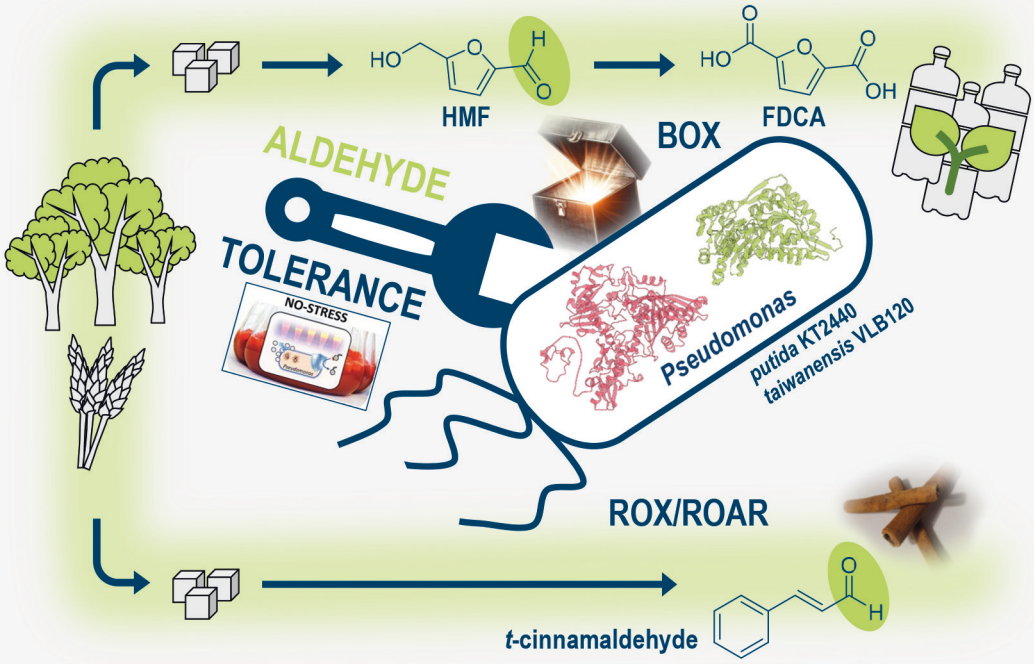

Tolerance engineering of *Pseudomonas* for the efficient conversion and production of aldehydes

Thorsten Lechtenberg

Schlüsseltechnologien / Key Technologies
Band / Volume 292
ISBN 978-3-95806-817-9

Mitglied der Helmholtz-Gemeinschaft

JÜLICH
Forschungszentrum

Schriften des Forschungszentrums Jülich
Reihe Schlüsseltechnologien / Key Technologies Band / Volume 292

Forschungszentrum Jülich GmbH
Institut für Bio- und Geowissenschaften (IBG)
Biotechnologie (IBG-1)

Tolerance engineering of *Pseudomonas* for the efficient conversion and production of aldehydes

Thorsten Lechtenberg

Schriften des Forschungszentrums Jülich
Reihe Schlüsseltechnologien / Key Technologies Band / Volume 292

ISSN 1866-1807 ISBN 978-3-95806-817-9

Bibliografische Information der Deutschen Nationalbibliothek.
Die Deutsche Nationalbibliothek verzeichnet diese Publikation in der
Deutschen Nationalbibliografie; detaillierte Bibliografische Daten
sind im Internet über http://dnb.d-nb.de abrufbar.

Herausgeber und Vertrieb:	Forschungszentrum Jülich GmbH Zentralbibliothek, Verlag 52425 Jülich Tel.: +49 2461 61-5368 Fax: +49 2461 61-6103 zb-publikation@fz-juelich.de www.fz-juelich.de/zb
Umschlaggestaltung:	Grafische Medien, Forschungszentrum Jülich GmbH
Druck:	Grafische Medien, Forschungszentrum Jülich GmbH
Copyright:	Forschungszentrum Jülich 2025

Schriften des Forschungszentrums Jülich
Reihe Schlüsseltechnologien / Key Technologies, Band / Volume 292

D 61 (Diss. Düsseldorf, Univ., 2024)

ISSN 1866-1807
ISBN 978-3-95806-817-9

Vollständig frei verfügbar über das Publikationsportal des Forschungszentrums Jülich (JuSER)
unter www.fz-juelich.de/zb/openaccess.

« Le premier regard de l'homme jeté sur l'univers n'y découvre que variété, diversité, multiplicité des phénomènes. Que ce regard soit illuminé par la science, — par la science qui rapproche l'homme de Dieu, — et la simplicité et l'unité brillent de toutes parts. »

“Man's first look at the universe discovers only variety, diversity, multiplicity of phenomena. Let this gaze be enlightened by science — by science which brings man closer to God — and simplicity and unity shine everywhere.”

Louis Pasteur (1822 – 1895)

Publications

The results of this thesis have been made available in the following original publications or are summarized in manuscripts intended for imminent submission:

LECHTENBERG, T., WYNANDS, B. & WIERCKX, N. 2024. Engineering 5-hydroxymethylfurfural (HMF) oxidation in *Pseudomonas* boosts tolerance and accelerates 2,5-furandicarboxylic acid (FDCA) production. *Metabolic Engineering*, 81, 262-272. **10.1016/j.ymben.2023.12.010**

LECHTENBERG, T., WYNANDS, B., POLEN. T & WIERCKX, N. 2024. Life with toxic substrates – PaoEFG forms the basis for growth of *Pseudomonas taiwanensis* VLB120 and *Pseudomonas putida* KT2440 on aromatic aldehydes. – to be submitted

LECHTENBERG, T., WYNANDS, B., MÜLLER, M. F., POLEN T., NOACK, S. & WIERCKX, N. 2024. Improving 5-(hydroxymethyl)furfural (HMF) tolerance of *Pseudomonas taiwanensis* VLB120 by automated adaptive laboratory evolution (ALE). – *Metabolic Engineering Communications*, 18, e00235. **10.1016/j.mec.2024.e00235**

LECHTENBERG, T., WYNANDS, B. & WIERCKX, N. 2024. *De novo* production of *t*-cinnamaldehyde by engineered solvent-tolerant and oxidation-deficient *Pseudomonas taiwanensis* VLB120. – to be submitted

Thesis-associated publications:

BITZENHOFER, N. L., KRUSE, L., THIES, S., WYNANDS, B., LECHTENBERG, T., RÖNITZ, J., KOZAEVA, E., WIRTH, N. T., EBERLEIN, C., JAEGER, K. E., NIKEL, P. I., HEIPIEPER, H. J., WIERCKX, N. & LOESCHCKE, A. 2021. Towards robust *Pseudomonas* cell factories to harbour novel biosynthetic pathways. *Essays in Biochemistry,* 65**,** 319-336. **10.1042/EBC20200173**

Additional publications not covered in this thesis:

KÖBBING, S., LECHTENBERG T., WYNANDS, B., BLANK L. M. & WIERCKX N. 2024. Reliable genomic integration sites in *Pseudomonas putida* identified by two-dimensional transcriptome analysis. *ACS Synthetic Biology*, 13, 2060-2072. **10.1021/acssynbio.3c00747**

Further contributions in form of oral presentations or posters:

Oral presentations:

LECHTENBERG, T., WYNANDS, B. & WIERCKX, N. 2022. Identification of aldehyde oxidizing enzymes in *Pseudomonas taiwanensis* VLB120 and generation of a tolerance-optimized chassis strain. *VAAM 2022 Jahrestagung der Vereinigung für Allgemeine und Angewandte Mikrobiologie*, online, February 2022

LECHTENBERG, T., WYNANDS, B. & WIERCKX, N. 2023. Unveiling *Pseudomonas*' enzymatic toolbox for 5-(hydroxymethyl)furfural (HMF) detoxification. *MICROBIAL STRESS 2023*, Vienna/Austria, September 2023

LECHTENBERG, T., WYNANDS, B. & WIERCKX, N. 2024. *De novo* production of valuable aromatic aldehydes and aldehyde-derived products by engineered solvent-tolerant and oxidation-deficient *P. taiwanensis* VLB120. *European Congress on Biotechnology 2024*, Rotterdam/The Netherlands, June 2024

Poster presentations:

LECHTENBERG, T., WYNANDS, B. & WIERCKX, N. 2022. *De novo* production of *t*-cinnamaldehyde using solvent-tolerant and redox-neutralized *Pseudomonas taiwanensis* VLB120. *BIOFLAVOUR 2022 - Biotechnology of Flavours, Fragrances and Functional Ingredients*, Frankfurt am Main/Germany, September 2022 (poster prize)

LECHTENBERG, T., WYNANDS, B. & WIERCKX, N. 2023. Engineering 5-(hydroxymethyl)furfural (HMF) oxidation in *Pseudomonas* boosts tolerance and accelerates 2,5-furandicarboxylic acid (FDCA) production. *3rd Pseudomonas Grassroots Meeting*, Garching/Germany, November 2023

LECHTENBERG, T., WYNANDS, B. & WIERCKX, N. 2023. Engineering 5-(hydroxymethyl)furfural (HMF) oxidation in *Pseudomonas* boosts tolerance and accelerates 2,5-furandicarboxylic acid (FDCA) production. *Topic 7 Fall Meeting - Towards a Sustainable Bioeconomy – Resources, Utilization, Engineering and AgroEcosystems*, Jülich/Germany, December 2023

List of abbreviations

4-CL	4-coumarate-CoA ligase
4-HB	4-hydroxybenzoate
4-HPAA	4-hydroxyphenylacetaldehyde
ADH	alcohol dehydrogenase
AdhP	ethanol-active dehydrogenase/acetaldehyde-active reductase
ADM	Archer Daniels Midland
AHADH	alpha-hydroxy acid dehydrogenase
AKR	aldo-keto reductase
AldB-I	aldehyde dehydrogenase B-I
AldB-II	aldehyde dehydrogenase B-II
AldB-I(I)	aldehyde dehydrogenases B-I and II
ALDH	aldehyde dehydrogenase
ALE	adaptive laboratory evolution
ATP	adenosine triphosphate
BCD2	bicistronic design 2
BIA	benzylisoquinoline alkaloids
BLAST	Basic Local Alignment Search Tool
BOX	Boosted OXidation
BOX-C/P	Boosted OXidation in the cytoplasm (C) and/or periplasm (P)
CAR	carboxylic acid reductase
CBP	consolidated bioprocessing
CoA	coenzyme A
CyT	cytidylyltransferase
del	deletion
DFF	2,5-diformylfuran
DHT	dehydratase
DMP	Dess-Martin periodinane
Ech	enoyl-CoA-hydratase/aldolase
ECT	electron transport chain

ED	Entner-Doudoroff
EDEMP	metabolic architecture relying on activities from the ED, EMP, and PP pathways
EG	ethylene glycol
EMP	Embden-Meyerhof-Parnas
FA	2-furoic acid
FAD	flavin adenine dinucleotide
Fcs	feruloyl-CoA-synthetase
FDCA	2,5-furandicarboxylic acid
FFA	5-formyl-2-furoic acid
GMC	glucose-methanol-choline
GRC	genome-reduced chassis
g-value	green value
HMF	5-(hydroxymethyl)furfural
HMFA	5-(hydroxymethyl)-2-furoic acid
HMFOH	5-(hydroxymethyl)furfuryl alcohol
HPLC	high-performance liquid chromatography
hyp	hypothetical
ISPR	*in situ* product removal
LB	lysogeny broth
LDMIC	lignocellulose-derived microbial inhibitory compounds
mfs	major facilitator superfamily
Moco	molybdopterin cofactor
MSM	minimal salts medium
NCS	norcoclaurine synthase
nt	nucleotide
OMP	outer membrane porin
OPA	ortho-phthaldehyde
PAC	phenylacetylcarbinol
PAL	phenylalanine ammonia lyase
Pao	periplasmic aldehyde oxidoreductase
PBS	polybutylene succinate
PCA	protocatechuate

PCC	pyridinium chlorochromate
PCR	polymerase chain reaction
PDC	pyruvate decarboxylase
PEF	polyethylene furanoate
PET	polyethylene terephthalate
pFMN	prenylated flavin mononucleotide
PHA	polyhydroxyalkanoate
PLA	polylactic acid
PLP	pyridoxal phosphate
PP	pentose phosphate
PPTase	phosphopantetheinyl transferase
PQQ	pyrroloquinoline quinone
PTF	polytrimethylene furandicarboxylate
PTFE	polytetrafluorethylen
RBS	ribosome-binding site
ROAR	Reduced Oxidation And Reduction
ROX	Reduced OXidation
sdr	short-chain dehydrogenase/reductase
SNV	single nucleotide variant
SSS	sodium/solute symporter
TA	terephthalic acid
TAT	Twin-Arginine Translocation
TAXI	TRAP-associated extracytoplasmic immunogenic
TCA	tricarboxylic acid
TEMPO	2,2,6,6-tetramethylpiperidinyloxyl
ThDP	thiamine diphosphate
TRAP	tripartite ATP-independent periplasmic
TTT	tripartite tricarboxylate transporter
Vdh	vanillin dehydrogenase
α/β hyd	alpha/beta hydrolase
α-KG	2-ketoglutaric acid

List of figures

Figure 1.3-1: Overview of the principle chemistry of aldehydes. 6

Figure 1.3-2: Aldehyde-mediated protein or DNA cross-linking via primary amino functionalities of biological macromolecules exemplarily shown for HMF as a stressor (adapted from (Jayakody and Jin, 2021)). 9

Figure 1.3-3: The furanic aldehydes HMF and furfural are promising biomass-derived platform chemicals, with HMF being largely further processed to the polymer building block FDCA. The dicarboxylic acid enables the production of PEF, a fully bio-based plastic material (adapted from (Xu et al., 2020a)). 10

Figure 1.3-4: Genetics and biochemistry of furanic compounds degradation. 23

Figure 2.1-1: HMF conversion by the biotechnological workhorses *P. taiwanensis* VLB120 GRC1, *P. putida* KT2440 and deletion mutants thereof unveiling the enzymes involved in this process. 38

Figure 2.1-2: Tracing of HMF-reducing enzymes in *P. taiwanensis* VLB120 GRC1 40

Figure 2.1-3: Importance of aldehyde oxidation for HMF tolerance. 41

Figure 2.1-4: Chromosomal overexpression of *paoEFGHI* and *aldB-I* enhances the oxidation ability of *P. taiwanensis* VLB120 GRC1 and leads to improved HMF tolerance. 44

Figure 2.1-5: FDCA production experiments with selected oxidation-optimized BOX-C/P strains. 48

Figure 2.1-6: Updated reaction scheme covering the entire oxidative pathway from HMF to FDCA. 49

Figure 2.2-1: Growth experiments with *P. taiwanensis* VLB120 GRC3, *P. putida* KT2440 and deletion mutants thereof lacking putative aromatic aldehyde-oxidizing enzymes on MSM agar plates containing different carbon sources. 60

Figure 2.2-2: Integration of the *hmf*-cluster into the genomes of *P. taiwanensis* VLB120 GRC1 and *P. putida* KT2440 and growth analysis of the resulting strains. 62

Figure 2.2-3: Complementation of the previously integrated *hmf*-cluster by *aldh* and *hmfR1* in *P. taiwanensis* VLB120 GRC1 and subsequent growth analysis. 64

Figure 2.2-4: Growth characteristics of selected strains resulting from the long-term ALE of GRC1 PVLB_23545-40::P_{tac}_*hmfFGABCDEHT* on HMFA as sole carbon and energy source (second generation). 66

Figure 2.2-5: BOX-derivatives of the evolved strain TL_666 show a high tolerance towards HMF, when utilizing the aldehyde as sole carbon and energy source. 71

Figure 2.3-1: ALE considerably accelerated growth of GRC1 ROX in the presence of HMF. 81

Figure 2.3-2: Analysis of isolated clones from the ALE. 83

Figure 2.3-3: Characterization of reverse-engineered GRC1 ROX mutants. 85

Figure 2.3-4: Deletion of *mexT* also confers a fitness advantage in strains with intact or boosted aldehyde oxidation machinery when exposed to HMF or furfural. 86

Figure 2.3-5: The main effect of MexT inactivation occurring during ALE is a shutdown of the MexEF-OprN efflux pump. 88

Figure 2.4-1: *t*-Cinnamaldehyde tolerance assessment of GRC1, GRC3, GRC3 PHE and their respective ROX derivatives. 97

Figure 2.4-2: Engineering of *P. taiwanensis* for *de novo* biosynthesis of *t*-cinnamaldehyde. 99

Figure 3.2-1: Possible applications of oxidation-deficient GRC3 ROX/ROAR in the biosynthesis of structurally more complex chiral building blocks. 113

Figure S5.1-1: BLAST analysis screening for *paoABCD* homologs in *P. taiwanensis* VLB120, *P. putida* KT2440, and *P. aeruginosa* PAO1. 139

Figure S5.1-2: HMF conversion assays in shake flasks (four-fold buffered MSM with 40 mM glycerol, 2 mM glucose, and 10 mM HMF) using whole-cells of *P. taiwanensis* VLB120 GRC1 and selected mutant strains thereof. 140

Figure S5.1-3: HMF conversion assays in 24-deepwell microplates (two-fold buffered MSM with 40 mM glycerol, 2 mM glucose, and 10 mM HMF) using whole-cells of *P. putida* KT2440 and deletion mutants thereof. 141

Figure S5.1-4: Bioinformatic prediction of promoter sequences upstream of *paoEFGHI* (**A**) and *aldB-I* (**B**). 142

Figure S5.1-5: HMF conversion assays in 24-deepwell microplates (two-fold buffered MSM with 40 mM glycerol, 2 mM glucose, and 10 mM HMF) using whole-cells of GRC1 and promoter exchange mutants thereof with optimized expression of identified genes encoding HMF-oxidizing enzymes. 143

Figure S5.1-6: FDCA production experiments with oxidation-optimized BOX-C/P-*hmfH-hmfT* strains. 144

Figure S5.1-7: FDCA production experiments with oxidation-optimized BOX-C/P-*hmfH-hmfT*(g) strains 145

Figure S5.2-1: Analysis of selected strains resulting from the ALE of GRC1 PVLB_23545-40::P_{tac}_*hmfFGABCDEHT* on HMFA as sole carbon and energy source (first generation). 147

Figure S5.3-1: Evaluation of optimal culture conditions for an ALE with GRC1 ROX. 149

Figure S5.3-2: Analysis of all isolated clones from the ALE. 150

Figure S5.3-3: MexT deletion also confers a fitness advantage in strains with intact aldehyde oxidation machinery including the oxidation-optimized BOX strains (control experiments). 151

Figure S5.3-4: HMF conversion assays in 24-deepwell microplates (two-fold buffered MSM with 40 mM glycerol, 2 mM glucose, and 10 mM HMF) using whole-cells of GRC1 and derived BOX strains (increased expression of *paoEFG* and *aldB-I*) with deletion of *mexT*. 152

Figure S5.3-5: Genomic context of *mexEF-oprN* in *P. taiwanensis* VLB120 highlighting the nod-box-like sequence containing two putative MexT binding sites upstream of the operon. 153

List of tables

Table 1.3-1: Selected standard reduction potentials (Berg et al., 2018). 5

Table 2.2-1: Genomic loci affected by the ALE experiment. 67

Table 2.3-1: Selected genomic loci affected by the ALE. 84

Table 2.3-2: Gradient method used for HPLC measurements. 93

Table S5.1-1: Overview of the 32 ALDH-encoding genes of *P. putida* KT2440 according to Julián-Sánchez et al. (Julian-Sanchez et al., 2020) and their corresponding homologs in *P. taiwanensis* VLB120. 137

Table S5.1-2: Aldehyde reducing enzymes deleted in the *E. coli* RARE strain and their homologs in *P. taiwanensis* VLB120. 138

Table S5.3-1: Overview of the growth parameters of all strains under the tested conditions in chapter 2.3. 154

Contents

Publications I

List of abbreviations III

List of figures VI

List of tables IX

Summary XIV

Zusammenfassung XV

1. Introduction 1

1.1. Biocatalysis – Exploring nature's chemical toolbox ... 1

1.2. Tolerance – A multifaceted prerequisite for efficient and competitive biotechnological processes ... 3

1.3. Aldehydes ... 4

1.3.1. Aldehydes in biology ... 7

1.3.1.1. Aldehyde toxicity ... 8

1.3.2. HMF and furfural – Green chemistry intermediates ... 9

1.3.3. FDCA as a plant-sourced polymer building block for PEF – Achieving fully bio-based plastics ... 12

1.3.3.1. Industrial production ... 13

1.3.3.2. Microbial catalysis as a sustainable alternative ... 14

1.3.4. Microbial degradation of furanic aldehydes and their derivatives ... 16

1.3.4.1. Genetic basis of the metabolic pathway ... 17

1.3.4.2. The degradation pathway and its biochemistry ... 19

1.4. *Pseudomonas* – A multi-talented and robust cell factory ... 24

1.5. Aim, scope, and outline of this thesis ... 26

2. Publications and manuscripts 29

2.1. Engineering 5-hydroxymethylfurfural (HMF) oxidation in *Pseudomonas* boosts tolerance and accelerates 2,5-furandicarboxylic acid (FDCA) production ... 31

2.1.1. Abstract ... 32

2.1.2. Introduction ... 34

2.1.3. Results and discussion ... 36

2.1.3.1. Identification of HMF-oxidizing enzymes in *P. taiwanensis* VLB120 and *P. putida* KT2440 ... 36

2.1.3.2. Identification of HMF-reducing enzymes in *P. taiwanensis* VLB120 ... 39

2.1.3.3. PaoEFG and AldB-I are crucial for tolerance towards HMF ... 41

2.1.3.4. Tolerance engineering enables GRC1 to withstand higher HMF concentrations ... 42

2.1.3.5. Optimized FDCA production ... 45

2.1.4. Conclusion and outlook ... 49

2.1.5. Materials and methods ... 50

2.1.5.1. Strains and culture conditions ... 50

2.1.5.2. Plasmid cloning and strain engineering ... 51

2.1.5.3. Analytical methods ... 52

2.1.5.4. Whole-cell HMF conversion assays in shake flasks ... 52

2.1.5.5. Whole-cell HMF conversion assays in 24-deepwell microplates (Duetz-System) ... 53

2.2. Life with toxic substrates – PaoEFG forms the basis for growth of *Pseudomonas taiwanensis* VLB120 and *Pseudomonas putida* KT2440 on aromatic aldehydes ... 55

2.2.1. Abstract ... 56

2.2.2. Introduction ... 57

2.2.3. Results and discussion ... 59

2.2.3.1. PaoEFG is essential for growth on 4-hydroxybenzaldehyde and vanillin ... 59

2.2.3.2. Genomic integration of the *hmf*-cluster into *P. taiwanensis* VLB120 GRC1 and *P. putida* KT2440 enabled growth on furfural, FA, and FDCA, but not on HMF and HMFA ... 61

2.2.3.3. Promoting growth on HMF and HMFA by adaptive laboratory evolution (ALE) ... 64
2.2.3.4. Whole-genome resequencing of the evolved strains ... 66
2.2.3.5. Evolved and tolerance-engineered GRC1 PVLB_23545-40::P_{tac}_*hmfFGABCDEHT* (TL_666 BOX-C/P) strains display superior growth on HMF compared to the native degrader *Paraburkholderia caribensis* ... 69
2.2.4. Conclusion ... 72
2.2.5. Materials and methods ... 72
2.2.5.1. Strains and culture conditions ... 72
2.2.5.2. Whole genome sequencing ... 73
2.2.5.3. Plasmid cloning and strain engineering ... 74
2.3. Improving 5-(hydroxymethyl)furfural (HMF) tolerance of *Pseudomonas taiwanensis* VLB120 by automated adaptive laboratory evolution (ALE) ... 76
2.3.1. Abstract ... 77
2.3.2. Introduction ... 78
2.3.3. Results and discussion ... 80
2.3.3.1. Increasing HMF tolerance of oxidation-deficient GRC1 ROX by ALE ... 80
2.3.3.2. Characterization of evolved strains ... 82
2.3.3.3. Reverse engineering ... 84
2.3.3.4. The benefit of *mexT* deletion lies in preventing *mexEF-oprN* expression ... 87
2.3.4. Conclusion ... 89
2.3.5. Materials and methods ... 90
2.3.5.1. Strains and culture conditions ... 90
2.3.5.2. Robotics-assisted ALE ... 91
2.3.5.3. Whole-genome sequencing ... 91
2.3.5.4. Plasmid cloning and strain engineering ... 92
2.3.5.5. Analytical methods ... 92
2.4. *De novo* production of *t*-cinnamaldehyde by engineered solvent-tolerant and oxidation-deficient *Pseudomonas taiwanensis* VLB120 ... 94
2.4.1. Abstract ... 95
2.4.2. Introduction ... 96

2.4.3. Results and discussion 96
2.4.4. Conclusion 100
2.4.5. Materials and methods 100
2.4.5.1. Media and culture conditions 100
2.4.5.2. Plasmid construction and genomic modifications 101
2.4.5.3. Analytics 101

3. General discussion and perspectives 103

3.1. Whole-cell biocatalytic FDCA production 103
3.2. Aromatic aldehydes as products or intermediates of microbial cell factories 108
3.3. Concluding remarks 115

4. References 117

5. Appendix 136

5.1. Supplementary material to chapter 2.1 136
5.2. Supplementary material to chapter 2.2 146
5.3. Supplementary material to chapter 2.3 148
5.4. Supplementary material to chapter 2.4 158
Table S1: Strains used in this thesis. 159
Table S2: Plasmids used in this thesis. 167
Table S3: Oligonucleotides (name, sequence, and description) 174

Danksagung 183

Eidesstattliche Erklärung 185

Summary

Biocatalysis holds promise to tackle the sustainability challenges faced by chemical industry due to climate change and depletion of fossil resources. However, obstacles emerge regarding the compatibility of several important chemicals, notably aldehydes, with biological systems, even if remarkably robust workhorses such as bacteria of the *Pseudomonas* clade are employed. This is related to the high and versatile reactivity of aldehydes, which is both their greatest asset and the root cause of their toxicity. Competitive biocatalytic processes involving these substances thus require tolerance-improved host organisms. In view of the constantly growing demand for renewable and ecologically produced plastics, the biocatalytic oxidation of the burgeoning platform chemical 5-(hydroxymethyl)furfural (HMF) to 2,5-furandicarboxylic acid (FDCA) is of particular interest since FDCA can substitute structurally similar and fossil-based terephthalic acid in polyesters. With the periplasmic oxidoreductase complex PaoEFG and the cytoplasmic dehydrogenases AldB-I and AldB-II, the primary enzymes responsible for the oxidation of HMF and further aromatic aldehydes like 4-hydroxybenzaldehyde and vanillin by *P. taiwanensis* VLB120 and *P. putida* KT2440 were uncovered. This marks a significant advancement from former black-box application of these strains to specialized biocatalysts with fine-tuned properties. To illustrate, overexpression of the newly characterized genes resulted in so-called BOX-strains (Boosted OXidation) with up to tenfold increased initial oxidation rates in comparison to the wild type. As a result, the new variants exhibited increased robustness when growing in presence of HMF and also proved to be more efficient for the complete oxidation of the aldehyde to the industrial target compound FDCA. Furthermore, tolerance mechanisms distinct from rapid oxidation were sought applying an adaptive laboratory evolution approach. A ROX (Reduced OXidation) deletion mutant with diminished aldehyde conversion ability was subjected to steady HMF stress. This yielded tolerance-improved strains through the unforeseen inactivation of the regulator MexT and the associated shutdown of the efflux pump MexEF-OprN. Another potential use for oxidation-deficient, yet solvent-tolerant, Pseudomonads is the biosynthesis of aromatic aldehydes, as showcased with the popular aroma compound *t*-cinnamaldehyde. In conclusion, this thesis contributes to the fundamental understanding of aromatic aldehyde conversion by *P. taiwanensis* VLB120 and *P. putida* KT2440 by unveiling the underlying enzymes which were shown to constitute the organisms' main tolerance mechanism against these toxic substances. Their overexpression in BOX strains strongly increases aldehyde tolerance, and enables improved FDCA production by boosted HMF oxidation. Reduced aldehyde oxidation and reduction (ROAR) unlocks *P. taiwanensis* VLB120 for the (*de novo*) production of valuable aromatic aldehydes or aldehyde-derived products, thereby expanding the product portfolio of this aspiring microbial cell factory.

Zusammenfassung

Die Biokatalyse ist ein vielversprechender Ansatz zur Lösung der durch den Klimawandel und die Erschöpfung der fossilen Ressourcen bedingten Problematik der Nachhaltigkeit in der chemischen Industrie. Allerdings sind einige wichtige Chemikalien, insbesondere Aldehyde, nur begrenzt mit biologischen Systemen verträglich, selbst wenn bemerkenswert robuste Bakterien der Gattung *Pseudomonas* eingesetzt werden. Dies hängt mit deren hoher und vielseitiger Reaktivität zusammen, die sowohl Chancen eröffnet, als auch Toxizitätsursache ist. Wettbewerbsfähige biokatalytische Prozesse mit diesen Stoffen erfordern daher toleranzverbesserte Wirtsorganismen. Angesichts der ständig wachsenden Nachfrage nach erneuerbaren und umweltfreundlich hergestellten Kunststoffen ist die biokatalytische Oxidation der zunehmend an Bedeutung gewinnenden Plattformchemikalie 5-(Hydroxymethyl)furfural (HMF) zu 2,5-Furandicarbonsäure (FDCA) von besonderem Interesse, da FDCA einen Ersatz für die strukturell ähnliche, aber auf fossilen Rohstoffen basierende Terephthalsäure in Polyestern darstellt. Mit dem periplasmatischen Oxidoreduktasekomplex PaoEFG und den cytoplasmatischen Dehydrogenasen AldB-I und AldB-II wurden die zentralen Enzyme identifiziert, die für die Oxidation von HMF und weiteren aromatischen Aldehyden wie 4-Hydroxybenzaldehyd und Vanillin durch *P. taiwanensis* VLB120 und *P. putida* KT2440 verantwortlich sind. Dies markiert einen wichtigen Fortschritt von der bisherigen Black-Box-Anwendung dieser Stämme hin zu spezialisierten Biokatalysatoren mit fein abgestimmten Eigenschaften. So führte die Überexpression der neu charakterisierten Gene zu so genannten BOX-Stämmen (Boosted OXidation) mit bis zu zehnfach höheren initialen Oxidationsraten im Vergleich zum Wildtyp. Daraus resultierend zeigten die neuen Varianten robusteres Wachstum in Gegenwart von HMF und erwiesen sich zusätzlich als effizienter bei der vollständigen Oxidation des Aldehyds zur industriellen Zielverbindung FDCA. Zudem wurde mittels einer Laborevolution nach anderen Toleranzmechanismen als der schnellen Oxidation gesucht. Eine ROX (Reduced OXidation) Deletionsmutante mit reduzierter Aldehydumwandlung wurde einem stetigen HMF-Stress ausgesetzt, was durch die unerwartete Inaktivierung des Regulators MexT und die damit verbundene Blockade der Effluxpumpe MexEF-OprN ebenfalls zu toleranzverbesserten Stämmen führte. Ein weiteres potentielles Einsatzgebiet für oxidationsdefiziente, gleichwohl lösungsmitteltolerante Pseudomonaden ist die Biosynthese aromatischer Aldehyde, was am Beispiel des bekannten Aromastoffs *t*-Zimtaldehyd demonstriert wurde. Im Ergebnis trägt die vorliegende Arbeit zum grundlegenden Verständnis der Umwandlung aromatischer Aldehyde durch *P. taiwanensis* VLB120 und *P. putida* KT2440 bei, indem sie die zugrundeliegenden Enzyme beschreibt, die nachweislich den zentralen Toleranzmechanismus der Organismen gegenüber diesen toxischen Substanzen bilden. Ihre Überexpression in BOX-Stämmen

bewirkt eine erhebliche Steigerung der Aldehydtoleranz und ermöglicht eine verbesserte FDCA-Produktion durch verstärkte HMF-Oxidation. Reduzierte Aldehyd-Oxidation und Reduktion (ROAR) erschließt *P. taiwanensis* VLB120 für die (*de novo*)-Produktion wertvoller aromatischer Aldehyde oder davon abgeleiteter Verbindungen und erweitert damit das Produktportfolio dieser aufstrebenden mikrobiellen Zellfabrik.

1. Introduction

A multitude of modern society's amenities heavily depend on the large-scale production of countless chemicals shaping our day-to-day life in manifold ways. Their vast impact extends to pharmaceuticals, fertilizers, pesticides, preservatives, fibers, dyes, and plastic material to just name a few examples. A world without synthetic chemistry is unthinkable, yet there is significant potential to drastically diminish the environmental footprint of its related industries. For this, alternative concepts for the future need to be outlined with a focus on transitioning away from oil as principal resource, transforming linear processes into cyclic ones and reducing energy consumption. The 12 principles of green chemistry can provide direction and guidance (Anastas and Warner, 1998).

1.1. Biocatalysis – Exploring nature's chemical toolbox

In the overarching pursuit of solutions towards a sustainable chemical industry, an ever-growing role is ascribed to biocatalysis, the use of isolated enzymes or entire cells to speed up chemical reactions (Bell et al., 2021). There is particular interest in the whole-cell variant owing to its ease of handling and the resulting cost reduction (Wachtmeister and Rother, 2016, Lin and Tao, 2017). The cell, henceforth with a particular focus on a microbe, can be considered a miniature chemical factory which possesses a number of similarities, but also specific differences compared to its customary macroscopic counterpart. For the production of a target compound, preparative organic synthesis typically relies on a stirred flask as a confined reaction space in which only the desired substrates, solvents and catalysts are present. Whether highly corrosive, explosive, harmful or completely harmless, there are practically no restrictions on their selection, since the reaction vessel is made of inert materials. In addition, the reaction mixture can be tempered or pressurized as required. Both heterogeneous catalytic systems, where the phase of the catalyst differs from that of the reactants or products, as well as homogeneous catalytic systems, where the catalyst is in the same phase, can be employed and are of similar importance to a future green chemistry (Lin et al., 2021, Deuss et al., 2014). Depending on the process, however, substrates derived from fossil resources, elevated energy demands, and the generation of hazardous waste, such as heavy metals or noxious solvents, are still frequently encountered.

Living cells likewise provide a distinct reaction environment enclosed by at least one biological membrane composed of a continuous lipid bilayer. Yet, they do not represent a completely leak-proof system, as cellular membranes are semi-permeable allowing especially small and

nonpolar molecules to pass through. Furthermore, integral membrane proteins such as transporters (Nikaido and Saier, 1992) or porins (Vergalli et al., 2020) facilitate a permanent exchange between the outside and inside, even of larger and charged compounds. Substrates and products can therefore be continuously taken up or released, presuming the existence of a functioning transport mechanism. Concerning solvents, the chemistry of life depends on water (Ball, 2017), generally considered the greenest option of all (Zhou et al., 2019a), but this does not mean that others cannot be tolerated as well (Isken and de Bont, 1998). Obviously, there is not just one specific chemical reaction taking place in a cell that could actually be used for a synthetic purpose, but a whole network of metabolic pathways and basic biochemical functions, constantly running in the background. These include vital operations, notably protein synthesis which yields new catalysts, DNA and RNA production required as construction manuals for them, along with core metabolism providing the necessary building blocks. Thus, a living cell is continuously bustling with a multitude of biochemical reactions of which those of value for biotechnology must be identified and accentuated where appropriate. This work illustrates the elucidation and systematic exploitation of a bacterium's distinct metabolic feature, specifically the oxidation of aromatic aldehydes by *Pseudomonas*, for production of compounds relevant to sustainable chemistry with a special focus on the bio-based plastic monomer 2,5-furandicarboxylic acid (FDCA). Nonetheless, it is also pointed out that whole-cell biocatalysis is often prone to unwanted side reactions jeopardizing the intended outcome. Therefore, genetic fine-tuning is needed to successfully harness microbes for industrial utilization. In modern days, sophisticated molecular biology techniques enable targeted interventions in the cell's physiological processes, a burgeoning strategy termed metabolic engineering which is finally heading towards designer cells for specific applications (Nielsen and Keasling, 2016, Lee et al., 2012, Kim et al., 2023, Yilmaz et al., 2022).

Even if microbes managed to occupy virtually all available environmental niches on earth (Merino et al., 2019), from a chemist's point of view, the intricate biochemical machinery, required for life, is only stable and functional under comparatively moderate conditions. Most organisms, at least those currently important for biotechnology including *Pseudomonas*, are mesophilic with optimal operating conditions at around 30 °C, neutral pH, and ambient pressure (Calero and Nikel, 2019). This adaptation to very mild conditions in combination with excellent selectivities, however, is the key advantage of biocatalysis, allowing process design with minimum energy expenditure. Enzymes, as highly efficient biological catalysts shaped by evolution, heavily reduce the activation barrier of chemical reactions, allowing them to proceed with modest thermal energy. Although reaction rates could be increased with rising temperatures, essential cell components such as proteins or DNA are only heat-stable to a limited extent, so that the temperature record for life is at the moment 122 °C, held by the

archaeon *Methanopyrus kandleri* (Takai et al., 2008). The integrity of vital cell functions in general is an important factor currently accountable for the partially still limited synthetic applicability of whole-cell biocatalysts, because it also affects the range of tolerated chemicals. These can potentially harm cells in various ways, for instance, by damaging biological (macro)molecules or membranes, and inhibition of central metabolic pathways (Nicolaou et al., 2010). One of the most problematic classes of compounds in this respect is constituted by aldehydes (Jayakody and Jin, 2021), which are in the spotlight of this thesis as challenging substrates, intermediates, and products.

Overall, whole-cell biocatalysis encompasses all fundamental characteristics to establish itself as a sustainable alternative for chemical industry (Woodley, 2022): Operation under exceptionally mild conditions, tunable properties through metabolic (Volk et al., 2023, Han et al., 2023) and protein engineering (Arnold, 2018, Chen and Arnold, 2020, Braun et al., 2023), growth on and/or conversion of renewable substances, and degradability or recyclability. The crucial aspect missing is enhanced compatibility with toxic chemicals like aldehydes. This study demonstrates how this issue can be addressed by analyzing and increasing the tolerance of the naturally robust host *Pseudomonas* through targeted engineering.

1.2. Tolerance – A multifaceted prerequisite for efficient and competitive biotechnological processes

The tolerance of a microorganism to a specific compound is a crucial property for its applicability as a whole-cell biocatalyst allowing higher substrate and product loads (Lo et al., 2013). It fundamentally describes the cell's ability to withstand the adverse conditions exerted by the toxicant. Next to the diverse chemical burden itself, these encompass among others stress related to osmolarity (Bremer and Krämer, 2019) and pH (Gao et al., 2021). A more detailed and precise definition of tolerance, however, is difficult and quantifying it is even more complicated (Brauner et al., 2017). The problem already begins with terminology, since next to tolerance, there exist several other expressions, essentially robustness, resistance, and persistence. The individual terms, originating from the field of antibiotics research, are each specified on their own (Brauner et al., 2016, Balaban et al., 2019), but commonly used interchangeably, which is also the case in this work, because they are often not clearly distinguishable in biotechnology. A further complexity arises from the biological fact that tolerance can be a phenotype associated with a multifactorial cellular response involving many genes and mechanisms. Gaining a deeper understanding of the individual aspects is already a major endeavor, and it becomes even more demanding to untangle their interconnections, thereby rendering targeted engineering of microbial tolerance highly challenging (Dunlop,

2011, Mukhopadhyay, 2015). Thus, next to elucidation of specific tolerance characteristics, large-scale systemic approaches, utilizing adaptive laboratory evolution (ALE) or omics-analyses, which both benefit from rapid progression in automation, provide promising options (Ling et al., 2014, Mohedano et al., 2022).

Moreover, tolerance acts at different tiers and it must be differentiated between the single-cell level and the survival of an entire population (Alnahhas and Dunlop, 2023). For the latter, the endurance of very few cells, which subsequently multiply rapidly, may be sufficient. Consequently, heterogeneity of microbial populations is an important point to reflect on, specifically under stress (Ackermann, 2015). This is also connected to the direct influence of a cell's stress response on its immediate environment and neighbors. The dynamic is exemplified when a toxicant is enzymatically degraded as a defense mechanism, such as hydrogen peroxide decomposition by a catalase or hydrolysis of an antibiotic by a β-lactamase. These processes not only serve the cell expressing the respective enzyme but also those in the vicinity. The situation is similar when considering the conversion of aldehydes discussed in this thesis. Recently, the intricate interplay between individual cells within a larger population has been described with the help of chaos theory (Choudhary et al., 2023).

A central factor of tolerance, where all aspects depicted above come together, is the lag phase, the initial delay in microbial growth to adapt to new conditions (Bertrand, 2019). It is therefore commonly used as a comparatively easy-to-measure read-out, particularly when furanic aldehydes like 5-(hydroxymethyl)furfural (HMF) or furfural are the chemical stressor (Heer and Sauer, 2008, Ma and Liu, 2010, Wordofa and Kristensen, 2018).

1.3. Aldehydes

Aldehydes constitute an essential class of organic compounds and their name is a blend originating from the Latin expression "alcohol(us) dehydrogenatus", which signifies "alcohol deprived of hydrogen". It was coined by the German scientist Justus von Liebig in 1835 and provides an illustrative description about what was observed upon the oxidation of ethanol to acetaldehyde, the formation of hydrogen gas. In the course of this reaction the primary alcohol with the formal carbon oxidation state -I is transformed into an aldehyde group with the carbon oxidation state +I releasing two protons and two electrons in the form of H_2 (Fig. 1.3-1A). The oxidized compound is characterized by its terminal carbonyl group C_{sp2}=O with a strong (720 kJ mol^{-1}) (Clayden et al., 2012), yet also considerably polarized carbon-oxygen double bond rendering aldehydes reactive substances. A fundamental reactivity is the release of two further electrons resulting in the formation of a carboxylic acid whose central carbon atom has the formal oxidation state +III. This second oxidation has a strong thermodynamic driving force

because of the additional resonance stabilization of the product (Fig. 1.3-1A). As a consequence, there is always a risk of overoxidation when attempting to chemically obtain aldehydes from alcohols. To solve this selectivity issue, organic chemists depend on sophisticated methods, amongst others the renowned Swern and Corey-Kim reactions (Mancuso et al., 1978, Corey and Kim, 1972). There are also further elaborate reagents, such as pyridinium chlorochromate (PCC), Dess-Martin periodinane (DMP), or TEMPO (Piancatelli et al., 1982, Yoshimura and Zhdankin, 2016, Cao et al., 2014b). As a result of the generally dehydrogenative mechanism being inoperative with aldehydes, overoxidation is usually not a concern for enzymatic reactions, at least when isolated oxidoreductases are employed. In the whole-cell context, of course, there is a variety of enzymes present, including those that catalyze potentially undesirable consecutive reactions (Dong et al., 2018). Certainly, these considerations only apply when aldehydes are the desired products and they become obsolete if obtaining the carboxylic acid is the main objective.

Aldehydes' pronounced tendency to deliver electrons is reflected by the highly negative standard reduction potential which is exemplarily given here for the redox couple acetic acid/acetaldehyde (Table 1.3-1). Even though biological redox conversions between alcohols, aldehydes, and carboxylic acids are the focus of this work, it should not remain unmentioned that the highest possible carbon oxidation level is +IV. This is found in carbon dioxide, but also in ortho esters or halogenated molecules, such as carbon tetrachloride (Fig. 1.3-1A).

Table 1.3-1: Selected standard reduction potentials (Berg et al., 2018).

oxidized form	reduced form	e^-	E0' in V at pH = 7
acetic acid, $2H^+$	**acetaldehyde, H_2O**	**2**	**-0.60**
NAD^+, $2H^+$	NADH, H^+	2	-0.32
$NADP^+$, $2H^+$	NADPH, H^+	2	-0.32
acetaldehyde, $2H^+$	**ethanol**	**2**	**-0.20**
cytochrome *c* (+3)	cytochrome *c* (+2)	1	0.22
½ O_2, $2H^+$	H_2O	2	0.82

Next to the described redox reactions, the chemistry of aldehydes is predominantly governed by their distinct electrophilicity. Owing to the high electronegativity of oxygen, the carbonyl carbon atom is significantly electron-deficient, a characteristic that can be further intensified by adjacent electron-withdrawing groups. Thus, aldehydes are easily attacked by a plethora of nucleophiles of which only a few can be stated at this point.

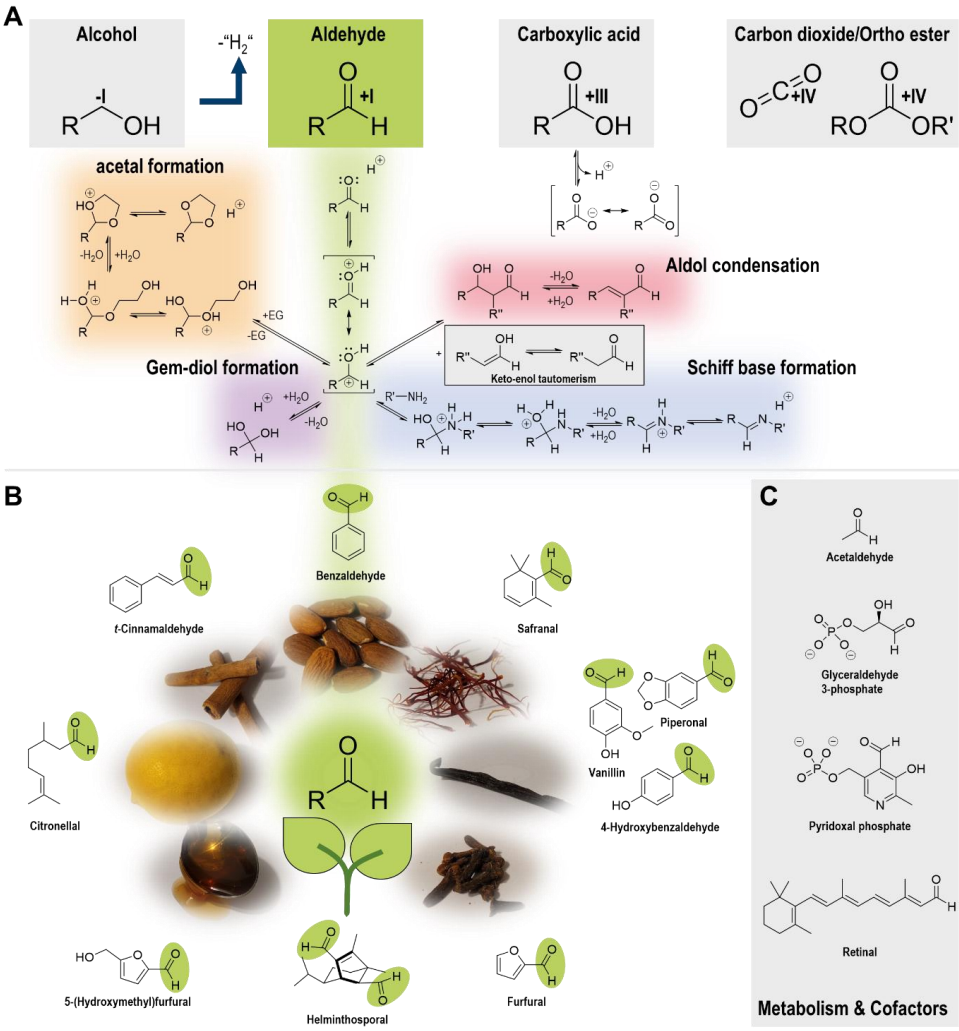

Figure 1.3-1: Overview of the principle chemistry of aldehydes. (**A**) Classification of functional groups according to the oxidation level of the central carbon atom. In this respect, aldehydes occupy an intermediate position between alcohol and carboxylic acid. Electrophilic aldehydes react with a multitude of nucleophiles. As examples with relevance for the chemistry of life, the acid-catalyzed formation of (hemi)acetals (orange), geminal diols (violet), and Schiff bases (blue) is portrayed. Additionally, the acid-catalyzed aldol condensation with an enolized second aldehyde molecule is shown (red). Aldehydes tend to be oxidized because of the resonance stabilization of the resulting carboxylic acid or carboxylate, respectively. (**B**) Important aldehydes occurring in nature and possible sources for their isolation. This thesis focuses on the furanic aldehydes 5-(hydroxymethlyl)furfural (HMF) and furfural and provides an example of how *t*-cinnamaldehyde can be produced by bacteria instead of being isolated from plants. (**C**) Selected aldehydes that occur as cofactors or intermediates in cellular metabolism.

Addition of primary amines and subsequent water elimination, for example, leads to reversible formation of imines, so-called Schiff bases frequently encountered in biochemistry (Fig. 1.3-1A) (Tidwell, 2008, Torrens-Spence et al., 2021). Alcohols, as nucleophiles, deliver (hemi)acetals, of which especially the cyclic ones formed by diols, are commonly used as

protecting groups for aldehydes in organic chemistry (Fig. 1.3-1A). (Hemi)acetals likewise have a pivotal function in sugar biochemistry (Clode, 1979). Water addition to aldehydes results in the generation of geminal diols, which, for instance, can play a role as intermediates in enzymatic oxidation reactions (1.3.4.2.) (Fig. 1.3-1A). However, they are only stable when the electron lone pairs of the two oxygen atoms, situated on the same carbon, are dispersed throughout the molecule preventing electrostatic repulsion. Important factors promoting distribution of electron density include neighboring electron-withdrawing groups and hydrogen bonding. The last and presumably most important aspect of aldehyde chemistry to be named in this setting is the aldol reaction, allowing the synthetically valuable formation of carbon-carbon bonds both in synthetic chemistry and in natural processes (Schmidt et al., 2016). Consider the production of fructose-1,6-bisphosphate in gluconeogenesis or the non-oxidative part of the pentose phosphate pathway as just two examples of this reaction type firmly anchored in cellular metabolism. Aldol addition, optionally followed by a dehydration step, involves a second carbonyl compound that must be enolizable, i.e. possess an acidic hydrogen atom in α-position. Under acidic conditions, this then acts as a nucleophile via the α-carbon atom of the enol form (Fig. 1.3-1A). Enzyme-catalyzed carbon-carbon bond-forming reactions are of particular interest for asymmetric synthesis (Brovetto et al., 2011, Windle et al., 2014).

1.3.1. Aldehydes in biology

Naturally produced mainly by plants, aldehydes, as volatile substances, are responsible for their unique aromas and flavors, which find applications in the food, pharmaceutical, and cosmetic industries (Schober et al., 2023, Kundu, 2017). Extracts of the orchid *Vanilla planifolia* even contain several of them, including the popular vanillin, as well as 4-hydroxybenzaldehyde and piperonal, also referred to as heliotropin (Fig. 1.3-1B) (Sinha et al., 2007). Further important examples are safranal, a monoterpene aldehyde from saffron; benzaldehyde, known for its almond-like odor; cinnamaldehyde, responsible for the flavor of cinnamon; and citronellal with its distinct lemon scent (Fig. 1.3-1B).

HMF and furfural are virtually absent in fresh edibles, but ubiquitous in sugar-rich and heat-treated foods, such as bakery products, fruit juices, dried fruits, and coffee (Quarta and Anese, 2012, Vignoli et al., 2014). For instance, HMF is a quality indicator for honey and high abundance indicates excessive heating during processing or inadequate storage (Fallico et al., 2004). As degradation product of cellulose and hemi-cellulose, the raw materials of paper, furfural contributes to the smell of old books and serves as a marker for age determination (Strlic et al., 2009). Both compounds are typically only found in trace amounts and all sources described are anthropogenic raising the question why degradation pathways for these substances evolved in nature (1.3.4.).

Furthermore, there are even complex natural products with aldehyde functionalities such as the phytotoxic helminthosporal isolated from the fungus *Bipolaris sorokiniana* (Fig. 1.3-1B) (de Mayo et al., 1962, Corey and Nozoe, 1963). Aldehydes also appear in cellular metabolism, as exemplified by the ethanol degradation product acetaldehyde or the glycolysis intermediate glyceraldehyde-3-phosphate (Fig. 1.3-1C). Both compounds are comparatively short-lived intermediates which rapidly undergo further oxidative processing. In particular, glyceraldehyde-3-phosphate and its conversion to 1,3-biphosphoglycerate is a prime example of how nature benefits from thermodynamics and conserves the energy released by aldehyde oxidation through concomitant substrate-level phosphorylation. The energy-rich phosphate bond can subsequently be used for adenosine triphosphate (ATP) generation.

Finally two fundamental biochemical cofactors bearing aldehyde groups are to be mentioned, retinal functioning as a chromophore for light sensing in both animals and microbes (Kiser et al., 2014, Rozenberg et al., 2021) and pyridoxal phosphate (PLP), amongst others involved in transamination reactions (Fig. 1.3-1C) (Eliot and Kirsch, 2004). Concerning retinal, the aldehyde function is in fact just used for coupling the cofactor to the protein via the ε-amino group of a lysine residue (Devine et al., 2013). Regarding PLP, the aldehyde group is needed for intermediate binding of the substrate, for example an amino acid, and thus actively takes part in catalysis (Eliot and Kirsch, 2004). In both cases, Schiff bases are formed (Fig. 1.3-1A).

Eventually the question arises, why a discussion about tolerance is required, when aldehydes are everywhere in nature.

1.3.1.1. Aldehyde toxicity

The very fact that aldehydes are common ingredients of disinfectants emphasizes their detrimental impact on microbes. Formaldehyde, glutaraldehyde, and *ortho*-phthalaldehyde (OPA) deserve specific mention in this context (Sagripanti et al., 1997, Simons et al., 2000). Despite the structural diversity, the toxicity of aldehydes can be attributed to a shared chemical property. In biological systems, their pronounced electrophilic nature poses challenges due to the presence of numerous nucleophiles, such as amino- or thiol- functionalities of proteins or DNA leading to cross-linking and thus damaging of the macromolecules (Fig. 1.3-2) (LoPachin and Gavin, 2014, O'Brien et al., 2005, Jayakody et al., 2022).

The extent of this noxious bridging of biological key players depends on the reactivity of the respective aldehyde which in turn is governed by various physiochemical parameters. These basically include the strength of the electrophilicity indicated by the energy of the lowest unoccupied molecular orbital (E_{LUMO}) or the electrophilicity index (ω) (Pal and Chattaraj, 2023), and steric hindrance (LoPachin and Gavin, 2014).

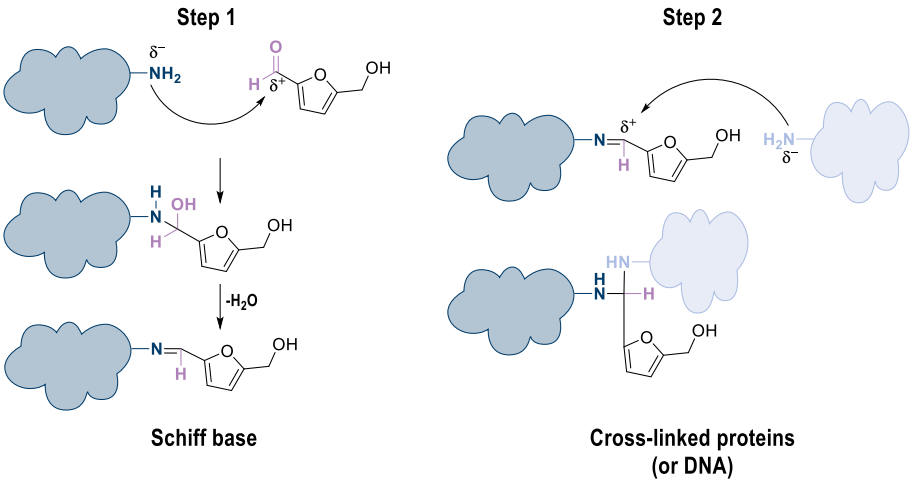

Figure 1.3-2: Aldehyde-mediated protein or DNA cross-linking via primary amino functionalities of biological macromolecules exemplarily shown for HMF as a stressor (adapted from (Jayakody and Jin, 2021)). Nucleophilic addition of the amino group to the aldehyde followed by dehydration yields a Schiff base intermediate. In a second step, this can be attacked by an amine functionality of another compound ultimately leading to a covalent linkage between two protein or DNA molecules through an aminoacetal.

For a comprehensive structure-inhibition analysis, the hydrophobicity of the compound, typically assessed by the $\log P_{o/w}$ (octanol/water partition coefficient) must also be taken into account (Jayakody and Jin, 2021). For the aldehydes HMF, furfural, vanillin, and 4-hydroxybenzaldehyde, which are relevant for this work, all these factors are available and compiled (Cao et al., 2014a). Defective proteins can partially be repaired by the control mechanisms of the cell, notably chaperones, but only under substantial investment of energy (Doyle et al., 2013, Saibil, 2013). However, there is evidence that engineering this machinery can lead to an increase in tolerance (Jayakody et al., 2018).

1.3.2. HMF and furfural – Green chemistry intermediates

A successful transformation to a chemical industry based on renewable resources demands novel platform molecules (Calvo-Flores and Martin-Martinez, 2022). In this respect, the sugar-derived furanic aldehydes HMF and furfural are considered of high potential, representing versatile building blocks that can be converted to a wide range of value-added compounds (Fig. 1.3-3A) (Bozell and Petersen, 2010, Xu et al., 2020a, Jiang et al., 2023). This flexibility is mainly driven by the reactivity of the aldehyde functionality which in the case of HMF is additionally complemented by a primary alcohol group, a bifunctionality rendering this substance particularly interesting. Both the dicarboxylic acid resulting from oxidative upgrading and the reductively obtained diol are suitable as monomers for plastic production (Fig. 1.3-3A) (Wang et al., 2014).

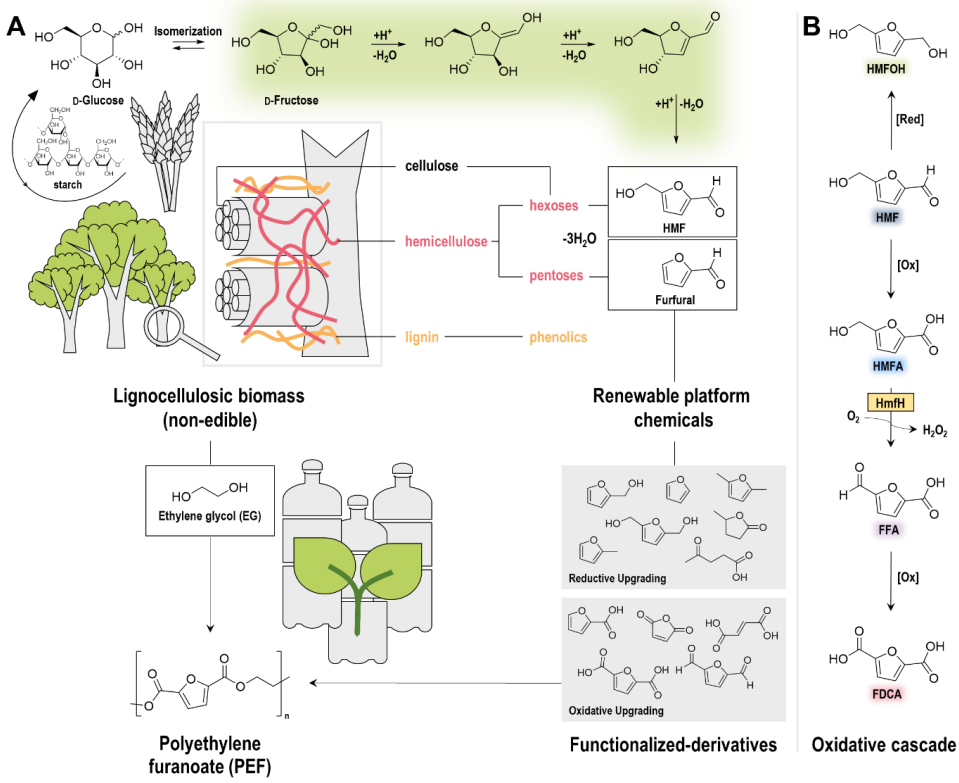

Figure 1.3-3: The furanic aldehydes HMF and furfural are promising biomass-derived platform chemicals, with HMF being largely further processed to the polymer building block FDCA. The dicarboxylic acid enables the production of PEF, a fully bio-based plastic material (adapted from (Xu et al., 2020a)). (**A**) Overview of HMF production from starch or lignocellulosic biomass and various examples of possible downstream products. For HMF synthesis, sugar dehydration via the presumably preferred route with cyclic intermediates, highlighted in green, is exemplarily depicted for fructose as the starting material (Antal et al., 1990, van Putten et al., 2013a). As an application example for PEF, the manufacturing of a so-called "plant bottle" made only from renewable biomass is showcased (Sheldon, 2014). (**B**) Three-step oxidation process from HMF to FDCA, which can be achieved with whole-cell biocatalysis under very mild conditions (Yuan et al., 2020). For clarity, the alternative pathway with an initial oxidation of the primary alcohol is omitted at this point.

HMF with its six-carbon backbone and the C_5-body furfural can be generated by acid-catalyzed dehydration of hexoses and pentoses, respectively, lowering the oxygen content while retaining all carbon atoms present in the starting carbohydrate (van Putten et al., 2013b, Rosatella et al., 2011, Teong et al., 2014). In total, three water molecules are eliminated resulting in the desaturated and planar heterocyclic core structure, where one electron lone pair of the oxygen atom is delocalized into the ring, thus fulfilling Hückel's rule for aromaticity (Fig. 1.3-3A). As all stereo centers are broken up, HMF can, in principle, be produced from any hexose. Yet, it is most efficiently synthesized from ketoses, consequently making fructose the predominant substrate (Kuster, 1990, van Putten et al., 2013a, Román-Leshkov et al., 2006).

Starchy plants such as wheat and corn are useful raw materials only requiring hydrolysis of the polymeric carbohydrate and isomerization of glucose into fructose (You et al., 2023). However, this leads to ethically questionable competition with food production, prompting recent efforts to increasingly utilize non-edible sources like abundant lignocellulosic biomass or other waste streams (Binder and Raines, 2009, Huynh et al., 2023, Shi et al., 2013, Kim et al., 2011, Caes et al., 2015, Lee et al., 2022, Xu et al., 2020a).

Overall, the yearly number of publications on HMF has grown drastically since the turn of the millennium (van Putten et al., 2013b, Messori et al., 2022), but despite intensive research the furanic aldehyde, often referred to as “the sleeping giant of sustainable chemistry”, is only slowly entering the awakening phase (Galkin and Ananikov, 2019). Currently, there appears to be just one company, AVA Biochem located in Muttenz, Switzerland, which is engaged in the larger-scale production of the compound for commercial purpose (Kläusli, 2014). Hence, HMF remains relatively costly at present (Rosenfeld et al., 2020). There are several challenges connected to the substance and its synthesis, mostly associated with the formation of unwanted byproducts. The dehydration reaction typically coincides with condensations resulting in complex, dark-colored, hardly soluble, and sticky furanic oligomers, known as humins (Xu et al., 2020c, Calderón et al., 2022, Liu et al., 2022). Although the actual composition and formation mechanism of these side products is still under investigation (Shen et al., 2020, Sailer-Kronlachner et al., 2022, Tsilomelekis et al., 2016, Echtermeyer and Viell, 2024), they should not be mixed up with similarly colored and equally intricate, fulvic acid-based humic material in soil which is structurally different (Rosenau et al., 2017). As a second issue, rehydration of HMF in an acidic aqueous milieu causes formation of levulinic acid and the simultaneous elimination of formic acid (Li et al., 2019). Levulinic acid is considered itself a promising platform chemical (Hayes and Becer, 2020), but represents only one of many follow-up chemicals (Xu et al., 2020a). Generally, next to yield loss, both processes provoke problems regarding separation and purification (Rosenfeld et al., 2020).

Despite the outlined difficulties, HMF is strongly promoted and profits from dynamic research that continually generates fresh ideas to alleviate these. For instance, thermal decomposition and self-polymerization of the furanic compound can be prevented by protecting the aldehyde function, amongst others, as a cyclic acetal (Kim et al., 2018, Coumans et al., 2022, He et al., 2024). Alternatively, new catalyst and solvent systems are proposed of which only a few can be mentioned here (Vu et al., 2023, Luan et al., 2022, Hou et al., 2022, Phan et al., 2022, He et al., 2023, Chen et al., 2022). Hence, it is assumed that HMF will become increasingly competitive and will be fully established as renewable platform in the near future (Galkin and Ananikov, 2019). The most important downstream product of HMF for this work is FDCA,

featuring fully-oxidized substituents on the furanic ring and serving as monomer for bio-based plastics.

1.3.3. FDCA as a plant-sourced polymer building block for PEF – Achieving fully bio-based plastics

Owing to its structural resemblance to the important industrial compound terephthalic acid (TA), FDCA is already mentioned in the very first list of particularly promising sugar-derived platform chemicals compiled by the US Department of Energy in 2004 (Werpy and Petersen, 2004). The primary application domain for both molecules is polymer synthesis. Polycondensation of TA with ethylene glycol (EG) yields polyethylene terephthalate (PET), one of the most important plastic materials with an annual global production predicted to exceed 35 million metric tons in 2024, corresponding to a market value of about 35 billion US dollars (Jaganmohan, 2024a, Jaganmohan, 2024b). At present, petroleum-derived PET finds extensive use, notably in the manufacturing of fibers and food packaging (Rabnawaz et al., 2017). Polyethylene furanoate (PEF) (Fig. 1.3-3A), synthesized from FDCA and EG, offers a comparable, yet sustainable alternative to conventional PET and could putatively replace it in the future (Fei et al., 2020, Hwang et al., 2020). Since EG can likewise be produced from renewable resources (Wong et al., 2023, Kandasamy et al., 2019, Yue et al., 2012), PEF constitutes an entirely bio-based material whose implementation instead of PET may additionally reduce greenhouse gas emissions over the entire life cycle up to about 50%, as suggested by a cradle-to-grave life cycle assessment (Eerhart et al., 2012). Both polymers exhibit similar physical, mechanical, and chemical characteristics, with PEF even outperforming PET in some aspects (Loos et al., 2020). The main advantage of the FDCA-based polymer is connected to the barrier properties with specific emphasis on gas permeability. This is significantly reduced for both O_2 and CO_2, which makes PEF especially appealing for longer-lasting carbonated beverages (Sheldon, 2014) and can be attributed to subtle chemical distinctions between FDCA and TA. These are essentially the differences in ring size and polarity stemming from the heteroaromatic nature of FDCA. Thereby, rotation movements typically observed for the benzene moieties of PET are prevented, resulting in PEF being more rigid (Burgess et al., 2014, Araujo et al., 2018). Next to carbon efficiency during production, the reduced gas transmission is a key benefit of PEF that sets it apart from other renewable polyesters such as polylactic acid (PLA), polybutylene succinate (PBS), and bioPET, the plant-based variant of PET (Rosenboom et al., 2022, Loos et al., 2020).

1.3.3.1. Industrial production

At present, FDCA is not yet produced on an industrial scale, but a first commercial factory is currently under construction at the Chemical Park Delfzijl in the Netherlands and scheduled to start operations in 2024. This demonstration plant, which is run by the Dutch company Avantium N.V. employing its YXY® technology, is intended to have an annual output of 5000 metric tons (Avantium, 2022, PEFerence, 2024, de Jong et al., 2022). The synthesis is based on wheat-sourced high-fructose syrup (F95) as the initial substrate (Tereos, 2022). Instead of HMF, the process predominantly relies on ether derivatives thereof as central intermediates resulting from the acid-catalyzed dehydration of the sugar in alcohol. These are less prone to decomposition at low pH (Gruter and Dautzenberg, 2007, Brown et al., 1982). The exact conditions for the subsequent oxidation to FDCA with molecular oxygen are not publicly available, but they can vaguely be deduced from the respective patents (Muñoz de Diego et al., 2011a, Muñoz de Diego et al., 2011b, Mazoyer et al., 2014, Baars et al., 2021). The procedure seems to involve an oxygen pressure between 3-15 bar, temperatures around 150-210 °C, an organic acid as a solvent, and a homogeneous metal catalyst (Co/Mn/Br) (Partenheimer and Grushin, 2000). These conditions resemble the reaction parameters that have long been used for the synthesis of TA from fossil-based *p*-xylene, known as the AMOCO process (Tomas et al., 2013). For the production of a completely colorless and clear plastic material, the crude FDCA needs to undergo an additional purification step before being used for polymer synthesis (de Jong et al., 2022).

Other companies, for instance the Scandinavian paper and packaging manufacturer Stora Enso with its FuraCore® process, also proclaim to have entered the pilot plant stage for commercial FDCA production (Stora Enso, 2023). The raw material here is again fructose, which is currently still starch-derived, but could potentially be obtained from non-food biomass in the future. The sugar is first dehydrated to HMF applying a method patented by the now-defunct American start-up Rennovia. Its key advantage consists in the avoidance of fouling and clogging by removal of viscous humins, occurring as inherent byproducts, through nanofiltration (Boussie et al., 2015). In a second step, HMF is converted to FDCA by a fixed-bed oxidation process, which according to present patents presumably relies on a heterogeneous noble metal catalyst (Sokolovskii et al., 2017). In addition, Stora Enso highlights that both dehydration and oxidation can be conducted in the same solvent (Stora Enso, 2024).

The US companies DuPont and Archer Daniel Midland (ADM) set their sights on the FDCA derivative furan dicarboxylic methyl ester (FDME) as a polymer building block and teamed up for a 60-metric-ton-per-year pilot plant opened in Decatur, Illinois, in 2018 (Bomgardner, 2018).

Dimethyl esters of dicarboxylic acids serve as alternative substrates for polyester synthesis. For example, PET, the petrochemical benchmark polymer, is produced from both dimethyl terephthalate (DMT) via transesterification and direct esterification of TA (Pang et al., 2006). Next to a higher shipping and storage stability, the primary objective of using the ester is to eliminate problematic humins. In contrast to FDCA, FDME can be more easily purified by distillation or sublimation resulting in better color properties of the final polymer (Metkar and Sengupta, 2017, Metkar et al., 2017). The downside is the need to manage methanol, a hazardous substance. The actual oxidation step from HMF to FDCA is carried out in a similar way to the Avantium process with the classical homogeneous metal catalyst (Co/Mn/Br) and molecular oxygen (Metkar et al., 2017). Offering an alternative to PEF, the two American companies specify polytrimethylene furandicarboxylate (PTF) as their target polymer utilizing bio-based 1,3-propanediol as a second monomer (Liauw et al., 2018).

In conclusion, chemical methods have brought FDCA and thus concomitantly PEF on the verge of industrial market launch (Rosenboom et al., 2022) and production conditions are already comparatively optimized and mild. However, they still leave room for improvement which could potentially be filled by whole-cell biocatalysis. The biological alternative does not require elevated temperatures, increased pressure, or noxious and costly metal catalysts.

1.3.3.2. Microbial catalysis as a sustainable alternative

Directly following the comprehensive elucidation of the genetic background behind microbial degradation of furanic compounds, notably HMF, described below (Koopman et al., 2010b) (1.3.4.), efforts were made to leverage this knowledge for synthetic application and thereby selectively produce the pathway intermediate FDCA under very mild conditions. For this, naturally robust bacteria of the *Pseudomonas* clade which have the ability to oxidize aromatic aldehydes like HMF, were selected as host organisms (Bitzenhofer et al., 2021, Hsu et al., 2020, Xu et al., 2020b). A first proof-of-concept study with *P. putida* S12, functionally expressing the oxidoreductase *hmfH*, delivered highly pure FDCA (99.4%) after acid precipitation and THF-extraction (Fig. 1.3-3B) (Koopman et al., 2010a, Ruijssenaars et al., 2011). This initial research attracted industrial interest and the strain was successively refined by introduction of a transporter and an additional aldehyde dehydrogenase (ALDH) with unidentified specificity. The optimized bacterium enables biocatalytic FDCA production in a fed-batch operation, without any accumulation of intermediates (Wierckx et al., 2012). Further investigations concentrated on alternative enzymes to HmfH, specifically dehydrogenases. This approach aimed at avoiding the formation of toxic H_2O_2, allowing conservation of the released energy from the oxidation step, and reducing the demand for molecular oxygen (Ruijssenaars, 2016). Even though functioning dehydrogenases have been found, this strategy

likely marks a dead end due to a central drawback: The oxidation of alcohols to aldehydes is an equilibrium reaction, capable of proceeding in either direction influenced by the concentrations of the redox cofactors involved (Table 1.3-1). Consequently, considerable amounts of 5-(hydroxymethyl)furfuryl alcohol (HMFOH) were observed because the employed dehydrogenase cannot only oxidize 5-(hydroxymethyl)-2-furoic acid (HMFA) to 5-formyl-2-furoic acid (FFA), but also reduce HMF to HMFOH likely resulting from the structural similarity between all molecules. In contrast, true oxidases, such as HmfH, circumvent this issue by using molecular oxygen as electron acceptor rendering the reaction irreversible (1.3.4.2.) (Jablonska and Tawfik, 2022). The latest reports on *Pseudomonas* as a host for whole-cell biocatalytic FDCA production originate from Taiwan. These do not introduce novel enzymes, but use CRISPR-based methods as a modern gene-editing technique. Furthermore, process parameters are adjusted, with a particular noteworthy supplementation of MnO_2 and $CaCO_3$ (Pham et al., 2020, Hu and Pham, 2021).

Despite several undeniable benefits of *Pseudomonas* cell factories (1.4.), additional organisms are equally harnessed for oxidation of HMF to FDCA. Amongst others, there are studies on *Escherichia coli* alone (Wang et al., 2020b), or in combination with *P. putida* KT2440 (Tan et al., 2020), *Raoultella ornithinolytica* BF60 (Hossain et al., 2017, Yuan et al., 2018a, Yuan et al., 2018b, Yuan et al., 2018c), *Burkholderia cepacia* H-2 (Yang and Huang, 2016), *Acinetobacter calcoaceticus* NL14 (Sheng et al., 2020), and *Klebsiella oxytoca* NCIM2694 (Parate et al., 2022). Certain eukaryotes, like the fungus *Penicillium brasilianum*, also possess the ability to natively convert HMF to FDCA. Upon heterologous expression, the genes required for this also enable commonly utilized biotechnological yeasts *Saccharomyces cerevisiae* or *Yarrowia lipolytica* to carry out the same process. Fungi can often be cultivated at lower pH facilitating downstream processing, specifically acid precipitation of FDCA, and makes the system less susceptible to contaminations. However, the product concentrations achieved so far are limited to the low millimolar range and the conversion is relatively slow (de Bont et al., 2017, de Bont et al., 2018). Another publication on fungi for FDCA synthesis directs attention to *Aspergillus flavus* APLS-1 (Rajesh et al., 2019).

Despite the described initiatives, the implementation of whole-cell biocatalysis for larger-scale FDCA production remains unattained at the moment, possibly not least due to a limited understanding of the specific biological aldehyde oxidation process and tolerance issues. Additionally, with regard to the entire value chain starting from biomass, solutions must be found as to how the comparatively harsh dehydration reaction in HMF synthesis, which appears to be possible only by chemical means, can be efficiently combined with a subsequent biocatalytic step. Whole-cell biocatalysis offers the advantage that complete conversion of the

sugar into HMF is not required, as any remaining substrate can serve as a carbon source for the employed organism. Thus, the dehydration process could be carried out under milder conditions and stopped earlier likely lowering formation of humins.

1.3.4. Microbial degradation of furanic aldehydes and their derivatives

Metabolization of HMF, furfural, and related compounds as sole carbon and energy sources is of interest for various reasons: In the first place, specialized or engineered organisms capable to grow on furanic compounds while not consuming sugars constitute a promising approach for biological detoxification of lignocellulosic hydrolysates (Koopman et al., 2011, Wierckx et al., 2011). The efficient fermentative utilization of the Earth's most abundant renewable feedstock is often hampered in particular by the toxic aldehydes HMF and furfural requiring their selective removal (Ujor and Okonkwo, 2022). Furthermore, the degradation pathway is a treasure trove for tailored proteins that have been shaped by long-term evolution, not least those whose importance is not immediately evident, such as transporters crucial for biotechnological applications like FDCA synthesis (Wierckx et al., 2015), or still completely uncharacterized enzymes. Related to that, furanic compounds-assimilating organisms can also play a beneficial role as screening platform for new or improved enzymatic activities. Specifically, there might be the endeavor to increase the activity of a protein with advantageous characteristics for a possible application, like enhanced stability, usage of simpler cofactors or a different cellular localization, but low catalytic performance. If the respective reactivity is vital for the degradation pathway and so far provided by another enzyme the corresponding gene could be replaced by the new variant and microbial growth be used as easy readout for enzyme activity. The resulting strain would be impaired first, but can subsequently be improved by growth-coupled adaptive laboratory evolution (ALE) potentially leading to activity-increasing mutations in the previously introduced target gene (Nielsen et al., 2023). This strategy can even be expanded to entire synthetic modules bypassing a naturally established metabolic route, disrupted beforehand, through an alternative pathway of interest to be engineered (Orsi et al., 2021). Lastly, furanic compound degradation, now with a focus on FDCA, represents an integral part of a circular bioeconomy, in a scenario where the dicarboxylic acid is used together with EG as bio-based polymer building blocks for PEF synthesis. To cope with plastic crisis, sustainable end-of life solutions for all produced materials, such as depolimerization (Weinberger et al., 2017) followed by assimilation of the monomers, are essential. In this way, the carbon is redirected into biomass or even employed for the biocatalytic synthesis of valued-added compounds (Ellis et al., 2021).

1.3.4.1. Genetic basis of the metabolic pathway

The earliest studies on microbial degradation of furanic compounds date back to the 1960s, when the first enrichment cultures on 2-furoic acid (FA) as a carbon and energy source were performed (Kakinuma and Yamatodani, 1964, Trudgill, 1969). However, significant progress in the field, notably the comprehensive elucidation of a gene cluster only occurred with the discovery of the HMF-degrading bacterium *Cupriavidus basilensis* HMF14 by Wierckx *et al.* about a decade ago (Wierckx et al., 2010, Koopman et al., 2010b). By screening a library of transposon mutant for clones which lost their capability to metabolize HMF and/or furfural and successive sequence analyses, eight genes (*hmfABCDEFGH*) encoding catalytically active proteins organized into two operons (*hmfABCDE* and *hmfFGH*), whose expression is controlled by LysR-type transcriptional regulators in reverse orientation (*hmfR1* and *hmfR2*), were initially identified (Koopman et al., 2010b). Upon further analysis, a gene encoding a major facilitator superfamily (mfs)-type transporter (Drew et al., 2021) was uncovered for each operon (*hmfT1* and *hmfT2*), along with an uncharacterized gene adjacent to *hmfH*, putatively corresponding to a hydroxylase (Wierckx et al., 2011). An overview of the complete bipartite *hmf*-cluster is shown in Fig. 1.3-4A. Simultaneously with the discovery in *C. basilensis* HMF14, the cluster or parts of it were likewise found in other bacteria. These included mostly closely related β-proteobacteria such as other *Cupriavidus* or *Paraburkholderia* species, but also α-proteobacteria and even gram-negatives (Koopman et al., 2010b, Wierckx et al., 2011). In recent years, tremendous advances in DNA-sequencing technologies triggered an explosion in the number of available microbial genomes (Loman and Pallen, 2015, Land et al., 2015), consequently also expanding the pool of potential furanic compound degraders. Thus, as one of the foundations of this work, a new BLASTp analysis using HmfA as query sequence was executed. The resulting strain collection (1.3-4A) does not claim to be complete, but rather focusses on easily obtainable organisms and those belonging to the *Pseudomonas* clade. Depending on the bacterium, the clusters vary in size and complexity, and genes are arranged differently. However it is noticeable that *hmfABCDE* always form the conserved core of the cluster which highlights a pivotal role of the corresponding proteins in the associated metabolic pathway (1.3.4.2.) (Wierckx et al., 2011). Excitingly, the ability to assimilate furanic compounds appears to be spread around the globe, because the list of potential degraders includes strains from Central Europe, the USA, Canada, China, Brazil, but also the Caribbean and even Antarctica.

Genes with particularly high sequence identities to the original isolate *C. basilensis* HMF14 were found in *Cupriavidus necator* H850, a bacterium known for its ability to degrade polychlorinated biphenyls (Abbey et al., 2003). The overall structure of the cluster is similar as

well, but the two original operons from *C. basilensis* HMF14 fused into a large one, resulting in the loss of both a transporter and a regulator gene. Moreover, the strain harbors an additional gene between *hmfG* and *hmfH* encoding a putative extracytoplasmic solute binding receptor subunit of a tripartite tricarboxylate transporter (TTT) (Rosa et al., 2018). *Paraburkholderia phytofirmans* PsJN is a well-studied plant-growth promoting endophyte (Esmaeel et al., 2018), which has already been included in previous homology searches and possesses a cluster with a slightly altered gene arrangement (Koopman et al., 2010b, Wierckx et al., 2011). The *hmfFG* genes are located directly upstream of *hmfA*, while *hmfH*, which here directly follows *hmfE*, completely changes position. Apart from the regulator and transporter genes, this cluster was transplanted successfully into *P. putida* KT2440, which enabled the strain to grow on HMF and furfural (Guarnieri et al., 2017). *Paraburkholderia caribensis* MWAP64 (Achouak et al., 1999) and *Paraburkholderia sacchari* IBT101 (Oliveira et al., 2021) were isolated from sugar-rich environments and are known exopolysaccharide producers. It is therefore not unlikely that they encounter HMF or furfural in their natural habitat. Their *hmf*-cluster matches that of *Paraburkholderia phytofirmans* described above. Additionally, it contains the *hyd* gene of unknown function and a gene encoding an ALDH rendering the mentioned strains suitable candidates as DNA donor for cloning purposes within this work. Alternatively, an identical cluster is also present in numerous likewise plant-associated *Caballeronia* species recently delineated from the genera *Paraburkholderia* and *Burkholderia* (Peeters et al., 2016, Dobritsa and Samadpour, 2016).

With regard to this project concentrating on *P. taiwanensis* VLB120 and *P. putida* KT2440 as promising biotechnological workhorses, furanic compounds-degrading members of the *Pseudomonas* clade were of high interest. The central genes *hmfABCDE* occur even twice in *P. umsongensis* GO16, which gained attention as natural degrader of the classical polyester monomers TA and EG (Narancic et al., 2021, Tiso et al., 2021) and was experimentally proven to degrade HMF (Rhys Orimaco, University College Dublin, Ireland, personal communication). However, one version is likely not functional due to multiple stop codons in the genes *hmfABCD* resulting from frameshifts, and a truncated form of *hmfE*. Special features of the remaining cluster comprise the split-up of *hmfF* and *hmfG*, the presence of a gene encoding a sodium solute symporter (SSS) in addition to the mfs-type transporter and the absence of *hmfH*. In return, extra genes occur encoding an alcohol dehydrogenase (ADH) of the short-chain dehydrogenase/reductase (sdr) family (Kavanagh et al., 2008), an alpha-beta hydrolase (α/β hyd) (Holmquist, 2000), a molybdenum cofactor insertion protein (*xdhC*) (Leimkühler and Klipp, 1999) and a helix-turn-helix transcriptional regulator of the AraC-family (Gallegos et al., 1997). Substantially identical clusters, but with only one copy of *hmfABCDE*, were identified in *P. putida* ALS1267, *P. silesiensis* A3^T, and *P. proteolytica* CMS 64^T with the latter also featuring

the uncharacterized *hyd* gene. Like *P. umsongensis* GO16, *P. putida* ALS1267 is an experimentally confirmed HMF and furfural degrader (Lee et al., 2016). To the best of our knowledge, both bacteria are currently the only organisms that can grow on HMF without possessing a homologue of *hmfH*. The occurrence of this gene was previously considered a clear indicator of the ability to degrade HMF (Wierckx et al., 2011), which must now be called into question. Interestingly, the cluster allows only assimilation of furfural but not HMF when heterologously expressed in *P. putida* KT2440 (Crigler et al., 2020). Further Pseudomonads, such as *P. borbori* R-20821 and *P. benzenivorans* 1477 contain an even larger *hmf*-cluster due to the presence of various supplementary genes mostly associated with transport. These include an mfs-type transporter different from *hmfT1* and *hmfT2* which belongs to the BenE family (Pao et al., 1998) and is directly connected to a gene encoding an outer membrane porin (OMP) *oprD* (Huang and Hancock, 1993). Such a structural configuration can also be found in the *ben*-cluster encoding the benzoate degradation pathway (www.pseudomonas.com (Winsor et al., 2016)). In addition, genes for a tripartite ATP-independent periplasmic (TRAP) transporter (Rabus et al., 1999, Peter et al., 2022, Davies et al., 2023) and a molybdenum cofactor cytidylyltransferase (CyT) (Neumann et al., 2011) were located. In total, the cluster variant described here measures 22.4 kb, whereas the one in the *Paraburkholderia* and *Caballeronia* strains is about 15.5 kb in size. Finally, *Alcanivorax dieselolei* B-5 was integrated into the portfolio owing to its halophilic lifestyle in the sea and its rather unusual alkane-degrading properties (Liu and Shao, 2005, Wang and Shao, 2014). It harbors the largest cluster of all notably comprising genes encoding two further TRAP transporter systems with substrate binding proteins of the TAXI-family (Mulligan et al., 2011). Furthermore, genes for the catalytic subunit of an acetolactate synthase 2 (ALS) (Chipman et al., 1998), an FMN-dependent alpha-hydroxy acid dehydrogenase (ADADH) (Maeda-Yorita et al., 1995), an OMP, a hypothetical protein, and a dehydratase (DHT) were detected. In light of the complex and quite differing cluster and the fact that is questionable whether furanic compounds even occur in the sea, it would be surprising if this strain could actually degrade these chemicals.

1.3.4.2. The degradation pathway and its biochemistry

Intriguingly, despite lacking knowledge on the genetic background, P.W. Trudgill accurately proposed the core metabolism for furanic compound degradation already in 1969. Using cell extracts from an FA-assimilating bacterium supplemented with ATP, coenzyme A (CoA), and an electron acceptor, he demonstrated the conversion of the carbon source into α-ketoglutaric acid (α-KG). The regular entry of α-KG into the tricarboxylic acid (TCA) cycle was blocked by the addition of arsenite, inhibiting α-KG-dehydrogenase (Trudgill, 1969). According to the

Trudgill pathway, FA is first activated in an ATP-dependent reaction to the corresponding CoA ester, which is then hydroxylated to 5-hydroxy-2-furoyl-CoA. This molecule undergoes keto-enol tautomerism and the lactone isomer can be hydrolytically cleaved yielding the enol form of linear 2-oxo-glutaroyl-CoA. After a spontaneous isomerization to the keto form, hydrolysis of the CoA ester ultimately results in α-KG formation (Fig. 1.3-4B). Later it was established that the central hydroxylation step was molybdenum-dependent (Koenig and Andreesen, 1989) and Koopman *et al.* eventually identified the individual proteins responsible for each reaction step, combining their genetic discoveries with expression of different parts of the *hmf*-cluster in a heterologous host (Koopman et al., 2010b). Accordingly, the CoA-activation of FA is catalyzed by the 2-furoyl-CoA synthetase HmfD and the hydroxylation step by the three-subunit 2-furoyl-CoA dehydrogenase HmfABC. HmfE belongs to the crotonase superfamily (Holden et al., 2001) and was postulated to catalyze the final CoA ester hydrolysis. Due to its ability to stabilize intermediates containing a negatively charged oxygen anion through the "oxyanion" hole, the protein could additionally facilitate lactone hydrolysis, but this reaction step might also occur abiotically (Wierckx et al., 2011). Moreover, it was proven that decarboxylation of FDCA to FA catalyzed by HmfF constitutes the connection between C-6 and C-5 furanic compound metabolism (Koopman et al., 2010b). HmfF is UbiD-type enzyme requiring a recently characterized prenylated flavin mononucleotide (prFMN) cofactor for its activity, which is generated by the UbiX-type prenyltransferase HmfG (Marshall et al., 2017, Bloor et al., 2023). This unusual cofactor enables a pericyclic reaction chemistry and the underlying mechanism was proposed to be based on a 1,3-dipolar cycloaddition (Payne et al., 2015). As the reaction is reversible, it can also be used for carbon fixation and production of FDCA from FA as substrate, but efficiencies are still low (Payne et al., 2019, Lopez-Lorenzo et al., 2023).

Recapitulating, the metabolism of HMF and furfural takes place via the central carboxylic acid intermediates FDCA and FA, from which a complete pathway including the responsible enzymes could be depicted. However, the oxidation reactions leading from the aldehydes or even alcohols to these compounds are not fully understood so far and might even be specific for each organism and its enzymatic equipment. Not every displayed gene cluster features the same genes encoding putative oxidoreductases (Fig. 1.3-4A) suggesting that in addition also proteins which are not encoded in the *hmf*-cluster could play a role. In case of HMF or the corresponding alcohol HMFOH the situation is further complicated by the existence of two potential oxidation pathways. One route involves the initial oxidation of the alcohol moiety of HMF leading to the formation of 2,5-diformylfuran (DFF) as an intermediate, which is then further converted to FFA. Alternatively, the aldehyde function of HMF can undergo the first oxidation resulting in the production of HMFA, followed by subsequent alcohol oxidation to

yield FFA which can finally be oxidized to FDCA (Fig. 1.3-4B). With HmfH, at least one oxidoreductase is consistently present in *C. basilensis* HMF14 as well as in its close relatives, and accumulation of HMFA in a respective deletion mutant points at alcohol oxidation as primary function (Koopman et al., 2010b). This is underlined by the fact that *P. putida* S12 with no capacity to grow on furanic compounds was able to produce HMFA from HMF natively, but required heterologous expression of *hmfH* from *C. basilensis* HMF14 to synthesize FDCA (Koopman et al., 2010a, Koopman et al., 2010b). The enzyme belongs to the glucose-methanol-choline (GMC) oxidoreductase family (Dijkman et al., 2013) and represents a true oxidase, which means that the electrons released during oxidation are directly shuttled via the FAD cofactor to molecular oxygen yielding H_2O_2 as a byproduct. Under anoxic conditions, the enzyme exhibited no activity (Koopman et al., 2010b). Reactions using O_2 as electron acceptor are highly exergonic and thus irreversible, enabling a substantial flux even with limited amounts of enzyme (Jablonska and Tawfik, 2022). As their mechanism involves a direct hydride transfer from the substrate to the cofactor, most of the GMC-type oxidoreductase described in literature are restricted to alcohol oxidation (Dijkman et al., 2013). Yet, through their hydrate forms, aldehydes could also indirectly be accepted as substrates (Ferreira et al., 2010, Dijkman and Fraaije, 2014). In most cases, geminal diol formation is thermodynamically unfavored, because the stable carbonyl function is destroyed. However, when electron-withdrawing groups are present as for instance in the case of chloral, the equilibrium is shifted towards hydrate formation. The same applies to DFF and to a lesser extent also to FFA, whereas no geminal diol is formed in the case of HMF, as demonstrated by NMR studies (Carro et al., 2015) (Fig. 1.3-4B).

Some of the clusters shown in Fig. 1.3-4A contain additional genes encoding ALDHs and ADHs which could likewise be involved in the oxidative pathways of HMF and furfural. ALDHs constitute a well-studied class of enzymes and operate according to the following mechanism: First, the substrate is covalently linked to a cysteine residue of the protein. The resulting thiohemiacetal is then oxidized via hydride transfer to a redox cofactor, either NAD^+ or $NADP^+$. Final hydrolysis of the thioester intermediate ultimately leads to carboxylic acid formation (Shortall et al., 2021). This reaction is highly exergonic and the reverse reduction requires the expense of energy to work under biological conditions (1.3.1). In contrast, ADHs are enzymes that catalyze both the reaction of alcohols to the corresponding aldehydes or ketones, as well as the reverse reaction from aldehydes to alcohols (Miranda et al., 2022).

This work finally provides conclusive experimental evidence on the enzymes required for the oxidative cascade from HMF or HMFOH to FDCA in the biotechnological workhorses *P. taiwanensis* VLB120 and *P. putida* KT2440.

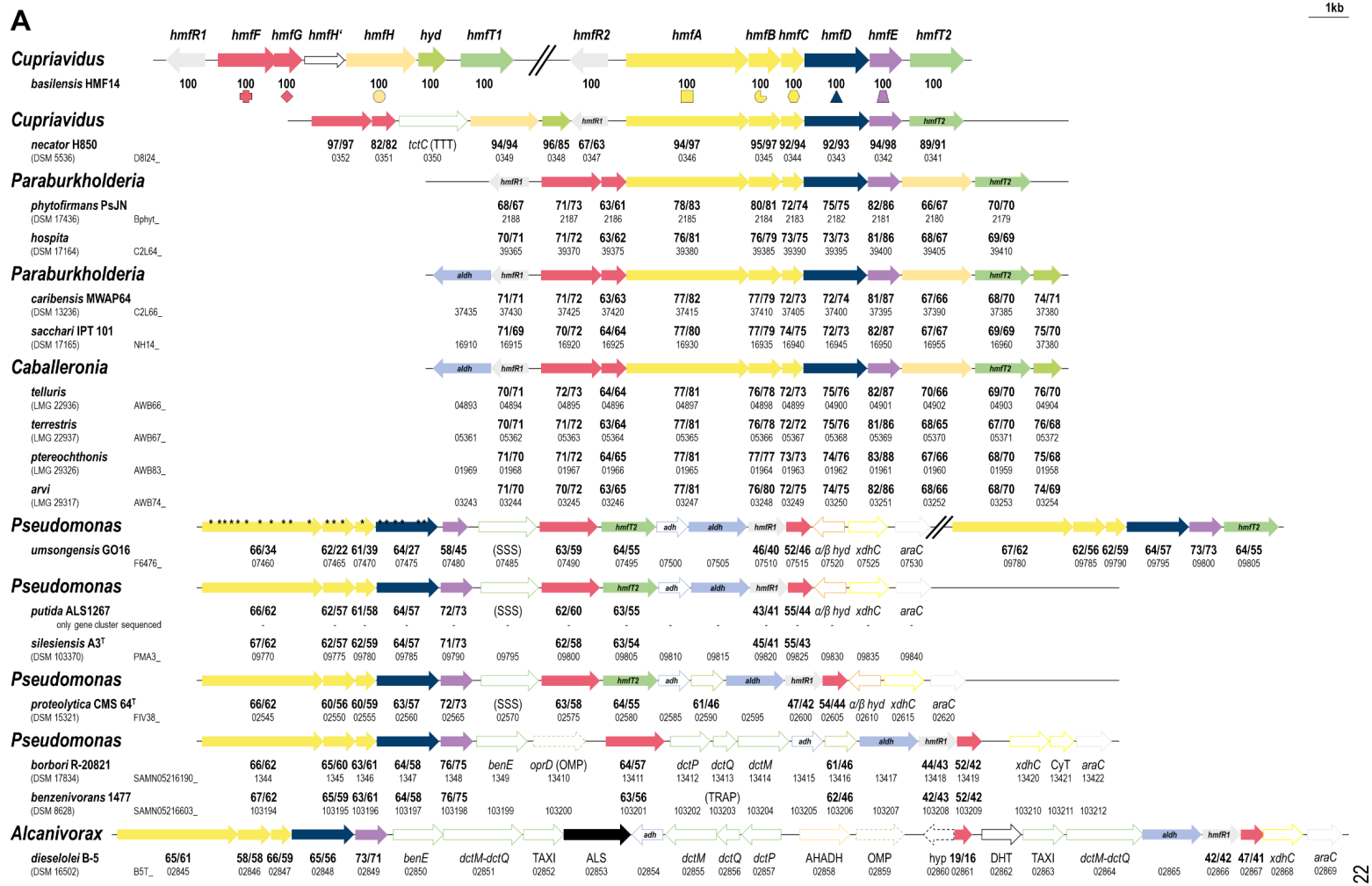
A
1kb
hmfR1 hmfF hmfG hmfH' hmfH hyd hmfT1 hmfR2 hmfA hmfB hmfC hmfD hmfE hmfT2
Cupriavidus basilensis HMF14
Cupriavidus necator H850 (DSM 5536) D8I24_
Paraburkholderia phytofirmans PsJN (DSM 17436) Bphyt_
Paraburkholderia hospita (DSM 17164) C2L64_
Paraburkholderia caribensis MWAP64 (DSM 13236) C2L66_
Paraburkholderia sacchari IPT 101 (DSM 17165) NH14_
Caballeronia telluris (LMG 22936) AWB66_
Caballeronia terrestris (LMG 22937) AWB67_
Caballeronia ptereochthonis (LMG 29326) AWB83_
Caballeronia arvi (LMG 29317) AWB74_
Pseudomonas umsongensis GO16 F6476_
Pseudomonas putida ALS1267 only gene cluster sequenced
Pseudomonas silesiensis A3T (DSM 103370) PMA3_
Pseudomonas proteolytica CMS 64T (DSM 15321) FIV38_
Pseudomonas borbori R-20821 (DSM 17834) SAMN05216190_
Pseudomonas benzenivorans 1477 (DSM 8628) SAMN05216603_
Alcanivorax dieselolei B-5 (DSM 16502) B5T_
hmfR1 hmfT2 adh aldh
(SSS) (TRAP) (OMP) benE oprD dctP dctQ dctM AHADH OMP hyp DHT TAXI ALS dctM-dctQ xdhC CyT araC α/β hyd

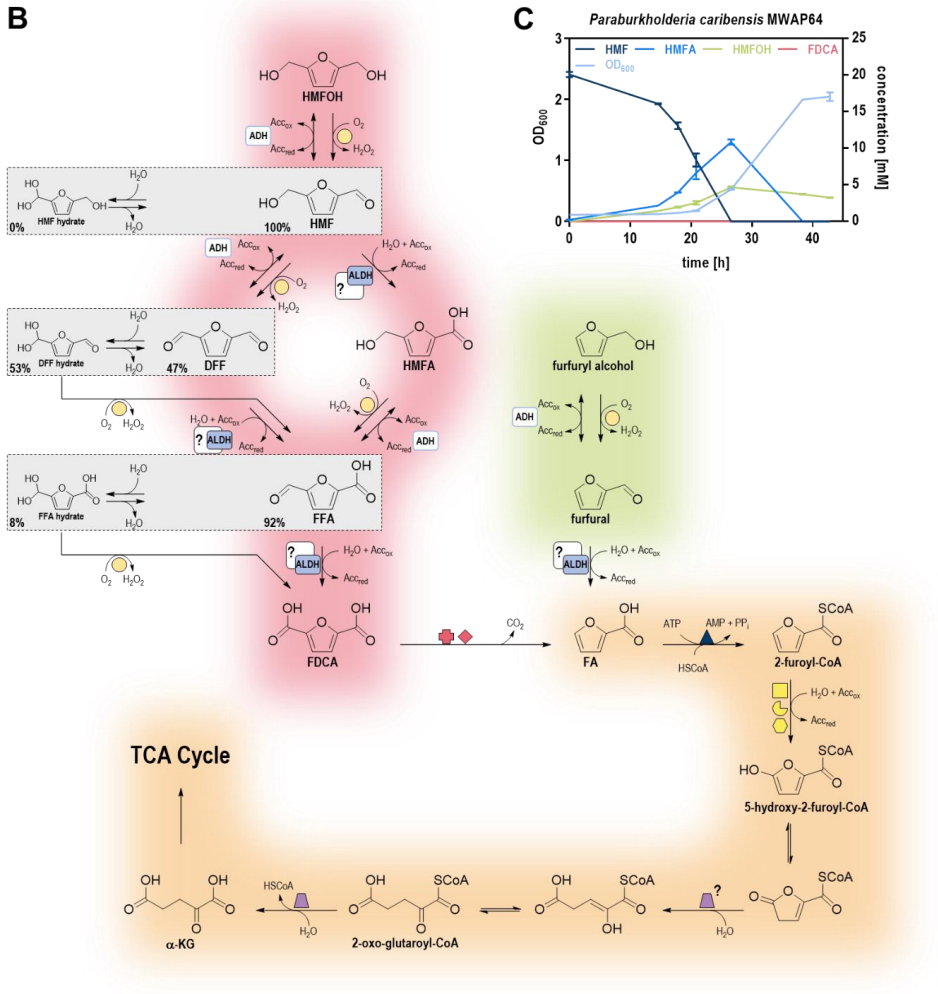

Figure 1.3-4: Genetics and biochemistry of furanic compounds degradation. (**A**) True-to-scale schematic representation of the two-part *hmf*-cluster of *C. basilensis* HMF14 and similar clusters of further bacteria. Colors and respective symbols relate the genes to the enzyme activities of their corresponding proteins shown in panel **B**. Bold numbers (**x**/**y**) below arrows denote the percentage identity on DNA (**x**) or protein (**y**) level with regard to *C. basilensis* HMF14 as a reference. Sequence identities were determined with the Emboss Needle pairwise sequence alignment tool (Madeira et al., 2022). If a cluster harbors genes not present in *C. basilensis* HMF14, the predicted protein family based on homology modelling is indicated. (**B**) Metabolic pathway for aerobic degradation of HMF, furfural and related compounds adapted from Koopman *et al.* (Koopman et al., 2010b). The central Trudgill pathway transforming FA into α-KG is highlighted in orange. Red (HMF) and green (furfural) colors mark the initial oxidation steps. In case of HMF, either the pathway via HMFA or the route via DFF is theoretically possible. Grey boxes depict hydrate formation of selected furanic aldehydes. The percentages describe the product distribution at equilibrium as determined by NMR (Carro et al., 2015). (**C**) Growth curve and substrate conversion of *Paraburkholderia caribensis* MWAP64 cultivated in MSM supplemented with 20 mM HMF as sole carbon and energy source. The mean and standard deviation of duplicates is shown. **Abbreviations:** ADH: alcohol dehydrogenase, AHADH: alpha-hydroxy acid dehydrogenase, ALDH: aldehyde dehydrogenase, CyT: cytidylyltransferase, DHT: dehydratase, OMP: outer membrane porin, SSS: sodium/solute symporter, TAXI: TRAP-associated extracytoplasmic immunogenic, TRAP: tripartite ATP-independent periplasmic, TTT: tripartite tricarboxylate transporter, α/β hyd: alpha/beta hydrolase.

1.4. *Pseudomonas* – A multi-talented and robust cell factory

The economically viable exploitation of whole-cell biocatalysis for chemical synthesis requires tolerant host organisms that can cope with stress caused by high concentrations of potentially toxic products, substrates, or further additives (Thorwall et al., 2020, Calero and Nikel, 2019). Hence, the focus is directed towards microbes featuring a diverse array of innate defense mechanisms, such as members of the *Pseudomonas* clade, which are, as soil-dwelling bacteria, naturally exposed to a multitude of environmental stresses (Bitzenhofer et al., 2021). Their reputation as extremely robust microbial cell factories is primarily rooted in their high solvent tolerance (Inoue and Horikoshi, 1989, Inoue and Horikoshi, 1991). In light of the precautions one has to take in a laboratory when handling organic solvents, which accumulate in and damage cell membranes, it is astonishing that numerous *Pseudomonas* sp. can live in presence of a second phase of these hazardous chemicals. The spectrum of tolerated solvents is broad and ranges from aliphatic alcohols like *n*-octanol to aromatics, such as toluene (Isken and de Bont, 1998, Schwanemann et al., 2023, Wynands et al., 2019). The basis for this special ability lies in the extrusion of the toxicant from the cytoplasm and the inner membrane by efflux pumps, membrane rigidification through *cis*-to-*trans* isomerization of unsaturated fatty acids, and formation of outer membrane vesicles (Bitzenhofer et al., 2021, Ramos et al., 2002, Ramos et al., 2015). Solvent tolerance is a beneficial feature for microbial production of aromatics that are typically highly lipophilic (Schwanemann et al., 2020), and allows bacterial cultivations in organic-aqueous two-phase systems addressing challenges related to toxicity and solubility of substrates and products (Heipieper et al., 2007, Kusumawardhani et al., 2018). The addition of a solvent immiscible with water not only provides a separate repository for potentially harmful substrates, but also serves as a method of *in situ* product removal (ISPR) (Freeman et al., 1993, Dafoe and Daugulis, 2014, Grundtvig et al., 2018).

Nonetheless, it would be a short-sighted view to consider Pseudomonads only for applications related to solvent stress, as their talents extend to defense against further chemicals, in particular aldehydes. Given that aldehyde toxicity primarily stems from the reactivity of the terminal carbonyl group (1.3.1.1.), a straightforward solution to overcome this problem is either reduction to the corresponding alcohol or oxidation to the respective carboxylic acid, both of which are less noxious. In this respect, *Pseudomonas* bacteria have the advantage that they preferentially use the oxidative route (Bitzenhofer et al., 2021, Xu et al., 2020b, Hsu et al., 2020, Kozono et al., 2020). This is not only thermodynamically favored (Table 1.3-1), i.e. representing a source of metabolic energy, but in the specific example of FDCA synthesis also proceeds towards the desired product (1.3.3.2.). A handicap is the lowering of the medium's pH value associated with acid formation and might be the explanation why various

other organisms including the biotechnologically relevant *E. coli*, *C. glutamicum*, or *S. cerevisiae* reductively detoxify aldehydes (Kunjapur et al., 2014, Kim et al., 2022, Wang et al., 2018). *Pseudomonas*' suitability for redox applications is further emphasized by the presence of approximately 80 oxidoreductases of different protein families, including about 30 ALDHs, in the genome of *P. putida* KT2440 (dos Santos et al., 2004).

An important criterion when selecting a strain for biotechnological exploitation is its safe handling. Microbial cell factories, cultivated in large scale, must not be pathogenic. However, several members of the *Pseudomonas* clade are categorized under biosafety level S2 in Germany. This includes the well-known *P. aeruginosa*, but also *P. putida* S12 playing an important role for the first studies on microbial FDCA production (1.3.3.2.). Yet, there are plenty of environmental isolates with similar aldehyde-oxidizing properties that are unproblematic and applicable to biotechnology. *P. taiwanensis* VLB120 (Panke et al., 1998) and *P. putida* KT2440 (Bagdasarian et al., 1981), employed in this work, are both free of virulence factors and classified S1 in Germany (Belda et al., 2016, Kohler et al., 2013). The latter is additionally certified HV1 implying a safe use in laboratory environments (Kampers et al., 2019).

While *P. taiwanensis* VLB120 is still considered an unconventional prokaryotic host (Blombach et al., 2022), *P. putida* KT2440 can meanwhile be counted among the most prominent workhorses of synthetic biology (Weimer et al., 2020, Loeschcke and Thies, 2020, Nikel and de Lorenzo, 2018, Nikel et al., 2016a, Poblete-Castro et al., 2012). Alongside the tolerance properties, the flexible metabolism is commonly cited as the main asset. The Pseudomonads described here cannot only utilize a wide range of different substrates, they are also distinguished by high NAD(P)H regeneration rates (Nikel and de Lorenzo, 2018). Reducing equivalents are required to provide the energy for maintaining the often ATP-intensive tolerance mechanisms mentioned above, such as efflux pumps or chaperones (Bitzenhofer et al., 2021). Furthermore, they are indispensable to withstand oxidative stress (Chavarría et al., 2013). In the context of FDCA, this is relevant, for example, when H_2O_2 is formed as a by-product of oxidation reactions (1.3.3.2.).

Customization and fine-tuning of the preferred organisms for each individual application demand an easy-to-handle toolbox that allows for fast and reliable genetic manipulations. Exploiting the repair mechanism of the bacterium built on homologous recombination, DNA fragments can be both, readily deleted from or inserted into the genome of *Pseudomonas*. Moreover, introduction of foreign DNA is possible via transposon-based methods or countless existing plasmids (Nikel et al., 2014, Martin-Pascual et al., 2021). For calibrated gene expression, a validated promoter library is available (Zobel et al., 2015). Additionally, there is an active community engaged in the development of further techniques. Currently, the portfolio

is complemented by CRISPR/Cas technologies which may further simplify and accelerate genetic engineering in the future (Volke et al., 2022, Kozaeva et al., 2024).

For biotechnological applications, the microbial cell is in certain aspects unnecessarily complex and specific natural bacterial features are superfluous or even disadvantageous including the ability to swim or to form biofilms. In the case of *P. taiwanensis* VLB120, the knockout of the respective genes encoding these traits, along with the deletion of several prophages and the megaplasmid, resulted in genome-reduced chassis (GRC) strains with improved properties, such as increased growth rate and better biomass yield (Wynands et al., 2019). This implies more energy available for important stress response mechanisms, which makes these strains ideal starting points for tolerance engineering. However, the genes *ttgGHI*, encoding an important efflux pump, are located on the megaplasmid and thus absent in unadjusted GRC1 rendering this variant solvent sensitive. While for the polar aldehyde HMF this does not play a role under solvent-free conditions, the tolerance to more lipophilic compounds depends on efficient extrusion, which is why two additional strains are available having the efflux pump reintegrated genomically either without (GRC2) or with (GRC3) the respective regulator genes *ttgVW* (Wynands et al., 2019). Analogously, similar genome reductions were also performed with *P. putida* KT2440 (Martinez-Garcia et al., 2014, Lieder et al., 2015).

1.5. Aim, scope, and outline of this thesis

While almost indispensable in organic chemistry, aldehydes are underexploited in the biological context, in particular with regard to whole-cell microbial catalysis. This arises from their toxicity, which is a result of the high reactivity, rendering them hardly compatible with the intricately balanced and in many respects delicate cellular processes of life. Consequently, living systems strive to minimize the presence of aldehydes and expeditiously transform them into less harmful alcohol or carboxylic acid derivatives. The focus of this work lies on the thermodynamically favored oxidative detoxification pathway holding particular significance for synthetic application. Although Pseudomonads are frequently employed as biotechnological workhorses for the rapid oxidation of HMF to FDCA, the specific mechanisms behind this feature are thus far poorly understood. To further improve these naturally robust organisms with regard to aldehyde tolerance through targeted strain engineering, the fundamental task consists of closing this knowledge gap.

The challenge is addressed in chapter 2.1 via a combination of literature-based rational selection and systematic analysis of multiple deletion mutants, resulting in the identification of the crucial HMF-oxidizing enzymes in both *P. taiwanensis* VLB120 and *P. putida* KT2440. Oxidation is confirmed as the central tolerance mechanism of these bacteria with respect to

aldehydes, since its absence causes significant growth defects in the presence of the stressor. Additionally, elimination of the predominant oxidation facilitates the elucidation of the two most prominent ADHs responsible for HMF reduction, which function as secondary but less efficient defense strategy in *Pseudomonas*. The novel insights on the key enzymes pave the way for rational engineering. Overexpression of the respective genes yields oxidation-optimized BOX strains (Boosted OXidation) associated with increased tolerance. As a final showcase, it is demonstrated that the accelerated initial oxidation step from HMF to the corresponding acid HMFA positively influences the entire reaction sequence towards the industrially relevant product FDCA, when these new mutants are endowed with the heterologous genes *hmfH* and *hmfT* from the HMF-degrading bacterium *Paraburkholderia caribensis*.

The following chapter deals with the usage of toxic aldehydes as sole carbon and energy source for *P. taiwanensis* VLB120 and *P. putida* KT2440 highlighting two core aspects: First, the activity of the newly discovered enzymes is not solely restricted to HMF but includes further aromatic aldehydes, such as vanillin and 4-hydroxybenzaldehyde, whose metabolism is similarly impaired when these proteins are lacking. This broadens the scope of this thesis beyond the biocatalytic production of FDCA, and the elucidated conversion processes bring *Pseudomonas* into play for the biosynthesis of these and potentially other (aromatic) aldehydes, as well as derived products thereof. Second, both organisms can be engineered to grow on HMF and related furanic compounds as carbon sources through genomic integration of the *hmf*-cluster and subsequent laboratory evolution. Upon implementation of strong and constitutive promoters for the now revealed HMF-oxidizing enzymes, significantly higher substrate concentrations can be employed also in this scenario. The tolerance of these rationally designed strains exceeds that of the native degrader *Paraburkholderia caribensis* serving as a donor for the required gene cluster.

Chapter 2.3. provides a vivid example of the occasional need of first taking a step backward to make significant progress afterwards. It describes the improvement of the oxidation-deficient and thus tolerance-reduced strain GRC1 ROX (Reduced OXidation) by a robotics-assisted ALE, representing an unbiased method to explore further “true” aldehyde tolerance mechanisms distinct from fast conversion. The evolved strains are subjected to whole-genome sequencing and ensuing mutations are reverse-engineered to resolve the genotype-phenotype relationship. Inactivation of the regulator MexT and the unexpected shut-down of the associated efflux pump MexEF-oprN emerge as new targets for tolerance improvement. The new findings, when ultimately combined with HMF oxidation, display a synergy between two entirely different tolerance mechanisms marking a step forward in chassis engineering for HMF-converting biocatalytic processes.

The last part of the results section is dedicated to the *de novo* production of aromatic aldehydes from glucose exemplified by the biosynthesis of *t*-cinnamaldehyde with *P. taiwanensis* VLB120. To this end, an existing *t*-cinnamate producer is rendered oxidation-deficient and equipped with a carboxylic acid reductase (CAR).

Accordingly, by identifying the key aromatic aldehyde-converting enzymes, this thesis makes dual contributions to the prospective utilization of these chemicals in whole-cell biocatalysis with *Pseudomonas*. On the one hand, there is the principal application regarding the production of FDCA from the bio-based model aldehyde HMF, where efficient oxidation is desired and can now be strengthened and fine-tuned, as evidenced by the BOX strains. On the other hand, aromatic aldehydes, such as the flavoring agent *t*-cinnamaldehyde can be appealing complements to the product portfolio of *Pseudomonas* cell factories. In this setting, the detoxification mechanism must be switched-off. The concluding discussion has likewise been divided into two parts. Next to the advances in the biocatalytic production of FDCA and pointing out further opportunities for strain engineering, attention is directed towards the manifold possibilities enabled by the biosynthesis of aldehydes, especially in producing complex derivatives like α-hydroxy ketones as building blocks for fine chemicals. The versatile aldehyde chemistry opens up a vast chemical space of valuable substances, which henceforth get into reach using the engineered *Pseudomonas* strains from this thesis.

2. Publications and manuscripts

This chapter includes four manuscripts that have either been published or are pending publication in peer-reviewed journals. Contributions of the authors to the respective manuscripts were described using the “Contributor Roles Taxonomy” (CRediT) (Allen et al., 2019).

Term	**Definition**
Conceptualization	Ideas; formulation or evolution of overarching research goals and aims
Methodology	Development or design of methodology; creation of models
Software	Programming, software development; designing computer programs; implementation of the computer code and supporting algorithms; testing of existing code components
Validation	Verification, whether as a part of the activity or separate, of the overall replication/reproducibility of results/experiments and other research outputs
Formal analysis	Application of statistical, mathematical, computational, or other formal techniques to analyze or synthesize study data
Investigation	Conducting a research and investigation process, specifically performing the experiments, or data/evidence collection
Resources	Provision of study materials, reagents, materials, patients, laboratory samples, animals, instrumentation, computing resources, or other analysis tools
Data curation	Management activities to annotate (produce metadata), scrub data and maintain research data (including software code, where it is necessary for interpreting the data itself) for initial use and later re-use
Writing – original draft	Preparation, creation and/or presentation of the published work, specifically writing the initial draft (including substantive translation)

Writing – review and editing	Preparation, creation and/or presentation of the published work by those from the original research group, specifically critical review, commentary or revision – including pre- or post-publication stages
Visualization Supervision	Preparation, creation and/or presentation of the published work, specifically visualization/ data presentation Oversight and leadership responsibility for the research activity planning and execution, including mentorship external to the core team
Project administration	Management and coordination responsibility for the research activity planning and execution
Funding acquisition	Acquisition of the financial support for the project leading to this publication

2.1. Engineering 5-hydroxymethylfurfural (HMF) oxidation in *Pseudomonas* boosts tolerance and accelerates 2,5-furandicarboxylic acid (FDCA) production

Thorsten Lechtenberg, Benedikt Wynands, Nick Wierckx* (2024)

Institute of Bio- and Geosciences IBG-1: Biotechnology, Forschungszentrum Jülich, 52425 Jülich, Germany
* Corresponding author

Status: published
Metabolic Engineering, 81, 262-272. **10.1016/j.ymben.2023.12.010**
(The version shown here contains minor editorial adjustments.)

CrediT authorship contribution statement:

T. Lechtenberg: Investigation, Writing - Original Draft, Writing - Review and editing, Visualization, Validation.

B. Wynands: Writing - Review and editing, Conceptualization, Supervision.

N. Wierckx: Writing - Review and editing, Conceptualization, Supervision, Funding acquisition, Project administration.

Overall contribution: 80%

The presented experimental work was conducted and validated by TL who likewise performed visualization of all data. BW acted as direct scientific advisor assisting with planning and evaluation of experiments. The entire project was led and supervised by NW. TL wrote the original draft which was reviewed and edited by BW and NW. Funding for the project was acquired by NW.

2.1.1. Abstract

Due to its tolerance properties, *Pseudomonas* has gained particular interest as host for oxidative upgrading of the toxic aldehyde 5-hydroxymethylfurfural (HMF) into 2,5-furandicarboxylic acid (FDCA), a promising biobased alternative to terephthalate in polyesters. However, until now, the native enzymes responsible for aldehyde oxidation are unknown. Here, we report the identification of the primary HMF-converting enzymes of *P. taiwanensis* VLB120 and *P. putida* KT2440 by extended gene deletions. The key players in HMF oxidation are a molybdenum-dependent periplasmic oxidoreductase and a cytoplasmic dehydrogenase. Deletion of the corresponding genes almost completely abolished HMF oxidation, leading instead to aldehyde reduction. In this context, two HMF-reducing dehydrogenases were also revealed. These discoveries enabled enhancement of *Pseudomonas'* furanic aldehyde oxidation machinery by genomic overexpression of the respective genes. The resulting BOX strains (Boosted OXidation) represent superior hosts for biotechnological synthesis of FDCA from HMF. The increased oxidation rates provide greatly elevated HMF tolerance, thus tackling one of the major drawbacks of whole-cell catalysis with this aldehyde. Furthermore, the ROX (Reduced OXidation) and ROAR (Reduced Oxidation And Reduction) deletion mutants offer a solid foundation for future development of Pseudomonads as biotechnological chassis notably for scenarios where rapid HMF conversion is undesirable.

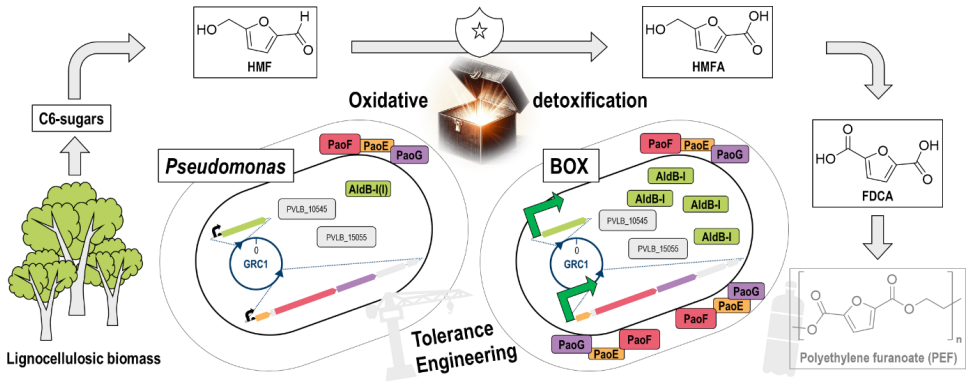

Keywords: 5-(Hydroxymethyl)furfural (HMF); 2,5-Furandicarboxylic acid (FDCA); *Pseudomonas*; Aldehyde stress; Periplasmic aldehyde oxidoreductase; Tolerance engineering

Highlights:

- Enzymatic toolbox for HMF redox detoxification in *Pseudomonas* revealed.
- Periplasm as first line of defense.
- Design of ROX, ROAR, and BOX strains with >400-fold HMF conversion rate difference.
- Tolerance-optimized BOX strains as superior biocatalysts for FDCA production.

2.1.2. Introduction

Non-pathogenic soil dwelling bacteria of the *Pseudomonas* clade, such as the aspiring biotechnological workhorses *P. putida* KT2440 and *P. taiwanensis* VLB120, show highly developed native tolerance traits towards various toxicants and are therefore promising starting points for the engineering of novel chassis strains with superior stress resistance (Bitzenhofer et al., 2021, Mukhopadhyay, 2015). This tolerance extends to aldehydes (Bitzenhofer et al., 2021) which, despite numerous possible applications enabled by their versatile reactivity, remain challenging for whole-cell biocatalytic processes (Zhou et al., 2020a). Aldehydes are potent electrophiles and easily undergo addition reactions with various biogenic nucleophiles like amino or thiol functionalities of proteins or nucleic acids, which can result in severe cell damage through misfolding and crosslinking (Lee and Park, 2017, LoPachin and Gavin, 2014). Consequently, living systems endeavor to avoid the presence of aldehydes and rapidly convert them to the less noxious alcohol or carboxylic acid derivatives (Wierckx et al., 2011). While many microbes, such as *Escherichia coli*, *Corynebacterium glutamicum* or *Saccharomyces cerevisiae* depend on energy-consuming alcohol formation, *P. putida* KT2440 preferentially uses oxidative aldehyde detoxification (Fig. 2.1-1A) (Kim et al., 2022, Kunjapur et al., 2014, Wang et al., 2018, Xu et al., 2020b). Their capability to rapidly oxidize aldehydes, along with their outstanding tolerance properties, renders Pseudomonads particularly attractive for whole-cell biocatalytic production of terephthalate-substituting plastic monomer FDCA from HMF (Troiano et al., 2020, Yuan et al., 2020). Together with ethylene glycol, FDCA can be used to synthesize the fully biobased and performance-advantaged polymer polyethylene furanoate (PEF) that features better barrier, thermal and mechanical qualities than conventional polyethylene terephthalate (PET) (Davidson et al., 2021, Loos et al., 2020).

Listed among the revised top chemical opportunities from biorefinery carbohydrates and often described as “Sleeping Giant” of sustainable chemistry, HMF, the dehydration product of hexoses, represents an industrially relevant model aldehyde that can be converted into a wide range of high-value products including FDCA (Bozell and Petersen, 2010, Galkin and Ananikov, 2019, van Putten et al., 2013b, Xu et al., 2020a). The oxidative cascade for the bioproduction of the dicarboxylic acid from HMF involves three sequential steps including two aldehyde and one alcohol oxidation resulting in the intermediates 5-hydroxymethyl-2-furoic acid (HMFA) and 5-formyl-2-furoic acid (FFA). The first whole-cell biocatalyst efficiently producing highly pure FDCA from HMF was described in 2010, using *P. putida* S12 expressing the alcohol oxidase *hmfH* from the HMF-degrading bacterium *Cupriavidus basilensis*

(Koopman et al., 2010a, Koopman et al., 2010b). This strain was subsequently improved by additional expression of an aldehyde dehydrogenase (ALDH) and the transporter *hmfT1* (Pham et al., 2020, Wierckx et al., 2015). Other examples comprising bacteria of the *Pseudomonas* clade for FDCA production employed either a different alcohol oxidase, a co-cultivation strategy, or a hybrid process combining whole-cell catalysis with purified enzymes (Hsu et al., 2020, Lin et al., 2020, Tan et al., 2020, Zou et al., 2020). Moreover, a few other species, such as *Raoultella ornithinolytica* BF60*,* were also applied to produce FDCA from HMF (Hossain et al., 2017, Sayed et al., 2022, Sheng et al., 2020, Yuan et al., 2018c).

Despite the extensive exploitation of *Pseudomonas*' native oxidative features, the enzyme(s) actually responsible for aldehyde detoxification remained unknown (Liu et al., 2020). The presence of many genes encoding ALDHs (32 for *P. putida* KT2440 and 25 for *P. taiwanensis* VLB120, Table S5.1-1) and numerous other putative aldehyde-converting oxidoreductases makes identifying these enzymes like a search for a needle in the haystack. Zheng *et al.* demonstrated that HMF oxidation of *P. putida* KT2440 was heavily affected by the deletion of the molybdate uptake system *modABC* (Zheng et al., 2020). This is in accordance with findings attributing a pivotal role to at least one molybdenum-dependent enzyme for the transformation of other aromatic aldehydes like vanillin, *p*-anisaldehyde, and piperonal (Adewunmi et al., 2020, Doi et al., 2016, Graf and Altenbuchner, 2014, Kozono et al., 2020). The PaoABC enzyme from *E. coli* is a well-described bacterial aldehyde-oxidizing enzyme depending on a molybdenum cofactor. It belongs to the xanthine oxidase family and is a periplasmic heterotrimer which consists of a large molybdenum-dependent subunit, a medium-size FAD-containing subunit and a small subunit harboring two iron-sulfur clusters (Correia et al., 2016, Neumann et al., 2009). *In vitro* experiments with purified enzyme proved a wide substrate spectrum of multiple mostly aromatic aldehydes including HMF and FFA (McKenna et al., 2017, Neumann et al., 2009). In an enzymatic cascade with a galactose oxidase variant, PaoABC was also successfully used to synthesize FDCA from HMF (McKenna et al., 2017).

In this work, we investigated the enzymatic furanic-aldehyde oxidation toolbox of *P. taiwanensis* VLB120 and *P. putida* KT2440. Consecutive gene deletions revealed a crucial role of a so far uncharacterized periplasmic molybdenum-dependent enzyme complex that is complemented by one or more cytoplasmic ALDHs. Strains deprived of their oxidation ability showed higher susceptibility to HMF and increased aldehyde reduction occurred as secondary tolerance mechanism, and we identified the main HMF-reducing enzymes. Overexpression of the newly discovered enzymes led to higher HMF tolerance through redox detoxification, while also enhancing FDCA production. Hence, this work uncovers the interplay between aldehyde

oxidation and tolerance, highlighting the periplasm as first line of defense in catalytic tolerance mechanisms.

2.1.3. Results and discussion

2.1.3.1. Identification of HMF-oxidizing enzymes in *P. taiwanensis* VLB120 and *P. putida* KT2440

The HMF-oxidizing properties of *P. taiwanensis* VLB120 and *P. putida* KT2440 were evaluated and shown to be very similar (Fig. 2.1-1B). Therefore, we expected both organisms to be equipped with a comparable set of aldehyde-converting enzymes and thus searched for candidates with homologs in both species. This excluded the PaoABC homolog of *P. putida* KT2440 since it is absent in *P. taiwanensis* VLB120. Additionally, the *P. putida* enzyme (PP_3308-10) lacks a TAT signal sequence unlike that of *E. coli*, which presumably prevents its export into the periplasm (Fig. S5.1-1). BLAST analysis revealed several related molybdenum-dependent enzymes as candidates for HMF oxidation in both species (Fig. S5.1-1). Since we had a genome-reduced chassis (GRC1) (Wynands et al., 2019) with improved process and tolerance features at hand and found only two promising operons in this strain, we decided to first elucidate HMF oxidation in *P. taiwanensis* VLB120. Initially, we verified the importance of one or more molybdenum-dependent enzyme(s) by deletion of the molybdate transporter system *modABC* in GRC1. Surprisingly, oxidation rates were only slightly affected under standard assay conditions, at first glance contradicting previous findings for *P. putida* KT2440 (Graf and Altenbuchner, 2014, Zheng et al., 2020). However, our minimal salts medium (MSM) contains 0.2 mg L^{-1} $Na_2MoO_4 \times 2H_2O$, which could be higher than the concentration in previously tested media such as the lysogeny broth (LB) used by Zheng *et al*. This may mask transport effects. Indeed, upon omission of this molybdenum source from the medium the initial oxidation rates of GRC1 Δ*modABC* were heavily impaired compared to the wild type, confirming the involvement of at least one molybdenum-dependent enzyme in HMF detoxification by *P. taiwanensis* VLB120 (Fig. 2.1-1C, Fig. S5.1-2).

The two operons encoding putative molybdenum-depending enzymes identified by BLAST analysis (Fig. S5.1-1) are designated by the locus tags PVLB_11305-PVLB_11325 and PVLB_10350-PVLB_10365. In both cases the molybdopterin-binding subunit harbors a putative TAT signal and shares a little more than 25% amino acid sequence similarity with PaoC (Fig. S5.1-1). In contrast to PaoABC, the third subunit is not FAD-binding, but a cytochrome according to *in silico* predictions (Winsor et al., 2016). The PVLB_11305-PVLB_11325 cluster additionally encodes a chaperone resembling PaoD and a MobA-like transferase that is probably involved in molybdopterin cofactor (Moco) biosynthesis. We

deleted the three catalytically relevant genes of this cluster and observed an 86% drop of initial HMF conversion rates similar to that of the transporter-deficient strain establishing an important function of this periplasmic molybdenum-dependent enzyme in HMF detoxification of *P. taiwanensis* VLB120 (Fig. 2.1-1). The newly discovered enzyme complex was named PaoEFG (Fig. 2.1-1A).

The *paoEFG* deletion reduced initial HMF oxidation considerably, but rates increased after 4 h and the mutant still completely converted the aldehyde in about 8 h. Consequently, at least one more enzyme is involved in the process and the delayed activity points to inducible expression (Fig. 2.1-1B). A participation of the second putative molybdenum-dependent oxidoreductase PVLB_10350-65 was excluded, since a double deletion mutant displayed the same oxidation rate as the single Δ*paoEFG* strain (Fig. 2.1-1C, Fig. S5.1-2). Therefore, we switched our focus to the plethora of predicted ALDHs (Table S5.1-1). Based on presence in both *P. taiwanensis* VLB120 and *P. putida* KT2440 and annotations related to aromatic aldehydes, *calB* (PVLB_01470, putative coniferyl aldehyde dehydrogenase), *peaE* (PVLB_12825, putative phenylacetaldehyde dehydrogenase) and *aldB-I* (PVLB_22390, putative aldehyde dehydrogenase B) were chosen for deletion. The initial HMF conversion rates were slightly reduced for GRC1 Δ*aldB-I* (Fig. 2.1-1C, Fig. S5.1-2). Thus, we generated the double deletion mutant GRC1 Δ*paoEFG* Δ*aldB-I*. This strain (hence called GRC1 ROX for Reduced OXidation) showed only marginal HMF oxidation activity producing less than 1 mM HMFA from 10 mM HMF in 24 h (Fig. 2.1-1B and C, Fig. S5.1-2). Accordingly, *P. taiwanensis* VLB120 has two main HMF oxidizing enzymes. In our set-up with externally added aldehyde, PaoEFG likely represents the primary defense system because its deletion had the most drastic effect. Theoretically, periplasmic oxidation of HMF would avoid its toxic effects inside the cell. In this proposition, AldB-I provides a second line of defense by detoxifying aldehyde molecules which pass this first barrier.

Both species analyzed in this study share high similarity, but also have a few conspicuous differences, such as the absence of the *ped*-cluster in *P. taiwanensis* VLB120, which among others contains several highly expressed alcohol and aldehyde dehydrogenases (*pedE*, *pedH*, *pedI*) (Li et al., 2020, Wehrmann et al., 2020, Winsor et al., 2016). We therefore investigated whether the results obtained for *P. taiwanensis* VLB120 could be transferred to the currently still more widely used *P. putida* KT2440. This strain harbors homologs to the newly identified PaoEFG (PP_3621-23) and AldB-I (PP_0545), both with amino acid sequence similarities greater than 90% (Fig. S5.1-1). As expected, deletion of the *paoEFG* operon led to a similar HMF oxidation deficiency as observed for GRC1 (Fig. 2.1-1B and D, Fig. S5.1-3).

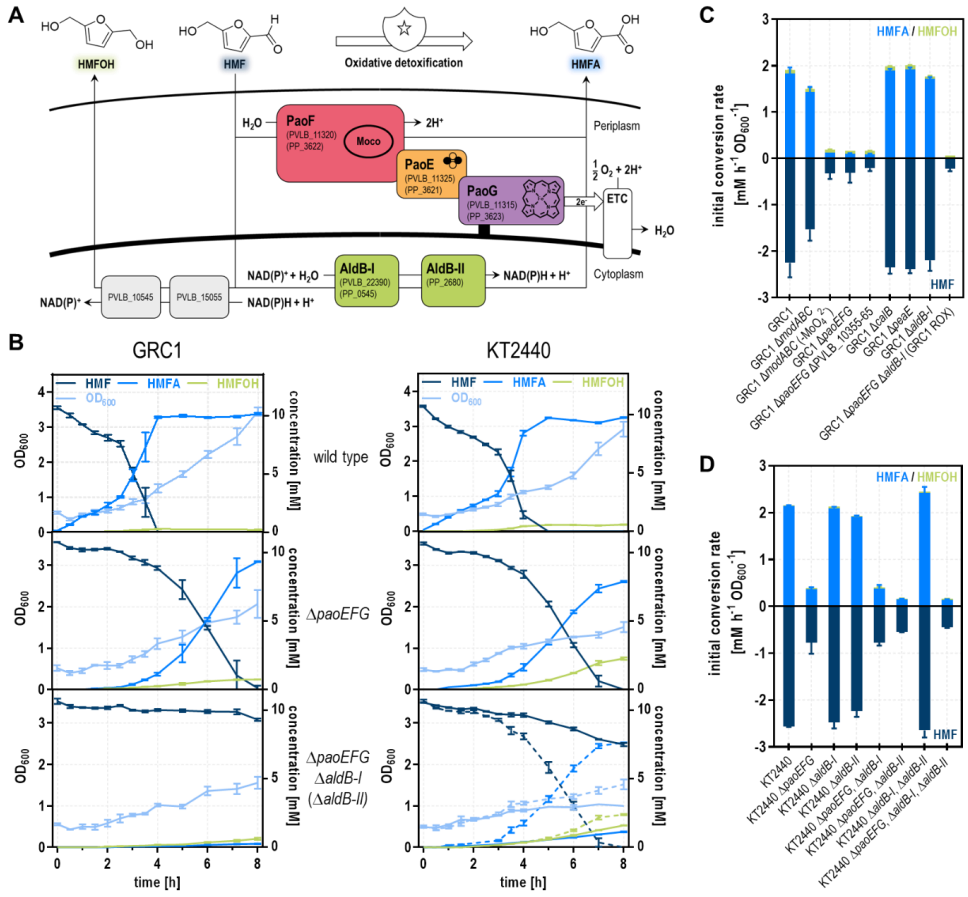

Figure 2.1-1: HMF conversion by the biotechnological workhorses *P. taiwanensis* VLB120 GRC1, *P. putida* KT2440 and deletion mutants thereof unveiling the enzymes involved in this process. (**A**) Reaction scheme depicting oxidative and reductive detoxification of HMF to HMFA and HMFOH. (**B**) HMF conversion in 24-deepwell microplates (two-fold buffered MSM with 40 mM glycerol, 2 mM glucose, and 10 mM HMF) using whole-cells of GRC1 and KT2440 compared to derived Δ*paoEFG* and Δ*aldB-I(I)* mutants. In the bottom graph of the KT2440 panel, dotted lines correspond to the double mutant KT2440 Δ*paoEFG* Δ*aldB-I* and solid lines to the triple mutant KT2440 Δ*paoEFG* Δ*aldB-I* Δ*aldB-II*. Error bars represent the mean ± standard deviation of three replicates. (**C**) Initial HMF depletion, as well as HMFA and HMFOH formation rates of GRC1 and selected mutant strains thereof in shake flasks. The data presented include the mean and standard error of at least two independent experiments each performed in duplicates. Full reaction courses are provided in the Supporting Information (Fig. S5.1-2). In case of a single dataset (GRC1 Δ*calB*, GRC1 Δ*peaE*, and GRC1 Δ*aldB-I*), the error bars correspond to the standard error of the slope of the linear regression. (**D**) Initial HMF depletion, as well as HMFA and HMFOH formation rates of KT2440 and selected mutant strains thereof in 24-deepwell microplates. The data presented include the mean and standard error of two independent experiments each performed in triplicates. Full reaction courses are provided in the Supporting Information (Fig. S5.1-3). Abbreviation: ETC, electron transport chain.

However, a higher residual activity remained upon additional deletion of AldB-I (PP_0545). This activity was further reduced by deletion of AldB-II (PP_2680, 87% identity to AldB-I from *P. taiwanensis*) also known as PedI (Table S5.1-1), although the residual HMF oxidation

activity was still slightly higher than that of GRC1 ROX (Fig. 2.1-1B and D, Fig. S5.1-3). In *P. putida* KT2440, AldB-II seems to be more important than AldB-I since, in the Δ*paoEFG* background, *aldB-I* deletion had little effect while *aldB-II* deletion yielded a lower activity (Fig. 2.1-1D, Fig. S5.1-3).

2.1.3.2. Identification of HMF-reducing enzymes in *P. taiwanensis* VLB120

Following the elucidation of the enzymatic toolbox for oxidative HMF detoxification, we aimed at discovering *Pseudomonas*' furanic aldehyde reduction machinery, which was focused on *P. taiwanensis* VLB120 GRC1 due to its potential process-oriented advantages (Wynands et al., 2019). In the ROX strain, about half of the HMF was reduced to 5-hydroxymethylfurfuryl alcohol (HMFOH) (Fig. S5.1-2) proving that *P. taiwanensis* VLB120 can use HMF reduction as alternative detoxification pathway. Diol formation is of biotechnological interest as well, because, like FDCA, HMFOH can serve as a symmetrical monomer for the production of plastics (Wu et al., 2023). Inspired by the *E. coli* RARE strain designed by the Prather lab (Kunjapur et al., 2014), we undertook to minimize HMF conversion. For this, we searched for homologs of the aldo-keto reductases (AKRs) (*dkgB*, *yeaE*, *dkgA*) and alcohol dehydrogenases (ADHs) (*yqhD*, *yahK*, *yjgB*) responsible for benzaldehyde reduction by *E. coli* (Kunjapur et al., 2014).

The three most similar AKRs and ADHs (PVLB_10970, PVLB_11635, PVLB_14845, PVLB_10545, PVLB_15055, PVLB_22390) were knocked out in GRC1 ROX (Table S5.1-2). Since HMF reduction was much slower than oxidation, cultivation time was prolonged to about 2 days, which allowed better detection of small differences in HMFOH formation. Remarkably, only removal of PVLB_10545 coding for an enzyme annotated as ethanol-active dehydrogenase/acetaldehyde-active reductase (AdhP) (www.pseudomonas.com (Winsor et al., 2016)) lowered HMFOH formation significantly by about 40% (Fig. 2.1-2). A second set of deletion mutants using GRC1 ROX Δ*adhP* (ΔPVLB_10545) as new background revealed that PVLB_15055 also contributed to a small but significant extent as the respective mutant produced about 13% less HMFOH compared to the Δ*adhP* reference (Fig. 2.1-2). Since its counterpart in *P. putida* KT2440 (PP_2426) has recently been proven responsible for vanillin reduction, we had assumed a more serious impact (Garcia-Hidalgo et al., 2020). The knockout of the other four tested genes did not significantly ($p > 0.01$) alter HMFOH production (Fig. 2.1-2). Nevertheless, we could identify AdhP and the ADH tagged PVLB_15055 as important members of GRC1's toolset for reductive HMF detoxification accounting for about half of the alcohol formation.

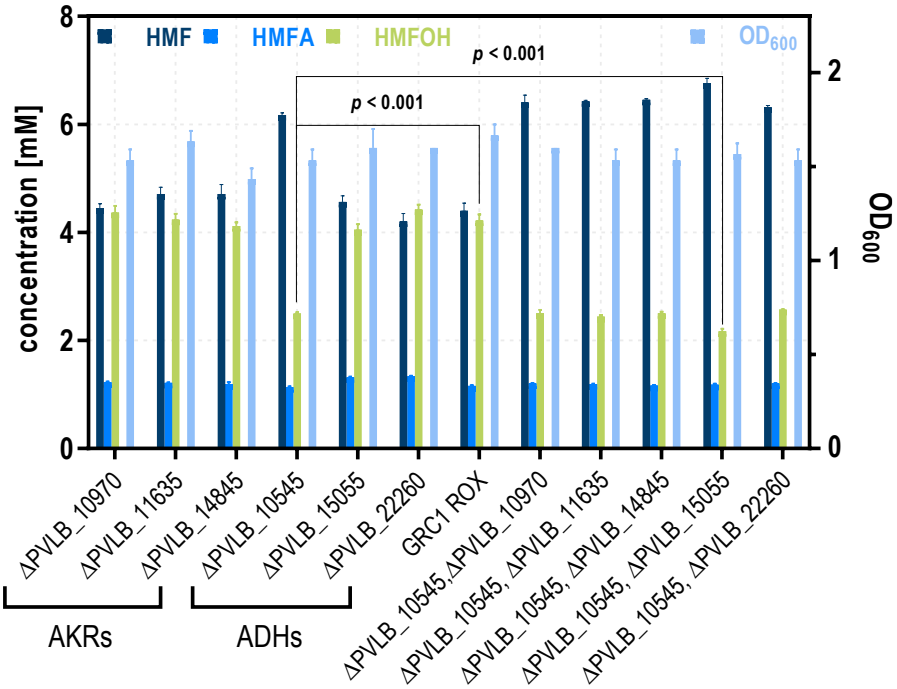

Figure 2.1-2: Tracing of HMF-reducing enzymes in *P. taiwanensis* VLB120 GRC1. Final furanics concentrations and OD_{600} of HMF conversion assays in shake flasks (four-fold buffered MSM with 40 mM glycerol, 2 mM glucose, and 10 mM HMF) using whole-cells of GRC1 ROX and derived deletion mutants lacking putative AKRs and ADHs. Samples were taken after 51 h. The mean and standard deviation of three replicates is shown. *P* values were calculated by two-tailed Student's *t*-tests.

In all, the redox-neutralized GRC1 Δ*paoEFG* Δ*aldB-I* Δ*adhP* ΔPVLB_15055 (GRC1 ROAR, Reduced Oxidation And Reduction, named according to a previously published *E. coli* variant with similar properties (Butler et al., 2023)) only metabolized HMF at an average rate of 47 ± 1 μM h^{-1} OD_{600}^{-1}, which is more than 40-fold slower than the GRC1 parent strain. Next to GRC1 ROX, it thus constitutes a promising novel chassis for redox-sensitive applications, for example future investigation of further HMF tolerance mechanisms which, in the wild type background, might be masked by predominant rapid oxidation. Moreover, if follow-up work can demonstrate, as observed for *Ec*PaoABC (Neumann et al., 2009), that the substrate spectrum of PaoEFG and the other identified enzymes includes additional aromatic aldehydes besides HMF, *Pseudomonas* strains with reduced oxidation and reduction properties can turn into alternative platforms for the microbial production of valuable aldehydes or aldehyde-derived compounds (Kunjapur and Prather, 2015, Zhou et al., 2020a).

2.1.3.3. PaoEFG and AldB-I are crucial for tolerance towards HMF

It is generally implied that oxidation and reduction of aldehydes are a major mechanism to abate their toxic effect, but this tolerance mechanism was until now not quantitatively investigated. We therefore assessed the importance of oxidative aldehyde detoxification for the viability of GRC1 in presence of HMF as a stressor.

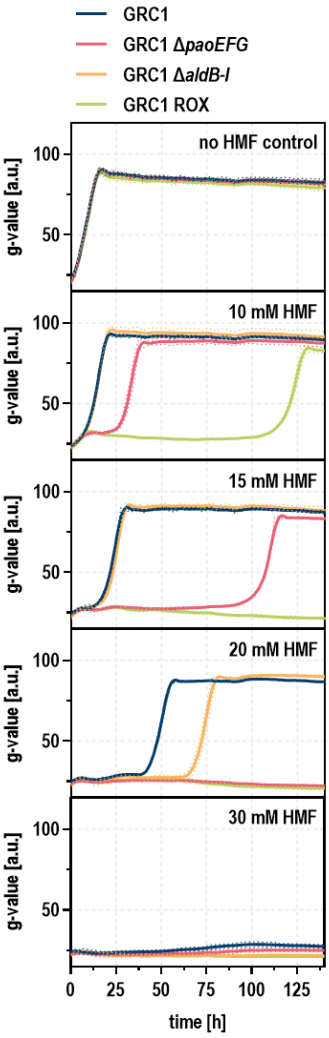

Figure 2.1-3: Importance of aldehyde oxidation for HMF tolerance. Four-fold buffered MSM supplemented with 40 mM glycerol and 2 mM glucose as carbon sources and increasing HMF concentrations was inoculated with the unmodified GRC1 (blue), the single deletion mutants GRC1 Δ*paoEFG* (red), GRC1 Δ*aldB-I* (yellow) and the double deletion mutant GRC1 ROX (green) to an OD_{600} of 0.1. Cells were cultivated in a Growth Profiler in 96-well microtiter plates. The growth curves result from a second-order smoothing to the mean values obtained from three replicates. The dots represent the standard deviation.

The oxidation-deficient strains were exposed to increasing concentrations of the toxic aldehyde and cell growth was monitored. The deletion mutants grew identically to the unmodified GRC1 in the absence of aldehyde stress, but showed notably prolonged lag phases when HMF was added (Fig. 2.1-3). Remarkably, the severity of the growth impairment followed exactly the oxidation capacity, indicating a cumulative effect of the two oxidoreductases on HMF tolerance.

In strains capable of detoxifying HMF in the periplasm, deletion of the cytoplasmic dehydrogenase *aldB-I* had only marginal influence on aldehyde conversion rates, and a retarded growth of the deletion mutant only became apparent at 20 mM HMF (Fig. 2.1-3). This indicates that PaoEFG can convert modest concentrations of the externally supplemented toxic aldehyde in the periplasm prior to its entry into the cell. Only at higher HMF concentrations is this first barrier breached, at which point the advantage of the cytoplasmic AldB-I manifests. In contrast, when GRC1 was deprived of its periplasmic detoxification mechanism, growth was already considerably impaired at 10 mM HMF and completely suppressed at concentrations above 15 mM (Fig. 2.1-3). The double deletion mutant GRC1 ROX performed even worse and growth in presence of 10 mM HMF only occurred after a lag phase of more than four days (Fig. 2.1-3). Under the tested conditions, these results corroborate the central role of PaoEFG for HMF tolerance, which heavily depends on fast aldehyde conversion. Furthermore, it can be concluded that cytoplasmic HMF oxidation by AldB-I can partially compensate lacking periplasmic detoxification, but it is not as efficient. This fits perfectly with the previously determined conversion rates and supports the theory that periplasmic oxidation is better than cytoplasmic oxidation for ameliorating HMF toxicity.

2.1.3.4. Tolerance engineering enables GRC1 to withstand higher HMF concentrations

Since disruption of the HMF-converting enzymes of *P. taiwanensis* VLB120 increased sensitivity towards the furanic aldehyde, we hypothesized that their overexpression would increase HMF tolerance. For this purpose, we employed the BacPP (de Avila et al., 2011) tool to identify the native promoter sequences of the *paoEFGHI* operon and *aldB-I* (Fig. S5.1-4). Expression of *paoEFGHI* and *aldB-I* was predicted to be controlled by stress-induced σ^{38}-promoters, which we substituted by the strong and constitutive P_{14f} promoter (Zobel et al., 2015). Commonly, this synthetic promoter is used together with a downstream BCD2 element encoding a short leader peptide which reduces gene-specific translation effects and increases expression levels (Mutalik et al., 2013), but introduction of this extended promoter sequence led to suppressor mutations indicating that the high expression of the *paoEFGHI* cluster was too stressful for the cells. Reasons for this could be the biochemically complex Moco synthesis,

an extensive demand for iron required for the cytochrome and the iron-sulfur clusters, or most likely membrane destabilization caused by intensive transport of folded proteins into the periplasm through the TAT system. This is supported by the fact that a similar promoter replacement with P_{14f} BCD2 for *aldB-I*, encoding the simpler cytoplasmic dehydrogenase, was successfully implemented (Fig. 2.1-4A). To attenuate the expression level, we generated alternative constructs omitting the translational coupler and keeping the native ribosome-binding sites (RBS) instead (Fig. 2.1-4A). In this case, correct clones were obtained as verified by Sanger sequencing. To further reduce metabolic burden, another strain was generated using the weaker P_{14c} promoter to control *paoEFGHI* expression. The resulting GRC1 BOX-C/P strains (Boosted OXidation in the cytoplasm (C) and/or periplasm (P)) were tested for their ability to oxidize HMF.

Strikingly, both the exchange to the moderately strong P_{14c} promoter and to the strong P_{14f} promoter upstream of the *paoEFGHI* cluster (BOX-P1 and BOX-P2) resulted in a more than five-fold increase in initial HMF conversion rates (Fig. 2.1-4B). This allowed the complete detoxification of 10 mM HMF to HMFA in less than 2 h when using a comparatively low starting OD_{600} of 0.5 (Fig. S5.1-5). In contrast to this, exchange of the *aldB-I* promoter affected aldehyde detoxification to a lesser extent. While BOX-C2 harboring the extended promoter sequence including BCD2 showed at least a doubling of the initial HMF oxidation rate, BOX-C1 possessing the native RBS only exhibited marginally improved oxidative properties (Fig. 2.1-4B). These findings are in accordance with the results obtained for the deletion mutants highlighting that periplasmic oxidation is clearly more efficient than the cytoplasmic reaction catalyzed by AldB-I. In this setting, with 10 mM externally supplemented HMF, oxidation rates were not further increased when *paoEFGHI* and *aldB-I* were simultaneously overexpressed. For BOX-C2P2 we even observed a slight deterioration which can presumably be attributed to an increased metabolic burden, since this strain also grew slightly slower without HMF (Fig. 2.1-4B and C). We hypothesized that with 10 mM HMF higher turnover rates were not possible due to substrate limitation, possibly caused by gradient-driven import into the cytoplasm.

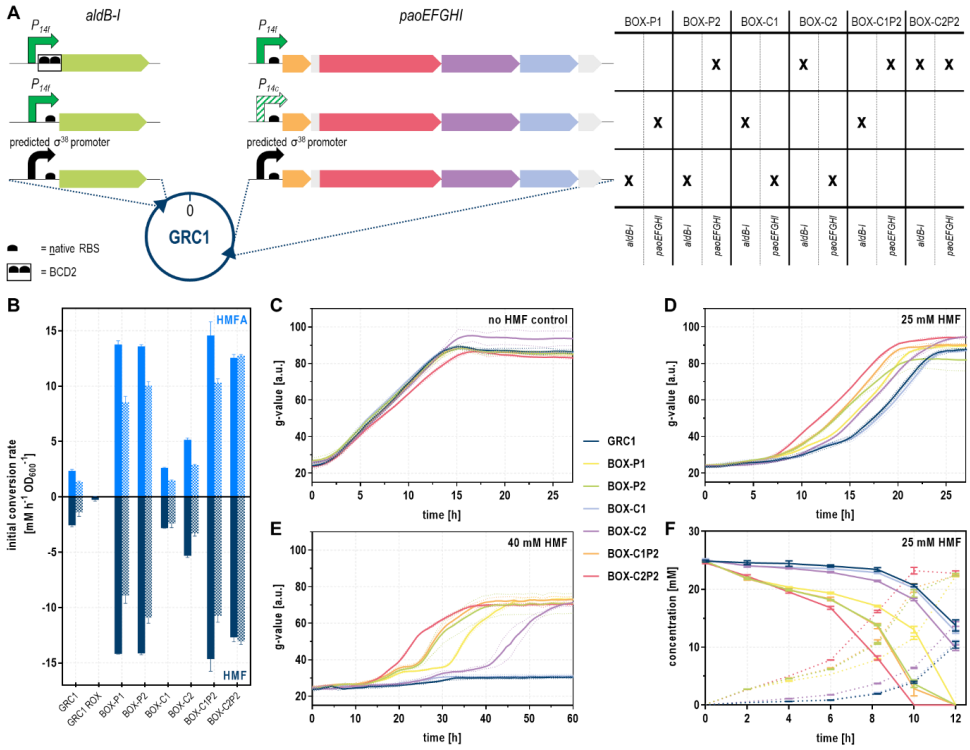

Figure 2.1-4: Chromosomal overexpression of *paoEFGHI* and *aldB-I* enhances the oxidation ability of *P. taiwanensis* VLB120 GRC1 and leads to improved HMF tolerance. (**A**) Genomic composition of the respective genes. Expression is modified by replacing the predicted native σ^{38} promoters with different strong and constitutively active ones. An overview of all combinations of promoter exchanges and their respective genotypes is given in the enclosed table. (**B**) Initial HMF depletion and HMFA formation rates of GRC1, GRC1 ROX as negative control, and the generated promoter exchange mutants. Filled bars show the mean and standard error of two independent experiments in 24-deepwell microplates (two-fold buffered MSM with 40 mM glycerol, 2 mM glucose, 10 mM HMF, starting OD_{600} = 0.5) each performed in triplicates. Full reaction courses are provided in the Supporting Information (Fig. S5.1-5). Shaded bars indicate the initial conversion rates of the growth experiment depicted in panel **D** and **F** (25 mM HMF, starting OD_{600} = 0.1) determined by linear regression limited to the first 6 h. The OD_{600} was assumed constant during this period and equaled the starting conditions. The error bars correspond to the standard error of the slope of the linear regression. Growth of the promoter exchange mutants (two-fold buffered MSM with 40 mM glycerol and 2 mM glucose) and the unmodified GRC1 without HMF (**C**) and with 25 mM (**D**) and 40 mM (**E**) HMF. Experiments were carried out in a Growth Profiler and growth curves result from a second-order smoothing to the mean values obtained from three replicates. The dots represent the standard deviation. (**F**) HMF (solid lines) and HMFA (dotted lines) concentrations observed during the growth experiments in presence of 25 mM HMF. The mean and standard deviation of three replicates is shown.

This was confirmed by cultures with 25 and 40 mM HMF, where BOX-C2P2 performed best (Fig. 2.1-4D and E). Under these conditions, when a lower cell density faced a higher HMF concentration, a differentiation occurred exactly as anticipated according to the relative importance of the two oxidoreductases and chosen promoter strengths. In contrast to oxidation rates determined with 10 mM HMF, weaker expression of *paoEFGHI* in BOX-P1 led to worse growth with 25 mM HMF compared to BOX-P2. However, the strain still performed slightly

better than BOX-C2 which solely relied on maximum expression of *aldB-I*. The hierarchy became even more pronounced when the HMF concentration was increased to 40 mM. In this case, GRC1 and BOX-C1 were no longer able to grow at all within the observation period, while all BOX strains headed by BOX-C2P2 withstood the high concentration of the toxicant (Fig. 2.1-4E). Analysis of HMF and HMFA concentrations during growth experiments in presence of 25 mM aldehyde confirmed rapid oxidation as primary tolerance mechanism (Fig. 2.1-4F). BOX-C2P2 equipped with the maximum amount of HMF-oxidizing enzymes showed fastest oxidation during the lag phase with ten-fold higher initial HMF conversion compared to the unmodified GRC1. The detoxification rates of the other strains also corresponded exactly to their growth performance (Fig. 2.1-4B, D, F).

In conclusion, the constitutive overexpression of *paoEFG* and *aldB-I* prepared the bacteria for growth under HMF stress, which is essential for competitive industrial bioprocesses involving this toxic aldehyde. Certainly, expression of the oxidoreductases will also be inherently induced upon exposure to the toxicant, which can be seen by increasing oxidation rates of the strains over time (Fig. 2.1-1B). Nevertheless, the primary effect of furanic aldehyde stress is a prolongation of the lag phase (Heer and Sauer, 2008), and the BOX strains are thus primed for HMF detoxification at the most critical time for tolerance, the initial stage of growth. Similarly, a previous study demonstrated that a constitutive solvent-tolerant strain (permanently expressing the efflux pump *ttgGHI*) exhibited superior growth properties than one with natural regulation when exposed to 4-ethylphenol as a stressor (Wynands et al., 2019). Additionally, handling becomes significantly simplified as the need for induction is eliminated. This is particularly advantageous in the case of HMF, where the inducer is continuously converted.

2.1.3.5. Optimized FDCA production

After identification of *paoEFG* and *aldB-I* as major genes for defense against HMF and optimization of their expression which resulted in markedly improved oxidation rates and tolerance, we hypothesized that the new BOX strains could also produce FDCA more efficiently. The oxidoreductase HmfH is needed to oxidize the hydroxy group of HMFA (Koopman et al., 2010a, Pham et al., 2020), while the HmfT transporter improves FDCA production likely by facilitating HMFA uptake (Pham et al., 2020, Wierckx et al., 2015). Starting from HMFA, the further reaction pathway then proceeds via FFA, another aldehyde, which was previously shown to be oxidized by *Pseudomonas* (Tan et al., 2020), ultimately yielding the dicarboxylic acid FDCA (Fig. 2.1-5A). Both heterologous genes required are part of the *hmf*-cluster enabling microbial growth on furanic aldehydes HMF and furfural (Koopman et al.,

2010b). In this study, *Paraburkholderia caribensis*, which can grow on both aldehydes as sole carbon and energy source (Fig. 1.3-4C), was chosen as donor strain for the mentioned genes (Achouak et al., 1999). Using a *tac*-promoter, which is constitutive in *Pseudomonas* lacking the *lacI* repressor, strong *hmfH* expression was achieved with plasmid pBT'T_*hmfH*. In contrast, excessive presence of transporter proteins negatively influences the cell's fitness due to membrane destabilization. Therefore, expression of *hmfT* was set under the control of the salicylate-inducible *nagR*/P_{nagAa} promoter on the lower-copy plasmid pJNN_*hmfT*. The resulting series of FDCA-producing strains is denoted as BOX-C/P-*hmfH-hmfT*. The heterologous expression of *hmfH* led to formation of FDCA in all tested strains and the beneficial role of the HmfT transporter was confirmed because induction of P_{nagAa} with 100 µM salicylate considerably improved production in all cases (Fig. 2.1-5, Fig. S5.1-6). The BOX-C2P2-*hmfH-hmfT* strain with maximized oxidation capacity significantly out-performed the GRC1 control, proving the benefit of enhanced aldehyde conversion on the overall oxidation process. In fact, both BOX-P2-*hmfH-hmfT* and BOX-C2P2-*hmfH-hmfT* achieved complete conversion of 10 mM HMF into 10 mM FDCA two hours faster than the unmodified control, constituting a 25% increased volumetric rate.

In relative terms, the initial HMF conversion rates remained comparable to those observed for the unmodified BOX-C/P strains, although absolute oxidation rates in these plasmid-harboring strains were reduced overall (Fig. 2.1-5B, Fig. S5.1-6). This can be attributed to the extra resources required for plasmid maintenance and selection. The strain based on BOX-P2 rapidly accumulated HMFA, whose further conversion by cytoplasmic HmfH seems to be limited by cellular uptake, as suggested by the flattening FDCA concentration curve (Fig. 2.1-5C). Expression of *hmfT* alleviated this limitation, making it likely that HMFA is the main substrate of the transporter. Yet, even upon full induction (100 µM salicylate), HMFA was still taken up slower than it was produced, indicating that HMF oxidation in the BOX strains was enhanced to such an extent that HMFA uptake became the rate-limiting reaction. This bottleneck was even more pronounced in a second set of BOX-C/P-*hmfH-hmfT*(g) strains with single copies of the *hmfT* and *hmfH* expression cassettes integrated into the genome, which showed even slower HMFA uptake (Fig. S5.1-7). The transport problem could be partly avoided by cytoplasmic HMF oxidation, because overexpression of *aldB-I* in BOX-C2-*hmfH-hmfT* led to transient accumulation of FFA. Increased AldB-I levels resulted in a higher proportion of HMFA formed in the cytoplasm, where it was directly available for further reaction of the co-localized HmfH. The secreted FFA was rapidly converted to FDCA only once HMF was completely consumed (Fig. 2.1-5). This indicates that PaoEFG has a higher affinity for HMF, which competitively inhibits FFA oxidation. BOX-C2P2-*hmfH-hmfT* with maximized HMF

oxidation capacity showed a mixed pattern characterized by the accumulation of both FFA and mostly HMFA so that a transport limitation occurred here as well (Fig. 2.1-5). Despite this newly emerged challenge, the overall results demonstrated that enhanced HMF oxidation not only increased aldehyde tolerance, but also accelerated FDCA production.

To test whether the HMFA transport limitation could be circumvented by a strain solely relying on boosted cytoplasmic HMF oxidation we deleted *paoEFG* in the BOX-C2 strain. Although periplasmic detoxification was proven crucial for HMF tolerance ensuring a lower intracellular stressor concentration, the colocalization of HMF and HMFA oxidation could alleviate the transport bottleneck. We conducted experiments with the genomically modified BOX-C2-*hmfH-hmfT*(g) Δ*paoEFG* as well as BOX-C2-*hmfH*(g) Δ*paoEFG* lacking the transporter gene (Fig. 2.1-5D and E). Surprisingly, FDCA production was almost completely abolished in both cases and FFA accumulated instead. Moreover, despite the absence of periplasmic detoxification, we still detected a large amount of about 5 mM HMFA in every culture broth, which was only further converted slowly in presence of HmfT (Fig. 2.1-5E). From this, the following conclusions might be drawn: 1) In BOX-*hmfH-hmfT* strains FFA is almost exclusively oxidized in the periplasm by PaoEFG. Either AldB-I has very low activity towards FFA, or FFA is exported and not taken back up into the cell. 2) The investigated strains are able to secrete HMFA from the cytoplasm, counteracting HmfT-mediated uptake. This probably explains the extracellular accumulation of the acid in previous FDCA production experiments. Incidentally, this also applies to FFA and FDCA as all concentration measurements could be performed without previous cell lysis. 3) In contrast to previous suggestions (Wierckx et al., 2015), HmfT does not contribute to HMF uptake because the initial rates of HMF decrease were virtually identical for BOX-C2-*hmfH-hmfT*(g) Δ*paoEFG* and BOX-C2-*hmfH*(g) Δ*paoEFG* lacking the transporter gene (Fig. 2.1-5D and E, Fig. S5.1-7). The very high metabolic rates and low hydrophobicity of HMF strongly suggest facilitated uptake, which has not been understood so far. This could explain why Guarnieri *et al.* had success in engineering *P. putida* KT2440 to grow on HMF and furfural by transplanting the *hmf*-cluster from *Paraburkholderia phytofirmans* without the transporter gene. Besides, they used a medium without molybdenum supplementation, which may have reduced periplasmic oxidation thereby preventing the HMFA uptake issue (Guarnieri et al., 2017).

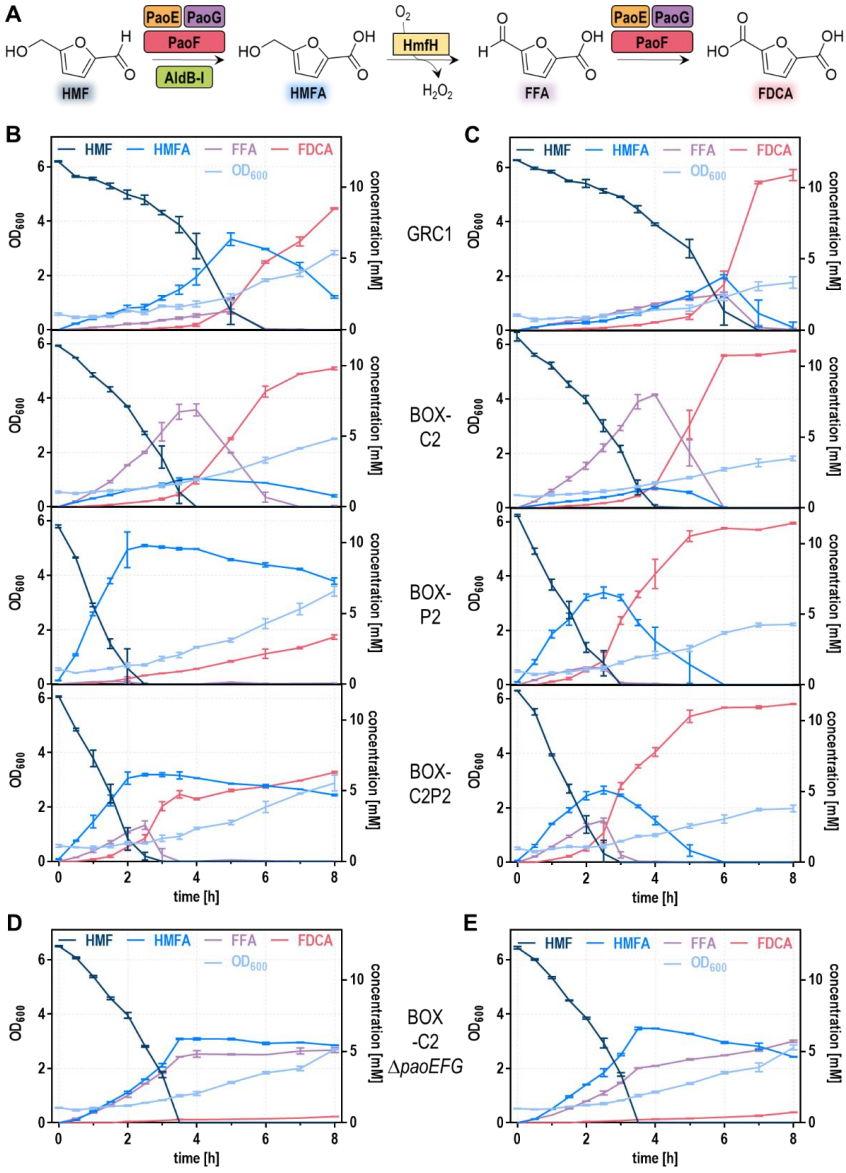

Figure 2.1-5: FDCA production experiments with selected oxidation-optimized BOX-C/P strains. After initial conversion of HMF to the respective carboxylic acid HMFA by PaoEFG and AldB-I, two further reaction steps, primary alcohol oxidation to FFA catalyzed by HmfH and a second aldehyde oxidation, are required for FDCA synthesis (**A**). Whole-cell HMF conversion assays in 24-deepwell microplates (two-fold buffered MSM with 40 mM glycerol, 2 mM glucose, and 10 mM HMF) using strains episomally expressing *hmfH* and *hmfT* from plasmids pBT'T_*hmfH* and pJNN_*hmfT* without transporter induction (**B**) and with induction of the transporter by addition of 100 µM salicylate (**C**). Additional experiments under the same conditions with supplementation of 100 µM salicylate were performed with BOX-C2-*hmfH*(g) Δ*paoEFG* (**D**) and BOX-C2-*hmfH*-*hmfT*(g) Δ*paoEFG* (**E**) underlining the importance of the periplasmic oxidoreductase PaoEFG for FFA oxidation. The mean and standard deviation of three replicates is shown.

The new findings prompted us to update the hitherto applied reaction scheme (Wierckx et al., 2015) for biocatalytic conversion of HMF to FDCA by *Pseudomonas* whole-cells (Fig. 2.1-6). In addition to the now established enzymes for the aldehyde oxidation steps and their respective cosubstrates, valuable insights into the cellular localization and respective transport routes could be gained. In the BOX strains engineered in this work, HMF oxidation rates are boosted to such an extent, that HMFA uptake becomes the rate-limiting step, even with strong episomal expression of the transporter gene. The uptake mechanism of the substrate HMF as well as the secretion of all furanic compounds from the cytoplasm remain cryptic, and should be the subject of further study.

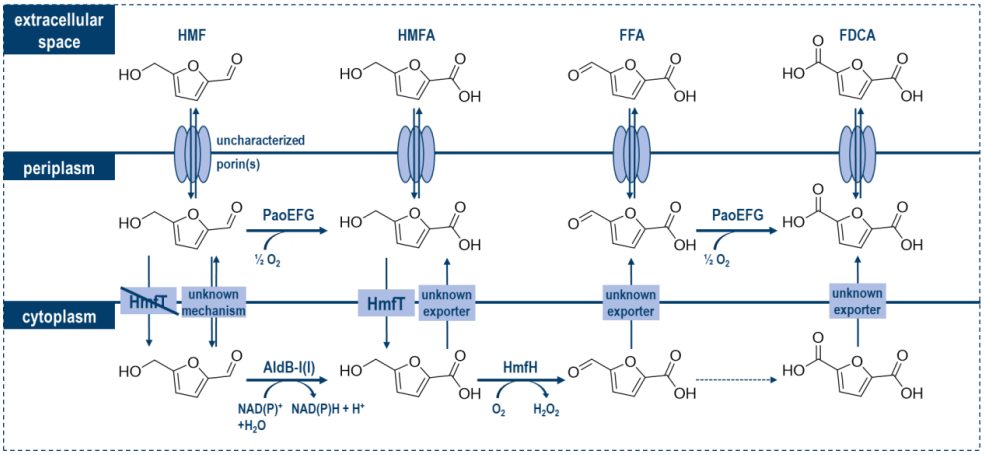

Figure 2.1-6: Updated reaction scheme covering the entire oxidative pathway from HMF to FDCA.

2.1.4. Conclusion and outlook

Aldehydes, such as the emerging renewable platform chemical HMF, are highly toxic for biological systems due to their reactivity. This study revealed the periplasmic PaoEFG and cytoplasmic AldB-I(I) enzymes involved in the oxidative detoxification of HMF by *P. taiwanensis* VLB120 and *P. putida* KT2440. Oxidation-enhanced BOX strains were generated by overexpression of the newly identified genes showing significantly improved tolerance, and HMF oxidation rates up to ten-fold higher than the progenitor GRC1. Thanks to their high oxidative capacity, these strains are perfectly suited for application in whole-cell HMF oxidation processes. The BOX strains also enabled faster FDCA production when equipped with the alcohol oxidase HmfH and the transporter HmfT. To further advance biotechnological FDCA synthesis from HMF, future efforts should focus on HMFA uptake, which emerged as new rate-limiting step in the BOX strains. Besides boosted oxidation, a strain with reduced

oxidation and reduction (ROAR) was also constructed which features more than 40-fold slower HMF conversion than GRC1, and even up to 400-fold slower than the best BOX strain. This ROAR strain can serve as valuable platform for a wide range of applications including targeted enzyme engineering for further optimization of HMF oxidation rates and exploration of additional tolerance mechanisms complementing fast aldehyde conversion. If the substrate spectrum of the newly identified enzymes extends beyond HMF, the ROAR strain is also an appropriate choice for microbial synthesis of valuable aromatic aldehydes and can serve as an alternative chassis to *E. coli* RARE/ROAR (Butler et al., 2023, Kunjapur et al., 2014), bringing all the advantages of *Pseudomonas* as platform host (Blombach et al., 2022, Nikel et al., 2016a, Nikel and de Lorenzo, 2018).

2.1.5. Materials and methods

2.1.5.1. Strains and culture conditions

For routine cultivation of bacterial strains premixed LB medium containing 10 g L^{-1} peptone, 5 g L^{-1} sodium chloride, and 5 g L^{-1} yeast extract or solid LB with additional 15 g L^{-1} agar (Carl Roth, Karlsruhe, Germany) was applied. All bacterial strains used in this study are listed in Table S1. *Paraburkholderia caribensis* DSM 13236 was acquired from DSMZ (Braunschweig, Germany). To select for *Pseudomonas* after mating procedures LB agar plates were supplemented with irgasan (25 mg L^{-1}). Growth and conversion experiments were conducted in MSM adapted from Hartmans *et al.* (Hartmans et al., 1989) notably containing $Na_2MoO_4 \times 2H_2O$ at a concentration of 0.2 mg L^{-1}, which was omitted as indicated for experiments involving the transporter deletion mutant GRC1 Δ*modABC*. As carbon sources, a mixture of glycerol (40 mM) and glucose (2 mM) was used. Employing glycerol avoided further acidification of the medium by gluconate, which already occurred through the formation of HMFA as product of oxidative HMF detoxification. Nevertheless, a small amount of glucose was added to prevent an extensive lag phase (Koopman et al., 2010a). The standard buffer capacity (22.3 mM K_2HPO_4 and 13.6 mM NaH_2PO_4) was commonly increased four-fold for HMF conversion assays or as indicated for the respective experiment. For plasmid maintenance and the selection of genomic recombination events the following antibiotics were employed: Kanamycin sulfate at 50 mg L^{-1}, gentamycin sulfate at 20 mg L^{-1}, ampicillin (only for *E. coli*) at 100 mg L^{-1}, and streptomycin sulfate at 50 mg L^{-1} (for *E. coli*) and 200 mg L^{-1} (for *Pseudomonas*). Induction of heterologous gene expression controlled by the *nagR*/P_{nagAa} promoter system was achieved by addition of 0.1 mM salicylate to the MSM preculture and the main experiment. *E. coli* was grown at 37 °C and *Pseudomonas* at 30 °C. Liquid cultures in shake flasks were incubated in a horizontal rotary shaker (Kuhner Shaker, Herzogenrath,

Germany) with a humidity of 80%, a throw of 50 mm, and a frequency of 200 rpm. For cultures in 24-deepwell microplates, the frequency was increased to 300 rpm. A Growth Profiler 960 (Enzyscreen, Heemstede, The Netherlands) monitoring cultures in microtiter plates with transparent bottoms by image analysis was used for online growth detection. The resulting green-values (g-values, based on green pixel counts) correlate with the optical density of a cell culture which is sufficient for qualitative statements. No conversion to OD_{600} values was performed, as calibrations depend on cell shape and size, which can vary in the presence of different stressor concentrations. This would require separate calibrations for each specific condition. Main cultures were conducted in 96-well plates (CR1496dg) with a volume of 200 µL at 30 °C and 225 rpm shaking speed with an amplitude of 50 mm. The starting OD_{600} was set to 0.1. The interval between two photos for growth analysis was 30 min. The growth curves displayed were generated by applying a second-order smoothing to all data points. All chemicals used in this study were obtained from Sigma-Aldrich (St. Louis, MO, USA), Carl Roth (Karlsruhe, Germany), or Merck (Darmstadt, Germany) unless stated otherwise.

2.1.5.2. Plasmid cloning and strain engineering

Genomic DNA of *P. taiwanensis* VLB120, *P. putida* KT2440 and *P. caribensis* was isolated using the Monarch® Genomic DNA Purification Kit (New England Biolabs, Ipswich, MA, USA). All Plasmids were constructed via Gibson assembly (Gibson et al., 2009) using the NEBuilder HiFi DNA Assembly (New England Biolabs, Ipswich, MA, USA) and verified by Sanger sequencing. Primers were obtained as unmodified DNA oligonucleotides from Eurofins Genomics (Ebersberg, Germany). All oligonucleotides and plasmids used in this study, accompanied by detailed information can be found in Table S2 and Table S3. DNA amplifications for cloning purpose were performed with Q5 High-Fidelity Polymerase (New England Biolabs, Ipswich, MA, USA). Restriction enzymes were purchased from New England Biolabs. Plasmid DNA and PCR amplicons were purified with the Monarch® Plasmid Miniprep Kit and Monarch® PCR & DNA Cleanup Kit, respectively (New England Biolabs, Ipswich, MA, USA). *E. coli* and *Pseudomonas* were transformed with DNA assemblies and purified plasmids by electroporation using a GenePulser Xcell (BioRad, Hercules, CA, USA) (settings: 2 mm cuvette gap, 2.5 kV, 200 Ω, 25 µF). Alternatively, a heat shock protocol was applied in case of *E. coli*. The correctness of cloned plasmids, obtained deletions and integrations, as well as genomic replacements was verified by colony PCR using the OneTaq 2X Master Mix with Standard Buffer (New England Biolabs, Ipswich, MA, USA). To increase efficiency, the template cell material was lysed in alkaline polyethylene glycol according to Chomczynski and Rymaszewski (Chomczynski and Rymaszewski, 2006).

Seamless genomic modifications were achieved using the I-SceI-based system developed by Martínez-García and de Lorenzo (Martinez-Garcia and de Lorenzo, 2011). For knockouts, the 500–800 bp upstream and downstream flanking regions of the deletion target (TS1 and TS2) were cloned between the two I-SceI restriction sites of pSNW2, pSNW4, or pEMG, and the resulting plasmid was transferred from *E. coli* PIR2 or *E. coli* EC100D™ *pir*$^{+}$ into the desired *Pseudomonas* recipient strain by conjugation. For this, mating procedures were performed as described by Wynands *et al.* (Wynands et al., 2018). Analogously, precisely positioned genomic integrations or exchanges were carried out with plasmids having the target DNA sequence inserted between the TS sites. Three randomly picked clones were transformed with I-SceI-encoding plasmid pSW-2 triggering the second homologous recombination event without induction by 3-methylbenzoate. Correct clones were cured of pSW-2 by restreaking on non-selective medium, and re-analyzed by PCR ensuring a pure culture. Additional Sanger sequencing verified strains with genomic exchanges such as modified promoter regions.

2.1.5.3. Analytical methods

Concentrations of furanic compounds were measured using a 1260 Infinity II HPLC system equipped with an InfinityLab Poroshell 120 EC-C18 column (3.0 x 150 mm, 2.7 µm) column and the respective InfinityLab Poroshell 120 EC-C18 (3.0 x 5 mm, 2.7 µm) guard column (all Agilent, Santa Clara, CA, USA). Chromatography was performed at 40 °C with potassium acetate buffer (10 mM, pH = 5.5) and acetonitrile as eluents at a flow rate of 0.8 mL min^{-1} for 7 min. From the starting ratio of 97% aqueous buffer and 3% acetonitrile the proportion of acetonitrile was first elevated linearly to 15% the first minute and then further increased to 40% the following 2 min. Thereafter, the proportion of acetonitrile remained constant for the next minute before it was gradually reduced to 3% within 2 min and kept constant for the rest of the run. UV detection was performed at distinct wavelengths for each compound: HMF at 280 nm, HMFA at 250 nm, FFA at 280 nm, FDCA at 250 nm, and HMFOH at 220 nm. Retention times were 2.44 min, 0.95 min, 1.14 min, 0.73 min, and 2.28 min for HMF, HMFA, FFA, FDCA, and HMFOH respectively. Standards of each chemical were purchased from Biosynth and used for quantification.

2.1.5.4. Whole-cell HMF conversion assays in shake flasks

MSM (10 mL) supplemented with 40 mM glycerol and 2 mM glucose was inoculated using glycerol stocks of the strains to be examined and incubated for approximately 18 h at 30 °C and 200 rpm. Precultures were concentrated by centrifugation (6,000 × g, rt, 5 min) and subsequent resuspension in one fifth of the medium, and used for inoculation of the main experiment. The main culture was carried out in four-fold buffered MSM (10 mL) supplemented

with 40 mM glycerol, 2 mM glucose, and 10 mM HMF (30 °C and 200 rpm). The starting OD_{600} was adjusted to 1.0 unless stated otherwise. The first sample was withdrawn directly after inoculation and then in regular intervals. Cell growth was monitored by measuring the optical density at 600 nm and concentrations of respective furanics were analyzed by HPLC. 20 µL of culture broth were diluted ten-fold by addition of 180 µL dH_2O and filtered (AcroPrep™ Advance 96-well, 0,2 µm, PTFE membrane, Pall Corporation, Port Washington, NY, USA). 1 µL of each sample was injected onto the HPLC. The initial conversion rates were defined as the decrease in the concentration of HMF or the increase in the concentration of HMFA normalized to the OD_{600} during the first two hours of the reaction or until HMF was completely consumed, and determined by linear regression. The OD_{600} was assumed constant during this period and equaled the starting conditions.

2.1.5.5. Whole-cell HMF conversion assays in 24-deepwell microplates (Duetz-System)

For parallel analyses of HMF conversion of multiple strains, polypropylene square 24-deepwell microplates capped with a sandwich cover with pins were employed (Enzyscreen, Heemstede, Netherlands). Cells used for inoculation of the main experiment were obtained as described above with an additional first passage in LB medium. The main culture was carried out in four-fold buffered MSM (1.5 mL) supplemented with 40 mM glycerol, 2 mM glucose, and 10 mM HMF (30 °C and 300 rpm). The starting OD_{600} was adjusted to 0.5 unless stated otherwise. Samples were taken in regular intervals of 30 min, which were prolonged to 1 h after 4 h of experiment (Sampling interval was shortened in case of fast-oxidizing strains). For each time point, a separate microplate was harvested. Measurements of cell growth and furanics concentrations, as well as determination of initial oxidation rates were carried out as described in the previous section.

Funding

This work was supported by the German Federal Ministry of Education and Research via the project NO-STRESS [grant number 031B0852A] and by the European Union's Horizon 2020 research and innovation program via the project UPLIFT [grant agreement number 953073].

Acknowledgements

We thank R. Schruff for her support with generating the deletion mutants of *P. putida* KT2440 and Pablo I. Nikel for kindly providing the pSNW2 and pSNW4 plasmids.

Competing Interest Statement

The authors declare no competing interests.

Data availability

Data will be made available on request.

2.2. Life with toxic substrates – PaoEFG forms the basis for growth of *Pseudomonas taiwanensis* VLB120 and *Pseudomonas putida* KT2440 on aromatic aldehydes

Thorsten Lechtenberg, Benedikt Wynands, Tino Polen, Nick Wierckx* (2024)

Institute of Bio- and Geosciences IBG-1: Biotechnology, Forschungszentrum Jülich, 52425 Jülich, Germany
* Corresponding author

Status: unpublished
manuscript in preparation

CrediT authorship contribution statement:

T. Lechtenberg: Investigation, Writing - Original Draft, Writing - Review and editing, Visualization, Validation.

B. Wynands: Writing - Review and editing, Conceptualization, Supervision.

T. Polen: Resources, Investigation

N. Wierckx: Writing - Review and editing, Conceptualization, Supervision, Funding acquisition, Project administration.

Overall contribution: 80%

Except for whole-genome sequencing conducted by TP, the shown experimental work was performed and validated by TL who also visualized all data. BW acted as direct scientific advisor assisting with planning and evaluation of experiments. The entire project was led and supervised by NW. TL wrote the original draft which was reviewed and edited by BW and NW. Funding for the project was acquired by NW.

2.2.1. Abstract

The biotechnological workhorses *P. taiwanensis* VLB120 and *P. putida* KT2440 can degrade a variety of aromatic compounds including a large number of carboxylates, such as benzoate, 4-hydroxybenzoate and vanillate whose metabolic pathways are extensively characterized. Moreover, they are able to catabolize many aldehyde derivatives of said chemicals including industrially important substances such as vanillin, although these are typically very toxic to microorganisms due to their high reactivity. However, the crucial enzyme(s) used by these bacteria to convert aldehydes into the corresponding carboxylates remained unknown so far. Here, we could demonstrate that the activity of the recently identified 5-(hydroxymethyl)furfural (HMF)-oxidizing periplasmic aldehyde oxidoreductase PaoEFG extends to further aromatic aldehydes, in particular 4-hydroxybenzaldehyde and vanillin, thereby closing the gap between aldehyde and carboxylate degradation. In addition, we engineered *P. taiwanensis* VLB120 GRC1 to grow on the furanic aldehyde HMF, representing both a lignocellulose-derived microbial inhibitory compounds and an auspicious bio-based platform chemical. Upon boosting the oxidation capacity through overexpression of *paoEFG* and *aldB-I*, the engineered strains outperformed the natural degrader *Paraburkholderia caribensis* in terms of tolerance. In the future, the newly generated strains might serve for biological detoxification of lignocellulosic hydrolysates or as screening vehicle for enhanced enzyme activities, for instance improved alcohol and aldehyde dehydrogenases or transporters, promoting efficient biotechnological production of the renewable plastic monomer 2,5-furandicarboxylic acid (FDCA) from HMF.

Keywords: *Pseudomonas*; Aromatic aldehyde degradation; Periplasmic aldehyde oxidoreductase PaoEFG; Vanillin; 5-(Hydroxymethyl)furfural

2.2.2. Introduction

Soil-inhabiting Pseudomonads like *P. taiwanensis* VLB120 and *P. putida* KT2440, which are non-pathogenic and hold great promise in biotechnology, display a multifaceted metabolism in particular with regard to catabolism of aromatic compounds (Nelson et al., 2002, Belda et al., 2016, Jiménez et al., 2002, dos Santos et al., 2004, Kohler et al., 2013). Among others, they degrade 4-hydroxybenzoate and vanillate via the common intermediate protocatechuate (PCA) (Nogales et al., 2019). PCA subsequently undergoes *ortho*-cleavage to β-carboxy-*cis*,*cis*-muconate which enters the β-ketoadipate pathway and is further metabolized to acetyl-CoA and succinyl-CoA, ultimately feeding into the tricarboxylic (TCA) cycle (Fig. 2.2-1) (Bull and Ballou, 1981, Harwood and Parales, 1996). In contrast to *P. taiwanensis* VLB120, *P. putida* KT2440 additionally harbors the so-called ferulic operon consisting of genes encoding an enoyl-CoA-hydratase/aldolase (*ech*), a vanillin dehydrogenase (*vdh*) and a feruloyl-CoA synthetase (*fcs*) (www.pseudomonas.com) (Winsor et al., 2016, Plaggenborg et al., 2003). Therefore, this strain can also grow on ferulate, which otherwise closely related *P. taiwanensis* VLB120 cannot (Plaggenborg et al., 2003, Zhou et al., 2020b, Wynands et al., 2023). The ferulate degradation pathway starts with CoA-activation of the substrate enabled by Fcs, followed by hydration and retro-aldol reaction catalyzed by Ech finally yielding vanillin (Fig. 2.2-1) (Graf and Altenbuchner, 2014). The aldehyde, in turn, can be oxidized to vanillate by Vdh, but the aldehyde dehydrogenase (ALDH) is not essential for ferulate and vanillin metabolization. This is confirmed by the fact that *P. taiwanensis* VLB120 can grow on vanillin despite the absence of the ferulic operon including *vdh* (Graf and Altenbuchner, 2014, Wordofa and Kristensen, 2018). Thus, there must exist one or more alternative enzymes capable of catalyzing the oxidation step that so far remained unidentified.

Vanillin (4-hydroxy-3-methoxybenzaldehyde) is a key aromatic flavor compound widely employed in both the food and fragrance industry. As conventional methods such as extraction from plant material or chemical synthesis either suffer from inefficiency or require fossil resources, alternative bio-based production routes leading to “natural” vanillin are highly sought after (Priefert et al., 2001, Gallage and Moller, 2015, Martau et al., 2021, Liu et al., 2023). However, biocatalytic production requires a thorough understanding of inherent degradation pathways in the selected host organism to avoid product loss (Muschiol et al., 2015). For instance, efficient vanillin *de novo* biosynthesis with *Escherichia coli* is only possible by employing a reduction-negative mutant, namely *E. coli* RARE, which prevents the undesired formation of vanillyl alcohol (Kunjapur et al., 2014, Kunjapur et al., 2016). Since vanillin is a cytotoxic compound exerting multidimensional stress through its electrophilic aldehyde

functionality as well as its lipophilic aromatic backbone, robust microbial chassis like Pseudomonads are advantageous hosts for handling this chemical (Nikel et al., 2016a, Weimer et al., 2020, Blombach et al., 2022). Bacteria of the *Pseudomonas* clade are characterized by multiple tolerance mechanisms including active extrusion of toxicants by various efflux pumps, the adaptation of membrane fatty acids for example through *cis-trans*-isomerization, as well as the release of outer membrane vesicles, and damage recovery systems, such as chaperones (Bitzenhofer et al., 2021). Furthermore, they exhibit a remarkable tolerance towards furanic aldehydes like the promising renewable platform chemical 5-(hydroxymethyl)furfural (HMF) owing to the ability to rapidly oxidize them to the corresponding carboxylic acids (Xu et al., 2020b). Recently, the enzymatic toolbox for this detoxification process was shown to be based on the central periplasmic and molybdenum-dependent oxidoreductase PaoEFG which is complemented by the cytoplasmic dehydrogenases AldB-I(I) (2.1.). It remains to be investigated whether these enzymes are also engaged in the metabolization of other (aromatic) aldehydes, such as 4-hydroxybenzaldehyde and vanillin. Considering earlier vanillin production experiments with *P. putida* KT2440, where aldehyde accumulation was only achieved upon deletion of the molybdate transporter *modABC*, this scenario seems plausible in light of chapter 2.1. (Graf and Altenbuchner, 2014).

P. taiwanensis VLB120 and *P. putida* KT2440 cannot natively degrade furanic aldehydes and require heterologous complementation of genes for this task. Koopman *et al.* published the first complete elucidation of a gene cluster enabling furfural and HMF degradation in 2010 identifying the involved genes through transposon mutant screening of the HMF-degrading bacterium *Cupriavidus basilensis* HMF14 (Fig. 2.2-2A) (Koopman et al., 2010b, Wierckx et al., 2010). Eight genes (*hmfABCDEFGH*) encoding catalytically active proteins, two regulatory genes (*hmfR1R2*), as well as two genes encoding major facilitator superfamily (mfs)-type transporters (*hmfT1T2*) were discovered. In addition, the cluster harbors an uncharacterized gene encoding a putative hydroxylase next to *hmfH* (Wierckx et al., 2011). Based on the results of the mutant studies, sequence homologies, and previous findings on 2-furoic acid (FA) degradation, a comprehensive pathway for furfural and HMF metabolization was proposed (Koopman et al., 2010b, Trudgill, 1969, Koenig and Andreesen, 1989). At first, oxidation of the aldehydes occurs. In the case of HMF, three sequential steps are required involving 5-hydroxymethlyl-2-furoic acid (HMFA) and 5-formyl-2-furoic acid (FFA) as intermediates. The fully oxidized product 2,5-furandicarboxylic acid (FDCA) subsequently undergoes decarboxylation by the UbiD/UbiX-like enzymes HmfF/HmfG to form FA which is the first common intermediate of HMF and furfural catabolism. Next, HmfD catalyzes the ATP-dependent conversion of FA to the respective CoA-ester 2-furoyl-CoA. After hydroxylation by

the molybdenum-dependent protein HmfABC, the lactone form of 5-hydroxy-2-furoyl-CoA can be cleaved hydrolytically yielding linear 2-oxo-glutaroyl-CoA. Finally, the CoA-ester is hydrolyzed resulting in α-ketoglutaric acid (α-KG) which is further metabolized via the TCA cycle (1.3.4.2.).

Well-adapted Pseudomonads can even catabolize toxic substrates such as aromatic aldehydes by converting them to less harmful acid intermediates. Here, we engineered *P. taiwanensis* VLB120 to efficiently metabolize HMF as the sole carbon and energy source. Boosting the initial oxidation step catalyzed by the recently identified PaoEFG and AldB-I, could significantly increase the organism's tolerance to this toxicant. On top of that, it was shown that the mentioned enzymes were not specific for HMF but equally important for degradation of other aromatic aldehydes, notably 4-hydroxybenzaldehyde and vanillin.

2.2.3. Results and discussion

2.2.3.1. PaoEFG is essential for growth on 4-hydroxybenzaldehyde and vanillin

To evaluate if PaoEFG and AldB-I(I) are involved in the degradation of aromatic aldehydes like vanillin and 4-hydroxybenzaldehyde, inducibly solvent-tolerant *P. taiwanensis* VLB120 GRC3 and *P. putida* KT2440 as well as previously generated Δ*paoEFG* and Δ*aldB-I(I)* deletion mutants were grown on minimal salt medium (MSM) agar plates supplemented with 5 mM of the respective aldehyde as sole carbon and energy source. The aldehyde concentration was kept low to minimize toxicity effects. As a control, all strains were cultivated on the corresponding carboxylates. Both *P. taiwanensis* VLB120 GRC3 and *P. putida* KT2440 showed decent growth on all carbon sources including the aldehydes (Fig. 2.2-1). To the best of our knowledge, 4-hydroxybenzaldehyde has not yet been described as sole carbon and energy source for *Pseudomonas*, thereby adding another compound to the already broad portfolio of substrates. The Δ*paoEFG* mutants did grow on the carboxylates, but not on any of the aldehydes. This confirms a central role of the encoded enzymes for the initial oxidation step of the degradation pathway (Fig. 2.2-1). Similar to PaoABC of *E. coli* (Neumann et al., 2009), the periplasmic aldehyde oxidoreductase PaoEFG appears to accept diverse substrates. This includes rather non-polar benzaldehyde derivatives such as 4-hydroxybenzaldehyde ($logP_{o/w}$ = 1.35 (Franden et al., 2013)) and vanillin ($logP_{o/w}$ = 1.21 (Franden et al., 2013)) with a six-membered ring backbone in addition to polar furanic aldehydes like HMF ($logP_{o/w}$ = -0.37 (Franden et al., 2013)) and furfural ($logP_{o/w}$ = 0.41 (Franden et al., 2013)) featuring a five-membered heterocycle core structure. Since *P. putida* KT2440 Δ*paoEFG* could also not grow on vanillin despite possessing a Vdh, it can be concluded that the aldehyde is not imported into the cytoplasm. This aligns with the previously

suggested theory, in the context of HMF oxidation, that aldehydes are primarily converted in the periplasm to avoid their toxic impact inside the cell (2.1.). This hypothesis is supported by the observation that single or combinatorial knockouts of the cytoplasmic dehydrogenases *aldB-I(I)* did not influence assimilation of 4-hydroxybenzaldehyde and vanillin by *P. putida* KT2440, although associated gene expression was reported to be upregulated in response to vanillin (Simon et al., 2014).

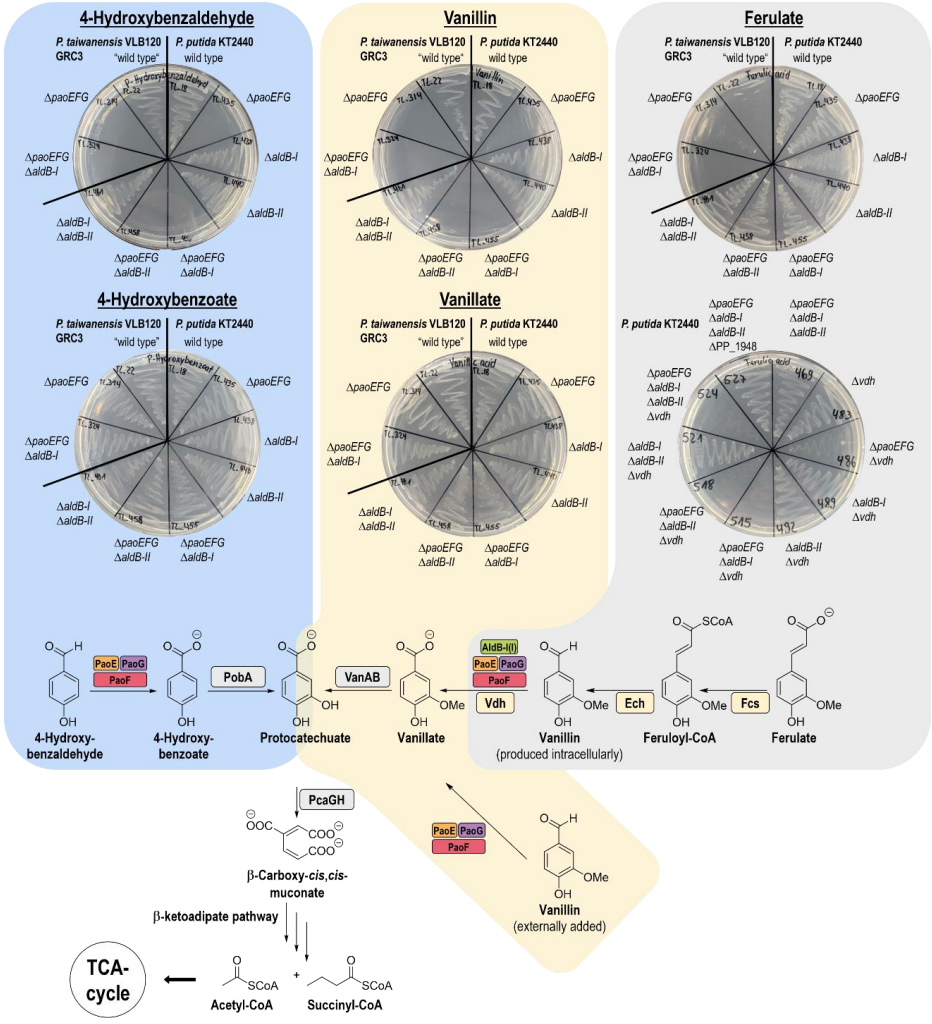

Figure 2.2-1: Growth experiments with *P. taiwanensis* VLB120 GRC3, *P. putida* KT2440 and deletion mutants thereof lacking putative aromatic aldehyde-oxidizing enzymes on MSM agar plates containing different carbon sources. Growth was evaluated with 5 mM of either 4-hydroxybenzaldehyde, vanillin, ferulate, or 4-hydroxybenzoate and vanillate as positive controls. The lower part of the figure shows the associated degradation pathways including the assigned enzymes for aldehyde oxidation steps. Photos were taken after 24 h of incubation at 30°C.

The situation changed when vanillin was formed intracellularly as a metabolic product of ferulate degradation in *P. putida* KT2440. In this case, the single knockout of *paoEFG* did not result in a visible growth defect likely due to the cytoplasmic activity of Vdh (Fig. 2.2-1). However, a Δ*vdh* mutant could also grow and only the double deletion mutant *P. putida* KT2440 Δ*paoEFG* Δ*vdh* exhibited severely reduced growth with ferulate as sole carbon and energy source. This might be explained as follows: When growing on ferulate, the intracellularly generated vanillin is rapidly converted to vanillate by cytoplasmic Vdh, which is supported by the fact that the corresponding gene forms an operon with *ech* and *fcs*. In absence of Vdh, vanillin cannot be processed in the cytosol leading to secretion of the toxicant using one of its numerous efflux systems (Simon et al., 2014). The aldehyde is then available as a substrate for periplasmic PaoEFG and can therefore be oxidized to vanillate, which is eventually reimported and further metabolized. As *P. putida* KT2440 Δ*paoEFG* Δ*vdh* still displayed weak growth on ferulate, *aldB-I* and *aldB-II* were additionally deleted which appeared to further reduce growth (Fig. 2.2-1). This indicates that these ALDHs can also oxidize vanillin, but quantitative growth analyses are required for a more conclusive statement. The experiments with *P. taiwanensis* VLB120 GRC3 and ferulate as a carbon source have to be regarded as controls, since the ferulic operon is absent in this organism. At last, it should be noted that other Pseudomonads such as *Pseudomonas* sp. 9.1 can grow on vanillin as sole carbon source, despite the absence of a PaoEFG homolog or another molybdenum-dependent aldehyde oxidase. This strain instead showed transient accumulation of vanillyl alcohol as an intermediate thereby indicating a different metabolic wiring (Ravi et al., 2018).

2.2.3.2. Genomic integration of the *hmf*-cluster into *P. taiwanensis* VLB120 GRC1 and *P. putida* KT2440 enabled growth on furfural, FA, and FDCA, but not on HMF and HMFA

In contrast to the compounds discussed thus far, HMF constitutes a much more polar heteroaromatic aldehyde that cannot natively be used as a feedstock by the *Pseudomonas* strains studied in this work. However, HMF represents not only a promising platform chemical but also an interesting carbon source, for example if the objective is to biologically detoxify lignocellulosic hydrolysates. The engineering towards furanic compounds-degrading *P. taiwanensis* VLB120 GRC1 and *P. putida* KT2440 started with the selection of a suitable donor strain for the required pathway genes. We chose to use *Paraburkholderia caribensis* which was easily accessible and, in contrast to the benchmark isolate *C. basilensis*, harbors all *hmf*-genes clustered in a single DNA segment thereby facilitating cloning procedures (Fig. 2.2-2A).

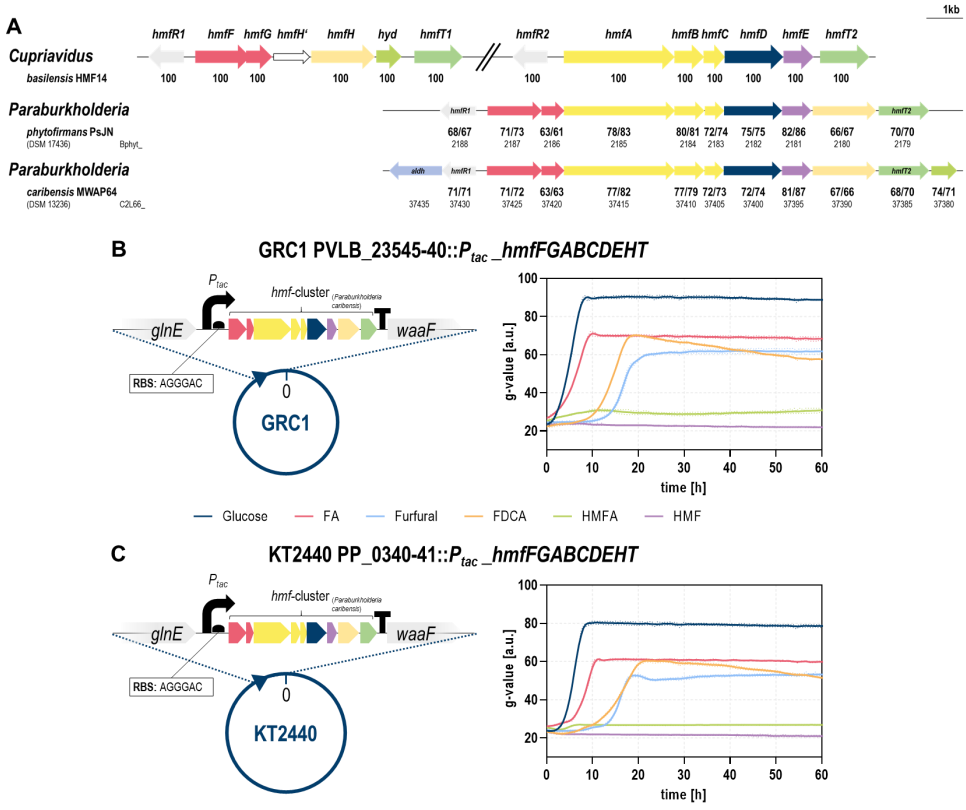

Figure 2.2-2: Integration of the *hmf*-cluster into the genomes of *P. taiwanensis* VLB120 GRC1 and *P. putida* KT2440 and growth analysis of the resulting strains. (**A**) Overview of the respective clusters of *Paraburkholderia phytofirmans* and *Paraburkholderia caribensis* employed as templates for genetic engineering**.** Numbers in bold print (**x**/**y**) next to each gene indicate the percentage identity on DNA (**x**) or protein (**y**) level with respect to the reference strain *C. basilensis* HMF14. Sequence identities were calculated with the Emboss Needle pairwise sequence alignment tool (Madeira et al., 2022). (**B**/**C**) Two-fold buffered MSM supplemented with 20 mM glucose (dark blue), FA (red), furfural (light blue), FDCA (orange), HMFA (green), and HMF (purple) was inoculated with GRC1 PVLB_23545-40::*P*$_{tac}$*_hmfFGABCDEHT* (**B**) and KT2440 PP_0340-41::*P*$_{tac}$*_hmfFGABCDEHT* (**C**) to an OD_{600} of 0.1. Cells were cultivated in a Growth Profiler in 96-well microtiter plates. The growth curves result from a second-order smoothing to the mean values obtained from three replicates. The dots represent the standard deviation.

P. taiwanensis VLB120 GRC1 and *P. putida* KT2440 were equipped with this cluster (*hmfFGABCDEHT*) which was genomically integrated via the I-SceI-based system developed by Martínez-García and de Lorenzo (Martinez-Garcia and de Lorenzo, 2011). For *P. putida* KT2440 a similar strain has already been constructed by Guarnieri *et al.* who employed the closely related *Paraburkholderia phytofirmans* PsJN as a donor (Guarnieri et al., 2017). They could show that the cluster's core fragment from *hmfF* to *hmfH* was sufficient to enable growth on HMF and furfural when expressed under the control of the constitutive *P*$_{tac}$ promoter. Thus, we likewise omitted the regulatory gene, as well as the putative ALDH and

hydroxylase. However, given its previously highlighted importance for HMFA uptake (2.1.), the transporter gene *hmfT* was included. Consequently, a segment of about 12 kb (*hmfF* to *hmfT*) from the entire cluster spanning 15,535 kb was transplanted into *P. taiwanensis* VLB120 GRC1 and *P. putida* KT2440. The authors of the above-mentioned publication chose a targeted integration site between two facing genes (*fpvA* and PP_4218) for the *hmf*-cluster to avoid damaging of potential regulatory elements. We opted for genomic insertion into a previously characterized landing pad between *glnE* and *waaF* which was shown to ensure high gene expression (Fig. 2.2-2B and C) (Köbbing et al., 2024).

A conserved GC-rich 11 bp region at the start of *hmfF*, which occurs more than ten times within the *hmf*-cluster of *P. caribensis*, but not *P. phytofirmans*, impeded PCR amplification of *hmfFGABCDEHT* through extensive false priming. This problem was circumvented by shifting the forward primer a few base pairs downstream and complementing the missing bases to the overhang of the primer for vector amplification. Upon plasmid assembly and *E. coli* transformation most colony PCR-positive clones whose plasmids were sequenced showed suppressor mutations in the promoter region or at the onset of *hmfF*. Apparently, there was a high selective pressure for clones with deactivated or at least reduced *hmfF* expression, which seemed thus to be toxic for *E. coli*. One plasmid was identified that instead only exhibited a mutation concerning the RBS, which was shortened from AGGAGAC to AGGGAC. Computational analysis revealed that this likely decreased translation initiation rates, but HmfF synthesis could remain active (Salis et al., 2009). This plasmid was therefore used to construct the intended strains (Fig. 2.2-2B and C).

The obtained strains were subjected to growth analysis using various carbon sources. These included HMF and furfural, the pathway intermediates FA, HMFA, and FDCA, together with glucose as a control. Both strains grew on FA, furfural and FDCA without further adaptation, but failed to assimilate HMF and HMFA. The best growth was observed with FA, followed by FDCA and furfural. Overall, the GRC1 variant showed slightly increased final cell densities in comparison to KT2440 highlighting the benefits of the genome-reduced chassis (Wynands et al., 2019). Both strains grew normally on glucose excluding negative side effects of *hmf*-cluster integration (Fig. 2.2-2B and C). The fact that we detected growth on FDCA, but not on HMFA or HMF was conspicuous as biotransformation of HMF into the dicarboxylic acid by GRC1 heterologously expressing *hmfH* and *hmfT* was already demonstrated (2.1.). Based on the previously performed oxidation assays (2.1.3.5.), where HMFA uptake was identified as rate-determining step, a hampered substrate uptake was assumed to be growth-inhibiting. However, a regulatory issue could also not be excluded and we therefore complemented the

cluster in GRC1 by addition of the two hitherto deliberately omitted genes encoding a LysR-type regulator (HmfR1) and an ALDH. Thereby, the P_{tac} promoter was replaced by the native promoter sequences from *Paraburkholderia caribensis* (Fig. 2.2-3). In comparison to its progenitor, the modified strain displayed reduced growth rates across all tested furanic compounds, with a particular pronounced decline observed in the case of FA and furfural. Nevertheless it could grow very slowly on HMFA as sole carbon and energy source (Fig. 2.2-3). The reasons for this remain elusive, but may be related to attuned expression of *hmfT*.

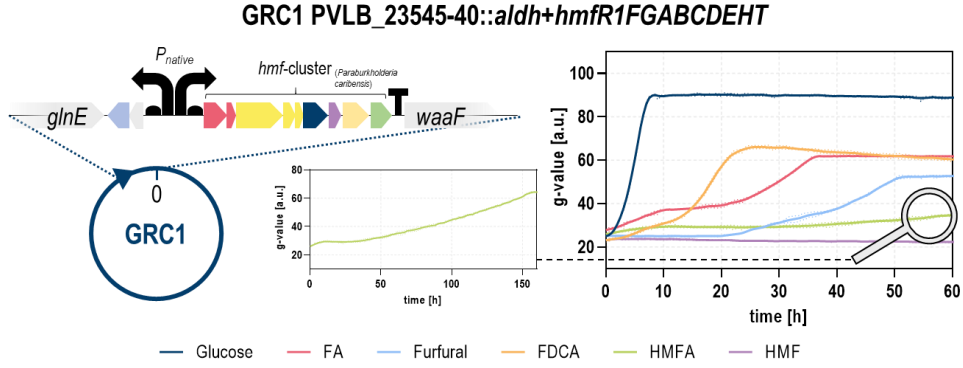

Figure 2.2-3: Complementation of the previously integrated *hmf*-cluster by *aldh* and *hmfR1* in *P. taiwanensis* VLB120 GRC1 and subsequent growth analysis. Two-fold buffered MSM supplemented with 20 mM glucose (dark blue), FA (red), furfural (light blue), FDCA (orange), HMFA (green), and HMF (purple) was inoculated with GRC1 PVLB_23545-40::aldh+hmfR1FGABCDEHT to an OD_{600} of 0.1. Slow growth on HMFA is highlighted in a separate graph. Cells were cultivated in a Growth Profiler in 96-well microtiter plates. The growth curves result from a second-order smoothing to the mean values obtained from three replicates. The dots represent the standard deviation.

2.2.3.3. Promoting growth on HMF and HMFA by adaptive laboratory evolution (ALE)

Despite its ability to slowly grow on HMFA, the work with the modified strain GRC1 PVLB_23545-40::*aldh+hmfR1FGABCDEHT* was abandoned due to the inferior overall growth characteristics, especially concerning the central pathway intermediate FA. Instead, we attempted to improve the growth of GRC1 PVLB_23545-40::P_{tac}_*hmfFGABCDEHT* on HMFA by ALE. As there was no observable growth with this strain using 20 mM HMFA (Fig. 2.2-2B), we first performed three passages in a medium containing a mixture of 10 mM FA and 10 mM HMFA. While FA was consumed overnight, it took about a week until a further increase in OD_{600} could be detected indicating the assimilation of HMFA. To increase the number of generations grown on HMFA (most doublings occur at low cell densities) we then switched to HMFA as sole carbon and energy source. However, it took about a month until the first culture was completely grown. The next reinoculation was carried out after ten days, after which the

cultivation time was reduced to three days for the best-growing cultures. Overall, 20 rounds of serial dilution (first 1:20, later 1:40) were performed eventually resulting in culture times of about 24 h. At this point, the cultures were spread on LB agar and single colonies were isolated. Selected clones from different evolutionary lineages were assessed for their growth on HMFA, FDCA, and glucose (Fig. S5.2-1). The strains obtained from the best-performing ALE culture (TL_626, TL_627, TL_629) required about 25 h to grow on 20 mM HMFA. In contrast, the strains from other evolutionary lineages (TL_637, TL_638, or TL_639, TL_640) also showed growth but were much slower. According to the hypothesis that the cellular uptake of the acid was growth-limiting, we speculated that improved HMFA assimilation was probably enabled by transporter evolution. Thus, the respective gene was PCR-amplified and sequenced. Intriguingly, the fastest-growing strains were those harboring the original *hmfT* gene from *Paraburkholderia caribensis* whereas slower growing bacteria showed at least one point mutation (Fig. S5.2-1). The evolutionary reason for such defective variants remain cryptic, especially considering that the transporter was previously characterized as indispensable for HMFA uptake (2.1.). One explanation could be a detrimental interplay between the heterologous uptake system and a native export machinery of the host. With regard to the other carbon sources, the improved metabolization of HMFA appeared to be correlated with slower growth on both FDCA and glucose (Fig. S5.2-1), which was unexpected.

After isolation of the first promising strains, the ALE was continued for another 15 reinoculation steps resulting in further improvements. While the first generation strains (TL_626, TL_627, TL_629) needed about one day to fully grow, the isolates TL_666, TL_671, and TL_676 all originating from the extended ALE experiment completely metabolized 20 mM HMFA in less than 15 h (Fig. 2.2-4A). Analogously, improved growth on HMF was found, but the aldehyde concentration had to be halved to reduce the associated stress (Fig. 2.2-4B). This was an expected outcome, since there is just one oxidation step needed to get from HMF to HMFA which can be catalyzed by the previously identified enzymes PaoEFG and AldB-I (2.1.). Growth on FA was similar to that of the progenitor and thus significantly better than that of *Paraburkholderia caribensis* on this carbon source (Fig. 2.2-4C). As already detected for the first generation ALE strains, the evolved strains grew worse on FDCA and glucose (Fig. 2.2-4D and E). While in the case of glucose only growth rates appeared to be reduced, TL_666, TL_671, and TL_676 also showed lower final biomass signal when metabolizing FDCA (Fig. 2.2-4D).

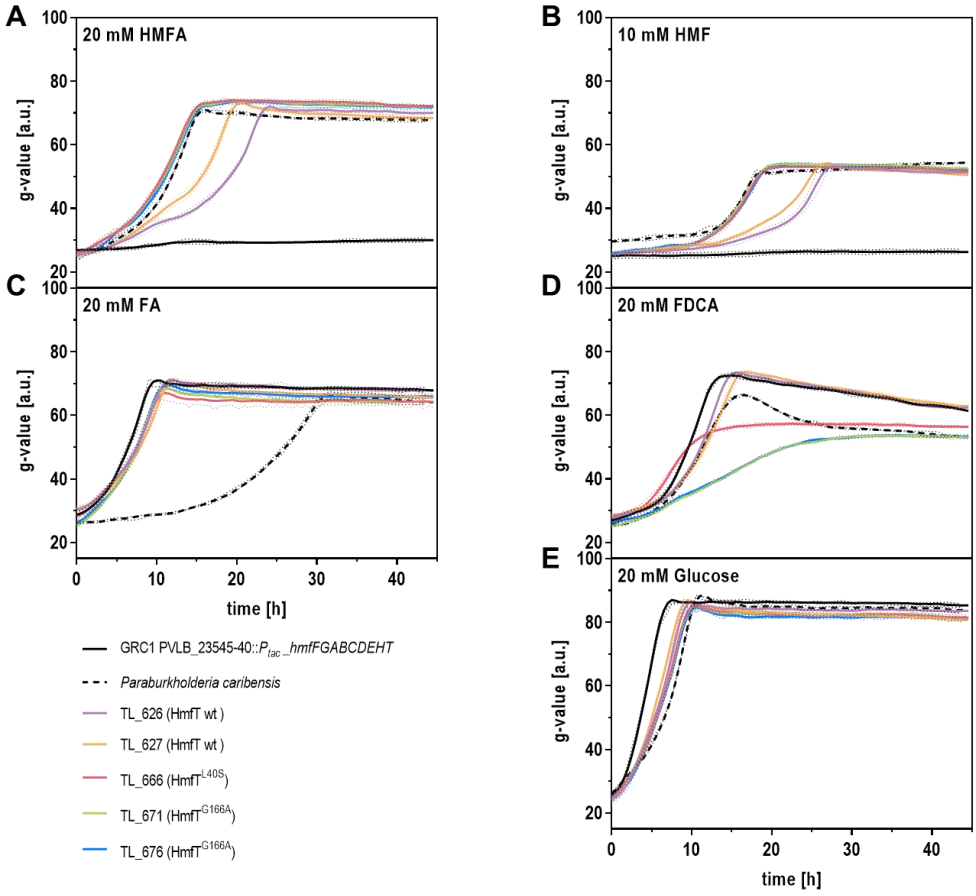

Figure 2.2-4: Growth characteristics of selected strains resulting from the long-term ALE of GRC1 PVLB_23545-40::*P*$_{tac}$*_hmfFGABCDEHT* on HMFA as sole carbon and energy source (second generation). Two-fold buffered MSM supplemented with 20 mM HMFA (**A**), 10 mM HMF (**B**), 20 mM FA (**C**), 20 mM FDCA (**D**) or 20 mM glucose (**E**) was inoculated with the evolved strains (refer to the legend for color-coding), the parent strain GRC1 PVLB_23545-40::*P*$_{tac}$*_hmfFGABCDEHT* (black), and *Paraburkholderia caribensis* (black, dashed) to an OD_{600} of 0.1. Two precultures, one using LB and the second using MSM supplemented with 20 mM glucose were conducted. Cells were cultivated in a Growth Profiler in 96-well microtiter plates. The growth curves result from a second-order smoothing to the mean values obtained from three replicates. The dots represent the standard deviation.

2.2.3.4. Whole-genome resequencing of the evolved strains

In order to explore the genetic basis of the results and identify the mutations associated to the enhanced growth on HMFA, the three strains were subjected to whole-genome sequencing. For comparison, the first generation ALE strains (TL_626 and TL_627) as well as the parent strain GRC1 PVLB_23545-40::*P*$_{tac}$*_hmfFGABCDEHT* were additionally analyzed (Table 2.2-1).

Table 2.2-1: Genomic loci affected by the ALE experiment. Abbreviations: nt, nucleotide; SNV, single nucleotide variant; del, deletion; ins, insertion.

nt pos.	mutation	affected locus	frequency (%)					
			TL_125	TL_626	TL_627	TL_666	TL_671	TL_676
467712	del_G_-	*hmfE*	-	100	100	100	100	100
2222021	SNV_C_T (R396W)	*clpA* (PVLB_14955) (ATP-dependent protease)	-	100	100	100	100	100
678125 ^678126	ins_-_G	*csiR* (PVLB_22555) (carbon starvation induced regulator)	-	95	97.5	93.2	92.6	98.9
4610697 ^4610698	ins_-_C	*dnaJ* (PVLB_03450) (molecular chaperone)	-	-	96.1	-	-	-
469675	SNV_T_C (L40S)	*hmfT1*	-	-	-	100	-	-
3379357-3379359	del_CTT_-	*infC* (PVLB_08890) (translation initiation factor IF-3)	-	-	-	83.7	98	94.2
470053	SNV_G_C (G166A)	*hmfT1*	-	-	-	-	100	100

Contrary to our hypothesis that we would discover mutations responsible for activating or enhancing a native uptake system or disabling an HMFA efflux machinery, sequencing revealed unexpected mutations in genes at first glance unrelated to cellular import or export processes (Table 2.2-1). All five evolved strains exhibited a single nucleotide variant in the ATP-dependent specificity component of the *clpAP* protease (*clpA*) leading to an R396W amino acid exchange in the corresponding protein. The ClpAP complex was previously reported to be involved in the regulation of lipopeptide biosynthesis in *P. fluorescens* (Song et al., 2015). Lipopeptides are versatile secondary metabolites that participate in critical cellular processes, including swarming motility and biofilm formation, among others (Raaijmakers et al., 2010). As biosurfactants, they have the ability to modify the cell surface, potentially influencing the properties of HMFA transport in the evolved strains. Second, a nucleotide insertion was found towards the end of the gene encoding the carbon starvation induced regulator CsiR which extends the corresponding protein by 246 amino acids due to a frame shift. This alteration probably influences folding and most likely renders the protein non-functional. CsiR is relatively well-characterized and known to act as transcriptional repressor for the *csiD-ygaF-gab* operon in *E. coli* (Metzner et al., 2004). However, there was no obvious link to furanic compound degradation, membrane modification, or cellular transport systems. The third common mutation concerns *hmfE* which is part of the integrated *hmf*-cluster. The deletion occurring at the terminal region of the gene changes the last three amino acids of the encoded protein and simultaneously extends the polypeptide by two amino acids. According

to the currently accepted HMF degradation pathway, HmfE is responsible for the hydrolysis of the final intermediate 2-oxo-glutaroyl-CoA to α-KG which is funneled into the TCA cycle (Koopman et al., 2010b). Since this reaction could also take place spontaneously and the mutation's influence on the protein level is marginal, this genomic locus was not considered important.

The faster growth of the second generation ALE strains on HMFA, as compared to TL_626 and TL_627, could be related to a three base pair deletion in the translation initiation factor *infC*. Due to the deletion of the bases CTT, which constitute a codon, the resulting protein is deficient in a single amino acid, specifically K77. This seems to be a minor variation but the respective residue could play a crucial role in maintaining the protein's proper functioning. InfC participates in the initiation of protein biosynthesis highlighting the potential for a mutation in this gene to have widespread effects, but there is also no explicit relationship to the cellular HMFA uptake properties (Butler et al., 1986). Mutations in this gene are possibly rather related to the ALE method in general, as the locus is commonly affected by evolutionary experiments (Conrad et al., 2011). Frequent re-inoculation from stationary phase cells favors cells that start re-growing sooner, which might be, among others, those with faster initiation of protein synthesis. Finally, there was one genomic locus affected by the ALE experiment with a direct link to HMFA transport, namely the *hmfT* transporter itself. In contrast to TL_626 and TL_627, which retained the wild-type configuration, the second-generation ALE strains each exhibited a point mutation resulting in a single amino acid substitution, either L40S or G166A (Table 2.2-1). Interestingly, the differences in the transporter gene directly correlated with the growth behavior on FDCA. The original transporter variant enabled TL_626 and TL_627 to grow similarly to the unevolved strain and to obtain comparable final cell densities. In sharp contrast, TL_666 (HmfT^{L40S}) displayed accelerated growth, albeit achieving a lower final g-value of approximately 60. The other two second-generation ALE strains, TL_671 and TL_676 (HmfT^{G166A}), exhibited severe growth impairments with a final g-value slightly above 50 (Fig. 2.2-4D). These results confirmed FDCA as an alternative substrate of HmfT and suggest that the observed mutations likely have a detrimental effect on the transporter's affinity for this substrate. They further question the current model of HMFA metabolization. Our previous research demonstrated that the aldehyde intermediate FFA can exclusively undergo oxidation to FDCA in the periplasmic space through the action of PaoEFG, rather than being oxidized by the cytoplasmic dehydrogenase AldB-I (2.1.). However, the subsequent decarboxylation of the dicarboxylic acid by HmfF definitely occurs inside the cell. Consequently, impaired FDCA uptake should also negatively affect HMFA assimilation. Surprisingly, this was not the case, as demonstrated by the ability of TL_671 and TL_676 to

readily grow on HMFA despite showing lower growth rates on FDCA (Fig. 2.2-4A and D). This contradiction cannot be resolved at the moment and requires further research, for example reverse engineering as next step for further elucidation of the individual mutations and their genotype-phenotype relationship.

2.2.3.5. Evolved and tolerance-engineered GRC1 PVLB_23545-40::P_{tac}_*hmfFGABCDEHT* (TL_666 BOX-C/P) strains display superior growth on HMF compared to the native degrader *Paraburkholderia caribensis*

Despite improved HMFA assimilation, the evolved strains could only grow with low concentrations of HMF due to aldehyde stress which comes into play as an additional factor in this context. We previously showed that this problem could be mitigated through targeted tolerance engineering (2.1.). For this, aldehyde conversion as main tolerance factor was enhanced by overexpression of HMF-oxidizing enzymes. The same process was applied to the evolved strain TL_666. Using previously constructed pSNW2-based plasmids (2.1.), promoters of the *paoEFGHI* operon and the *aldB-I* gene were exchanged to P_{14f} via double-strand breaks and targeted homologous recombination-mediated repair resulting in a new set of BOX-strains (Boosted OXidation). In a first round, this yielded the variants TL_666 BOX-P2, TL_666 BOX-C1, and TL_666 BOX-C2. Subsequently, strains with a double promoter exchange, TL_666 BOX-C1P2 and TL_666 BOX-C2P2, were also generated (for nomenclature refer to (2.1.)). Similar to preceding experiments, where HMF was added as a stressor, the promoter exchanges led to a considerable tolerance increase when the aldehyde served as a carbon source. While the unmodified ALE strain TL_666 could not grow at all during the observation period, TL_666 BOX-P2 with an overexpressed periplasmic aldehyde oxidoreductase PaoEFG managed to metabolize 20 mM HMF in about 30 h. The counterpart TL_666 BOX-C2 with an overexpressed cytoplasmic dehydrogenase AldB-I showed a longer lag phase, but still grew slightly better than *Paraburkholderia caribensis*. TL_666 BOX-C1, like its parental strain, did not show any growth (Fig. 2.2-5A). Despite the improvement in growth for TL_666 BOX-P2 and TL_666 BOX-C2, our expectations for further enhancement using strains with both promoter exchanges were not met: TL_666 BOX-C1P2 and TL_666 BOX-C2P2 behaved similar to TL_666 BOX-P2 (Fig. 2.2-5A). Nevertheless, the TL_666 BOX-strains represent a significant step forward. They clearly outperformed the *Paraburkholderia caribensis* reference, rendering them highly suitable candidates, for instance, for the efficient removal of the toxic fermentation inhibitor HMF from lignocellulosic hydrolysates. Additionally, they could function as screening platform for elevated or new enzyme activities. Their high potential became even more evident when the aldehyde concentration was increased to

30 mM. Under these conditions, only the TL_666 BOX-derivatives were able to grow (Fig. 2.2-5B). In contrast, the evolved *P. putida* KT2440 mutant, previously published by Guarnieri *et al.*, was just fed a maximum concentration of 1 g L^{-1} corresponding to a molar concentration of about 8 mM HMF (Guarnieri et al., 2017).

A series of control experiments with less challenging carbon sources was conducted to assess any potential side effects resulting from the promoter exchanges. Growth on HMFA, the substrate employed in the ALE experiment, and FDCA remained unaffected following the modification of the promoter regions (Fig. 2.2-5C and E). All strains with increased expression of the *paoEFGHI* operon grew even better on the central pathway intermediate FA as compared to TL_666 (Fig. 2.2-5D). One explanation for this could be a positive impact resulting from an increased level of the chaperone PaoH. Following the initial activation of FA to 2-furoyl-CoA, the second step in the degradation pathway involves the hydroxylation of the aromatic ring by the enzyme complex HmfABC, which like PaoEFG belongs to the xanthine dehydrogenase family. Therefore, its activity also relies on a molybdopterin cofactor, which needs to be inserted into the apoprotein. It is possible that PaoH also facilitates this incorporation process. If this hypothesis is true, though, we should also observe a positive effect on growth when utilizing other furanic compounds, unless this effect is masked by other growth-limiting factors. Finally, growth on standard substrates glucose and glycerol, typically used for oxidation assays, was tested. Especially in the case of glycerol, the intensified overexpression of *aldB-I* with an additional BCD2 element (TL_666 BOX-C2 and TL_666 BOX-C2P2) led to growth deficits probably due to aggravated metabolic burden (Fig. 2.2-5F and G). The significantly slower growth of the evolved strains on glycerol in general represents an unforeseen and undesirable outcome and must be taken into account when using these mutants for further experiments.

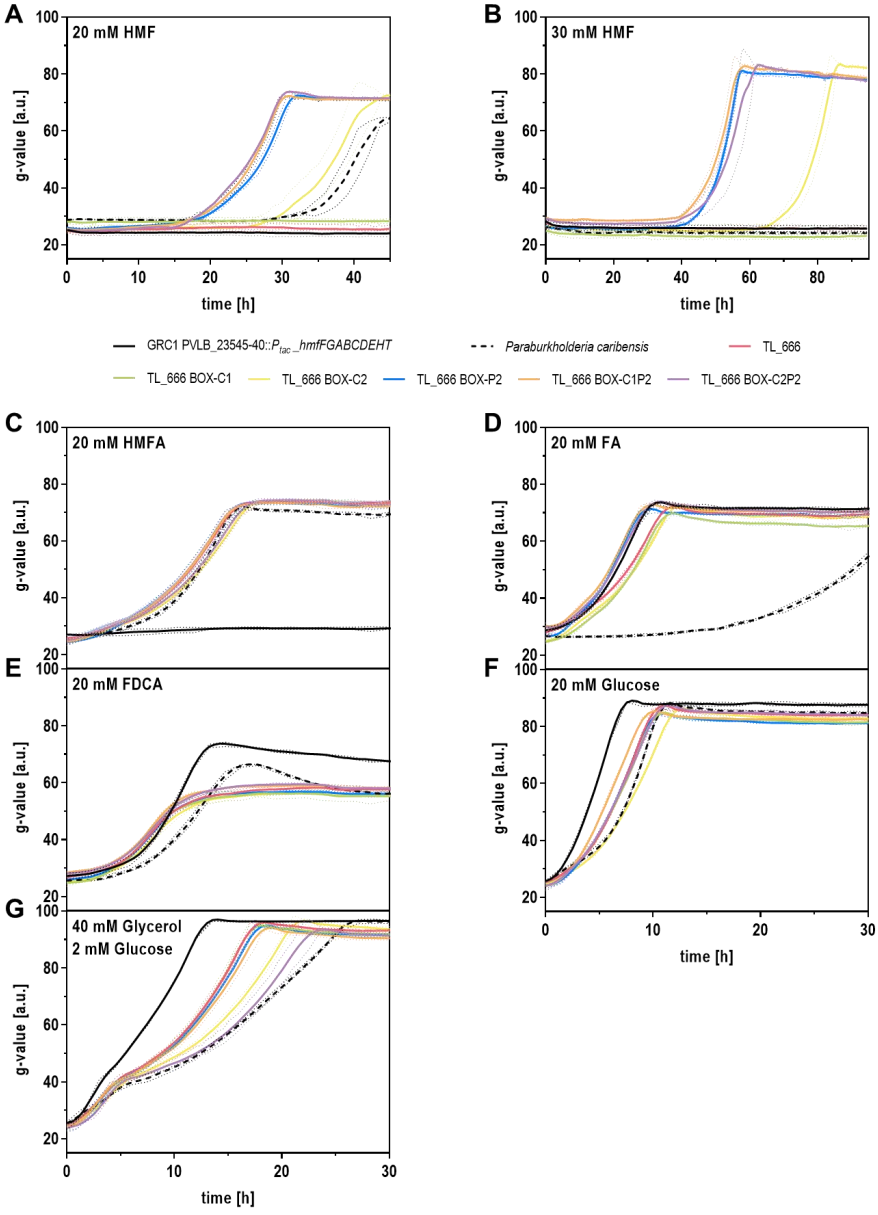

Figure 2.2-5: BOX-derivatives of the evolved strain TL_666 show a high tolerance towards HMF, when utilizing the aldehyde as sole carbon and energy source. Two-fold buffered MSM supplemented with 20 mM HMF (**A**), 30 mM HMF (**B**), 20 mM HMFA (**C**), 20 mM FA (**D**), 20 mM FDCA (**E**), 20 mM glucose (**F**), or 40 mM glycerol and 2 mM glucose (**G**) was inoculated with BOX-mutants of the evolved strain TL_666 (refer to the legend for color-coding), the parent strain GRC1 PVLB_23545-40::*Ptac_hmfFGABCDEHT* (black), and *Paraburkholderia caribensis* (black, dashed) to an OD_{600} of 0.1. Two precultures, one using LB and the second using MSM supplemented with 20 mM glucose were conducted. Cells were cultivated in a Growth Profiler in 96-well microtiter plates. The growth curves result from a second-order smoothing to the mean values obtained from three replicates. The dots represent the standard deviation.

2.2.4. Conclusion

P. taiwanensis VLB120 and *P. putida* KT2440 are robust bacteria which can effectively manage stress caused by the emerging renewable bio-based platform chemical HMF through conversion of the toxicant to the less harmful carboxylic acid. This study highlights the earlier established thesis that periplasmic oxidation is crucial for the detoxification and provides additional evidence for the significance of the previously identified HMF-oxidizing enzymes PaoEFG and AldB-I(I) for aromatic aldehyde tolerance in a broader context. Growth analyses with either 4-hydroxybenzaldehyde or vanillin as sole carbon source revealed that the substrate scope of the periplasmic aldehyde oxidoreductase PaoEFG, which so far was only experimentally proven to include HMF and FFA extends beyond furanic aldehydes. Additional ALDHs such as Vdh and AldB-I(I) play a role when aldehydes occur in the cytoplasm. This is the case when the bacterium cannot completely keep the toxicant outside, as observed for HMF, or when aldehydes are formed as intermediates of catabolic pathways, such as in the degradation of ferulate. By clarifying the initial oxidative step in the degradation pathway of 4-hydroxybenzaldehyde and vanillin, the microbial production of these aromatic aldehydes or derived products thereof with *P. taiwanensis* VLB120 or *P. putida* KT2440 can now be envisioned.

Moreover, another example of the importance of PaoEFG and AldB-I for HMF tolerance was provided by engineering *P. taiwanensis* GRC1 to utilize this aldehyde as sole carbon and energy source. The metabolization of furanic compounds was enabled by genomic integration of the *hmf*-cluster from the native degrader *Paraburkholderia caribensis*. Unexpectedly, this did not lead directly to growth with HMF and HMFA, instead requiring a subsequent prolonged ALE. One of the evolved strains was finally optimized for HMF catabolism by overexpression of the two HMF-oxidizing enzymes. The modified strains could grow with up to 30 mM HMF and were therefore shown to be significantly more tolerant than *P. caribensis* whose growth was fully impaired at this concentration.

2.2.5. Materials and methods

2.2.5.1. Strains and culture conditions

All strains used in this study are listed in Table S1. *Paraburkholderia caribensis* DSM 13236 was obtained from the DSMZ (Braunschweig, Germany). Bacteria were routinely cultivated in LB medium (10 g L^{-1} peptone, 5 g L^{-1} sodium chloride, and 5 g L^{-1} yeast extract) or on solid LB (1.5% agar) (Carl Roth, Karlsruhe, Germany). Growth experiments were executed in buffer-adjusted MSM (one-fold concentrations: 22.3 mM K_2HPO_4 and 13.6 mM NaH_2PO_4) according

to Hartmans *et al.* (Hartmans et al., 1989) which was supplemented with the respective carbon source as indicated for each experiment (MSM plates contained 1% agar). *Pseudomonas* was incubated at 30 °C and *E. coli* at 37 °C. Liquid cultures in shake flasks or plastic tubes were performed in a horizontal rotary shaker (Kuhner Shaker, Herzogenrath, Germany) with a humidity of 80%, a throw of 50 mm, and a frequency of 200 rpm. Parallelized analysis of various strains was carried out in a Growth Profiler 960 (Enzyscreen, Heemstede, The Netherlands) realizing online growth measurements through image analysis of cultures in 96-well microtiter plates with transparent bottoms (CR1496dg). The g-values obtained (based on green pixel counts) correlate with the optical density of a cell culture, allowing for qualitative evaluations. Due to dependency on cell shape and size, which can vary with different stressor concentrations requiring a separate calibration for each condition, g-values were not converted into OD_{600}. For cultures in the 96-well format a volume of 200 µL, a temperature of 30 °C and a shaking speed of 225 rpm with an amplitude of 50 mm was used. The interval between two photos taken for growth analysis was 30 minutes. Irgasan (25 mg L^{-1}) was used for isolation of *Pseudomonas* after mating procedures. For selection of genomic recombination events and plasmid maintenance, kanamycin sulfate (50 mg L^{-1}) and gentamycin sulfate (20 mg L^{-1}) were employed. All chemicals used in this study were purchased from Sigma-Aldrich (St. Louis, MO, USA), Carl Roth (Karlsruhe, Germany), Merck (Darmstadt, Germany) or Biosynth (Bratislava, Slovakia).

2.2.5.2. Whole genome sequencing

Genomic DNA to be sequenced was extracted using the Monarch® Genomic DNA Purification Kit (New England Biolabs, Ipswich, MA, USA). DNA concentrations were determined with a Qubit 2.0 fluorometer (Thermo Fisher Scientific, Waltham, MA, USA) and 1 µg of DNA was used for library preparation carried out with the NEBNext® Ultra™ II DNA Library Prep Kit for Illumina® (New England Biolabs, Ipswich, MA, USA). The library was evaluated by qPCR using the KAPA library quantification Kit (PEQLAB, Erlangen, Germany). Following normalization for pooling, paired-end sequencing with a read length of 2 × 150 bases was conducted on a MiSeq system (Illumina, San Diego, CA, USA). The sequencing output (base calls) were obtained as demultiplexed fastq files. Data processing (e.g. trimming, mapping, coverage extraction) was performed with the CLC Genomic Workbench software (QIAGEN Aarhus A/S, Aarhus, Denmark). Reads were mapped against an adapted version of the *P. taiwanensis* VLB120 genome containing the *hmf*-cluster. The identified mutations were manually evaluated for their significance.

2.2.5.3. Plasmid cloning and strain engineering

The standard method for plasmid construction was Gibson assembly (Gibson et al., 2009) which was performed with the NEBuilder HiFi DNA Assembly kit (New England Biolabs, Ipswich, MA, USA). Alternatively, a restriction/ligation approach was utilized in case of modification of large integrative plasmids for *hmf*-cluster implementation. Primers were acquired as unmodified DNA oligonucleotides from Eurofins Genomics (Ebersberg, Germany). Amplicons for cloning purposes were generated with Q5 High-Fidelity Polymerase (New England Biolabs, Ipswich, MA, USA). For large fragments, Platinum SuperFi II DNA Polymerase (Thermo Fisher Scientific, Waltham, MA, USA) was used. Restriction enzymes were purchased from New England Biolabs (Ipswich, MA, USA). Plasmid DNA and PCR amplicons were purified with the Monarch® Plasmid Miniprep Kit and Monarch® PCR & DNA Cleanup Kit, respectively (New England Biolabs, Ipswich, MA, USA). All plasmids were verified by Sanger sequencing. Summaries of oligonucleotides and plasmids used in this study are provided in Table S2 and Table S3. *E. coli* was transformed with DNA assemblies and purified plasmids by electroporation using a GenePulser Xcell (BioRad, Hercules, CA, USA) (settings: 2 mm cuvette gap, 2.5 kV, 200 Ω, 25 µF) or applying a standard heat shock protocol (New England Biolabs, Ipswich, MA, USA). Cloned plasmids, deletions, and integrations, were mapped by colony PCR employing the OneTaq 2X Master Mix with Standard Buffer (New England Biolabs, Ipswich, MA, USA). An additional cell lysis step in alkaline polyethylene glycol increased efficiencies according to Chomczynski and Rymaszewski (Chomczynski and Rymaszewski, 2006). For seamless genomic modifications, the I-SceI-based system developed by Martínez-García and de Lorenzo (Martinez-Garcia and de Lorenzo, 2011) was utilized as described previously. For knockouts, the 500 bp upstream and downstream flanking regions of the target (TS1 and TS2) were cloned between the two I-SceI restriction sites of pSNW2 or pEMG and the resulting plasmid was conjugationally transferred from *E. coli* PIR2 to the intended *Pseudomonas* recipient strain via mating procedures according to Wynands et al. (Wynands et al., 2018). Analogously, the integration of the *hmf*-cluster was carried out with a plasmid having the respective DNA section inserted between the TS-sites. Three clones were randomly selected for transformation with I-SceI-encoding plasmid pSW-2 triggering the second homologous recombination event without requiring induction by 3-methylbenzoate. Correct clones were cured of pSW-2 by repeated cultivation in non-selective medium, and re-analyzed by PCR confirming pure cultures. Successful integration of heterologous genes was further verified by Sanger sequencing.

Acknowledgements

This work was supported by the German Federal Ministry of Education and Research via the project NO-STRESS [grant number 031B0852A] and by the European Union's Horizon 2020 research and innovation program via the project UPLIFT [grant agreement number 953073]. We thank R. Schruff for laboratory assistance in generating the deletion mutants of *P. putida* KT2440 and performing the plate assays.

Competing Interest Statement

The authors declare no competing interests.

Data availability

Data will be made available on request.

2.3. Improving 5-(hydroxymethyl)furfural (HMF) tolerance of *Pseudomonas taiwanensis* VLB120 by automated adaptive laboratory evolution (ALE)

Thorsten Lechtenberg, Benedikt Wynands, Moritz-Fabian Müller, Tino Polen, Stephan Noack, Nick Wierckx* (2024)

Institute of Bio- and Geosciences IBG-1: Biotechnology, Forschungszentrum Jülich, 52425 Jülich, Germany
* Corresponding author

Status: published
Metabolic Engineering Communications, 18, e00235. **10.1016/j.mec.2024.e00235**
(The version shown here contains minor editorial adjustments.)

CrediT authorship contribution statement:

T. Lechtenberg: Investigation, Writing - Original Draft, Writing - Review and editing, Visualization, Validation.

B. Wynands: Writing - Review and editing, Conceptualization, Supervision.

M.-F. Müller: Investigation, Visualization, Validation.

T. Polen: Resources, Investigation.

S. Noack: Writing - Review and editing, Resources, Methodology, Conceptualization

N. Wierckx: Writing - Review and editing, Conceptualization, Supervision, Funding acquisition, Project administration.

Overall contribution: 75%

The presented experimental work was conducted by TL, with support from MM for robotics-assisted ALE and TP for genome sequencing. Visualization and validation was done by TL and MM. BW acted as direct scientific advisor assisting with planning and evaluation of experiments. SN provided the robotics platform. The entire project was led and supervised by NW. TL wrote the original draft which was reviewed and edited by BW, SN, and NW. Funding for the project was acquired by NW.

2.3.1. Abstract

The aldehyde 5-(hydroxymethyl)furfural (HMF) is of great importance for a circular bioeconomy. It is a renewable platform chemical that can be converted into a range of useful compounds to replace petroleum-based products such as the green plastic monomer 2,5-furandicarboxylic acid (FDCA). However, it also exhibits microbial toxicity for example hindering the efficient biotechnological valorization of lignocellulosic hydrolysates. Thus, there is an urgent need for tolerance-improved organisms applicable to whole-cell biocatalysis. Here, we engineer an oxidation-deficient derivative of the naturally robust and emerging biotechnological workhorse *P. taiwanensis* VLB120 by robotics-assisted adaptive laboratory evolution (ALE). The deletion of HMF-oxidizing enzymes enabled for the first time evolution under constant selection pressure by the aldehyde, yielding strains with consistently improved growth characteristics in presence of the toxicant. Genome sequencing of evolved clones revealed loss-of function mutations in the LysR-type transcriptional regulator-encoding *mexT* preventing expression of the associated efflux pump *mexEF-oprN*. This knowledge allowed reverse engineering of strains with enhanced aldehyde tolerance, even in a background of active or overexpressed HMF oxidation machinery, demonstrating a synergistic effect of two distinct tolerance mechanisms.

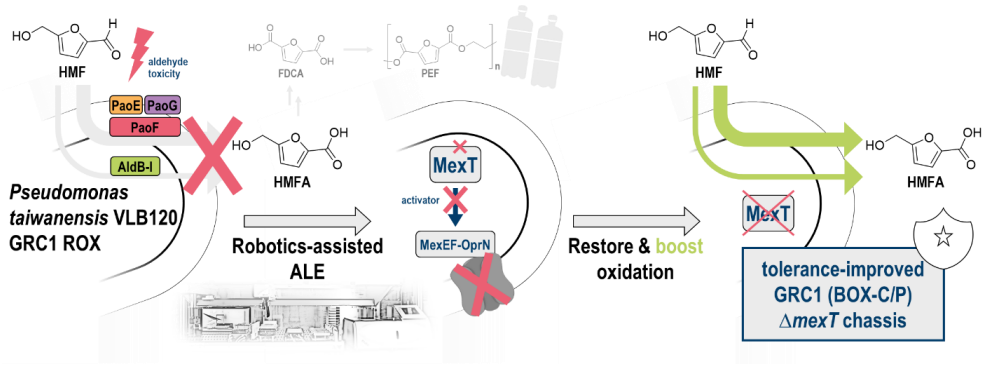

Keywords: 5-(hydroxymethyl)furfural (HMF); Adaptive laboratory evolution (ALE); *Pseudomonas;* Aldehyde stress; MexT; MexEF-OprN

Highlights:

- Robotics-assisted ALE in presence of HMF without interfering conversion.
- New and unforeseen mechanism of furanic aldehyde tolerance.
- Disruption of HMF-responsive regulator MexT prevents *mexEF-oprN* expression.
- Previously tolerance-enhanced BOX strains are further improved by *mexT* deletion.

2.3.2. Introduction

Climate change is progressing rapidly and earth's fossil resources are dwindling fast thereby urgently suggesting a switch to more sustainable technologies like microbial biocatalysis with renewable carbon sources (de Lorenzo, 2022, Ragauskas et al., 2006). Particular potential as future feedstock is assigned to lignocellulosic biomass, non-edible plant waste material. However, rendering the locked sugars available to enzymes and microbes requires harsh pretreatment (Brethauer and Studer, 2015, Galbe and Wallberg, 2019, Prasad et al., 2023). This process typically involves mechanical grinding, heating and acidification resulting in the formation of unwanted by-products, so-called lignocellulose-derived microbial inhibitory compounds (LDMICs), e.g. phenolic aldehydes and acids (Ujor and Okonkwo, 2022). Especially under acidic conditions, pentoses and hexoses dehydrate to form the highly reactive and toxic furanic aldehydes furfural and 5-(hydroxymethyl)furfural (HMF) (Almeida et al., 2009, Jonsson and Martin, 2016). Their electrophilicity, caused by the polarity of the carbonyl function, makes them an easy target for all kinds of nucleophiles, among others, amino or thiol functionalities of proteins or DNA crosslinking the biological macromolecules and leading to malfunctions (Jayakody et al., 2018, Lee and Park, 2017, LoPachin and Gavin, 2014). As LDMICs prevent the efficient production of chemicals from biomass by non-tolerant microorganisms, they have to be removed in a laborious and costly manner prior to fermentation or avoided entirely through complex processes (Ujor and Okonkwo, 2022, Wang et al., 2020a). Alternatively, this problem can be bypassed utilizing robust microbial species that display higher tolerance to the inhibitors (Jonsson et al., 2013).

Non-pathogenic soil-dwelling Pseudomonads like *P. taiwanensis* VLB120 can readily cope with various toxicants, most notably aromatics (Kohler et al., 2013, Volmer et al., 2014, Wynands et al., 2019). In addition, this emerging host for biotechnological applications convinces with its natural resilience to other compounds including aldehydes (Blombach et al., 2022, Wordofa and Kristensen, 2018). Recently, it was demonstrated that this tolerance mainly stems from the organism's ability to rapidly oxidize HMF to the less noxious carboxylic acid (Xu et al., 2020b). This process predominantly occurs in the periplasmic space avoiding damage inside the cell (2.1.). Moreover, it was found that the tolerance could be increased by promoting oxidation through overexpression of the responsible enzymes in a genome-reduced chassis (GRC1) resulting in improved BOX (Boosted OXidation) strains (2.1.) (Wynands et al., 2019). However, conversion as tolerance mechanism has its limitations, especially when low cell densities face high aldehyde concentrations leading to prolonged lag phases (Heer and Sauer, 2008, López et al., 2021). This is especially relevant in the context of HMF

biotransformation, where high initial substrate concentrations could simplify process operation. HMF hence plays a dual role, not only as an LDMIC but also as a promising platform chemical for a biobased chemical industry (Bozell and Petersen, 2010, Galkin and Ananikov, 2019, van Putten et al., 2013b, Xu et al., 2020a). This opens up a wide array of potential biotechnological applications for tolerance-optimized bacteria the most important one being complete oxidation of HMF to 2,5-furandicarboxylic acid (FDCA), a renewable substitute for the plastic monomer terephthalic acid (Koopman et al., 2010a, Pham et al., 2020, Troiano et al., 2020).

Adaptive laboratory evolution (ALE) provides an unbiased and natural selection process for advantageous mutations that can result in a diverse array of genetic variations. It is therefore a suitable method for microbial tolerance engineering, because this is typically a complex feature depending on numerous parameters, such as stressor-converting enzymes, energy supply, redox balance, membrane alteration, efflux pumps, and damage recovery through chaperones (Bitzenhofer et al., 2021, Dragosits and Mattanovich, 2013, Sandberg et al., 2019). Several of these factors (e.g. transporters and chaperones) are energy-dependent requiring tolerance evolution experiments to be precisely monitored and controlled (Hartl et al., 2011, Murakami et al., 2006). In order to preserve energy-consuming tolerance traits and avoid death caused by starvation in the toxic environment, cells should be permanently maintained under exponentially growing conditions, which can most effectively be achieved using a robotics platform (LaCroix et al., 2017). Automation brings further advantages including a higher passage frequency and an elevated number of possible replicates due to independency of human resources. Additionally, it leads to reduced fluctuation of inoculum density and permits real-time monitoring of culture parameters (Hirasawa and Maeda, 2023, Lee and Kim, 2020).

In this study, *P. taiwanensis* VLB120 GRC1 Δ*paoEFG* Δ*aldB-I* (GRC1 ROX, Reduced OXidation), deprived of aldehyde oxidation as its primary defense mechanism, was subjected to an automated ALE experiment. Continuous exposure of the bacterium to HMF stress yielded evolved strains with permanently increased tolerance towards the toxic aldehyde as well as to the related compound furfural. This performance advantage was attributed to loss-of-function mutations in the transcriptional regulator *mexT* identified by whole-genome sequencing and subsequent reverse engineering. Inactivation of *mexT* was shown to suppress *mexEF-oprN* expression, as a respective knockout of the efflux pump exhibited a similar phenotype. Furthermore, deletion of *mexT* was likewise beneficial in the wild type or BOX background proving an additive effect of two distinct tolerance mechanisms.

2.3.3. Results and discussion

2.3.3.1. Increasing HMF tolerance of oxidation-deficient GRC1 ROX by ALE

Hitherto, performing ALE experiments in the presence of aldehydes has been challenging due to the difficulty of maintaining a constant selection pressure. This is especially true if the investigated microorganism, as in the case of HMF oxidation by *P. taiwanensis* VLB120, promptly converts the stressor. The rapid oxidation often takes place in the span of about one microbial generation (2.1.), and thus ALE would only lead to an increased tolerance towards the corresponding 5-(hydroxymethyl)-2-furoic acid (HMFA), rather than the far more toxic aldehyde. The recent deciphering of *Pseudomonas*' enzymatic toolbox for oxidative HMF detoxification yielded the double deletion mutant GRC1 ROX, which lacks both the primary periplasmic aldehyde oxidoreductase PaoEFG as well as the supportive cytoplasmic dehydrogenase AldB-I thereby displaying drastically reduced HMF oxidation (Fig. 2.3-1A) (2.1.). In an alternative pathway, this strain can still reduce HMF to 5-(hydroxymethyl)furfuryl alcohol (HMFOH), but this process is very slow in *Pseudomonas* and can be neglected (2.1.3.2.). Therefore, GRC1 ROX was chosen for ALE, selecting for the activation of so far not expressed HMF-converting enzymes or the development of alternative tolerance traits. We hypothesized that this would help to uncover secondary aldehyde tolerance mechanisms by characterization of emerging mutations.

Due to severely reduced HMF tolerance in absence of oxidizing enzymes, growth of GRC1 ROX under various conditions was assessed in the BioLector to identify an optimal balance between high selection pressure and sufficient growth to enable ALE. Two-fold buffered minimal salt medium (MSM) containing 80 mM glycerol and 2 mM glucose as carbon sources, supplemented with HMF concentrations ranging from 4 to 5 mM, and inoculated to an OD_{600} of 0.1 was found to be suitable. These conditions ensured culture times of about one day spanning approximately six generations, pH stability, and exposure to the stressor throughout growth phase (Fig. S5.3-1). Using a dual carbon source is a common strategy for whole-cell biocatalytic conversion of HMF (Koopman et al., 2010a, Pham et al., 2020) (2.1.). Glycerol constituted the main carbon source instead of glucose to prevent acidification from gluconate formation and a small amount of the sugar was added to reduce the lag phase. Six parallel ALE experiments were performed of which three were constantly exposed to 4 mM HMF and the other three to gradually increasing concentrations from 4 mM to 6 mM HMF (Fig. 2.3-1B). The threshold for automated reinoculation of the following batch was set to a backscatter value of 40 corresponding to late exponential growth phase (Fig. 2.3-1C, Fig. S5.3-1). While the initial cultures all grew almost identically, the second batch already reached the threshold

considerably faster in five out of six cases (Fig. 2.3-1C). Despite some slower outliers, this trend continued until the end of the experiment with the final cultures requiring on average only 14.7 h to attain the target backscatter value. This was more than twice as fast as the initial cultures (Fig. 2.3-1D). No difference was observed between the two setups of constant or slightly increasing HMF concentrations. After a comparatively short ALE experiment of about one week with seven serial passages spanning approximately 40 generations, cultures with substantially improved HMF tolerance were obtained. For subsequent analysis, the cultures of well columns 7 and 8 were spread on LB agar and two single colonies isolated for each evolutionary line.

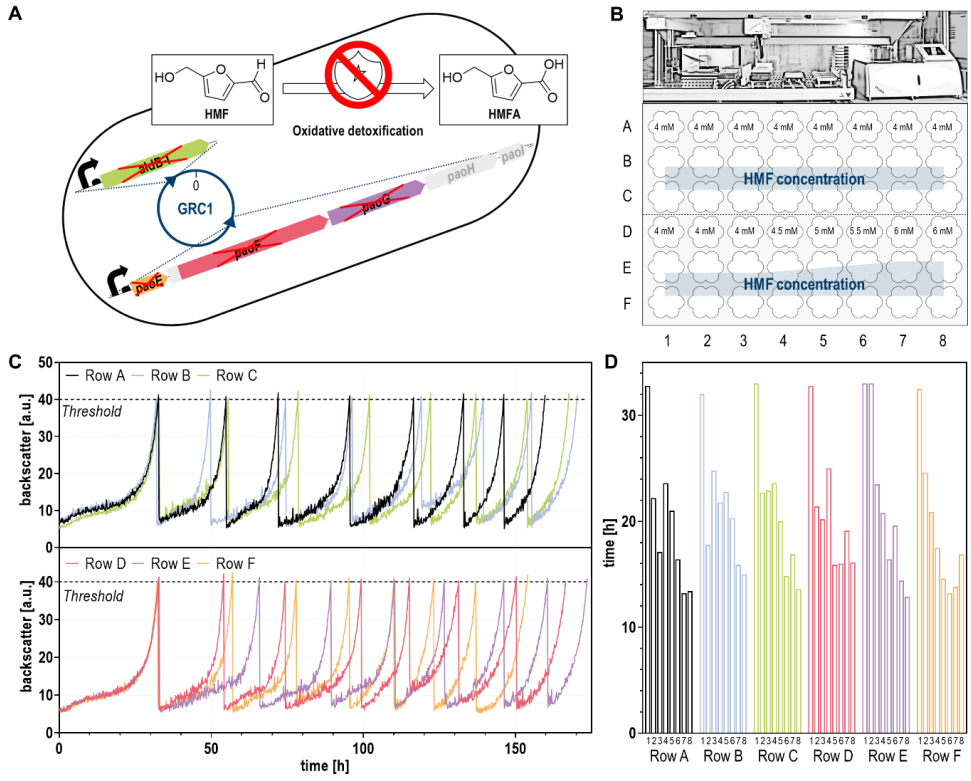

Figure 2.3-1: ALE considerably accelerated growth of GRC1 ROX in the presence of HMF. (**A**) Schematic representation of the employed oxidation-deficient starting strain, GRC1 ROX lacking PaoEFG and AldB-I. (**B**) Overview on the experimental setup. ALE was performed through automated serial passages in a 48-well FlowerPlate in a BioLector using MSM supplemented with 80 mM glycerol, 2 mM glucose and indicated HMF concentrations. Initial OD_{600} was set to 0.1 and subsequent batches were inoculated with 20 µL of the preceding culture. (**C**) Time course of the ALE experiment. Growth was monitored by scattered light intensities. Cultures were transferred to the next well, when a backscatter threshold of 40 was reached. (**D**) Elapsed time for each batch.

2.3.3.2. Characterization of evolved strains

To verify whether the enhanced bacterial fitness was due to a temporal adaptation effect or beneficial genomic mutations, the evolved strains were tested for HMF tolerance in the Growth Profiler after undergoing an intermediate culture in aldehyde-free full medium. As expected, the generated strains showed similar behavior in the absence of stress compared to both the parental deletion mutant GRC1 ROX and the original GRC1 strain with intact aldehyde oxidation machinery (Fig. 2.3-2A). Slight differences for example in the case of strain F8.1 might be explained by the putative development of an energy-demanding tolerance trait (e.g. upregulation of an efflux pump) constituting a burden in a non-stressful environment (Wynands et al., 2019). When exposed to 8 mM HMF, most ALE-derived strains outperformed unevolved GRC1 ROX, which could not grow at all under these conditions (Fig. 2.3-2B, Fig. S5.3-2).

Next, the underlying physiological mechanisms behind the improved HMF tolerance were examined. Since the evolved strains did not surpass the parental control in absence of the stressor, it was unlikely that their fitness advantage was solely a result of adaptation to the utilized MSM or glycerol as a carbon source. This was verified by assessing their growth in presence of HMF using glucose as a feedstock (Fig. 2.3-2C), where the strains showed the same tendencies as on glycerol. The evolved strains could grow on glucose with 10 mM HMF, whereas the starting strain GRC1 ROX could not (Fig. 2.3-2D). Restored oxidation ability or increased reductive detoxification was likewise excluded. *P. taiwanensis* VLB120 possesses a plethora of aldehyde oxidoreductases (2.1.) leading to the hypothesis that, due to mutations, for example, in regulatory sequences, one or more of these enzymes could potentially replace the deleted principal HMF-converting enzymes PaoEFG and AldB-I. However, HPLC analysis at the end of the tolerance assays revealed no increased oxidation or reduction rates and the ratio between acid and alcohol formation remained almost constant (Fig. 2.3-2E). The observed differences in final acid and alcohol titers could rather be associated with minor growth variations. Specifically, faster-growing strains have higher average biomass density over the whole cultivation time, leading to higher volumetric conversions (Fig. 2.3-2E, Fig. S5.3-2). Thus, the observed improvement was likely a consequence of tolerance traits different from aldehyde conversion. In contrast to that, a previously furfural-tolerance-evolved *P. putida* KT2440, with functioning aldehyde oxidation, primarily featured a better conversion performance (Zou et al., 2022). For further insights, three selected evolved strains (A7.1, E7.2, F8.1) and the unevolved reference GRC1 ROX were subjected to whole-genome resequencing.

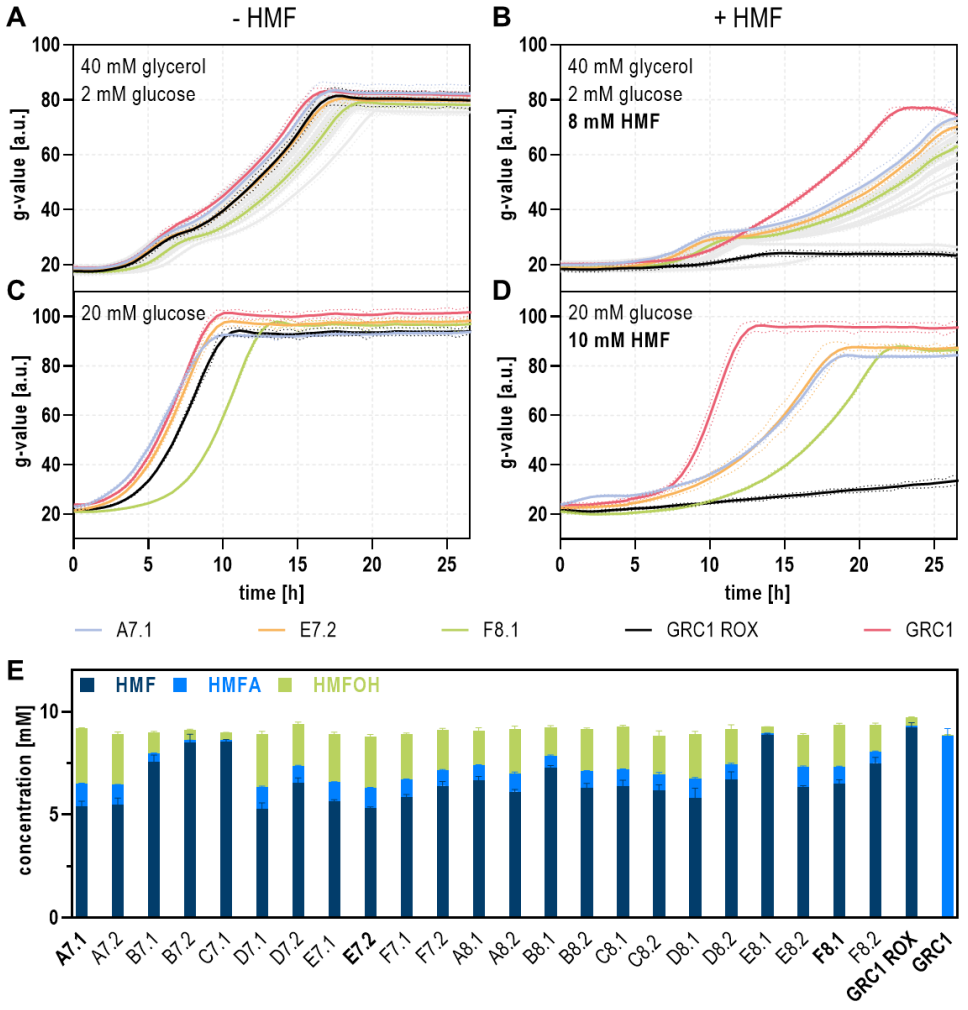

Figure 2.3-2: Analysis of isolated clones from the ALE. Growth comparison between all evolved clones (grey), the unevolved GRC1 ROX reference (black), and the oxidation-positive GRC1 (red) in absence (**A**/**C**) or presence of 8 mM (**B**) or 10 mM (**D**) HMF. Selected strains A7.1 (light blue), E7.2 (orange), and F8.1 (green) subsequently analyzed by whole-genome sequencing are highlighted by color. Cells were cultivated in a Growth Profiler in 96-well microtiter plates using two-fold buffered MSM supplemented with 40 mM glycerol and 2 mM glucose (**A**/**B**) or 20 mM glucose (**C**/**D**) as carbon sources. The initial OD_{600} of the cultures was set to 0.1. The growth curves result from a second-order smoothing to the mean values obtained from three replicates. The dots represent the standard deviation. (**E**) HPLC analysis of HMF tolerance assays with glycerol as principal carbon source (compare Fig. 2.3-2B, Fig. S5.3-2). Samples were taken after 25 h. The mean and standard deviation of three replicates is shown.

Genomic analysis uncovered only a few mutations compared to the reference sequence based on the published genome of *P. taiwanensis* VLB120 (GenBank accession number NC_022738) (Kohler et al., 2013), most of which were also present in the control strain. This

narrowed down the list of potential factors for the increased HMF tolerance to a very limited number of promising candidates (Table 2.3-1), which was anticipated given the relatively short ALE with only seven or eight consecutive cultures. Since all analyzed evolved clones showed consistent behavior in presence of the stressor, similar genomic modifications were expected. The only gene found to be modified in all evolved strains, but not in the control, was *mexT* (PVLB_13900) encoding a LysR-type transcriptional regulator (www.pseudomonas.com (Winsor et al., 2016)). Strains A7.1 and F8.1 exhibited a point mutation leading to an amino acid exchange from glycine (G) to glutamate (E) at position 231, while E7.2 had a two-base-pair deletion resulting in a frameshift and a truncated protein version (Table 2.3-1). A premature stop codon in the *tig* (PVLB_08210) gene, which encodes a trigger factor involved in protein folding (Wu et al., 2022), was not considered critical, as it was exclusive to A7.1 (Table 2.3-1). To check whether the alteration of *mexT* was responsible for the increased HMF tolerance of the evolved strains, reverse engineering of GRC1 ROX was performed. This was based on the mutation in strains A7.1 and F8.1, which was verified by PCR and Sanger sequencing.

Table 2.3-1: Selected genomic loci affected by the ALE. Abbreviations: nt, nucleotide; SNV, single nucleotide variant; del, deletion.

nt pos.	mutation	affected locus	frequency [%]			
			GRC1 ROX	A7.1	E7.2	F8.1
1845845	SNV_C_T (Q255*)	*tig* (PVLB_08210)	-	96.2	-	-
2954511	SNV_G_A (G231E)	*mexT* (PVLB_13900)	-	91.1	-	59.5
2954557	del_GG_-	*mexT* (PVLB_13900)	-	-	13.4	-

2.3.3.3. Reverse engineering

The native *mexT* gene of GRC1 ROX was replaced by *mexT*^{G231E} using the homologous recombination-based I-SceI system (Martinez-Garcia and de Lorenzo, 2011) and the growth behavior of the resulting strain was analyzed. Similar to the evolved strains and in contrast to the unevolved progenitor, the reverse-engineered GRC1 ROX *mexT*^{G231E} mutant was able to grow in presence of 8 mM HMF, whereas growth was nearly unaffected without HMF (Fig. 2.3-3). Therefore, it could be concluded that the G231E amino acid exchange in MexT was responsible for the higher HMF tolerance of the ALE strains. The underlying SNV (G to A) likely represents a null mutation considering that E7.2 alternatively harbors a two-base-pair deletion generating a frameshift (Table 2.3-1). This hypothesis was confirmed by complete deletion of *mexT*, which led to the same phenotype as observed for the point mutation

(Fig. 2.3-3B). Hence, we could prove that loss-of-function mutations in *mexT* were causal to the improved HMF tolerance.

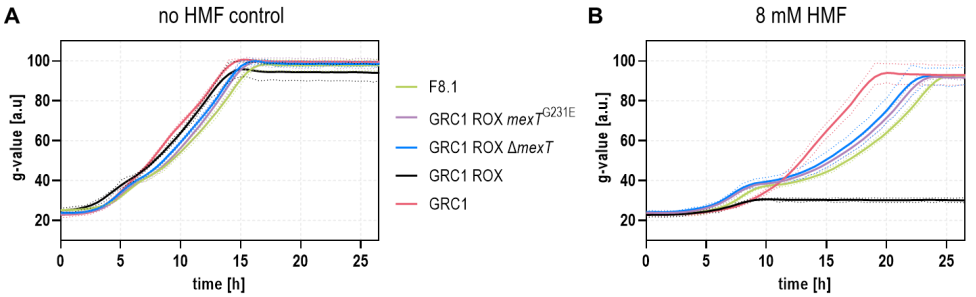

Figure 2.3-3: Characterization of reverse-engineered GRC1 ROX mutants. Two-fold buffered MSM supplemented with 40 mM glycerol and 2 mM glucose as carbon sources was inoculated with ALE strain F8.1 (green), GRC1 ROX *mexT*^{G231E} (purple), GRC1 ROX Δ*mexT* (dark blue), GRC1 ROX (black), and GRC1 (red) to an OD_{600} of 0.1. Cells were cultivated in a Growth Profiler in 96-well microtiter plates without HMF (**A**) and in presence of 8 mM HMF (**B**). The growth curves result from a second-order smoothing to the mean values obtained from three replicates. The dots represent the standard deviation.

Next, we sought to determine whether MexT inactivation would also have a beneficial effect in a strain with an intact aldehyde oxidation system, by deleting *mexT* in *P. taiwanensis* GRC1. Again, no difference between GRC1 and GRC1 Δ*mexT* was detected in absence of the stressor, but the deletion mutant showed a small growth advantage in the presence of 8 mM HMF, which became much more evident when the stressor concentration was increased to 20 mM (Fig. 2.3-4A). Under these conditions, the GRC1 strain was completely inhibited, whereas the Δ*mexT* mutant could still grow. A similar trend was observed when furfural was used as a toxicant (Fig. 2.3-4A). In accordance with previous determinations of EC_{50} values carried out with *P. putida* KT2440 (Jayakody et al., 2018), furfural had lower toxicity than HMF, and thus did not lead to a complete inhibition of the unmodified GRC1 at a concentration of 20 mM. Overall, these results confirmed that the MexT-related tolerance mechanism was compatible and even combinable with fast oxidation as *Pseudomonas*' main line of defense against furanic aldehydes.

Recently, we reported the development of oxidation-optimized BOX strains, which showed increased HMF detoxification rates through different levels of overexpression of the central periplasmic aldehyde oxidoreductase *paoEFG* and the cytoplasmic aldehyde dehydrogenase *aldB-I* (Fig. 2.3-4B) (2.1.). Even though these strains tolerate considerably higher aldehyde concentrations, this tolerance could still be further enhanced through additional deletion of *mexT*.

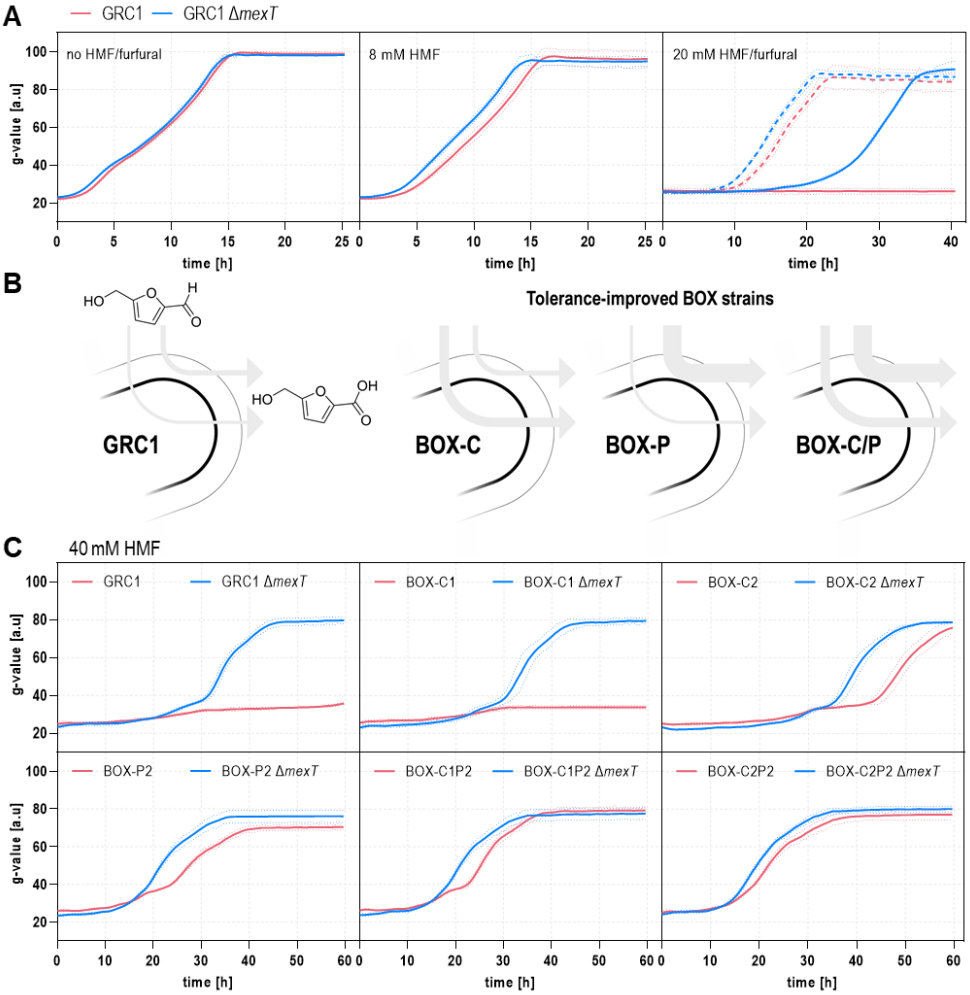

Figure 2.3-4: Deletion of *mexT* also confers a fitness advantage in strains with intact or boosted aldehyde oxidation machinery when exposed to HMF or furfural. (**A**) Growth of GRC1 (red) and GRC1 Δ*mexT* (blue) in absence of a stressor and in presence of 8 mM or 20 mM HMF (solid lines), or 20 mM furfural (dashed lines). (**B**) Overview of tolerance-improved BOX strains with increased HMF conversion in the cytoplasm, periplasm or both (2.1.). (**C**) Growth of GRC1, the BOX derivatives (red) and the respective *mexT* deletion mutants (blue) in presence of 40 mM HMF. Control experiments without stressor addition are provided in Fig. S5.3-3. All experiments were carried out in two-fold buffered MSM supplemented with 40 mM glycerol and 2 mM glucose as carbon sources and an initial OD_{600} of 0.1. Cells were cultivated in a Growth Profiler in 96-well microtiter plates. The growth curves result from a second-order smoothing to the mean values obtained from three replicates. The dots represent the standard deviation.

A new series of BOX-C/P Δ*mexT* strains were grown in presence of 40 mM HMF (Fig. 2.3-4C). Under these harsh conditions, the *mexT* knockout variants consistently grew better than the respective unmodified control without exhibiting altered HMF oxidation rates (Fig. S5.3-4). However, the relative growth advantage was more pronounced as the oxidative capacity of the

specific strain decreased, with the most substantial impact observed in the unmodified GRC1 and the only marginally improved BOX-C1 (Fig. 2.3-4C). This seems plausible, because these strains were exposed longer to high aldehyde stress, resembling the conditions during the ALE, not benefiting from improved fast periplasmic conversion. Interestingly, BOX-C2 Δ*mexT* had a longer lag phase than BOX-C1 Δ*mexT* although the parental BOX-C2 was considerably more tolerant than BOX-C1 pointing at a negative interference between the MexT-related tolerance mechanism and reinforced cytoplasmic HMF oxidation. That would also explain why the *mexT* deletion in BOX-C2P2 caused a weaker improvement than in BOX-P2 and BOX-C1P2 (Fig. 2.3-4C). On the other hand, it has also to be taken into account that BOX-C2P2 already showed a remarkable tolerance level *per se*, reducing the effect of further improvements. Considering this, it is even more notable that in the best-performing BOX strains an advancement by *mexT* deletion was still observed.

2.3.3.4. The benefit of *mexT* deletion lies in preventing *mexEF-oprN* expression

We attempted to further elucidate how inactivation of MexT mechanistically increased tolerance to furanic aldehydes. The protein is mainly characterized as transcriptional activator of the *mexEF-oprN* (PVLB_11800, PVLB_11795, and PVLB_11790) operon encoding a versatile RND-type efflux pump associated with antibiotic resistance in *Pseudomonas aeruginosa* (Juarez et al., 2018, Kohler et al., 1997, Kohler et al., 1999). In *P. aeruginosa*, *mexEF-oprN* expression is increased upon exposure to aldehydes, such as cinnamaldehyde or citral (Tetard et al., 2019, Tetard et al., 2021). However, the regulon is not restricted to the efflux pump and extends to at least 40 other targets, which is why MexT is generally more seen as redox-responsive regulator (Fargier et al., 2012, Tian et al., 2009). Recently the crystal structure of the regulatory domain of the *P. aeruginosa* homolog was elucidated, and the purified full-length protein employed in a DNase I footprinting assay to identify MexT binding sites (Kim et al., 2019). Comparing the established consensus sequence (ATCA$(N)_7$CGAT) with the upstream region of *mexEF-oprN* in *P. taiwanensis* VLB120, we also found two putative MexT binding sites suggesting a similar regulatory network in the biotechnological workhorse (Fig. S5.3-5).

We initially hypothesized that furanic compounds like HMF or furfural might also be substrates of MexEF-OprN, which could thus contribute to increased tolerance by extrusion. This was supported by the fact that all three components, MexE, MexF, and OprN, were among the most upregulated, both at the transcriptional and translational levels, when *P. putida* KT2440 was exposed to thermochemical wastewater streams containing glycolaldehyde, HMF, and furfural as main toxicants (Jayakody et al., 2018). Moreover, the efflux pump was shown to be induced

by formaldehyde and susceptibility to this aldehyde was elevated in a *mexE*-deficient background (Roca et al., 2008). However, this would have implied reverse regulation in *P. taiwanensis* VLB120 in comparison to *P. aeruginosa*, because *mexT* was actually disrupted during the ALE. Surprisingly, it was in fact the lack of activation of *mexEF-oprN* expression that was mostly responsible for the fitness advantage in the presence of HMF. This was confirmed by a GRC1 Δ*mexEF-oprN* deletion mutant, which, similar to GRC1 Δ*mexT*, could also grow in the presence of the stressor whereas no difference was observed in the control experiment without aldehyde addition (Fig. 2.3-5). In contrast to GRC1 Δ*mexT* or the double knockout GRC1 Δ*mexT* Δ*mexEF-oprN*, the growth rate appeared to be marginally reduced, especially towards the end of the growth period (Fig. 2.3-5B), indicating a slight impact of MexT beyond activation of the *mexEF-oprN* operon. This is certainly possible given the intricate MexT regulon.

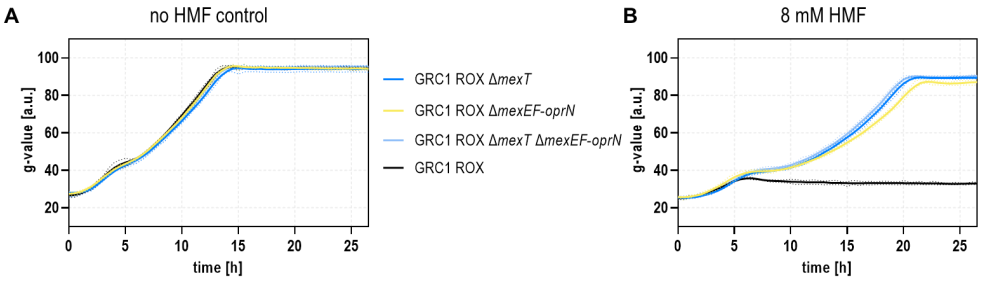

Figure 2.3-5: The main effect of MexT inactivation occurring during ALE is a shutdown of the MexEF-OprN efflux pump. Two-fold buffered MSM supplemented with 40 mM glycerol and 2 mM glucose as carbon sources was inoculated with GRC1 ROX Δ*mexT* (dark blue), GRC1 ROX Δ*mexEF-oprN* (yellow), GRC1 ROX Δ*mexT* Δ*mexEF-oprN* (light blue), and GRC1 ROX (black) to an OD_{600} of 0.1. Cells were cultivated in a Growth Profiler in 96-well microtiter plates without HMF (**A**) and in presence of 8 mM HMF (**B**). The growth curves result from a second-order smoothing to the mean values obtained from three replicates. The dots represent the standard deviation.

An adverse effect of MexEF-OprN was not expected, but might be explained as follows: First, HMF could be an extremely strong effector molecule, resulting in MexT-mediated expression levels of *mexEF-oprN* which are high above a useful amount, only harming the cells through severe fitness costs of overexpressed transporter proteins (Du Toit, 2017). As RND-type efflux systems are proton antiporters, an increased efflux pump concentration likely disturbs proton potential gradient (Olivares et al., 2014). Moreover, it is possible that HMF is actually secreted by MexEF-OprN, but can diffuse back into the cell even faster, thereby generating a futile cycle of export and uptake, which again would only be a waste of energy. This kind of negative impact of a highly expressed efflux pump has already been discussed for the solvent efflux pump TtgGHI with regard to phenol tolerance (Wynands et al., 2019). Based on the role of

MexT and MexEF-OprN in *P. aeruginosa,* a third possible explanation came up. It has been reported that MexEF-OprN could modulate quorum sensing through secretion of a signaling molecule belonging to the HAQ (4-hydroxy-2-alkylquinolines) family (Lamarche and Deziel, 2011). Although most publications focus on the influence of quorum sensing on virulence factors of *P. aeruginosa*, not relevant for *P. taiwanensis* VLB120, the bacterial signaling system could also be very important for tolerance mechanisms (Luong et al., 2014, Oshri et al., 2018). It is conceivable, for example, that the natural response of *P. taiwanensis* VLB120 to HMF stress is biofilm formation as protection against the toxicant. That would mean that the cells sense the toxic aldehyde (possibly through MexT) and retard growth until it is removed by oxidative conversion. As the GRC strains are deprived of the ability to form biofilms, this signaling cascade may be disturbed in our strains. Consequently, the bacteria keep up the precaution to not grow in presence of the stressor, although they could handle a moderate HMF concentration even without biofilm formation. The MexT inactivation might release this protective brake, but more experiments are necessary to gain further insights into the influence of quorum sensing on HMF tolerance.

2.3.4. Conclusion

Throughout evolution, microorganisms have encountered a diverse array of environmental conditions and effectively adapted to them. Nevertheless, employing even very robust bacteria such as *P. taiwanensis* VLB120 under industrial conditions represents a particular challenge (Blombach et al., 2022, Tan et al., 2022). We could improve tolerance of this promising biotechnological workhorse towards the increasingly important bio-based platform chemical HMF by a robotics-assisted ALE. This was enabled by taking two steps back: The rapid oxidation of furanic aldehydes to the less harmful acid derivatives was avoided by using the reduced oxidation mutant GRC1 ROX (2.1.). We obtained considerably enhanced strains whose elevated tolerance was a result of a mechanism different from fast conversion, which is an interesting feature especially for biosynthetic endeavors where aldehydes occur as products or important intermediates (Bayer et al., 2017, Kunjapur and Prather, 2015, Narcross et al., 2016). The uncovered *mexT* disruption and associated MexEF-oprN repression were foundational for the increased HMF tolerance in a counter-intuitive fashion, considering that efflux pumps constitute a well-established mechanism for solvent tolerance and antibiotic resistance (Bitzenhofer et al., 2021, Henderson et al., 2021, Li et al., 2015). The *mexT* deletion could be synergistically combined with boosted oxidation in engineered BOX mutants (2.1.) to further enhance HMF tolerance. This marks another step forward in the pursuit of generating an ideal chassis for whole-cell biocatalytic production of renewable plastic building block FDCA

from HMF (Cui et al., 2023). With regard to a potential application of the improved strains as robust hosts for fermentative exploitation of lignocellulosic hydrolysates, future work will need to determine if LDMICs other than HMF and furfural, such as glycolaldehyde, or for example vanillin or *p*-hydroxybenzaldehyde derived from lignin depolimerization, are similarly well-endured (Hu et al., 2022, Jayakody et al., 2022). Additionally, it would be interesting to test how the engineered strains perform in the simultaneous presence of multiple stressors, some of which, unlike the furanic aldehydes HMF and furfural, may be better tolerated with a functional MexEF-OprN efflux pump.

2.3.5. Materials and methods

2.3.5.1. Strains and culture conditions

Chemicals used in this study were purchased from Sigma-Aldrich (St. Louis, MO, USA), Carl Roth (Karlsruhe, Germany), or Merck (Darmstadt, Germany) unless stated otherwise. Bacteria (refer to Table S1 for a list of all strains used in this study) were routinely cultivated in LB medium containing 10 g L^{-1} peptone, 5 g L^{-1} sodium chloride, and 5 g L^{-1} yeast extract or on solid LB with additional 15 g L^{-1} agar (Carl Roth, Karlsruhe, Germany). To isolate *Pseudomonas* strains following mating procedures irgasan (25 mg L^{-1}) was supplemented. Growth experiments were performed using buffer-adjusted MSM (one-fold concentrations: 22.3 mM K_2HPO_4 and 13.6 mM NaH_2PO_4) according to Hartmans *et al*. (Hartmans et al., 1989) with a mixture of glycerol (40 mM) and glucose (2 mM) as carbon sources unless stated otherwise. The use of glycerol prevented medium acidification due to gluconate formation resulting from *Pseudomonas*' preference for metabolizing glucose via the Entner–Doudoroff pathway (Chavarría et al., 2013). This is important for all experiments involving HMF whose oxidative detoxification to HMFA can also lead to pH drop. Nevertheless, a low concentration of glucose was beneficial preventing an extensive lag phase. For the selection of genomic recombination events and plasmid maintenance, kanamycin sulfate (50 mg L^{-1}) and gentamycin sulfate (20 mg L^{-1}) were employed. *E. coli* was cultivated at 37 °C and *Pseudomonas* at 30 °C. Liquid cultures in shake flasks were incubated in a horizontal rotary shaker (Kuhner Shaker, Herzogenrath, Germany) with a humidity of 80%, a throw of 50 mm, and a frequency of 200 rpm. For cultures in 24-deepwell microplates (System Duetz), the frequency was raised to 300 rpm. High-throughput strain characterizations were performed with a Growth Profiler 960 (Enzyscreen, Heemstede, The Netherlands) allowing online growth measurements through image analysis of cultures in 96-well microtiter plates with transparent bottoms (CR1496dg). The resulting g-values (based on green pixel counts) correlate with the optical density of a cell culture, providing sufficient data for qualitative assessments. G-values

were not converted into OD_{600}, because calibrations hinge on cell shape and size, factors that may vary with different stressor concentrations, therefore requiring adjustments for each specific condition. Cultures in the 96-well format were conducted with a volume of 200 µL at 30 °C and 225 rpm shaking speed with an amplitude of 50 mm. The time gap between two photos used for growth analysis was 30 min. An overview of the growth parameters of all shown experiments is given Table S5.3-1. Whole-cell HMF bioconversion assays in 24-deepwell microplates (System Duetz) were carried out as described previously (2.1.5.5.).

2.3.5.2. Robotics-assisted ALE

The ALE experiments were done on a Mini Pilot Plant covering a JANUS® liquid handler (PerkinElmer, Waltham MA, USA) and a BioLector I® (Beckmann Coulter Life Sciences, CA, United States). Repetitive batch cultivations were performed in 48-well FlowerPlates® (Beckmann Coulter Life Sciences, CA, United States) of the category BOH-1 (with optodes). All BioLector cultures were performed at 30 °C, shaking frequency of 1200 rpm, humidity of 85% and oxygen-ratio of 20.95% (air). Biomass (gain 20), pH and pO_2 filters were used to monitor the growth progress. All media for the consecutive batches were stored sterile in a plate at room temperature on the deck of the platform and sealed with non-woven, gas-permeable sealing foil to minimize evaporation. The execution of the ALE was controlled by the Beckman RoboLection software, using the backscatter signal of the current batch as a trigger. When the culture reached a backscatter value of 40, a new batch was started so that the liquid handler pipetted 20 µL of the actual batch as inoculum and 780 µL of the specifically stored medium from the plate in an empty well.

2.3.5.3. Whole-genome sequencing

Genomic DNA for sequencing was isolated using the Monarch® Genomic DNA Purification Kit (New England Biolabs, Ipswich, MA, USA). DNA concentrations were determined employing a Qubit 2.0 fluorometer (Thermo Fisher Scientific, Waltham, MA, USA). Afterwards, 1 µg of DNA was used for library preparation with the NEBNext® Ultra™ II DNA Library Prep Kit for Illumina® (New England Biolabs, Ipswich, MA, USA). The library was subsequently evaluated by qPCR using the KAPA library quantification Kit (PEQLAB, Erlangen, Germany). After normalization for pooling, paired-end sequencing with a read length of 2 × 150 bases was performed on a MiSeq system (Illumina, San Diego, CA, USA). The sequencing output (base calls) were obtained as demultiplexed fastq files. The data was processed (e.g. trimming, mapping, coverage extraction) using the CLC Genomic Workbench software (QIAGEN Aarhus A/S, Aarhus, Denmark). Reads were mapped against an adapted version of the *P. taiwanensis* VLB120 genome that included the GRC modifications and the deletions of *paoEFG* and *aldB-I*.

The significance of the identified mutations was manually assessed. Sequencing data are stored in the NCBI Sequence Read Archive under BioProject PRJNA1061370 with the accession numbers SAMN39267274 (A7.1), SAMN39267275 (E7.2), and SAMN39267276 (F8.1).

2.3.5.4. Plasmid cloning and strain engineering

Plasmids were constructed via Gibson assembly (Gibson et al., 2009) using NEBuilder HiFi DNA Assembly (New England Biolabs, Ipswich, MA, USA) and verified by Sanger sequencing. Primers were obtained as unmodified DNA oligonucleotides from Eurofins Genomics (Ebersberg, Germany). All oligonucleotides and plasmids used in this study are summarized in Table S2 and Table S3. DNA for cloning purposes was amplified with Q5 High-Fidelity Polymerase (New England Biolabs, Ipswich, MA, USA). Restriction enzymes were purchased from New England Biolabs. Plasmid DNA and PCR amplicons were purified with the Monarch® Plasmid Miniprep Kit and Monarch® PCR & DNA Cleanup Kit, respectively (New England Biolabs, Ipswich, MA, USA). *E. coli* was transformed with DNA assemblies and purified plasmids utilizing a standard heat shock protocol (New England Biolabs, Ipswich, MA, USA). Cloned plasmids, deletions, and substitutions, were verified by colony PCR using the OneTaq 2X Master Mix with Standard Buffer (New England Biolabs, Ipswich, MA, USA). For improved efficiency, the template cell material was lysed in alkaline polyethylene glycol as described by Chomczynski and Rymaszewski (Chomczynski and Rymaszewski, 2006). The I-SceI-based system developed by Martínez-García and de Lorenzo (Martinez-Garcia and de Lorenzo, 2011) enabled seamless genomic modifications and was utilized as described previously. For knockouts, the 500 bp upstream and downstream flanking regions of the target (TS1 and TS2) were cloned between the two I-SceI restriction sites of pSNW2 and the resulting plasmid was transferred from *E. coli* PIR2 to the intended *Pseudomonas* recipient strain through conjugation. For this, mating procedures were executed according to Wynands *et al*. (Wynands et al., 2018). Analogously, the single-base pair exchange was carried out with a plasmid having the mutated *mexT* sequence inserted between the TS-sites. Three random clones underwent transformation with I-SceI-encoding plasmid pSW-2 initiating the second homologous recombination event without the need for induction by 3-methylbenzoate. Correct clones were cured of pSW-2 by restreaking on non-selective medium, and re-analyzed by PCR ensuring a pure culture. The single-base pair exchange in *mexT* was verified by Sanger sequencing.

2.3.5.5. Analytical methods

Optical densities of cell suspensions were measured at a wavelength of 600 nm (OD_{600}) with an Ultrospec 10 photometer (Biochrom, Cambridge, UK). Furanic compound concentrations

were determined using a 1260 Infinity II HPLC system equipped with an InfinityLab Poroshell 120 EC-C18 column (3.0 × 150 mm, 2.7 µm) column and the corresponding InfinityLab Poroshell 120 EC-C18 (3.0 × 5 mm, 2.7 µm) guard column (all Agilent, Santa Clara, CA, USA). Chromatography was carried out at a temperature of 40 °C using potassium acetate buffer (10 mM, pH = 5.5, A) and acetonitrile (B) as mobile phases, with a flow rate of 0.8 mL min^{-1} for a duration of 7 min. The gradient method for elution is shown in Table 2.3-2. UV detection was performed at distinct wavelengths for each compound: HMF at 280 nm, HMFA at 250 nm, and HMFOH at 220 nm. Retention times were 2.44 min, 0.95 min, and 2.28 min for HMF, HMFA, and HMFOH respectively. Standards of each chemical were purchased from Biosynth (Staad, Switzerland) and used for quantification.

Table 2.3-2: Gradient method used for HPLC measurements.

time [min]	A [%]	B [%]
0	97	3
1	85	15
3	60	40
4	60	40
6	97	3
7	97	3

Funding

This work was supported by the German Federal Ministry of Education and Research via the project NO-STRESS [grant number 031B0852A] and by the European Union's Horizon 2020 research and innovation program via the project UPLIFT [grant agreement number 953073].

Declaration of competing interest

The authors declare that they have no known competing financial interests or personal relationships that could have appeared to influence the work reported in this paper.

Data availability

Data will be made available on request.

2.4. *De novo* production of *t*-cinnamaldehyde by engineered solvent-tolerant and oxidation-deficient *Pseudomonas taiwanensis* VLB120

Thorsten Lechtenberg, Benedikt Wynands, Nick Wierckx* (2024)

Institute of Bio- and Geosciences IBG-1: Biotechnology, Forschungszentrum Jülich, 52425 Jülich, Germany
* Corresponding author

Status: unpublished
manuscript in preparation

CrediT authorship contribution statement:

T. Lechtenberg: Investigation, Writing - Original Draft, Writing - Review and editing, Visualization, Validation.

B. Wynands: Writing - Review and editing, Conceptualization, Supervision.

N. Wierckx: Writing - Review and editing, Conceptualization, Supervision, Funding acquisition, Project administration.

Overall contribution: 90%

The presented experimental work was conducted and validated by TL who likewise performed visualization of all data. BW acted as direct scientific advisor assisting with planning and evaluation of experiments. The entire project was led and supervised by NW. TL wrote the original draft which was reviewed and edited by BW and NW. Funding for the project was acquired by NW.

2.4.1. Abstract

Whole-cell biocatalytic *de novo* production of aromatic aldehydes is challenging due to the toxicity caused by their high reactivity. All common production hosts defend themselves by rapid conversion to the less harmful alcohol or acid derivatives. When this primary defense mechanism is disrupted allowing aldehyde accumulation, most organisms have no further protective capacity and require rich media to survive. Here we report the first bioproduction of *t*-cinnamaldehyde in a minimal medium using distinctly robust *Pseudomonas taiwanensis* VLB120 which was shown to benefit from active extrusion of the product by the efflux pump TtgGHI. This work thus promotes this host as alternative platform for microbial synthesis of valuable aromatic aldehydes or aldehyde-derived compounds.

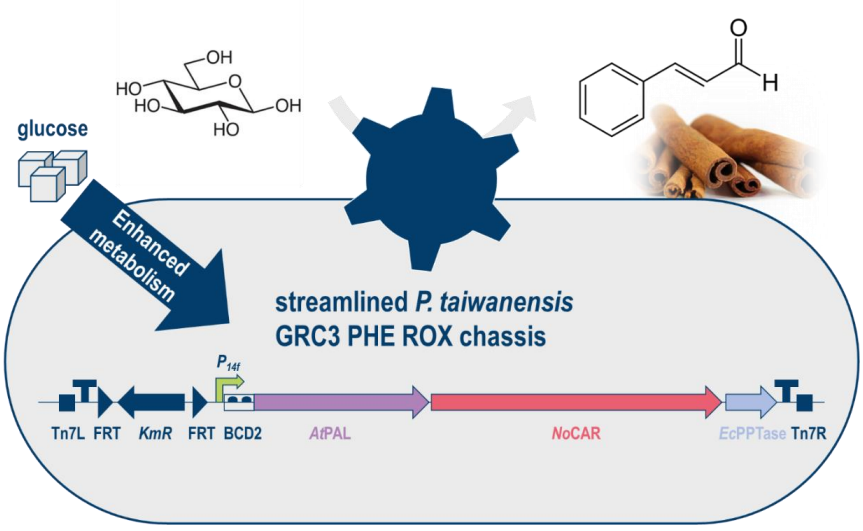

Keywords: *t*-Cinnamaldehyde; *Pseudomonas*; *De novo* biosynthesis; minimal medium; efflux pump; tolerance

2.4.2. Introduction

t-Cinnamaldehyde is a widespread natural aroma compound considered safe to use by both American and European authorities (Friedman, 2017). Besides its applications in the food sector, it exhibits insecticidal activity and is a promising natural biological pesticide (Lu et al., 2020). Currently, the production relies on extraction from plant material suffering from a low natural abundance of the target molecule, or on aldol condensation of hazardous and fossil-based chemicals benzaldehyde and acetaldehyde. Alternatively, natural flavor and fragrance compounds could be sustainably produced using microorganisms (Carroll et al., 2016). Although multiple enzymatic pathways exist for aldehyde synthesis (Schober et al., 2023), examples of whole-cell *de novo* bioproduction from renewable resources are scarce so far, because microbes typically do not accumulate them due to their toxicity (Kunjapur and Prather, 2015, Zhou et al., 2020a, Kazimírová and Rebros, 2021). Owing to its tolerance properties *Pseudomonas taiwanensis* VLB120 stands out as a chassis for the biosynthesis of compounds that exert chemical stress on the bacterial host. This strain was already engineered for production of various aromatics including phenol, benzoate, *t*-cinnamate, 4-coumarate and even complex (hydroxy) benzoate-derived polyketides (Wynands et al., 2018, Otto et al., 2020, Otto et al., 2019, Wynands et al., 2023, Schwanemann et al., 2023). Recently, the oxidative aldehyde detoxification of *P. taiwanensis* was revealed to be based on a periplasmic oxidoreductase PaoEFG and a cytoplasmic dehydrogenase AldB-I (2.1.). This discovery renders aromatic aldehydes accessible as potential products or intermediates by utilizing an oxidation-deficient ROX (Reduced OXidation) mutant. In contrast, many other biotechnological production hosts like *Escherichia coli*, *Corynebacterium glutamicum* and *Saccharomyces cerevisiae* reduce aldehydes to the corresponding alcohols (Visvalingam et al., 2013, Son et al., 2022, Gottardi et al., 2017) requiring elaborately constructed reduction-deficient strains, such as *E. coli* RARE, for aldehyde production (Kunjapur et al., 2014). Here, we report the engineering of the L-phenylalanine overproducing strain GRC3 PHE (Otto et al., 2019) into an oxidation-deficient ROX variant which was subsequently employed for the first microbial *de novo* synthesis of *t*-cinnamaldehyde in minimal salts medium (MSM) without any additives.

2.4.3. Results and discussion

Thus far, only an oxidation-deficient version of the solvent sensitive *P. taiwanensis* GRC1 lacking the efflux pump encoding operon *ttgVWGHI* - a key determinant for solvent tolerance of this organism - was available (Wynands et al., 2019, Bitzenhofer et al., 2021) (2.1.). To explore the interplay between aldehyde- and solvent-tolerance, the inducibly solvent-tolerant

GRC3 and a previously engineered L-phenylalanine overproducing strain GRC3 PHE (Otto et al., 2019) were modified into ROX variants by deletion of *paoEFG* and *aldB-I*.

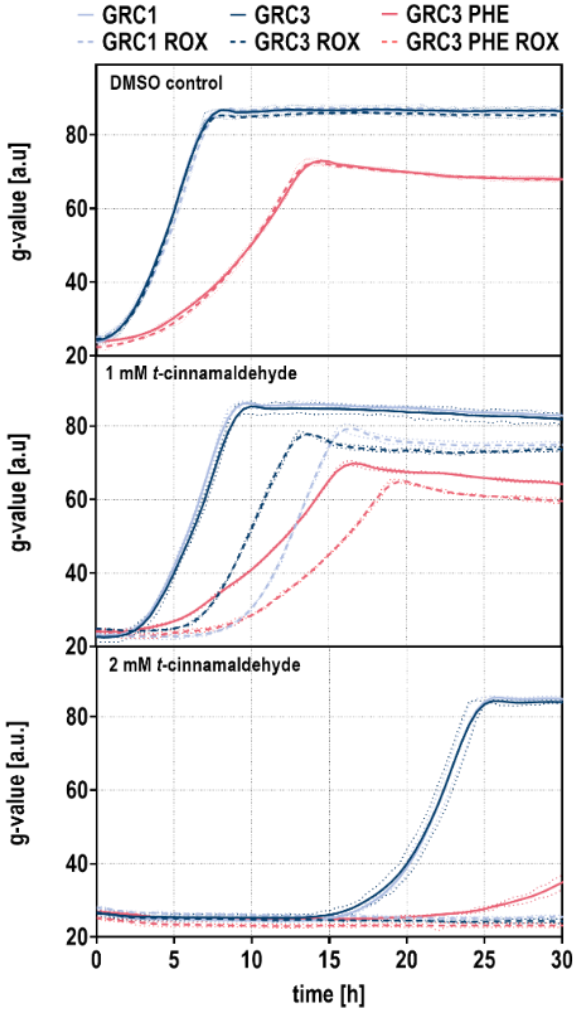

Figure 2.4-1: *t*-Cinnamaldehyde tolerance assessment of GRC1, GRC3, GRC3 PHE and their respective ROX derivatives. Two-fold buffered MSM supplemented with 20 mM glucose as carbon source and different *t*-cinnamaldehyde concentrations was inoculated to an OD_{600} of 0.1. Cells were cultivated in a Growth Profiler in 96-well microtiter plates. The growth curves result from a second-order smoothing to the mean values obtained from three replicates. The dots represent the standard deviation.

As expected, GRC1, GRC3, and the respective ROX mutants behaved identically in absence of a stressor, whereas the L-phenylalanine overproducers grew slower due to the genomic modifications in the shikimate pathway. As soon as *t*-cinnamaldehyde was added, the growth of all oxidation-deficient strains lagged behind their oxidation-positive counterparts (Fig. 2.4-1).

Intriguingly, GRC3 ROX, harboring the TtgGHI solvent efflux pump, grew better in the presence of the toxicant than GRC1 ROX (Fig. 2.4-1). Both GRC3 and GRC1 likely rapidly oxidized *t*-cinnamaldehyde to the corresponding acid which existed as a charged anion in the pH-neutral growth medium and was therefore not exported by TtgGHI. In the oxidation-deficient ROX derivatives the aldehyde was not converted and available as non-polar substrate for the efflux pump present in GRC3 ROX. Its $logP_{o/w}$ value around 2 (Shreaz et al., 2016) is in a similar range to that of typical aromatic TtgGHI substrates and the observed growth advantage is indirect evidence that *t*-cinnamaldehyde was indeed transported highlighting *P. taiwanensis* as suitable alternative for production of apolar aromatic aldehydes.

To enable GRC3 PHE to accumulate *t*-cinnamaldehyde instead of *t*-cinnamate, the previously employed production module harboring a phenylalanine ammonia lyase from *Arabidopsis thaliana* (*At*PAL) (Otto et al., 2019) was complemented by a carboxylic acid reductase (CAR) from *Nocardia otitidiscaviarum* and a phosphopantetheinyl transferase (PPTase) from *E. coli*, posttranslationally transferring a 4'-phosphopantetheine arm to the CAR (Weber et al., 2021). This step is indispensable for the reaction during which the carboxylic acid is first activated by adenylation, then covalently attached to the phosphopantetheine arm via a thioester bond, and finally moved to the reductase domain where the actual reduction is carried out using NADPH as cofactor (Finnigan et al., 2017). The newly designed synthetic operon encoding the pathway from L-phenylalanine to *t*-cinnamaldehyde under the control of a strong and constitutive P_{14f} promoter (Zobel et al., 2015) was integrated via Tn7 transposition into GRC3, GRC3 PHE and the respective oxidation-deficient variants (Fig. 2.4-2). All resulting strains were tested for accumulation of *t*-cinnamaldehyde and its acid and alcohol derivatives after 24 h of cultivation in closed glass vials preventing evaporation of the volatile aldehyde (Rönitz et al., 2024). Consistent with previous findings (Otto et al., 2019), the control strain GRC3 PHE ROX harboring only the *At*PAL reached a titer of 3.0 mM *t*-cinnamate. As no aldehydes were formed, the oxidation deficiency had no impact. Despite expressing the *No*CAR, oxidation-positive GRC3 and GRC3 PHE strains also exclusively produced the carboxylic acid, probably due to fast re-oxidation. This caused an energy-wasting futile cycle which would explain why the final titer of GRC3 PHE *attTn7*::Kan_FRT_P_{14f}_*At*PAL_*No*CAR_*Ec*PPTase was slightly reduced. As the GRC3 and GRC3 ROX strains are not optimized for aromatic amino acid accumulation, they grew better, but produced only low concentrations of *t*-cinnamate. However, the oxidation-deficient strain delivered trace amounts of the target aldehyde. Implementing the *At*PAL and *No*CAR expression cassette into GRC3 PHE ROX finally led to substantial formation of 0.89 mM (118 mg L^{-1}) *t*-cinnamaldehyde which corresponded to a yield of 6.7% Cmol/Cmol. There was only minimal over-reduction to the alcohol, but a significant concentration of

t-cinnamate was still produced indicating that CAR activity is the major bottleneck. To the best of our knowledge, these production parameters surpass the best shake flask titer obtained so far with *E. coli* cultivated in glucose-supplemented nutrient-rich medium (Bang et al., 2016).

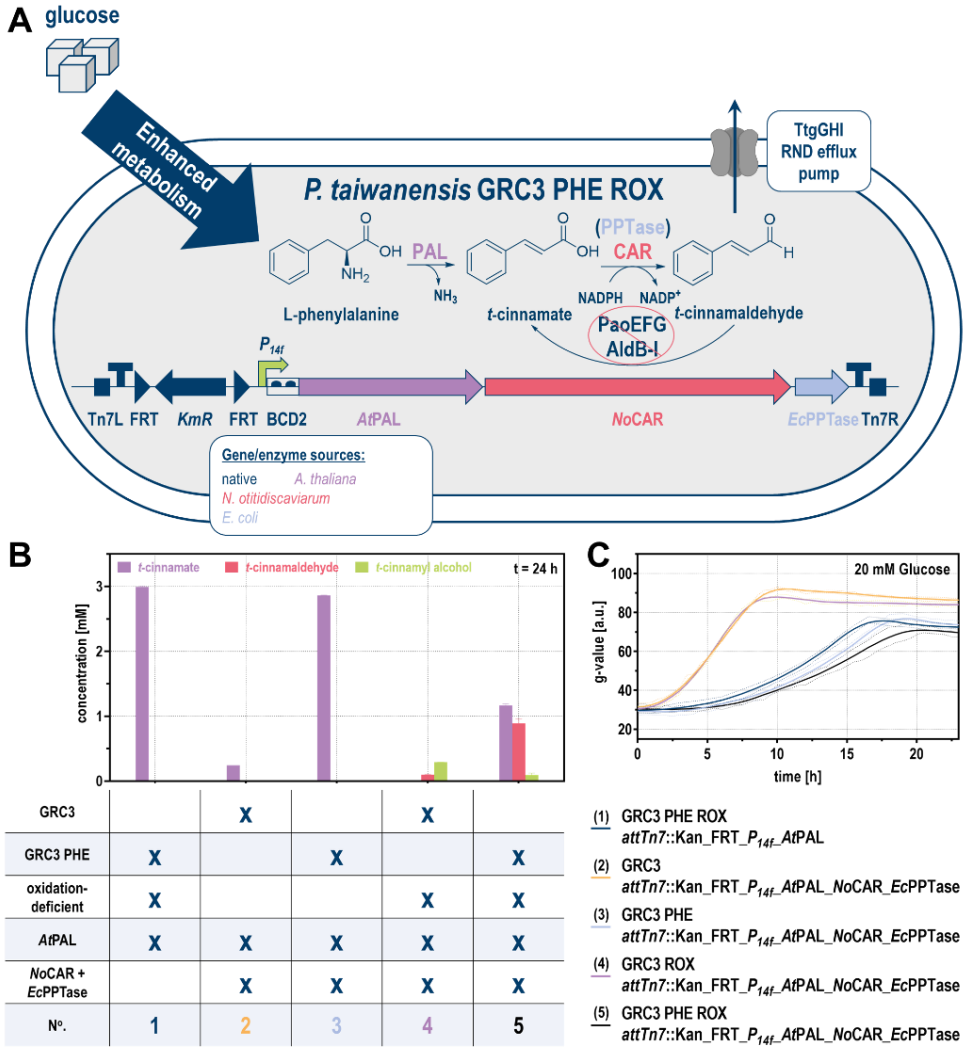

Figure 2.4-2: Engineering of *P. taiwanensis* for *de novo* biosynthesis of *t*-cinnamaldehyde. (**A**) Overview of the engineered GRC3 PHE ROX chassis and the synthetic pathway to convert L-phenylalanine into *t*-cinnamaldehyde. Aldehyde re-oxidation is avoided by deletion of *paoEFG* and *aldB-I*. (**B**) *t*-cinnamate, *t*-cinnamaldehyde and *t*-cinnamyl alcohol production of GRC3, GRC3 PHE and derived ROX mutants either equipped with the extended production module including *No*CAR and *Ec*PPtase or a control with only the *At*PAL. Strains were cultivated in closed glass vials with two-fold buffered MSM with 20 mM glucose (starting OD_{600} = 0.08) in a Growth Profiler for 24 h. The mean and standard deviation of triplicates is shown. (**C**) Respective growth curve for each strain. The growth curves result from a second-order smoothing to the mean values obtained from three replicates. The dots represent the standard deviation.

Recently, however, a significantly improved version of this *E. coli* strain was reported, featuring gram scale aldehyde formation through high biomass fed batch cultivations combined with *in situ* product removal (Bang et al., 2023). This was enabled by several adjustments, such as deletion of various reductases and dehydrogenases, use of an auto-inducible genomically integrated expression cassette, as well as increased pools of the important cofactors NADPH, CoA, and ATP. In particular, the use of the cell density-dependent promoter separating growth and production phase without addition of a costly inducer is an elegant way of increasing the host's tolerance to a toxic product. Nonetheless, our findings indicate that highly robust microbes such as *P. taiwanensis* can survive in simple MSM even if *t*-cinnamaldehyde is formed directly through constitutive expression of the production module. This is where the advantageous solvent tolerance of the bacterium comes into play. It does not only ensure a higher tolerance to the product itself, but also provides a wider degree of freedom for selection of solvents for *in situ* product removal (Schwanemann et al., 2023, Heipieper et al., 2007).

2.4.4. Conclusion

This study describes the adaptation of the previously engineered L-phenylalanine-overproducing chassis GRC3 PHE for microbial production of *t*-cinnamaldehyde by disruption of aldehyde oxidation and genomic expression of a new production module consisting of a PAL, a CAR and a PPTase. The resulting strain produced 0.89 mM (118 mg L^{-1}) *t*-cinnamaldehyde from 20 mM glucose using purely minimal medium in closed glass-vial small scale cultivations. As an extremely robust chassis, *P. taiwanensis* profits from its numerous efflux pumps like TtgGHI which was indirectly proven to export *t*-cinnamaldehyde because GRC3, harboring the solvent efflux pump, was more tolerant towards the aldehyde than the solvent-sensitive GRC1. This renders this organism a promising chassis for the bioproduction of natural *t*-cinnamaldehyde and further aldehydes or aldehyde-derived products although further optimization and upscaling for example in fed-batch reactors is required to achieve industrial competitiveness.

2.4.5. Materials and methods

2.4.5.1. Media and culture conditions

Strains, plasmids, and oligonucleotides employed in this study can be found in Tables S1 - S3. *P. taiwanensis* and *E. coli* cells were routinely cultivated at 30 or 37 °C, respectively, in liquid LB-Lennox medium or on LB-Lennox agar plates (with 1.5% w/v agar) (Carl Roth, Karlsruhe, Germany). Irgasan (25 mg L^{-1}) was applied for selection of *Pseudomonas* after conjugational mating procedures. Kanamycin sulfate (50 mg L^{-1}) was added to cultures or plates when

necessary. Growth and production experiments were performed in a Growth Profiler 960 (Enzyscreen, Heemstede, The Netherlands) (225 rpm with an amplitude of 50 mm) utilizing buffer-adjusted MSM (standard buffer capacity: 22.3 mM K_2HPO_4 and 13.6 mM NaH_2PO_4) (Hartmans et al., 1989) supplemented with 20 mM glucose. Tolerance assays were carried out in 96-well plates (CR1496dg) with a culture volume of 200 µL and production experiments in closed glass vials with a culture volume of 600 µL (Rönitz et al., 2024). The interval between two photos for growth analysis was 30 min.

2.4.5.2. Plasmid construction and genomic modifications

Plasmids for Tn7 transposition were constructed as described in detail in the Supporting Information and transformed into *E. coli* PIR2 or EC100D™ *pir*$^+$ cells. Integration at the *attTn7*-site was achieved by four-parental patch mating (Wynands et al., 2018). ROX strains were generated by stepwise genomic deletion with the I-SceI-based system (Martinez-Garcia and de Lorenzo, 2011) using previously constructed integrative plasmids (2.1.) and following a streamlined protocol (Wynands et al., 2018). Genomic modifications were confirmed through colony PCR with an additional cell lysis step (Chomczynski and Rymaszewski, 2006)

2.4.5.3. Analytics

Culture supernatants were analyzed at 40 °C and a flow rate of 0.8 mL min^{-1} using a 1260 Infinity II HPLC system equipped with an InfinityLab Poroshell 120 EC-C18 column (3.0 x 150 mm, 2.7 µm) column and the respective InfinityLab Poroshell 120 EC-C18 (3.0 x 5 mm, 2.7 µm) guard column (all Agilent, Santa Clara, CA, USA). Chromatography was performed with a binary mixture of 0.1% (v/v) trifluoroacetic acid and acetonitrile in ratios as follows: 0-2 min: 5% acetonitrile; 2-10 min: linear increase to 70% acetonitrile; 10-12 min: 70% acetonitrile; 12-13 min: linear decrease to 5% acetonitrile; 13-14 min: 5% acetonitrile. *t*-Cinnamaldehyde was detected at 250 nm (RT = 8.47 min), *t*-cinnamate at 240 nm (RT = 7.93 min), and *t*-cinnamyl alcohol at 270 nm (RT = 7.74 min).

Funding

This work was supported by the German Federal Ministry of Education and Research via the project NO-STRESS [grant number 031B0852A] and by the European Union's Horizon 2020 research and innovation program via the project UPLIFT [grant agreement number 953073].

Declaration of competing interest

The authors declare no competing interests.

Data availability

Data will be made available on request.

3. General discussion and perspectives

3.1. Whole-cell biocatalytic FDCA production – Tackling the new boundaries

Bacteria of the *Pseudomonas* clade have been employed extensively as whole-cell biocatalysts for the oxidative conversion of the furanic aldehyde HMF to the polymer building block FDCA, but thus far, without detailed understanding of the involved enzyme(s). To optimize the oxidation process, this work aimed at a deeper understanding of *Pseudomonas*' enzymatic equipment for HMF conversion going beyond a mere black box application and allowing targeted engineering. In fact, through combinatorial testing of numerous deletion mutants, the needle in the haystack was found. The genomes of *P. taiwanensis* VLB120 and *P. putida* KT2440 harbor over 30 potential ALDHs and a plethora of further oxidoreductases of different types, from which the key candidates could be identified. It was demonstrated that the bacteria's oxidative properties are primarily based on a periplasmic molybdenum-dependent aldehyde oxidoreductase PaoEFG, named according to a similar complex previously characterized in *E. coli* (Neumann et al., 2009). In addition, supplementary cytoplasmic ALDHs AldB-I(I) were uncovered (2.1.).

As a first step towards a rationally improved chassis for FDCA production, the newly established genes were overexpressed by genomic implementation of strong and constitutive synthetic promoters leading to tolerance-optimized BOX strains that oxidize HMF to the corresponding acid HMFA up to ten times faster than the unmodified reference. HMFA, alternatively abbreviated in literature as HMFCA and HFCA, is typically seen as just an intermediate *en route* to FDCA, but represents also itself a versatile and renewable precursor for the synthesis of polyesters due to its alcohol and carboxylic acid functionality (Hu et al., 2018, Todea et al., 2019). Additionally, bio-based plasticizers were developed (Hao et al., 2021) and very recently, the biological synthesis of new-to-nature polyhydroxyalkanoates (PHAs) using HMFA as a cosubstrate was discussed (Averesch et al., 2023). Moreover, there are even possible applications in the medical sector, firstly because antitumor activity has been reported (Munekata and Tamura, 1981), and secondly as part of an interleukin-2 inhibitor (Braisted et al., 2003).

Nevertheless, further oxidation of HMFA to FDCA remains of far greater importance drawing high industrial interest (Milic et al., 2023). Upon heterologous expression of *hmfH*, which is

required for the oxidation of HMFA's primary alcohol function (Pham et al., 2020), the BOX strains exhibited promising initial results in this regard as well. However, the observed improvements were less pronounced than expected, despite a drastically accelerated first oxidation step from HMF to HMFA. Specifically, the strains with increased periplasmic HMF oxidation showed a strong accumulation of HMFA, whereas those with enhanced cytoplasmic HMF oxidation displayed a buildup of FFA pointing at new bottlenecks in the enzymatic cascade which have to be addressed in further research (2.1.). As increasing expression levels of the transporter *hmfT* mitigated HMFA accumulation, this problem was attributed to slow uptake of the carboxylic acid into the cytoplasm where the subsequent primary alcohol oxidation catalyzed by HmfH occurs. Transport limitations, imposed by cellular membranes, are common challenges of whole-cell biocatalysis (Lin and Tao, 2017), especially when, as here, the individual steps of a reaction sequence partially take place in different cellular compartments. In general, the rate of whole-cell biocatalysts is one to two orders of magnitude lower than that of isolated enzymes (Chen, 2007). It is therefore an alternative concept to synthesize FDCA from HMF by means of purified proteins, for which multiple examples exist (Troiano et al., 2020, Yuan et al., 2020, Cajnko et al., 2020). Yet, this approach is considerably inferior to whole-cell biocatalysis in several other aspects. Protein purification is often laborious and costly, notably when multiple enzymes are required for a complicated cascade (Wachtmeister and Rother, 2016). As part of this work, the purification of the three-subunit enzyme complex PaoEFG from *P. taiwanensis* VLB120 with multiple cofactors was attempted through His-tagging and affinity chromatography, but the membrane-bound cytochrome could not be obtained. Even if this had been successful, an *in vitro* functionality would not have been guaranteed, because of the requirement for artificial reconstruction of the intricate electron transport chain. One could, of course, switch to the less complex ALDHs AldB-I(I), but the shown experiments clearly suggested better efficiencies for PaoEFG (2.1.). In both cases, the problem of efficient cofactor recycling arises which in turn is automatically solved by the host's inherent metabolism when whole-cells are employed (Wachtmeister and Rother, 2016, Lin and Tao, 2017). The same applies to toxic byproducts, such as hydrogen peroxide, formed by HmfH, which is naturally removed in the whole-cell setup thanks to endogenous catalases or glutathione-dependent mechanisms. *Pseudomonas*, in particular, has the ability to redirect its central carbon metabolism upon oxidative stress (cycling operation of the so-called EDEMP pathway), thereby providing reducing power in the form of NADPH to detoxify reactive oxygen species (Nikel et al., 2021, Nikel et al., 2015). Furthermore, transhydrogenases allow the interconversion between NADH, produced in excess by the aldehyde dehydrogenases AldB-I(I), and NADPH (Nikel et al., 2016b). In this way the energy set free by aldehyde oxidation cannot only be conserved via the respiratory chain, but utilized flexibly, for instance,

to drive anabolic reactions. Lastly, in whole-cell biocatalysis, the required enzymes work in their natural environment, where they are much better protected, and thus have a longer lifespan (Kadisch et al., 2017). Accordingly, it is not a viable option to just circumvent the transport issue of whole-cell biocatalytic FDCA production by use of purified enzymes. On the contrary, there are already some promising alternative solutions under consideration to tackle and overcome this challenge.

First of all, current experiments have been restricted to HmfT from *Paraburkholderia caribensis* and further transporters could be screened. For this, the BLAST analysis presented in the introduction (1.3.4.) provides a large collection of possible candidates (Fig. 1.3-4A). The greatest potential may lie in a variant from an HMF-degrading *Pseudomonas* bacterium, for example *P. umsongensis* GO16. Perhaps such a homolog fits better with the membrane properties of the workhorses applied within this thesis because it originates from a bacterium of the same genus. Some of the expanded *hmf*-clusters found in *Pseudomonas* sp., included in the BLAST analysis (Fig. 1.3-4A), harbor genes for supplementary transporters in addition to HmfT such as an SSS or a TRAP system which could also be tested. TRAP transporters are of particular interest with regard to HMFA as they need a carboxylate function for target recognition making organic acids their primary substrates (Mulligan et al., 2011). However, due to their localization in the *hmf*-cluster these proteins are just candidates for transporting furanic compounds, and experimental evidence about their substrate scope, especially concerning HMFA, is still pending (Donoso et al., 2021). They might also act as importers of FDCA, which would be counterproductive for a strain intended to produce the dicarboxylic acid.

If the moderate HMFA uptake rate is a general issue extending over all selected homologs and variants, targeted transporter engineering could be an alternative solution approach (van der Hoek and Borodina, 2020, Zhu et al., 2020, Kell et al., 2015). However, this requires in-depth knowledge about the protein, and although there are numerous characterized representatives of the mfs (Pao et al., 1998, Drew et al., 2021), HmfT has not yet been studied in detail. Notably, structural data are missing which could provide evidence about the precise transport mechanism and explain why uptake of FDCA, which is likewise negatively charged under physiological conditions, seemed to work much better than that of HMFA (2.2.). One interesting difference between the two molecules is their charge distribution which is symmetric in FDCA, but single-sided for HMFA. Considering that transporter characterization demands specialized methods, a non-directed strategy based on ALE holds more promise. The engineering of an HMF(A)-degrading *P. taiwanensis* VLB120 (2.2.) laid a solid foundation in this direction: Besides transporter evolution, this unbiased approach could likewise address a native HMFA export machinery of the host strain which has not yet been deciphered and potentially

counteracts uptake of the carboxylic acid. Such a mechanism is likely to exist, since HMFA could also be detected in culture supernatants of the BOX-C2 Δ*paoEFG* deletion mutant by which HMFA was exclusively formed through boosted cytoplasmic HMF oxidation (2.1.). In initial evolutionary experiments, though, unexpected mutations were identified in genes that appeared unrelated to cellular import or export processes (2.2.).

In terms of tolerance, the ideal process would be a completely periplasmic oxidation route, founded on PaoEFG, rendering rate-limiting HMFA uptake into the cytoplasm obsolete and keeping the toxicant away from where it can cause harm. The porous outer membrane permits easy passage of small molecules and represents a much lower barrier than the inner membrane. To accomplish fully periplasmic FDCA biosynthesis, a replacement for HmfH, catalyzing the oxidation of HMFA's primary alcohol in the periplasm is necessary. However, the natural variety of such catalysts is scarce probably due to lacking cofactor availability outside the cytosol. All standard ADHs depending on $NAD(P)^+$, for example, are not worth considering due to the absence of the cofactor in the periplasm. One of the few promising candidates is the pyrroloquinoline quinone (PQQ)-dependent ADH PedH from *P. putida* KT2440 which was recently engineered to expand its substrate spectrum to include HMFA (Wehrmann et al., 2020). Evidence of *in vivo* functionality, as well as applicability to whole-cell biocatalysis has yet to be confirmed, though.

Instead of shifting primary alcohol oxidation out of the cytosol, the opposite direction of performing HMF conversion to HMFA exclusively in the cytoplasm is also conceivable, but may be detrimental with respect to tolerance and is therefore only discussed here as a secondary option. Cellular uptake of the aldehyde appears to be much easier, likely because it is not charged, and with the cytoplasmic ALDHs AldB-I(I) alone decent conversion to the carboxylic acid was possible which was underlined by the BOX-C2 Δ*paoEFG* strain (2.1.). Thus far, however, the precise mechanism by which HMF enters the cytosol remains unclear and must be subject of further research. Without additional evidence, the presence of one or more so far uncharacterized transporter(s) would be the initial assumption. Besides the tolerance issue, the main problem with enhanced cytoplasmic oxidation is that the aldehyde intermediate FFA accumulates, since it competes with HMF as the preferred substrate for PaoEFG and can only be converted to the final product FDCA once the starting material is fully depleted. FFA oxidation by AldB-I(I) is not possible as demonstrated by the BOX-C2 Δ*paoEFG* mutant (2.1.). A simple solution to this scenario entails the expression of an additional ALDH, commonly present in the majority of *hmf*-clusters (Fig.1.3-4) (Wierckx et al., 2015). Certainly, such an enzyme should have FFA as its preferred substrate. Alternatively, there is also a technical approach that is typically applied: a fed-batch biotransformation (Koopman et al., 2010a). With

a continuous HMF-feed, the concentration of the initial substrate in the bioreactor (and thus in the cell) can be kept low, thereby avoiding competitive inhibition of PaoEFG.

Besides the development of the BOX strains and the associated improvement of FDCA production, the elucidation of *Pseudomonas*' enzymatic toolbox for oxidative detoxification of HMF paved the way for further applications. Growth experiments with the GRC1 ROX mutant in presence of HMF clearly highlighted oxidation as primary tolerance mechanism (2.1.), but this did not rule out the existence of any others. As these can be diverse (Bitzenhofer et al., 2021), an unbiased evolution approach was employed to find potential candidates. This strategy was so far limited in its application for selection of aldehyde tolerance because prevailing oxidation to the less toxic acid impeded continuous exposure of the bacteria to the target compound HMF. The use of GRC1 ROX allowed to circumvent this boundary, although this was initially linked to a significant loss of tolerance. The following ALE finally established a negative influence on HMF tolerance by the regulator MexT and the dependent efflux pump MexEF-OprN, revealing an entirely novel aspect that would have otherwise remained concealed (2.3.). In parallel with mechanistic elucidation of this phenomenon, putative benefits of the newly identified targets on FDCA production should be assessed. Moreover, the evolutionary improvement can be further pursued using the already tolerance-enhanced GRC1 ROX Δ*mexT* or GRC1 ROX Δ*mexEF-oprN* as starting points. Given that aldehyde tolerance is a manifold property and only a brief ALE with seven serial passages was conducted so far, there remains plenty of opportunity for additional refinements (Bitzenhofer et al., 2021, Wang et al., 2023). Incidentally, utilizing a robotics platform for ALE as outlined in chapter 2.3. provides a glimpse of the future – a continuously progressing automation in microbial strain development in general, ranging from cloning to upscaling (Tenhaef et al., 2021, Hemmerich et al., 2018, Janzen et al., 2019). This should accelerate research and establish biotechnology even faster as an alternative method for the production of valuable chemicals, such as FDCA (Holland and Davies, 2020, Gurdo et al., 2022, Abbate et al., 2023).

Next to the entire bacterium, the important enzymes for HMF oxidation, PaoEFG and AldB-I(I), could likewise undergo targeted protein engineering individually (Vidal et al., 2023, McLure et al., 2022, Gargiulo and Soumillion, 2021). Although both biocatalysts have been subject to natural selection for ages and thus should be quite optimized *per se*, the cell's intended application in an industrial process has special demands in contrast to pure survival in the natural environment. This does not necessarily mean only a further improvement in activity, but can also address other parameters important for biocatalysis, such as enzyme stability or pH tolerance. Efficient protein engineering by directed evolution requires simple high-throughput screening methods for extensive mutant libraries. In this context, aldehydes,

whether as substrates or products, prove to be convenient. Owing to their high and versatile reactivity, there are a variety of derivatization methods available facilitating easy readout by direct detection in the reaction mixture (Hecko et al., 2023).

In conclusion, the most efficient way to manage aldehyde toxicity, here exemplarily analyzed with HMF as a model substance, is evidently straightforward: minimizing the time the cell is exposed to the stressor by converting it to a less toxic form. Following thermodynamics the favored reaction for this purpose is the oxidation to the corresponding carboxylic acid as performed by the biotechnologically-promising bacteria *P. taiwanensis* VLB120 and *P. putida* KT2440. The process could be boosted by overexpression of the responsible enzymes which were revealed in the course of this work. The up to ten-fold higher oxidation rates considerably enhanced HMF tolerance, effectively addressing a key limitation of whole-cell catalysis with this aldehyde which is important as an environmentally benign route to the renewable plastic monomer FDCA. Thus far, only a slight improvement in the production of this important platform chemical can be proclaimed, but several suggestions were made to tackle the newly occurring bottlenecks, most notably the slow cellular uptake of the monocarboxylic acid intermediate HMFA. Overall, the by now fully elucidated oxidation cascade from HMF to FDCA will foster research focusing on *Pseudomonas* as whole-cell catalyst for this process and advance it further towards industrial application.

3.2. Aromatic aldehydes as products or intermediates of microbial cell factories – Oxidation-deficient *Pseudomonas* as auspicious chassis for *de novo* synthesis of flavorings and chiral building blocks

In the context of the previously discussed redox chemistry, whole-cell biocatalysis is appealing as alternative to chemical synthesis due to high selectivity, mild reaction conditions, and efficient cofactor recycling. However, its true strength emerges when stereochemistry comes into play as an additional factor, particularly when carbon-carbon bonds are formed, for example through aldol reactions or carboligations (Schmidt et al., 2016). Enzymes, acting as catalysts, are built-up themselves of stereospecific units, L-amino acids. Their intricate 3D-structure provides a defined reaction environment generally resulting in high stereoselectivity. Aldehydes are essential as substrates for both mentioned types of reaction and can be externally supplied or even generated *in vivo* with various enzymatic reactions available (Schober et al., 2023). The reduction of carboxylic acids using a CAR enzyme is the most frequently employed route (Winkler and Ling, 2022, Gahloth et al., 2020, Finnigan et al., 2017).

Of particular synthetic interest is the coupling of two aldehyde molecules, enabled by the thiamin-diphosphate (ThDP)-mediated “Umpolung” of one of the reactants (Dünkelmann et al., 2002, de Maria et al., 2007, Hoyos et al., 2010). To perform aldol reactions or carboligations within whole cells, it is crucial to ensure that substrates and products are not lost to unintended side reactions, such as oxidations or reductions, caused by the innate metabolism of the host organism (Muschiol et al., 2015). The simplest strategy is to delete the genes encoding the responsible enzymes for these processes, assuming that these are known and their absence has no negative influence on cell growth. With *E. coli* RARE (Kunjapur et al., 2014), a chassis is by now available in which native aldehyde reduction is disabled through deletion of six genes encoding ADHs and AKRs. By heterologous expression of a carboligation-performing pyruvate decarboxylase, this strain was shown to stereoselectively produce the pharmaceutically important building block (*R*)-phenylacetylcarbinol (PAC) from externally supplemented benzaldehyde and pyruvate derived from its own central carbon metabolism (Kunjapur et al., 2014). This reaction was not possible in the wild type background due to the unwanted detoxification of benzaldehyde to benzyl alcohol. Conducting the carboligation inside a bacterial cell offers various advantages: There is no need for laborious purification of enzymes which furthermore benefit from the cell envelope as an inherent barrier, shielding them from external influences and increasing stability (Kadisch et al., 2017, Duetz et al., 2001). Additionally, complex enzyme cascades can be carried out which are barely feasible in an *in vitro* approach due to the immense complexity regarding the number of substrates, enzymes, and cofactors required (Ladkau et al., 2014, France et al., 2017).

In analogy to *E. coli* RARE, aldehyde conversion-deficient *Pseudomonas* strains GRC ROX/ROAR were generated in the course of this work. This was enabled by the identification of PaoEFG and AldB-I(I) as central enzymes for aromatic aldehyde oxidation in this organism (2.1.). Despite the strong focus on HMF as a model aldehyde, the enzymes’ significance extended to the degradation of vanillin and 4-HB, indicating a relatively broad substrate spectrum of different types of aromatic aldehydes (2.2.). Moreover, it remains to be tested whether even aliphatic aldehydes can be oxidized by PaoEFG and/or the ALDHs AldB-I(I). In any case, with only two central aldehyde-oxidizing enzymes, or a total of four aldehyde-converting enzymes, including the minor activities of the identified ADHs, the situation is somewhat simpler compared to the six ADHs and AKRs deleted in *E. coli* RARE. This facilitates the modification of any production strain to render it conversion-deficient, which was achieved so far by the relatively time-consuming, but reliable consecutive deletion of the uncovered genes using the homologous recombination-based I-SceI system (Martinez-Garcia and de Lorenzo, 2011). Yet, with the advent of new genome engineering tools, this process could be streamlined in the future. For instance, a CRISPR/nCas9-assisted cytidine base

editor was reported permitting gene disruption via stop codon integration. If the safe option is selected and two stop codons per gene are introduced to avoid the occurrence of revertants, simultaneous functional knockouts of up to six genes are possible (Volke et al., 2022). This single-step engineering technique allows the transformation of every strain of interest into a ROX or ROAR variant within about one week, but comes with the typical drawbacks of CRISPR, especially potential off-target mutations (Ding et al., 2020, Blin et al., 2016).

Regardless of how the genes encoding the aldehyde-converting enzymes are ultimately deactivated, *Pseudomonas* was unlocked as alternative platform for the synthesis of aldehyde-derived compounds and aldehydes themselves. Initial evidence of this potential was demonstrated by *t*-cinnamaldehyde production with the oxidation-deficient L-phenylalanine overproducer GRC3 PHE ROX (2.4.). Certainly, considering the highly toxic nature of the product, it should be noted that the observed titers, even with a not fully optimized strain, approached the tolerance limit. Because of the knockouts and missing aldehyde conversion, the maximum *t*-cinnamaldehyde concentration tolerated by GRC3 PHE ROX was only in the range between 1 and 2 mM which is far too low for industrial applications. A potential solution would be to try to increase the robustness of the chassis through methods such as ALE (Sandberg et al., 2019, Lennen et al., 2023). Admittedly, it might even make more sense to simply circumvent the tolerance issue by producing the corresponding carboxylic acid with a whole-cell biocatalyst. The reduction step to the aldehyde would then be performed in a separate reaction, either enzymatically (Winkler and Ling, 2022) or chemically (Iyer et al., 2023). Thus, the highest potential is probably not found in the microbial production of valuable aldehydes themselves. Although there are numerous interesting targets, particularly in the flavor and fragrance sector, such as benzaldehyde, anisaldehyde, piperonal, or vanillin, the production strains would always have to withstand extremely high aldehyde concentrations for commercial viability. This goes hand in hand with enormous selection pressure for less or even non-producing strains and endangers long-term genetic stability of the production host (Wassenaar and Zimmermann, 2020). Furthermore, it is doubtful whether the requirements for tolerance could ever be achieved with either rational or random-based engineering. In nature, the rapid conversion of aldehydes, either through oxidation or reduction, has not emerged as a central mechanism in evolutionary progression without reason. The problem might be alleviated if the product is continuously removed from the bioreactor. For this, the typically high volatility of aldehydes could be leveraged by means of off-gas stripping, as already successfully performed for an acetaldehyde production process (Mengers et al., 2022). Alternatively, the solvent-tolerant *Pseudomonas* is applicable for two-phase fermentations involving continuous extraction of the product by a suitable organic solvent (Schwanemann et al., 2023). In the case of vanillin, nature itself has developed a protective storage mechanism

where the aldehyde is transiently caged as non-toxic vanillin β-D-glucoside (Hansen et al., 2009).

For multistep enzyme cascades, such as the described production of chiral α-hydroxy ketones, aldehyde intermediates are inevitable. In this context, however, the toxicant does not need to be accumulated in the cell and optimal pathway design secures the rapid conversion to the desired downstream product, which is often less harmful. This mitigates the tolerance problem, although it should still not be neglected. Thus, it stands to reason that the most promising application of the newly generated set of aldehyde conversion-deficient *Pseudomonas* strains will be the *de novo* production of this kind of complex and high-value building blocks. *Pseudomonas* cell factories offer several beneficial features in comparison to the so far established alternatives like *E. coli* RARE (Schwanemann et al., 2020). A clear advantage of *P. taiwanensis* VLB120 in particular is its high solvent tolerance primarily mediated by the efflux pump TtgGHI (Volmer et al., 2014, Wynands et al., 2019). This vastly enlarges the opportunities for process design, notably by enabling a wider degree of freedom in the choice of extractant in the aforementioned two-phase fermentation. An auxiliary water-immiscible solvent can act as both a reservoir for substrates and a sink for products (de María and Hollmann, 2015), which can be important, for example, in the case of benzaldehyde as quite hydrophobic intermediate in the biosynthesis of (*R*)-PAC. In addition, solvent tolerance contributes positively to mitigating the challenges exerted by the target molecule itself. Aromatic aldehydes, such as *t*-cinnamaldehyde, are multifaceted stressors due to the aldehyde chemistry on the one hand and the apolar carbon backbone on the other hand and the experiments performed in this work proved that this aldehyde is a substrate of the TtgGHI efflux pump which thereby contributes to a higher tolerance (2.4.). Another advantage is that numerous *Pseudomonas* platform strains for the production of a plethora of aromatic carboxylates, such as benzoate (Otto et al., 2020), 4-hydroxybenzoate (Lenzen et al., 2019), *t*-cinnamate (Otto et al., 2019), or 4-coumarate (Wynands et al., 2023) are already available as starting point for future research. Moreover, the development of strains for microbial synthesis of further compounds including additional hydroxybenzoates and protocatechuate is currently ongoing. All these strains can be readily modified for the production of the corresponding aldehydes by transforming them into the respective ROX/ROAR variants and implementing a CAR enzyme.

So how might a future *Pseudomonas* microbial cell factory, capable of stereoselectively producing (*R*)-PAC solely from glucose as a renewable feedstock, concretely look like? A promising design is proposed with the following (Fig. 3.2-1A): First of all, the strain should be able to synthesize the central precursor benzaldehyde through its own metabolic network

eliminating the need for external supplementation as required for the current state-of-the-art approach using *E. coli* RARE (Kunjapur et al., 2014). This can be achieved by setting the engineering process on the basis of the already existing benzoate overproducer GRC3 PHE Δ*benABCD attTn7*::P_{14f}-*phdBCDE-4cl-pal* (Otto et al., 2020). With identical modifications in the central carbon metabolism as the one utilized for *t*-cinnamaldehyde production (2.4.), this strain exhibits enhanced flux through the shikimate pathway resulting in an increased L-phenylalanine pool. The amino acid is subsequently converted to *t*-cinnamate catalyzed by a PAL. Instead of being reduced to the aldehyde (2.4.), the carboxylate undergoes CoA-activation. This is followed by a β-oxidation like cascade enabled by the enzymes PhdBCDE yielding benzoate whose usage as a carbon source is prevented by deletion of the respective *benABCD* degradation cluster. This is where the new findings on the oxidative conversion of aromatic aldehydes come into play. Implementation of the ROX deletions Δ*paoEFG* and Δ*aldB-I* to evade reoxidation, and possibly the additional knockout of the ADHs PVLB_10545 and PVLB_15055 (their substrate scope has not yet been determined) to avoid the over reduction to the alcohol, permit the reduction of benzoate to benzaldehyde by a CAR enzyme. The sole limitation may arise from the enzyme also potentially reducing the pathway intermediate *t*-cinnamate. Nonetheless, the competing CoA-ligase is expected to be considerably faster.

Alternatively, benzaldehyde could, in theory, be synthesized directly from β-hydroxyphenylpropionyl-CoA via a retro-aldol cleavage to sidestep the energy-demanding reduction of benzoate (Fig. 3.2-1A) (Kallscheuer et al., 2016). This pathway, previously demonstrated to be the most efficient by *in silico* flux response analysis (Luo and Lee, 2020), effectively functions for hydroxylated aromatic compounds, such as ferulate (2.2.). Here, the well-characterized enzyme Ech ensures both the hydration of the double bond and the subsequent non-oxidative C-C bond cleavage (Gasson et al., 1998). However, a respective enzyme performing this reaction with unsubstituted substrates like β-hydroxyphenylpropionyl-CoA has not yet been discovered or engineered (Luo and Lee, 2020).

The strain design is completed by a pyruvate decarboxylase (PDC) catalyzing the carboligation of benzaldehyde with acetaldehyde, which is generated *in situ* by decarboxylation of pyruvate gathered from the central carbon metabolism, ultimately yielding completely bio-based (*R*)-PAC. For this reaction, an optimized enzyme variant PDC^{E473Q} from *Zymomonas mobilis* exists among others (Meyer et al., 2011, Yun and Kim, 2008).

A very similar example involves the enzymatic cascade for the synthesis of the pharmaceutical ingredient metaraminol. This substance is produced by carboligation of 3-hydroxybenzaldehyde and acetaldehyde, followed by transamination (Labib et al., 2022). It

was shown that the process can be carried out using bio-based pyruvate and L-alanine, generated with *C. glutamicum*, in addition to 3-hydroxybenzoate for which a microbial production route has also been demonstrated (Zhou et al., 2019b). Yet, the *in vivo* generation of the indispensable aldehyde intermediate was not implemented so far. Choosing oxidation-deficient *Pseudomonas* as whole-cell biocatalyst, we can probably combine optimized aromatics production with reduced aldehyde conversion, as well as enhanced aldehyde tolerance, and thereby perform the process in a one-step fermentation.

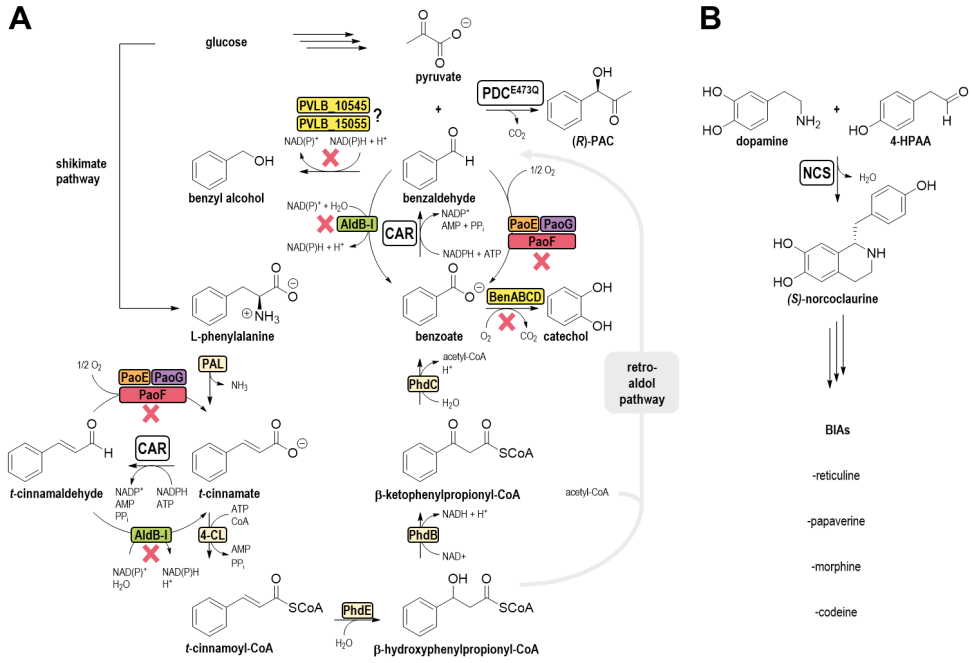

Figure 3.2-1: Possible applications of oxidation-deficient GRC3 ROX/ROAR in the biosynthesis of structurally more complex chiral building blocks. (**A**) Theoretical outline for microbial *de novo* production of (*R*)-PAC based on a previously published benzoate-overproducing *Pseudomonas* strain (Otto et al., 2020). (**B**) Initial step of the biosynthesis pathway towards complex benzylisoquinoline alkaloids (BIAs): NCS-catalyzed Pictet-Spengler condensation of dopamine and 4-HPAA yielding (*S*)-norcoclaurine, the universal precursor of important natural products such as morphine or codeine. **Abbreviations:** CAR: carboxylic acid reductase, PAL: phenylalanine ammonia lyase, 4-CL: 4-coumarate-CoA ligase, PDC: pyruvate decarboxylase, NCS: norcoclaurine synthase.

Looking ahead more broadly, *Pseudomonas* could become a suitable alternative for the production of even more complex plant natural products used as drugs, e. g. benzylisoquinoline alkaloids (BIAs) (Hagel and Facchini, 2013). The biosynthetic pathway of these compounds likewise includes an aldehyde as central intermediate, namely 4-hydroxyphenylacetaldehyde (4-HPAA) (Marienhagen and Bott, 2013). This undergoes Pictet-Spengler condensation with dopamine to form (*S*)-norcoclaurine representing a

precursor to important opioids, such as codeine or morphine. The respective reaction is catalyzed by the norcoclaurine synthase (NCS) (Fig. 3.2-1B). To reduce reliance from natural production by plants, alternative microbial production systems for these opioids are highly sought after (Keasling, 2008). Pioneering advances were achieved both with *S. cerevisiae* and *E. coli* (Hawkins and Smolke, 2008, Galanie et al., 2015, Minami et al., 2008). Intriguingly, aldehyde scavenging by oxidation or reduction, restricting the available 4-HPAA pool, was explicitly pointed out as problem with regard to existing producer strains (Narcross et al., 2016). If it occurs that the aliphatic aldehyde 4-HPAA is also part of the substrate spectrum of PaoEFG and/or AldB-I, this should not pose an issue when using *Pseudomonas*. The corresponding acid of the required aldehyde, 4-hydroxyphenylacetate is already part of *Pseudomonas*' product portfolio and, like dopamine, is derived from L-tyrosine (Wynands et al., 2023), so that all prerequisites for *de novo* biosynthesis of (*S*)-norcoclaurine with this organism are met. The chemical diversification from this intermediate to the actual pharmaceutically-used substances could be the only drawback of *Pseudomonas*, as it involves various cytochrome P450 enzymes that are often difficult to functionally express in prokaryotes (Nguyen and Dang, 2021, Durairaj and Li, 2022).

On the basis of the above, it can be concluded that owing to their versatile reactivity aldehydes are key elements of a future preparative synthetic biology representing an environmentally benign alternative to many chemical processes. However, whole-cell biocatalysts naturally avoid the accumulation of these key compounds because of their toxicity so that *in vivo* enzymatic cascades involving aldehydes are barely possible, as large proportions of the intermediates are diverted by cellular defense mechanisms. Here, we could access the robust biotechnological workhorses *P. taiwanensis* VLB120 and *P. putida* KT2440 for production of aromatic aldehydes and aldehyde-derived products by identification and deletion of the inherent redox conversion machinery. Future research can now combine the biosynthesis of aromatic precursors, their conversion into aldehydes and the construction of complex carbon frameworks in a single strain profiting from all assets of *Pseudomonas* as cell factory (Blombach et al., 2022, Bitzenhofer et al., 2021, Weimer et al., 2020). As a result, the already wide range of aromatic compounds synthesized with this organism will be expanded considerably (Schwanemann et al., 2020). This scenario is finally headed towards a kind of consolidated bioprocessing (CBP) approach, i.e. a single-step production of valuable (fine) chemicals directly from biomass in a single bioreactor (Singhania et al., 2022, Banner et al., 2021).

3.3. Concluding remarks – The importance of aldehydes in whole-cell biocatalysis: From bio-based polymers to fine chemicals

Plastics are indispensable materials for a modern society bringing benefits such as versatility, lightweight, chemical- and corrosion-resistance, cost-effectiveness, and durability. Nonetheless, we are in the midst of a dramatic plastics crisis with two major problems: heavy reliance on depleting fossil resources and a lack of adequate end-of-life solutions, leading to large amounts of waste accumulating in the environment. Thus, bio-based alternatives produced from renewable feedstock, ideally with recyclability, have to be promoted and can significantly contribute to a more sustainable plastic life cycle within the broader context of a circular bioeconomy (Rosenboom et al., 2022, Stegmann et al., 2022). One of these substitutes is PEF, whose central building block FDCA can be synthesized, amongst others, by whole-cell biocatalytic oxidation of the sugar-derived precursor HMF representing an environmentally benign process in view of its mild reaction conditions as outlined in this thesis. Robust bacteria of the *Pseudomonas* clade manifested as suitable hosts for this application which is supported by several patent filings (Ruijssenaars et al., 2011, Wierckx et al., 2012, Ruijssenaars, 2016, Hu and Pham, 2021). However, progress has been limited in recent years due to a lack of knowledge particularly concerning the enzymatic toolbox with which the organism handles the toxic aldehyde substrate HMF. Owing to the versatile reactivity of the carbonyl function, aldehydes have always been cornerstones of organic synthesis and for the same reason will also play a crucial role in a future bioeconomy coined by synthetic biology, despite their limited compatibility with the biochemistry of life. Although this is a challenge, the mechanistic insights into the physiological processes related to *Pseudomonas*' aldehyde tolerance gained in the course of this project are likely to stimulate further development of biotechnological activities involving these chemicals. With the design of the oxidation-optimized BOX strains and the tolerance-improvement related to *mexT* or *mexEF-oprN* deletion, initial application examples were presented enhancing the efficiency of FDCA synthesis by *Pseudomonas* and bringing it closer to industrial implementation. Establishing a competitive and sustainable production route for its central building block will also boost PEF manufacturing utilizing existing PET facilities. This would be a significant contribution towards eventually increasing the percentage of petroleum-independent material on the global plastic market which currently still stands below 1% (Kunamaneni, 2023). PEF likewise addresses the second aspect of the plastic crisis and comes with mechanical, chemical and biological recycling solutions, whereby the mild enzymatic hydrolysis of the polyester is particularly appealing (Loos et al., 2020, Agostinho et al., 2022, Pellis et al., 2016, Austin et al., 2018). With the help of the furanic compounds-

degrading strains, constructed as part of this thesis, and previously engineered bacteria the monomers FDCA and EG can serve as a resource for the production of new valuable chemicals (Tiso et al., 2022, Blank et al., 2020, Franden et al., 2018).

Pseudomonas' oxidative detoxification of (aromatic) aldehydes extends to various substrates, which confers relevance to this work beyond HMF and the topic of bio-based polymers. While the tolerance issue remains important, this organism is now generally available for (*de novo*) biosynthesis of aromatic aldehydes and derived products thereof. These compounds are valuable not only as flavorings, such as *t*-cinnamaldehyde and vanillin, but also as central intermediates towards complex fine chemicals (Zhou et al., 2020a). Microbial cell factories, operating under mild conditions and processing simple, readily available, and renewable starting materials have the potential to complement or even replace established chemical synthesis methods which often rely on fossil resources and harsh reaction environments (Keasling, 2010, Cho et al., 2022, Jullesson et al., 2015). Their strength is particularly evident when complex metabolic pathways turn simple precursors into intricate molecules which would otherwise require labor-intensive multistep organic synthesis (Rudroff, 2019). Whole-cell biocatalysis offers a sustainable "one-pot alternative" and thanks to versatile aldehyde (bio)chemistry, the product portfolio of *Pseudomonas* cell factories will be extended further.

4. References

ABBATE, E., ANDRION, J., APEL, A., BIGGS, M., CHAVES, J., CHEUNG, K., CIESLA, A., CLARK-ELSAYED, A., CLAY, M., CONTRIDAS, R., FOX, R., HEIN, G., HELD, D., HORWITZ, A., JENKINS, S., KALLBARCZYK, K., KRISHNAMURTHY, N., MIRSIAGHI, M., NOON, K., ROWE, M., SHEPHERD, T., TARASAVA, K., TARASOW, T. M., THACKER, D., VILLA, G. & YERRAMSETTY, K. 2023. Optimizing the strain engineering process for industrial-scale production of bio-based molecules. *Journal of Industrial Microbiology & Biotechnology,* 50.

ABBEY, A. M. I., BEAUDETTE, L. A., LEE, H. & TREVORS, J. T. 2003. Polychlorinated biphenyl (PCB) degradation and persistence of a *gfp*-marked *Ralstonia eutropha* H850 in PCB-contaminated soil. *Applied Microbiology and Biotechnology,* 63**,** 222-230.

ACHOUAK, W., CHRISTEN, R., BARAKAT, M., MARTEL, M. H. & HEULIN, T. 1999. *Burkholderia caribensis* sp. nov., an exopolysaccharide-producing bacterium isolated from vertisol microaggregates in Martinique. *International Journal of Systematic Bacteriology,* 49**,** 787-794.

ACKERMANN, M. 2015. A functional perspective on phenotypic heterogeneity in microorganisms. *Nature Reviews Microbiology,* 13**,** 497-508.

ACKERMANN, Y. S., LI, W. J., OP DE HIPT, L., NIEHOFF, P. J., CASEY, W., POLEN, T., KÖBBING, S., BALLERSTEDT, H., WYNANDS, B., O'CONNOR, K., BLANK, L. M. & WIERCKX, N. 2021. Engineering adipic acid metabolism in *Pseudomonas putida*. *Metabolic Engineering,* 67**,** 29-40.

ADEWUNMI, Y., NAMJILSUREN, S., WALKER, W. D., AMATO, D. N., AMATO, D. V., MAVRODI, O. V., PATTON, D. L. & MAVRODI, D. V. 2020. Antimicrobial Activity of, and Cellular Pathways Targeted by, *p*-Anisaldehyde and Epigallocatechin Gallate in the Opportunistic Human Pathogen *Pseudomonas aeruginosa*. *Applied and Environmental Microbiology,* 86.

AGOSTINHO, B., SILVESTRE, A. J. D. & SOUSA, A. F. 2022. From PEF to rPEF: disclosing the potential of deep eutectic solvents in continuous de-/re-polymerization recycling of biobased polyesters. *Green Chemistry,* 24**,** 3115-3119.

ALLEN, L., O'CONNELL, A. & KIERMER, V. 2019. How can we ensure visibility and diversity in research contributions? How the Contributor Role Taxonomy (CRediT) is helping the shift from authorship to contributorship. *Learned Publishing,* 32**,** 71-74.

ALMEIDA, J. R. M., BERTILSSON, M., GORWA-GRAUSLUND, M. F., GORSICH, S. & LIDEN, G. 2009. Metabolic effects of furaldehydes and impacts on biotechnological processes. *Applied Microbiology and Biotechnology,* 82**,** 625-638.

ALNAHHAS, R. N. & DUNLOP, M. J. 2023. Advances in linking single-cell bacterial stress response to population-level survival. *Current Opinion in Biotechnology,* 79.

ANASTAS, P. T. & WARNER, J. C. 1998. *Green Chemistry: Theory and Practice*, Oxford University Press: New York.

ANTAL, M. J., MOK, W. S. L. & RICHARDS, G. N. 1990. Mechanism of formation of 5-(hydroxymethyl-2-furaldehyde from D-fructose and sucrose. *Carbohydrate Research,* 199**,** 91-109.

ARAUJO, C. F., NOLASCO, M. M., RIBEIRO-CLARO, P. J. A., RUDIC, S., SILVESTRE, A. J. D., VAZ, P. D. & SOUSA, A. F. 2018. Inside PEF: Chain Conformation and Dynamics in Crystalline and Amorphous Domains. *Macromolecules,* 51**,** 3515-3526.

ARNOLD, F. H. 2018. Directed Evolution: Bringing New Chemistry to Life. *Angewandte Chemie-International Edition,* 57**,** 4143-4148.

AUSTIN, H. P., ALLEN, M. D., DONOHOE, B. S., RORRER, N. A., KEARNS, F. L., SILVEIRA, R. L., POLLARD, B. C., DOMINICK, G., DUMAN, R., EL OMARI, K., MYKHAYLYK, V., WAGNER, A., MICHENER, W. E., AMORE, A., SKAF, M. S., CROWLEY, M. F., THORNE, A. W., JOHNSON, C. W., WOODCOCK, H. L., MCGEEHAN, J. E. & BECKHAM, G. T. 2018. Characterization and engineering of a plastic-degrading aromatic polyesterase. *Proceedings of the National Academy of Sciences of the United States of America,* 115**,** E4350-E4357.

AVANTIUM. 2022. *Avantium reaches Financial Close for its FDCA Flagship Plant* [Online]. Available: https://www.avantium.com/wp-content/uploads/2022/03/20220331-Avantium-reaches-Financial-Close-for-its-FDCA-Flagship-Plant.pdf [Accessed 23.02.2024].

AVERESCH, N. J. H., PANE, V. E., KRACKE, F., ZIESACK, M., NANGLE, S. N., WAYMOUTH, R. W. & CRIDDLE, C. S. 2023. Towards high-performance polyesters from carbon dioxide: novel polyhydroxyarylates from engineered *Cupriavidus necator*. *Research Square, preprint (01/31/24)*.

BAARS, H. J., BLANK, J. H., KOLSTAD, J. J. & DE SOUSA DIAS, A. S. V. 2021. *Process for producing 2,5-furandicarboxylic acid from ethers of 5-hydroxymethylfurfural*. World Intellectual Property Organization patent application WO 2021/123189 A1. 24.06.2021.

4. References

BAGDASARIAN, M., LURZ, R., RUCKERT, B., FRANKLIN, F. C., BAGDASARIAN, M. M., FREY, J. & TIMMIS, K. N. 1981. Specific-purpose plasmid cloning vectors. II. Broad host range, high copy number, RSF1010-derived vectors, and a host-vector system for gene cloning in *Pseudomonas*. *Gene,* 16**,** 237-47.

BALABAN, N. Q., HELAINE, S., LEWIS, K., ACKERMANN, M., ALDRIDGE, B., ANDERSSON, D. I., BRYNILDSEN, M. P., BUMANN, D., CAMILLI, A., COLLINS, J. J., DEHIO, C., FORTUNE, S., GHIGO, J. M., HARDT, W. D., HARMS, A., HEINEMANN, M., HUNG, D. T., JENAL, U., LEVIN, B. R., MICHIELS, J., STORZ, G., TAN, M. W., TENSON, T., VAN MELDEREN, L. & ZINKERNAGEL, A. 2019. Definitions and guidelines for research on antibiotic persistence. *Nature Reviews Microbiology,* 17**,** 441-448.

BALL, P. 2017. Water is an active matrix of life for cell and molecular biology. *Proceedings of the National Academy of Sciences of the United States of America,* 114**,** 13327-13335.

BANG, H. B., LEE, Y. H., KIM, S. C., SUNG, C. K. & JEONG, K. J. 2016. Metabolic engineering of *Escherichia coli* for the production of cinnamaldehyde. *Microbial Cell Factories,* 15**,** 16.

BANG, H. B., SON, J., KIM, S. C. & JEONG, K. J. 2023. Systematic metabolic engineering of *Escherichia coli* for the enhanced production of cinnamaldehyde. *Metabolic Engineering,* 76**,** 63-74.

BANNER, A., TOOGOOD, H. S. & SCRUTTON, N. S. 2021. Consolidated Bioprocessing: Synthetic Biology Routes to Fuels and Fine Chemicals. *Microorganisms,* 9.

BAYER, T., MILKER, S., WIESINGER, T., WINKLER, M., MIHOVILOVIC, M. D. & RUDROFF, F. 2017. In Vivo Synthesis of Polyhydroxylated Compounds from a "Hidden Reservoir" of Toxic Aldehyde Species. *ChemCatChem,* 9**,** 2919-2923.

BELDA, E., VAN HECK, R. G. A., LOPEZ-SANCHEZ, M. J., CRUVEILLER, S., BARBE, V., FRASER, C., KLENK, H. P., PETERSEN, J., MORGAT, A., NIKEL, P. I., VALLENET, D., ROUY, Z., SEKOWSKA, A., DOS SANTOS, V. A. P. M., DE LORENZO, V., DANCHIN, A. & MÉDIGUE, C. 2016. The revisited genome of *Pseudomonas putida* KT2440 enlightens its value as a robust metabolic *chassis*. *Environmental Microbiology,* 18**,** 3403-3424.

BELL, E. L., FINNIGAN, W., FRANCE, S. P., GREEN, A. P., HAYES, M. A., HEPWORTH, L. J., LOVELOCK, S. L., NIIKURA, H., OSUNA, S., ROMERO, E., RYAN, K. S., TURNER, N. J. & FLITSCH, S. L. 2021. Biocatalysis. *Nature Reviews Methods Primers,* 1.

BERG, J. M., TYMOCZKO, J. L., JR., G. J. G. & STRYER, L. 2018. *Stryer Biochemie*, Springer Spektrum.

BERTRAND, R. L. 2019. Lag Phase Is a Dynamic, Organized, Adaptive, and Evolvable Period That Prepares Bacteria for Cell Division. *Journal of Bacteriology,* 201.

BINDER, J. B. & RAINES, R. T. 2009. Simple Chemical Transformation of Lignocellulosic Biomass into Furans for Fuels and Chemicals. *Journal of the American Chemical Society,* 131**,** 1979-1985.

BITZENHOFER, N. L., KRUSE, L., THIES, S., WYNANDS, B., LECHTENBERG, T., RÖNITZ, J., KOZAEVA, E., WIRTH, N. T., EBERLEIN, C., JAEGER, K. E., NIKEL, P. I., HEIPIEPER, H. J., WIERCKX, N. & LOESCHCKE, A. 2021. Towards robust *Pseudomonas* cell factories to harbour novel biosynthetic pathways. *Essays in Biochemistry,* 65**,** 319-336.

BLANK, L. M., NARANCIC, T., MAMPEL, J., TISO, T. & O'CONNOR, K. 2020. Biotechnological upcycling of plastic waste and other non-conventional feedstocks in a circular economy. *Current Opinion in Biotechnology,* 62**,** 212-219.

BLIN, K., PEDERSEN, L. E., WEBER, T. & LEE, S. Y. 2016. CRISPy-web: An online resource to design sgRNAs for CRISPR applications. *Synthetic and Systems Biotechnology,* 1**,** 118-121.

BLOMBACH, B., GRUNBERGER, A., CENTLER, F., WIERCKX, N. & SCHMID, J. 2022. Exploiting unconventional prokaryotic hosts for industrial biotechnology. *Trends in Biotechnology,* 40**,** 385-397.

BLOOR, S., MICHURIN, I., TITCHINER, G. R. & LEYS, D. 2023. Prenylated flavins: structures and mechanisms. *FEBS Journal,* 290**,** 2232-2245.

BOMGARDNER, M. M. 2018. *DuPont, ADM pilot the biobased monomer FDME* [Online]. Available: https://cen.acs.org/business/biobased-chemicals/DuPont-ADM-pilot-biobased-monomer/96/i19 [Accessed 04.03.2024].

BOUSSIE, T. R., DIAS, E. L., MURPHY, V. J. & SHOEMAKER, J. A. 2015. *Conversion of fructose-containing feedstocks to HMF-containing product*. World Intellectual Property Organization patent application WO 2015/113060 A2. 30.07.2015.

BOZELL, J. J. & PETERSEN, G. R. 2010. Technology development for the production of biobased products from biorefinery carbohydrates—the US Department of Energy's "Top 10" revisited. *Green Chemistry,* 12.

BRAISTED, A. C., OSLOB, J. D., DELANO, W. L., HYDE, J., MCDOWELL, R. S., WAAL, N., YU, C., ARKIN, M. R. & RAIMUNDO, B. C. 2003. Discovery of a potent small molecule IL-2 inhibitor through fragment assembly. *Journal of the American Chemical Society,* 125**,** 3714-3715.

BRAUN, M., GRUBER, C. C., KRASSNIGG, A., KUMMER, A., LUTZ, S., OBERDORFER, G., SIIROLA, E. & SNAJDROVA, R. 2023. Accelerating Biocatalysis Discovery with Machine Learning: A Paradigm Shift in Enzyme Engineering, Discovery, and Design. *ACS Catalysis,* 13**,** 14454-14469.

BRAUNER, A., FRIDMAN, O., GEFEN, O. & BALABAN, N. Q. 2016. Distinguishing between resistance, tolerance and persistence to antibiotic treatment. *Nature Reviews Microbiology,* 14**,** 320-330.

BRAUNER, A., SHORESH, N., FRIDMAN, O. & BALABAN, N. Q. 2017. An Experimental Framework for Quantifying Bacterial Tolerance. *Biophysical Journal,* 112**,** 2664-2671.

BREMER, E. & KRÄMER, R. 2019. Responses of Microorganisms to Osmotic Stress. *Annual Review of Microbiology,* 73**,** 313-334.

BRETHAUER, S. & STUDER, M. H. 2015. Biochemical Conversion Processes of Lignocellulosic Biomass to Fuels and Chemicals - A Review. *Chimia,* 69**,** 572-581.
BROVETTO, M., GAMENARA, D., MÉNDEZ, P. S. & SEOANE, G. A. 2011. C-C Bond-Forming Lyases in Organic Synthesis. *Chemical Reviews,* 111**,** 4346-4403.
BROWN, D. W., FLOYD, A. J., KINSMAN, R. G. & ROSHANALI, Y. 1982. Dehydration Reactions of Fructose in Non-Aqueous Media. *Journal of Chemical Technology and Biotechnology,* 32**,** 920-924.
BULL, C. & BALLOU, D. P. 1981. Purification and Properties of Protocatechuate 3,4-Dioxygenase from *Pseudomonas putida* - a New Iron to Subunit Stoichiometry. *Journal of Biological Chemistry,* 256**,** 2673-2680.
BURGESS, S. K., LEISEN, J. E., KRAFTSCHIK, B. E., MUBARAK, C. R., KRIEGEL, R. M. & KOROS, W. J. 2014. Chain Mobility, Thermal, and Mechanical Properties of Poly(ethylene furanoate) Compared to Poly(ethylene terephthalate). *Macromolecules,* 47**,** 1383-1391.
BUTLER, J. S., SPRINGER, M., DONDON, J., GRAFFE, M. & GRUNBERG-MANAGO, M. 1986. *Escherichia coli* protein synthesis initiation factor IF3 controls its own gene expression at the translational level *in vivo*. *Journal of Molecular Biology,* 192**,** 767-80.
BUTLER, N. D., ANDERSON, S. R., DICKEY, R. M., NAIN, P. & KUNJAPUR, A. M. 2023. Combinatorial gene inactivation of aldehyde dehydrogenases mitigates aldehyde oxidation catalyzed by *E. coli* resting cells. *Metabolic Engineering,* 77**,** 294-305.
CAES, B. R., TEIXEIRA, R. E., KNAPP, K. G. & RAINES, R. T. 2015. Biomass to Furanics: Renewable Routes to Chemicals and Fuels. *ACS Sustainable Chemistry & Engineering,* 3**,** 2591-2605.
CAJNKO, M. M., NOVAK, U., GRILC, M. & LIKOZAR, B. 2020. Enzymatic conversion reactions of 5-hydroxymethylfurfural (HMF) to bio-based 2,5-diformylfuran and 2,5-furandicarboxylic acid (FDCA) with air: mechanisms, pathways and synthesis selectivity. *Biotechnology for Biofuels,* 13.
CALDERÓN, J. C. V., ARORA, J. S. & MUSHRIF, S. H. 2022. Mechanistic Investigation into the Formation of Humins in Acid-Catalyzed Biomass Reactions. *ACS Omega,* 7**,** 44786-44795.
CALERO, P. & NIKEL, P. I. 2019. Chasing bacterial *chassis* for metabolic engineering: a perspective review from classical to non-traditional microorganisms. *Microbial Biotechnology,* 12**,** 98-124.
CALVO-FLORES, F. G. & MARTIN-MARTINEZ, F. J. 2022. Biorefineries: Achievements and challenges for a bio-based economy. *Frontiers in Chemistry,* 10.
CAO, D. X., TU, M. B., XIE, R., LI, J., WU, Y. N. & ADHIKARI, S. 2014a. Inhibitory Activity of Carbonyl Compounds on Alcoholic Fermentation by *Saccharomyces cerevisiae*. *Journal of Agricultural and Food Chemistry,* 62**,** 918-926.
CAO, Q., DORNAN, L. M., ROGAN, L., HUGHES, N. L. & MULDOON, M. J. 2014b. Aerobic oxidation catalysis with stable radicals. *Chemical Communications,* 50**,** 4524-4543.
CARRO, J., FERREIRA, P., RODRIGUEZ, L., PRIETO, A., SERRANO, A., BALCELLS, B., ARDA, A., JIMENEZ-BARBERO, J., GUTIERREZ, A., ULLRICH, R., HOFRICHTER, M. & MARTINEZ, A. T. 2015. 5-hydroxymethylfurfural conversion by fungal aryl-alcohol oxidase and unspecific peroxygenase. *FEBS Journal,* 282**,** 3218-29.
CARROLL, A. L., DESAI, S. H. & ATSUMI, S. 2016. Microbial production of scent and flavor compounds. *Current Opinion in Biotechnology,* 37**,** 8-15.
CHAVARRÍA, M., NIKEL, P. I., PÉREZ-PANTOJA, D. & LORENZO, V. 2013. The Entner-Doudoroff pathway empowers *Pseudomonas putida* KT2440 with a high tolerance to oxidative stress. *Environmental Microbiology,* 15**,** 1772-1785.
CHEN, K. & ARNOLD, F. H. 2020. Engineering new catalytic activities in enzymes. *Nature Catalysis,* 3**,** 203-213.
CHEN, L. F., XIONG, Y. H., QIN, H. & QI, Z. W. 2022. Advances of Ionic Liquids and Deep Eutectic Solvents in Green Processes of Biomass-Derived 5-Hydroxymethylfurfural. *ChemSusChem,* 15.
CHEN, R. R. Z. 2007. Permeability issues in whole-cell bioprocesses and cellular membrane engineering. *Applied Microbiology and Biotechnology,* 74**,** 730-738.
CHIPMAN, D., BARAK, Z. A. & SCHLOSS, J. V. 1998. Biosynthesis of 2-aceto-2-hydroxy acids: acetolactate synthases and acetohydroxyacid synthases. *Biochimica et Biophysica Acta-Protein Structure and Molecular Enzymology,* 1385**,** 401-419.
CHO, J. S., KIM, G. B., EUN, H., MOON, C. W. & LEE, S. Y. 2022. Designing Microbial Cell Factories for the Production of Chemicals. *JACS Au,* 2**,** 1781-1799.
CHOI, K. H., GAYNOR, J. B., WHITE, K. G., LOPEZ, C., BOSIO, C. M., KARKHOFF-SCHWEIZER, R. R. & SCHWEIZER, H. P. 2005. A Tn7-based broad-range bacterial cloning and expression system. *Nature Methods,* 2**,** 443-448.
CHOMCZYNSKI, P. & RYMASZEWSKI, M. 2006. Alkaline polyethylene glycol-based method for direct PCR from bacteria, eukaryotic tissue samples, and whole blood. *Biotechniques,* 40**,** 454-458.
CHOUDHARY, D., FOSTER, K. R. & UPHOFF, S. 2023. Chaos in a bacterial stress response. *Current Biology,* 33.
CLAYDEN, J., GREEVES, N. & WARREN, S. 2012. *Organic Chemistry 2nd edition*, Oxford University Press.
CLODE, D. M. 1979. Carbohydrate Cyclic Acetal Formation and Migration. *Chemical Reviews,* 79**,** 491-513.
CONRAD, T. M., LEWIS, N. E. & PALSSON, B. O. 2011. Microbial laboratory evolution in the era of genome-scale science. *Molecular Systems Biology,* 7**,** 509.
COREY, E. J. & KIM, C. U. 1972. New and Highly Effective Method for Oxidation of Primary and Secondary Alcohols to Carbonyl-Compounds. *Journal of the American Chemical Society,* 94**,** 7586-7587.

COREY, E. J. & NOZOE, S. 1963. Total Synthesis of Helminthosporal. *Journal of the American Chemical Society,* 85**,** 5728-5733.

CORREIA, M. A. S., OTRELO-CARDOSO, A. R., SCHWUCHOW, V., CLAUSS, K. G. V. S., HAUMANN, M., ROMAO, M. J., LEIMKUHLER, S. & SANTOS-SILVA, T. 2016. The *Escherichia coli* Periplasmic Aldehyde Oxidoreductase Is an Exceptional Member of the Xanthine Oxidase Family of Molybdoenzymes. *ACS Chemical Biology,* 11**,** 2923-2935.

COUMANS, F. J. A. G., OVERCHENKO, Z., WIESFELD, J. J., KOSINOV, N., NAKAJIMA, K. & HENSEN, E. J. M. 2022. Protection Strategies for the Conversion of Biobased Furanics to Chemical Building Blocks. *ACS Sustainable Chemistry & Engineering,* 10**,** 3116-3130.

CRIGLER, J., EITEMAN, M. A. & ALTMAN, E. 2020. Characterization of the Furfural and 5-Hydroxymethylfurfural (HMF) Metabolic Pathway in the Novel Isolate *Pseudomonas putida* ALS1267. *Applied Biochemistry and Biotechnology,* 190**,** 918-930.

CUI, Y. A., DENG, C., FAN, L. Q., QIU, Y. J. & ZHAO, L. M. 2023. Progress in the biosynthesis of bio-based PET and PEF polyester monomers. *Green Chemistry,* 25**,** 5836-5857.

DAFOE, J. T. & DAUGULIS, A. J. 2014. In situ product removal in fermentation systems: improved process performance and rational extractant selection. *Biotechnology Letters,* 36**,** 443-460.

DAVIDSON, M. G., ELGIE, S., PARSONS, S. & YOUNG, T. J. 2021. Production of HMF, FDCA and their derived products: a review of life cycle assessment (LCA) and techno-economic analysis (TEA) studies. *Green Chemistry,* 23**,** 3154-3171.

DAVIES, J. S., CURRIE, M. J., NORTH, R. A., SCALISE, M., WRIGHT, J. D., COPPING, J. M., REMUS, D. M., GULATI, A., MORADO, D. R., JAMIESON, S. A., NEWTON-VESTY, M. C., ABEYSEKERA, G. S., RAMASWAMY, S., FRIEMANN, R., WAKATSUKI, S., ALLISON, J. R., INDIVERI, C., DREW, D., MACE, P. D. & DOBSON, R. C. J. 2023. Structure and mechanism of a tripartite ATP-independent periplasmic TRAP transporter. *Nature Communications,* 14.

DE AVILA, E. S. S., ECHEVERRIGARAY, S. & GERHARDT, G. J. 2011. BacPP: Bacterial promoter prediction-A tool for accurate sigma-factor specific assignment in enterobacteria. *Journal of Theoretical Biology,* 287**,** 92-9.

DE BONT, J. A., RUIJSSENAARS, H. J. & WERIJ, J. 2017. *Fungal production of FDCA*. World Intellectual Property Organization patent application WO 2017/050815 A1. 30.03.2017.

DE BONT, J. A., RUIJSSENAARS, H. J. & WERIJ, J. 2018. *FDCA-decarboxylating monooxygenase-deficient host cells for producing FDCA*. World Intellectual Property Organization patent application WO 2018/172401 A1. 27.09.2018.

DE JONG, E., VISSER, H. A., DIAS, A. S., HARVEY, C. & GRUTER, G. J. M. 2022. The Road to Bring FDCA and PEF to the Market. *Polymers,* 14.

DE LORENZO, V. 2022. 15 years of microbial biotechnology: the time has come to think big-and act soon. *Microbial Biotechnology,* 15**,** 240-246.

DE MARÍA, P. D. & HOLLMANN, F. 2015. On the (Un)greenness of Biocatalysis: Some Challenging Figures and Some Promising Options. *Frontiers in Microbiology,* 6.

DE MARIA, P. D., POHL, M., GOCKE, D., GRÖGER, H., TRAUTHWEIN, H., STILLGER, T., WALTER, L. & MÜLLER, M. 2007. Asymmetric synthesis of aliphatic 2-hydroxy ketones by enzymatic carboligation of aldehydes. *European Journal of Organic Chemistry,* 2007**,** 2940-2944.

DE MAYO, P., SPENCER, E. Y. & WHITE, R. W. 1962. Constitution of Helminthosporal. *Journal of the American Chemical Society,* 84**,** 494-495.

DEUSS, P. J., BARTA, K. & DE VRIES, J. G. 2014. Homogeneous catalysis for the conversion of biomass and biomass-derived platform chemicals. *Catalysis Science & Technology,* 4**,** 1174-1196.

DEVINE, E. L., OPRIAN, D. D. & THEOBALD, D. L. 2013. Relocating the active-site lysine in rhodopsin and implications for evolution of retinylidene proteins. *Proceedings of the National Academy of Sciences of the United States of America,* 110**,** 13351-13355.

DIJKMAN, W. P., DE GONZALO, G., MATTEVI, A. & FRAAIJE, M. W. 2013. Flavoprotein oxidases: classification and applications. *Applied Microbiology and Biotechnology,* 97**,** 5177-5188.

DIJKMAN, W. P. & FRAAIJE, M. W. 2014. Discovery and Characterization of a 5-Hydroxymethylfurfural Oxidase from *Methylovorus* sp Strain MP688. *Applied and Environmental Microbiology,* 80**,** 1082-1090.

DING, W. T., ZHANG, Y. & SHI, S. B. 2020. Development and Application of CRISPR/Cas in Microbial Biotechnology. *Frontiers in Bioengineering and Biotechnology,* 8.

DITTA, G., STANFIELD, S., CORBIN, D. & HELINSKI, D. R. 1980. Broad Host Range DNA Cloning System for Gram-Negative Bacteria: Construction of a Gene Bank of *Rhizobium meliloti*. *Proceedings of the National Academy of Sciences of the United States of America,* 77**,** 7347-7351.

DOBRITSA, A. P. & SAMADPOUR, M. 2016. Transfer of eleven species of the genus *Burkholderia* to the genus *Paraburkholderia* and proposal of *Caballeronia* gen. nov. to accommodate twelve species of the genera *Burkholderia* and *Paraburkholderia*. *International Journal of Systematic and Evolutionary Microbiology,* 66**,** 2836-2846.

DOI, S., HASHIMOTO, Y., TOMITA, C., KUMANO, T. & KOBAYASHI, M. 2016. Discovery of piperonal-converting oxidase involved in the metabolism of a botanical aromatic aldehyde. *Scientific Reports,* 6**,** 38021.

DONG, J. J., FERNÁNDEZ-FUEYO, E., HOLLMANN, F., PAUL, C. E., PESIC, M., SCHMIDT, S., WANG, Y. H., YOUNES, S. & ZHANG, W. Y. 2018. Biocatalytic Oxidation Reactions: A Chemist's Perspective. *Angewandte Chemie-International Edition,* 57**,** 9238-9261.

DONOSO, R. A., GONZÁLEZ-TORO, F. & PÉREZ-PANTOJA, D. 2021. Widespread distribution of *hmf* genes in Proteobacteria reveals key enzymes for 5-hydroxymethylfurfural conversion. *Computational and Structural Biotechnology Journal,* 19**,** 2160-2169.

DOS SANTOS, V. A. P. M., HEIM, S., MOORE, E. R. B., STRÄTZ, M. & TIMMIS, K. N. 2004. Insights into the genomic basis of niche specificity of *Pseudomonas putida* KT2440. *Environmental Microbiology,* 6**,** 1264-1286.

DOYLE, S. M., GENEST, O. & WICKNER, S. 2013. Protein rescue from aggregates by powerful molecular chaperone machines. *Nature Reviews Molecular Cell Biology,* 14**,** 617-629.

DRAGOSITS, M. & MATTANOVICH, D. 2013. Adaptive laboratory evolution - principles and applications for biotechnology. *Microbial Cell Factories,* 12.

DREW, D., NORTH, R. A., NAGARATHINAM, K. & TANABE, M. 2021. Structures and General Transport Mechanisms by the Major Facilitator Superfamily (MFS). *Chemical Reviews,* 121**,** 5289-5335.

DU TOIT, A. 2017. Bacterial physiology: Efflux pumps, fitness and virulence. *Nature Reviews Microbiology,* 15**,** 512-513.

DUETZ, W. A., VAN BEILEN, J. B. & WITHOLT, B. 2001. Using proteins in their natural environment: potential and limitations of microbial whole-cell hydroxylations in applied biocatalysis. *Current Opinion in Biotechnology,* 12**,** 419-425.

DÜNKELMANN, P., KOLTER-JUNG, D., NITSCHE, A., DEMIR, A. S., SIEGERT, P., LINGEN, B., BAUMANN, M., POHL, M. & MÜLLER, M. 2002. Development of a donor-acceptor concept for enzymatic cross-coupling reactions of aldehydes: The first asymmetric cross-benzoin condensation. *Journal of the American Chemical Society,* 124**,** 12084-12085.

DUNLOP, M. J. 2011. Engineering microbes for tolerance to next-generation biofuels. *Biotechnology for Biofuels,* 4.

DURAIRAJ, P. & LI, S. 2022. Functional expression and regulation of eukaryotic cytochrome P450 enzymes in surrogate microbial cell factories. *Engineering Microbiology,* 2**,** 100011.

ECHTERMEYER, A. W. W. & VIELL, J. 2024. Integrated Humin Formation and Separation Studied In Situ by Centrifugation. *ACS Omega,* 9**,** 6432-6441.

EERHART, A. J. J. E., FAAIJ, A. P. C. & PATEL, M. K. 2012. Replacing fossil based PET with biobased PEF; process analysis, energy and GHG balance. *Energy & Environmental Science,* 5**,** 6407-6422.

ELIOT, A. C. & KIRSCH, J. F. 2004. Pyridoxal phosphate enzymes: Mechanistic, structural, and evolutionary considerations. *Annual Review of Biochemistry,* 73**,** 383-415.

ELLIS, L. D., RORRER, N. A., SULLIVAN, K. P., OTTO, M., MCGEEHAN, J. E., ROMÁN-LESHKOV, Y., WIERCKX, N. & BECKHAM, G. T. 2021. Chemical and biological catalysis for plastics recycling and upcycling. *Nature Catalysis,* 4**,** 539-556.

ESMAEEL, Q., MIOTTO, L., RONDEAU, M., LECLÈRE, V., CLÉMENT, C., JACQUARD, C., SANCHEZ, L. & BARKA, E. A. 2018. *Paraburkholderia phytofirmans* PsJN-Plants Interaction: From Perception to the Induced Mechanisms. *Frontiers in Microbiology,* 9.

FALLICO, B., ZAPPALÀ, M., ARENA, E. & VERZERA, A. 2004. Effects of conditioning on HMF content in unifloral honeys. *Food Chemistry,* 85**,** 305-313.

FARGIER, E., MAC AOGÁIN, M., MOOIJ, M. J., WOODS, D. F., MORRISSEY, J. P., DOBSON, A. D. W., ADAMS, C. & O'GARA, F. 2012. MexT Functions as a Redox-Responsive Regulator Modulating Disulfide Stress Resistance in *Pseudomonas aeruginosa*. *Journal of Bacteriology,* 194**,** 3502-3511.

FEI, X., WANG, J. G., ZHU, J., WANG, X. Z. & LIU, X. Q. 2020. Biobased Poly(ethylene 2,5-furanoate): No Longer an Alternative, but an Irreplaceable Polyester in the Polymer Industry. *ACS Sustainable Chemistry & Engineering,* 8**,** 8471-8485.

FERREIRA, P., HERNÁNDEZ-ORTEGA, A., HERGUEDAS, B., RENCORET, J., GUTIÉRREZ, A., MARTÍNEZ, M. J., JIMÉNEZ-BARBERO, J., MEDINA, M. & MARTÍNEZ, A. T. 2010. Kinetic and chemical characterization of aldehyde oxidation by fungal aryl-alcohol oxidase. *Biochemical Journal,* 425**,** 585-593.

FIGURSKI, D. H. & HELINSKI, D. R. 1979. Replication of an origin-containing derivative of plasmid RK2 dependent on a plasmid function provided in *trans*. *Proceedings of the National Academy of Sciences of the United States of America,* 76**,** 1648-1652.

FINNIGAN, W., THOMAS, A., CROMAR, H., GOUGH, B., SNAJDROVA, R., ADAMS, J. P., LITTLECHILD, J. A. & HARMER, N. J. 2017. Characterization of Carboxylic Acid Reductases as Enzymes in the Toolbox for Synthetic Chemistry. *ChemCatChem,* 9**,** 1005-1017.

FRANCE, S. P., HEPWORTH, L. J., TURNER, N. J. & FLITSCH, S. L. 2017. Constructing Biocatalytic Cascades: In Vitro and in Vivo Approaches to de Novo Multi-Enzyme Pathways. *ACS Catalysis,* 7**,** 710-724.

FRANDEN, M. A., JAYAKODY, L. N., LI, W. J., WAGNER, N. J., CLEVELAND, N. S., MICHENER, W. E., HAUER, B., BLANK, L. M., WIERCKX, N., KLEBENSBERGER, J. & BECKHAM, G. T. 2018. Engineering *Pseudomonas putida* KT2440 for efficient ethylene glycol utilization. *Metabolic Engineering,* 48**,** 197-207.

FRANDEN, M. A., PILATH, H. M., MOHAGHEGHI, A., PIENKOS, P. T. & ZHANG, M. 2013. Inhibition of growth of *Zymomonas mobilis* by model compounds found in lignocellulosic hydrolysates. *Biotechnology for Biofuels,* 6.

FREEMAN, A., WOODLEY, J. M. & LILLY, M. D. 1993. *In Situ* Product Removal as a Tool for Bioprocessing. *Bio/Technology,* 11**,** 1007-1012.

FRIEDMAN, M. 2017. Chemistry, Antimicrobial Mechanisms, and Antibiotic Activities of Cinnamaldehyde against Pathogenic Bacteria in Animal Feeds and Human Foods. *Journal of Agricultural and Food Chemistry,* 65**,** 10406-10423.

GAHLOTH, D., ALEKU, G. A. & LEYS, D. 2020. Carboxylic acid reductase: Structure and mechanism. *Journal of Biotechnology,* 307**,** 107-113.

GALANIE, S., THODEY, K., TRENCHARD, I. J., INTERRANTE, M. F. & SMOLKE, C. D. 2015. Complete biosynthesis of opioids in yeast. *Science,* 349**,** 1095-1100.

GALBE, M. & WALLBERG, O. 2019. Pretreatment for biorefineries: a review of common methods for efficient utilisation of lignocellulosic materials. *Biotechnology for Biofuels,* 12.

GALKIN, K. I. & ANANIKOV, V. P. 2019. When Will 5-Hydroxymethylfurfural, the "Sleeping Giant" of Sustainable Chemistry, Awaken? *Chemsuschem,* 12**,** 2976-2982.

GALLAGE, N. J. & MOLLER, B. L. 2015. Vanillin-Bioconversion and Bioengineering of the Most Popular Plant Flavor and Its Biosynthesis in the Vanilla Orchid. *Molecular Plant,* 8**,** 40-57.

GALLEGOS, M. T., SCHLEIF, R., BAIROCH, A., HOFMANN, K. & RAMOS, J. L. 1997. AraC/XylS family of transcriptional regulators. *Microbiology and Molecular Biology Reviews,* 61**,** 393-410.

GAO, X. P., XU, K., AHMAD, N., QIN, L. & LI, C. 2021. Recent advances in engineering of microbial cell factories for intelligent pH regulation and tolerance. *Biotechnology Journal,* 16.

GARCIA-HIDALGO, J., BRINK, D. P., RAVI, K., PAUL, C. J., LIDEN, G. & GORWA-GRAUSLUND, M. F. 2020. Vanillin Production in *Pseudomonas*: Whole-Genome Sequencing of *Pseudomonas* sp. Strain 9.1 and Reannotation of *Pseudomonas putida* CalA as a Vanillin Reductase. *Applied and Environmental Microbiology,* 86.

GARGIULO, S. & SOUMILLION, P. 2021. Directed evolution for enzyme development in biocatalysis. *Current Opinion in Chemical Biology,* 61**,** 107-113.

GASSON, M. J., KITAMURA, Y., MCLAUCHLAN, W. R., NARBAD, A., PARR, A. J., LINDSAY, E., PARSONS, H., PAYNE, J., RHODES, M. J. C. & WALTON, N. J. 1998. Metabolism of ferulic acid to vanillin - A bacterial gene of the enoyl-SCoA hydratase/isomerase superfamily encodes an enzyme for the hydration and cleavage of a hydroxycinnamic acid SCoA thioester. *Journal of Biological Chemistry,* 273**,** 4163-4170.

GIBSON, D. G., YOUNG, L., CHUANG, R. Y., VENTER, J. C., HUTCHISON, C. A. & SMITH, H. O. 2009. Enzymatic assembly of DNA molecules up to several hundred kilobases. *Nature Methods,* 6**,** 343-345.

GOTTARDI, M., KNUDSEN, J. D., PRADO, L., OREB, M., BRANDUARDI, P. & BOLES, E. 2017. De novo biosynthesis of *trans*-cinnamic acid derivatives in *Saccharomyces cerevisiae*. *Applied Microbiology and Biotechnology,* 101**,** 4883-4893.

GRAF, N. & ALTENBUCHNER, J. 2014. Genetic engineering of *Pseudomonas putida* KT2440 for rapid and high-yield production of vanillin from ferulic acid. *Applied Microbiology and Biotechnology,* 98**,** 137-49.

GRUNDTVIG, I. P. R., HEINTZ, S., KRÜHNE, U., GERNAEY, K. V., ADLERCREUTZ, P., HAYLER, J. D., WELLS, A. S. & WOODLEY, J. M. 2018. Screening of organic solvents for bioprocesses using aqueous-organic two-phase systems. *Biotechnology Advances,* 36**,** 1801-1814.

GRUTER, G. J. M. & DAUTZENBERG, F. 2007. *Method for the synthesis of 5-alkoxymethyl furfural ethers and their use*. World Intellectual Property Organization patent application WO 2007/104514 A2. 20.09.2007.

GUARNIERI, M. T., ANN FRANDEN, M., JOHNSON, C. W. & BECKHAM, G. T. 2017. Conversion and assimilation of furfural and 5-(hydroxymethyl)furfural by *Pseudomonas putida* KT2440. *Metabolic Engineering Communications,* 4**,** 22-28.

GURDO, N., VOLKE, D. C. & NIKEL, P. I. 2022. Merging automation and fundamental discovery into the design-build-test-learn cycle of nontraditional microbes. *Trends in Biotechnology,* 40**,** 1148-1159.

HAGEL, J. M. & FACCHINI, P. J. 2013. Benzylisoquinoline Alkaloid Metabolism: A Century of Discovery and a Brave New World. *Plant and Cell Physiology,* 54**,** 647-672.

HAN, T., NAZARBEKOV, A., ZOU, X. & LEE, S. Y. 2023. Recent advances in systems metabolic engineering. *Current Opinion in Biotechnology,* 84.

HANSEN, E. H., MOLLER, B. L., KOCK, G. R., BUNNER, C. M., KRISTENSEN, C., JENSEN, O. R., OKKELS, F. T., OLSEN, C. E., MOTAWIA, M. S. & HANSEN, J. 2009. De novo biosynthesis of vanillin in fission yeast (*Schizosaccharomyces pombe*) and baker's yeast (*Saccharomyces cerevisiae*). *Applied and Environmental Microbiology,* 75**,** 2765-74.

HAO, Y. Y., WANG, G. Y., SHUI, X. X., TIAN, A. P., YANG, Y. & ZHU, J. 2021. Design and synthesis of HFCA-based plasticizers with asymmetrical alkyl chains for poly(vinyl chloride). *Journal of Applied Polymer Science,* 138.

HARTL, F. U., BRACHER, A. & HAYER-HARTL, M. 2011. Molecular chaperones in protein folding and proteostasis. *Nature,* 475**,** 324-332.

HARTMANS, S., SMITS, J. P., VAN DER WERF, M. J., VOLKERING, F. & DE BONT, J. A. 1989. Metabolism of Styrene Oxide and 2-Phenylethanol in the Styrene-Degrading *Xanthobacter* Strain 124X. *Applied and Environmental Microbiology,* 55**,** 2850-5.

HARWOOD, C. S. & PARALES, R. E. 1996. The β-ketoadipate pathway and the biology of self-identity. *Annual Review of Microbiology,* 50**,** 553-590.

HAWKINS, K. M. & SMOLKE, C. D. 2008. Production of benzylisoquinoline alkaloids in *Saccharomyces cerevisiae*. *Nature Chemical Biology,* 4**,** 564-573.

HAYES, G. C. & BECER, C. R. 2020. Levulinic acid: a sustainable platform chemical for novel polymer architectures. *Polymer Chemistry,* 11**,** 4068-4077.

HE, J., QIANG, Q., BAI, L., SU, W., YU, H. & LIU, S. 2024. Acetalization strategy in biomass valorization: a review. *Industrial Chemistry & Materials,* 2**,** 30-56.

HE, L. J., CHEN, L., ZHENG, B. H., ZHOU, H., WANG, H., LI, H., ZHANG, H., XU, C. C. & YANG, S. 2023. Deep eutectic solvents for catalytic biodiesel production from liquid biomass and upgrading of solid biomass into 5-hydroxymethylfurfural. *Green Chemistry,* 25**,** 7410-7440.

HECKO, S., SCHIEFER, A., BADENHORST, C. P. S., FINK, M. J., MIHOVILOVIC, M. D., BORNSCHEUER, U. T. & RUDROFF, F. 2023. Enlightening the Path to Protein Engineering: Chemoselective Turn-On Probes for High-Throughput Screening of Enzymatic Activity. *Chemical Reviews,* 123**,** 2832-2901.

HEER, D. & SAUER, U. 2008. Identification of furfural as a key toxin in lignocellulosic hydrolysates and evolution of a tolerant yeast strain. *Microbial Biotechnology,* 1**,** 497-506.

HEIPIEPER, H. J., NEUMANN, G., CORNELISSEN, S. & MEINHARDT, F. 2007. Solvent-tolerant bacteria for biotransformations in two-phase fermentation systems. *Applied Microbiology and Biotechnology,* 74**,** 961-973.

HEMMERICH, J., NOACK, S., WIECHERT, W. & OLDIGES, M. 2018. Microbioreactor Systems for Accelerated Bioprocess Development. *Biotechnology Journal,* 13.

HENDERSON, P. J. F., MAHER, C., ELBOURNE, L. D. H., EIJKELKAMP, B. A., PAULSEN, I. T. & HASSAN, K. A. 2021. Physiological Functions of Bacterial "Multidrug" Efflux Pumps. *Chemical Reviews,* 121**,** 5417-5478.

HIRASAWA, T. & MAEDA, T. 2023. Adaptive Laboratory Evolution of Microorganisms: Methodology and Application for Bioproduction. *Microorganisms,* 11.

HOLDEN, H. M., BENNING, M. M., HALLER, T. & GERLT, J. A. 2001. The crotonase superfamily: Divergently related enzymes that catalyze different reactions involving acyl coenzyme A thioesters. *Accounts of Chemical Research,* 34**,** 145-157.

HOLLAND, I. & DAVIES, J. A. 2020. Automation in the Life Science Research Laboratory. *Frontiers in Bioengineering and Biotechnology,* 8.

HOLMQUIST, M. 2000. Alpha/Beta-Hydrolase Fold Enzymes: Structures, Functions and Mechanisms. *Current Protein & Peptide Science,* 1**,** 209-235.

HOSSAIN, G. S., YUAN, H. B., LI, J. H., SHIN, H. D., WANG, M., DU, G. C., CHEN, J. & LIU, L. 2017. Metabolic Engineering of *Raoultella ornithinolytica* BF60 for Production of 2,5-Furandicarboxylic Acid from 5-Hydroxymethylfurfural. *Applied and Environmental Microbiology,* 83.

HOU, Q. D., BAI, C. Y. L., BAI, X. Y., QIAN, H. L., NIE, Y. F., XIA, T. L., LAI, R. T., YU, G. J., REHMAN, M. L. U. & JU, M. T. 2022. Roles of Ball Milling Pretreatment and Titanyl Sulfate in the Synthesis of 5-Hydroxymethylfurfural from Cellulose. *ACS Sustainable Chemistry & Engineering,* 10**,** 1205-1213.

HOYOS, P., SINISTERRA, J. V., MOLINARI, F., ALCÁNTARA, A. R. & DE MARÍA, P. D. 2010. Biocatalytic Strategies for the Asymmetric Synthesis of α-Hydroxy Ketones. *Accounts of Chemical Research,* 43**,** 288-299.

HSU, C. T., KUO, Y. C., LIU, Y. C. & TSAI, S. L. 2020. Green conversion of 5-hydroxymethylfurfural to furan-2,5-dicarboxylic acid by heterogeneous expression of 5-hydroxymethylfurfural oxidase in *Pseudomonas putida* S12. *Microb Biotechnol,* 13**,** 1094-1102.

HU, L., HE, A. Y., LIU, X. Y., XIA, J., XU, J. X., ZHOU, S. Y. & XU, J. M. 2018. Biocatalytic Transformation of 5-Hydroxymethylfurfural into High-Value Derivatives: Recent Advances and Future Aspects. *ACS Sustainable Chemistry & Engineering,* 6**,** 15915-15935.

HU, Y. C. & PHAM, N. N. 2021. *Transformant for producing 2,5-furandicarboxylic acid and preparation method for 2,5-furandicarboxylic acid*. United States patent application US 2021/0189443 A1. 24.06.2021.

HU, Y. Z., LI, S., ZHAO, X. L., WANG, C. G., ZHANG, X. H., LIU, J. G., MA, L. L., CHEN, L. G. & ZHANG, Q. 2022. Catalytic oxidation of native lignin to phenolic monomers: Insight into aldehydes formation and stabilization. *Catalysis Communications,* 172.

HUANG, H. J. & HANCOCK, R. E. W. 1993. Genetic Definition of the Substrate Selectivity of Outer-Membrane Porin Protein OprD of *Pseudomonas aeruginosa*. *Journal of Bacteriology,* 175**,** 7793-7800.

HUYNH, Q. T., ZHONG, C. T., HUANG, Q., LIN, Y. C., CHEN, K. F., LIAO, C. S., DONG, C. D. & CHANG, K. L. 2023. Highly effective synthesis of 5-hydroxymethylfurfural from lignocellulosic biomass over a green and one-pot reaction in biphasic system. *Bioresource Technology,* 387.

HWANG, K. R., JEON, W., LEE, S. Y., KIM, M. S. & PARK, Y. K. 2020. Sustainable bioplastics: Recent progress in the production of bio-building blocks for the bio-based next-generation polymer PEF. *Chemical Engineering Journal,* 390.

INOUE, A. & HORIKOSHI, K. 1989. A *Pseudomonas* Thrives in High-Concentrations of Toluene. *Nature,* 338**,** 264-266.

INOUE, A. & HORIKOSHI, K. 1991. Estimation of solvent-tolerance of bacteria by the solvent Parameter log P. *Journal of Fermentation and Bioengineering,* 71**,** 194-196.

ISKEN, S. & DE BONT, J. A. M. 1998. Bacteria tolerant to organic solvents. *Extremophiles,* 2**,** 229-238.

IYER, K. S., NELSON, C. & LIPSHUTZ, B. H. 2023. Facile, green, and functional group-tolerant reductions of carboxylic acids ... in, or with, water. *Green Chemistry,* 25**,** 2663-2671.

JABLONSKA, J. & TAWFIK, D. S. 2022. Innovation and tinkering in the evolution of oxidases. *Protein Science,* 31.

JAGANMOHAN, M. 2024a. *Market value of polyethylene terephthalate worldwide from 2015 to 2022, with a forecast for 2023 to 2030* [Online]. Available: https://www.statista.com/statistics/964331/market-value-polyethylene-terephthalate-worldwide/ [Accessed 07.03.2024].

JAGANMOHAN, M. 2024b. *Production capacity of polyethylene terephthalate worldwide from 2014 to 2024* [Online]. Available: https://www.statista.com/statistics/242764/global-polyethylene-terephthalate-production-capacity/ [Accessed 07.03.2024].

JANZEN, N. H., STRIEDNER, G., JARMER, J., VOIGTMANN, M., ABAD, S. & REINISCH, D. 2019. Implementation of a Fully Automated Microbial Cultivation Platform for Strain and Process Screening. *Biotechnology Journal,* 14.

JAYAKODY, L. N., CHINMOY, B. & TURNER, T. L. 2022. Trends in valorization of highly-toxic lignocellulosic biomass derived-compounds via engineered microbes. *Bioresource Technology,* 346.

JAYAKODY, L. N. & JIN, Y. S. 2021. In-depth understanding of molecular mechanisms of aldehyde toxicity to engineer robust. *Applied Microbiology and Biotechnology,* 105**,** 2675-2692.

JAYAKODY, L. N., JOHNSON, C. W., WHITHAM, J. M., GIANNONE, R. J., BLACK, B. A., CLEVELAND, N. S., KLINGEMAN, D. M., MICHENER, W. E., OLSTAD, J. L., VARDON, D. R., BROWN, R. C., BROWN, S. D., HETTICH, R. L., GUSS, A. M. & BECKHAM, G. T. 2018. Thermochemical wastewater valorization *via* enhanced microbial toxicity tolerance. *Energy & Environmental Science,* 11**,** 1625-1638.

JIANG, Z. W., ZENG, Y. J., HU, D., GUO, R. C., YAN, K. & LUQUE, R. 2023. Chemical transformations of 5-hydroxymethylfurfural into highly added value products: present and future. *Green Chemistry,* 25**,** 871-892.

JIMÉNEZ, J. I., MIÑAMBRES, B., GARCÍA, J. L. & DÍAZ, E. 2002. Genomic analysis of the aromatic catabolic pathways from *Pseudomonas putida* KT2440. *Environmental Microbiology,* 4**,** 824-841.

JONSSON, L. J., ALRIKSSON, B. & NILVEBRANT, N. O. 2013. Bioconversion of lignocellulose: inhibitors and detoxification. *Biotechnology for Biofuels,* 6.

JONSSON, L. J. & MARTIN, C. 2016. Pretreatment of lignocellulose: Formation of inhibitory by-products and strategies for minimizing their effects. *Bioresource Technology,* 199**,** 103-112.

JUAREZ, P., BROUTIN, I., BORDI, C., PLESIAT, P. & LLANES, C. 2018. Constitutive Activation of MexT by Amino Acid Substitutions Results in MexEF-OprN Overproduction in Clinical Isolates of *Pseudomonas aeruginosa*. *Antimicrobial Agents and Chemotherapy,* 62.

JULIAN-SANCHEZ, A., CASTREJON-GONZAGA, A. P., MORENO-HAGELSIEB, G., MUNOZ-CLARES, R. A. & RIVEROS-ROSAS, H. 2020. Metabolic role of aldehyde dehydrogenases in *Pseudomonas putida* KT2440. *FASEB Journal,* 34.

JULLESSON, D., DAVID, F., PFLEGER, B. & NIELSEN, J. 2015. Impact of synthetic biology and metabolic engineering on industrial production of fine chemicals. *Biotechnology Advances,* 33**,** 1395-1402.

KADISCH, M., WILLRODT, C., HILLEN, M., BÜHLER, B. & SCHMID, A. 2017. Maximizing the stability of metabolic engineering-derived whole-cell biocatalysts. *Biotechnology Journal,* 12.

KAKINUMA, A. & YAMATODANI, S. 1964. L-Glutamic Acid Formation from 2-Furoic Acid by Soil Bacteria. *Nature,* 201**,** 420-421.

KALLSCHEUER, N., VOGT, M., KAPPELMANN, J., KRUMBACH, K., NOACK, S., BOTT, M. & MARIENHAGEN, J. 2016. Identification of the *phd* gene cluster responsible for phenylpropanoid utilization in *Corynebacterium glutamicum*. *Applied Microbiology and Biotechnology,* 100**,** 1871-1881.

KAMPERS, L. F. C., VOLKERS, R. J. M. & DOS SANTOS, V. A. P. M. 2019. *Pseudomonas putida* KT2440 is HV1 certified, not GRAS. *Microbial Biotechnology,* 12**,** 845-848.

KANDASAMY, S., SAMUDRALA, S. P. & BHATTACHARYA, S. 2019. The route towards sustainable production of ethylene glycol from a renewable resource, biodiesel waste: a review. *Catalysis Science & Technology,* 9**,** 567-577.

KAVANAGH, K. L., JORNVALL, H., PERSSON, B. & OPPERMANN, U. 2008. Medium- and short-chain dehydrogenase/reductase gene and protein families : the SDR superfamily: functional and structural diversity within a family of metabolic and regulatory enzymes. *Cellular and Molecular Life Sciences,* 65**,** 3895-3906.

KAZIMÍROVÁ, V. & REBROS, M. 2021. Production of Aldehydes by Biocatalysis. *International Journal of Molecular Sciences,* 22.

KEASLING, J. 2008. From yeast to alkaloids. *Nature Chemical Biology,* 4**,** 524-525.

KEASLING, J. D. 2010. Manufacturing Molecules Through Metabolic Engineering. *Science,* 330**,** 1355-1358.

KELL, D. B., SWAINSTON, N., PIR, P. & OLIVER, S. G. 2015. Membrane transporter engineering in industrial biotechnology and whole cell biocatalysis. *Trends in Biotechnology,* 33**,** 237-46.

KIM, B., JEONG, J., LEE, D., KIM, S., YOON, H. J., LEE, Y. S. & CHO, J. K. 2011. Direct transformation of cellulose into 5-hydroxymethyl-2-furfural using a combination of metal chlorides in imidazolium ionic liquid. *Green Chemistry,* 13**,** 1503-1506.

KIM, G. B., CHOI, S. Y., CHO, I. J., AHN, D. & LEE, S. Y. 2023. Metabolic engineering for sustainability and health. *Trends in Biotechnology,* 41**,** 425-451.

KIM, H. S., CHOI, J. A., KIM, B. Y., FERRER, L., CHOI, J. M., WENDISCH, V. F. & LEE, J. H. 2022. Engineered *Corynebacterium glutamicum* as the Platform for the Production of Aromatic Aldehydes. *Frontiers in Bioengineering and Biotechnology,* 10.

KIM, M., SU, Y. Q., FUKUOKA, A., HENSEN, E. J. M. & NAKAJIMA, K. 2018. Aerobic Oxidation of 5-(Hydroxymethyl)furfural Cyclic Acetal Enables Selective Furan-2,5-dicarboxylic Acid Formation with CeO_2-Supported Gold Catalyst. *Angewandte Chemie-International Edition,* 57**,** 8235-8239.

KIM, S., KIM, S. H., AHN, J., JO, I., LEE, Z. W., CHOI, S. H. & HA, N. 2019. Crystal Structure of the Regulatory Domain of MexT, a Transcriptional Activator of the MexEFOprN Efflux Pump in Pseudomonas aeruginosa. *Mol Cells,* 42**,** 850-857.

KISER, P. D., GOLCZAK, M. & PALCZEWSKI, K. 2014. Chemistry of the Retinoid (Visual) Cycle. *Chemical Reviews,* 114**,** 194-232.

KLÄUSLI, T. 2014. AVA Biochem: commercialising renewable platform chemical 5-HMF. *Green Processing and Synthesis,* 3**,** 235-236.

KÖBBING, S., LECHTENBERG, T., WYNANDS, B., BLANK, L. M. & WIERCKX, N. 2024. Reliable Genomic Integration Sites in *Pseudomonas putida* Identified by Two-Dimensional Transcriptome Analysis. *ACS Synthetic Biology*.

KOENIG, K. & ANDREESEN, J. R. 1989. Molybdenum Involvement in Aerobic Degradation of 2-Furoic Acid by *Pseudomonas putida* Fu1. *Applied and Environmental Microbiology,* 55**,** 1829-34.

KOHLER, K. A. K., RUCKERT, C., SCHATSCHNEIDER, S., VORHOLTER, F. J., SZCZEPANOWSKI, R., BLANK, L. M., NIEHAUS, K., GOESMANN, A., PUHLER, A., KALINOWSKI, J. & SCHMID, A. 2013. Complete genome sequence of *Pseudomonas* sp. strain VLB120 a solvent tolerant, styrene degrading bacterium, isolated from forest soil. *Journal of Biotechnology,* 168**,** 729-730.

KOHLER, T., EPP, S. F., CURTY, L. K. & PECHERE, J. C. 1999. Characterization of MexT, the regulator of the MexE-MexF-OprN multidrug efflux system of *Pseudomonas aeruginosa*. *Journal of Bacteriology,* 181**,** 6300-5.

KOHLER, T., MICHEA-HAMZEHPOUR, M., HENZE, U., GOTOH, N., CURTY, L. K. & PECHERE, J. C. 1997. Characterization of MexE-MexF-OprN, a positively regulated multidrug efflux system of *Pseudomonas aeruginosa*. *Molecular Microbiology,* 23**,** 345-54.

KOOPMAN, F., WIERCKX, N., DE WINDE, J. H. & RUIJSSENAARS, H. J. 2010a. Efficient whole-cell biotransformation of 5-(hydroxymethyl)furfural into FDCA, 2,5-furandicarboxylic acid. *Bioresource Technology,* 101**,** 6291-6296.

KOOPMAN, F., WIERCKX, N., DE WINDE, J. H. & RUIJSSENAARS, H. J. 2010b. Identification and characterization of the furfural and 5-(hydroxymethyl)furfural degradation pathways of *Cupriavidus basilensis* HMF14. *Proceedings of the National Academy of Sciences of the United States of America,* 107**,** 4919-24.

KOOPMAN, F. W., RUIJSSENAARS, H. J. & WIERCKX, N. J. P. 2011. *Novel microorganism and its use in lignocellulose detoxification*. World Intellectual Property Organization patent application WO 2011/026906 A2. 10.03.2011.

KOZAEVA, E., NIELSEN, Z. S., NIETO-DOMÍNGUEZ, M. & NIKEL, P. 2024. The pAblo·pCasso self-curing vector toolset for unconstrained cytidine and adenine base-editing in Gram-negative bacteria. *Nucleic Acids Research,* 52.

KOZONO, I., HIBI, M., TAKEUCHI, M. & OGAWA, J. 2020. Purification and characterization of molybdenum-containing aldehyde dehydrogenase that oxidizes benzyl maltol derivative from *Pseudomonas nitroreducens* SB32154. *Bioscience Biotechnology and Biochemistry,* 84**,** 2390-2400.

KUNAMANENI, S. 2023. Bioplastics innovation: commercialization strategies for polyethylene furanoate (PEF) and polyhydroxy alkanoates (PHA). *Biofuels, Bioproducts and Biorefining,* 17**,** 421-436.

KUNDU, A. 2017. Vanillin biosynthetic pathways in plants. *Planta,* 245**,** 1069-1078.

KUNJAPUR, A. M., HYUN, J. C. & PRATHER, K. L. J. 2016. Deregulation of *S*-adenosylmethionine biosynthesis and regeneration improves methylation in the *E. coli* de novo vanillin biosynthesis pathway. *Microbial Cell Factories,* 15.

KUNJAPUR, A. M. & PRATHER, K. L. J. 2015. Microbial Engineering for Aldehyde Synthesis. *Applied and Environmental Microbiology,* 81**,** 1892-1901.

KUNJAPUR, A. M., TARASOVA, Y. & PRATHER, K. L. J. 2014. Synthesis and Accumulation of Aromatic Aldehydes in an Engineered Strain of *Escherichia coli*. *Journal of the American Chemical Society,* 136**,** 11644-11654.

KUSTER, B. F. M. 1990. 5-Hydroxymethylfurfural (HMF) - a Review Focusing on Its Manufacture. *Starch-Stärke,* 42**,** 314-321.

KUSUMAWARDHANI, H., HOSSEINI, R. & DE WINDE, J. H. 2018. Solvent Tolerance in Bacteria: Fulfilling the Promise of the Biotech Era? *Trends in Biotechnology,* 36**,** 1025-1039.

LABIB, M., GRABOWSKI, L., BRUSSELER, C., KALLSCHEUER, N., WACHTENDONK, L., FUCHS, T., JUPKE, A., WIECHERT, W., MARIENHAGEN, J., ROTHER, D. & NOACK, S. 2022. Toward the Sustainable Production of the Active Pharmaceutical Ingredient Metaraminol. *ACS Sustainable Chemistry & Engineering,* 10**,** 5117-5128.

LACROIX, R. A., PALSSON, B. O. & FEIST, A. M. 2017. A Model for Designing Adaptive Laboratory Evolution Experiments. *Applied and Environmental Microbiology,* 83.

LADKAU, N., SCHMID, A. & BÜHLER, B. 2014. The microbial cell - functional unit for energy dependent multistep biocatalysis. *Current Opinion in Biotechnology,* 30**,** 178-189.

LAMARCHE, M. G. & DEZIEL, E. 2011. MexEF-OprN efflux pump exports the *Pseudomonas* quinolone signal (PQS) precursor HHQ (4-hydroxy-2-heptylquinoline). *PLoS One,* 6**,** e24310.

LAND, M., HAUSER, L., JUN, S. R., NOOKAEW, I., LEUZE, M. R., AHN, T. H., KARPINETS, T., LUND, O., KORA, G., WASSENAAR, T., POUDEL, S. & USSERY, D. W. 2015. Insights from 20 years of bacterial genome sequencing. *Functional & Integrative Genomics,* 15**,** 141-161.

LEE, C. & PARK, C. 2017. Bacterial Responses to Glyoxal and Methylglyoxal: Reactive Electrophilic Species. *International Journal of Molecular Sciences,* 18.

LEE, J., CHEN, W. H. & PARK, Y. K. 2022. Recent achievements in platform chemical production from food waste. *Bioresource Technology,* 366.

LEE, J. W., NA, D., PARK, J. M., LEE, J., CHOI, S. & LEE, S. Y. 2012. Systems metabolic engineering of microorganisms for natural and non-natural chemicals. *Nature Chemical Biology,* 8**,** 536-546.

LEE, S. & KIM, P. 2020. Current Status and Applications of Adaptive Laboratory Evolution in Industrial Microorganisms. *Journal of Microbiology and Biotechnology,* 30**,** 793-803.

LEE, S. A., WRONA, L. J., CAHOON, A. B., CRIGLER, J., EITEMAN, M. A. & ALTMAN, E. 2016. Isolation and Characterization of Bacteria That Use Furans as the Sole Carbon Source. *Applied Biochemistry and Biotechnology,* 178**,** 76-90.

LEIMKÜHLER, S. & KLIPP, W. 1999. Role of XDHC in molybdenum cofactor insertion into xanthine dehydrogenase of *Rhodobacter capsulatus*. *Journal of Bacteriology,* 181**,** 2745-2751.

LENNEN, R. M., LIM, H. G., JENSEN, K., MOHAMMED, E. T., PHANEUF, P. V., NOH, M. H., MALLA, S., BORNER, R. A., CHEKINA, K., OZDEMIR, E., BONDE, I., KOZA, A., MAURY, J., PEDERSEN, L. E., SCHONING, L. Y., SONNENSCHEIN, N., PALSSON, B. O., NIELSEN, A. T., SOMMER, M. O. A., HERRGARD, M. J. & FEIST, A. M. 2023. Laboratory evolution reveals general and specific tolerance mechanisms for commodity chemicals. *Metabolic Engineering,* 76**,** 179-192.

LENZEN, C., WYNANDS, B., OTTO, M., BOLZENIUS, J., MENNICKEN, P., BLANK, L. M. & WIERCKX, N. 2019. High-Yield Production of 4-Hydroxybenzoate From Glucose or Glycerol by an Engineered *Pseudomonas taiwanensis* VLB120. *Frontiers in Bioengineering and Biotechnology,* 7.

LI, W. J., NARANCIC, T., KENNY, S. T., NIEHOFF, P. J., O'CONNOR, K., BLANK, L. M. & WIERCKX, N. 2020. Unraveling 1,4-Butanediol Metabolism in *Pseudomonas putida* KT2440. *Frontiers in Microbiology,* 11.

LI, X. Y., XU, R., YANG, J. X., NIE, S. X., LIU, D., LIU, Y. & SI, C. L. 2019. Production of 5-hydroxymethylfurfural and levulinic acid from lignocellulosic biomass and catalytic upgradation. *Industrial Crops and Products,* 130**,** 184-197.

LI, X. Z., PLÉSIAT, P. & NIKAIDO, H. 2015. The Challenge of Efflux-Mediated Antibiotic Resistance in Gram-Negative Bacteria. *Clinical Microbiology Reviews,* 28**,** 337-418.

LIAUW, A. Y., POLADI, R. H. & SUNKARA, H. B. 2018. *Process for preparing poly(trimethylene furandicarboxylate)*. World Intellectual Property Organization patent application WO 2018/071383 A1. 19.04.2018.

LIEDER, S., NIKEL, P. I., DE LORENZO, V. & TAKORS, R. 2015. Genome reduction boosts heterologous gene expression in *Pseudomonas putida*. *Microbial Cell Factories,* 14.

LIN, B. & TAO, Y. 2017. Whole-cell biocatalysts by design. *Microbial Cell Factories,* 16**,** 106.

LIN, L. F., HAN, X., HAN, B. X. & YANG, S. H. 2021. Emerging heterogeneous catalysts for biomass conversion: studies of the reaction mechanism. *Chemical Society Reviews,* 50**,** 11270-11292.

LIN, T. Y., WEN, R. C., SHEN, C. R. & TSAI, S. L. 2020. Biotransformation of 5-Hydroxymethylfurfural to 2,5-Furandicarboxylic Acid by a Syntrophic Consortium of Engineered *Synechococcus elongatus* and *Pseudomonas putida*. *Biotechnology Journal,* 15**,** 1900357.

LING, H., TEO, W. S., CHEN, B. B., LEONG, S. S. J. & CHANG, M. W. 2014. Microbial tolerance engineering toward biochemical production: from lignocellulose to products. *Current Opinion in Biotechnology,* 29**,** 99-106.

LIU, C. L. & SHAO, Z. Z. 2005. *Alcanivorax dieselolei* sp. nov., a novel alkane-degrading bacterium isolated from sea water and deep-sea sediment. *International Journal of Systematic and Evolutionary Microbiology,* 55**,** 1181-1186.

LIU, P., XIE, J., TAN, H., ZHOU, F., ZOU, L. & OUYANG, J. 2020. Valorization of *Gelidium amansii* for dual production of D-galactonic acid and 5-hydroxymethyl-2-furancarboxylic acid by chemo-biological approach. *Microbial Cell Factories,* 19**,** 104.

LIU, S. W., ZHU, Y. T., LIAO, Y. H., WANG, H. Y., LIU, Q. Y., MA, L. L. & WANG, C. G. 2022. Advances in understanding the humins: Formation , prevention and application. *Applications in Energy and Combustion Science,* 10.

LIU, Y., SUN, L. C., HUO, Y. X. & GUO, S. Y. 2023. Strategies for improving the production of bio-based vanillin. *Microbial Cell Factories,* 22.

LO, T. M., TEO, W. S., LING, H., CHEN, B. B., KANG, A. & CHANG, M. W. 2013. Microbial engineering strategies to improve cell viability for biochemical production. *Biotechnology Advances,* 31**,** 903-914.

LOESCHCKE, A. & THIES, S. 2020. Engineering of natural product biosynthesis in *Pseudomonas putida*. *Current Opinion in Biotechnology,* 65**,** 213-224.

LOMAN, N. J. & PALLEN, M. J. 2015. Twenty years of bacterial genome sequencing. *Nature Reviews Microbiology,* 13**,** 787-794.

LOOS, K., ZHANG, R., PEREIRA, I., AGOSTINHO, B., HU, H., MANIAR, D., SBIRRAZZUOLI, N., SILVESTRE, A. J. D., GUIGO, N. & SOUSA, A. F. 2020. A Perspective on PEF Synthesis, Properties, and End-Life. *Frontiers in Chemistry,* 8**,** 585.

LOPACHIN, R. M. & GAVIN, T. 2014. Molecular Mechanisms of Aldehyde Toxicity: A Chemical Perspective. *Chemical Research in Toxicology,* 27**,** 1081-1091.

LOPEZ-LORENZO, X., ASEM, H., STAMM, A., SUBRAMANIYAN, S., HAKKARAINEN, M. & SYRÉN, P. O. 2023. Whole-cell Mediated Carboxylation of 2-Furoic Acid Towards the Production of Renewable Platform Chemicals and Biomaterials. *ChemCatChem,* 15.

LÓPEZ, P. C., PENG, C. T., ARNEBORG, N., JUNICKE, H. & GERNAEY, K. 2021. Analysis of the response of the cell membrane of *Saccharomyces cerevisae* during the detoxification of common lignocellulosic inhibitors. *Scientific Reports,* 11.

LU, L., SHU, C., CHEN, L., YANG, Y., MA, S., ZHU, K. & SHI, B. 2020. Insecticidal activity and mechanism of cinnamaldehyde in *C. elegans*. *Fitoterapia,* 146**,** 104687.

LUAN, S., LI, W., GUO, Z. W., LI, W. X., HOU, X. J., SONG, Y., WANG, R. & WANG, Q. 2022. Synthesis of ordered hierarchically mesoporous/microporous carbon materials via compressed CO_2 for fructose-to-HMF transformation. *Green Energy & Environment,* 7**,** 1033-1044.

LUO, Z. W. & LEE, S. Y. 2020. Metabolic engineering of *Escherichia coli* for the production of benzoic acid from glucose. *Metabolic Engineering,* 62**,** 298-311.

LUONG, P. M., SHOGAN, B. D., ZABORIN, A., BELOGORTSEVA, N., SHROUT, J. D., ZABORINA, O. & ALVERDY, J. C. 2014. Emergence of the P2 Phenotype in *Pseudomonas aeruginosa* PAO1 Strains Involves Various Mutations in *mexT* or *mexF*. *Journal of Bacteriology,* 196**,** 504-513.

MA, M. G. & LIU, Z. L. 2010. Comparative transcriptome profiling analyses during the lag phase uncover *YAP1*, *PDR1*, *PDR3*, *RPN4*, and *HSF1* as key regulatory genes in genomic adaptation to the lignocellulose derived inhibitor HMF for *Saccharomyces cerevisiae*. *BMC Genomics,* 11.

MADEIRA, F., PEARCE, M., TIVEY, A. R. N., BASUTKAR, P., LEE, J., EDBALI, O., MADHUSOODANAN, N., KOLESNIKOV, A. & LOPEZ, R. 2022. Search and sequence analysis tools services from EMBL-EBI in 2022. *Nucleic Acids Research***,** W276–W279.

MAEDA-YORITA, K., AKI, K., SAGAI, H., MISAKI, H. & MASSEY, V. 1995. L-Lactate Oxidase and L-Lactate Monooxygenase - Mechanistic Variations on a Common Structural Theme. *Biochimie,* 77**,** 631-642.

MANCUSO, A. J., HUANG, S. L. & SWERN, D. 1978. Oxidation of Long-Chain and Related Alcohols to Carbonyls by Dimethyl-Sulfoxide Activated by Oxalyl Chloride. *Journal of Organic Chemistry,* 43**,** 2480-2482.

MARIENHAGEN, J. & BOTT, M. 2013. Metabolic engineering of microorganisms for the synthesis of plant natural products. *Journal of Biotechnology,* 163**,** 166-178.

MARSHALL, S. A., PAYNE, K. A. P. & LEYS, D. 2017. The UbiX-UbiD system: The biosynthesis and use of prenylated flavin (prFMN). *Archives of Biochemistry and Biophysics,* 632**,** 209-221.

MARTAU, G. A., CALINOIU, L. F. & VODNAR, D. C. 2021. Bio-vanillin: Towards a sustainable industrial production. *Trends in Food Science & Technology,* 109**,** 579-592.

MARTIN-PASCUAL, M., BATIANIS, C., BRUINSMA, L., ASIN-GARCIA, E., GARCIA-MORALES, L., WEUSTHUIS, R. A., VAN KRANENBURG, R. & DOS SANTOS, V. A. P. M. 2021. A navigation guide of synthetic biology tools for *Pseudomonas putida*. *Biotechnology Advances,* 49.

MARTINEZ-GARCIA, E. & DE LORENZO, V. 2011. Engineering multiple genomic deletions in Gram-negative bacteria: analysis of the multi-resistant antibiotic profile of *Pseudomonas putida* KT2440. *Environmental Microbiology,* 13**,** 2702-2716.

MARTINEZ-GARCIA, E., NIKEL, P. I., APARICIO, T. & DE LORENZO, V. 2014. Pseudomonas 2.0: genetic upgrading of *P. putida* KT2440 as an enhanced host for heterologous gene expression. *Microbial Cell Factories,* 13.

MAZOYER, E., DE SOUSA DIAS, A. S. V., MCKAY, B., BAARS, H. J., VREEKEN, V. P. C. & GRUTER, G. J. M. 2014. *Process for the preparation of 2,5-furan-dicarboxylic acid*. World Intellectual Property Organization patent application WO 2014/163500 A1. 09.10.2014.

MCKENNA, S. M., MINES, P., LAW, P., KOVACS-SCHREINER, K., BIRMINGHAM, W. R., TURNER, N. J., LEIMKUHLER, S. & CARNELL, A. J. 2017. The continuous oxidation of HMF to FDCA and the immobilisation and stabilisation of periplasmic aldehyde oxidase (PaoABC). *Green Chemistry,* 19**,** 4660-4665.

MCLURE, R. J., RADFORD, S. E. & BROCKWELL, D. J. 2022. High-throughput directed evolution: a golden era for protein science. *Trends in Chemistry,* 4**,** 378-391.

MENGERS, H. G., WESTARP, W. G. V., BRUCKER, D., JUPKE, A. & BLANK, L. M. 2022. Yeast-based production and in situ purification of acetaldehyde. *Bioprocess and Biosystems Engineering,* 45**,** 761-769.

MERINO, N., ARONSON, H. S., BOJANOVA, D. P., FEYHL-BUSKA, J., WONG, M. L., ZHANG, S. & GIOVANNELLI, D. 2019. Living at the Extremes: Extremophiles and the Limits of Life in a Planetary Context *Frontiers in Microbiology,* 10.

MESSORI, A., FASOLINI, A. & MAZZONI, R. 2022. Advances in Catalytic Routes for the Homogeneous Green Conversion of the Bio-Based Platform 5-Hydroxymethylfurfural. *ChemSusChem,* 15.

METKAR, P. S., OZER, R. & RAJAGOPALAN, B. 2017. *Process for preparing 2,5-furandicarboxylic acid and esters thereof*. World Intellectural Property Organization patent application WO 2017/017441 A1. 02.02.2017.

METKAR, P. S. & SENGUPTA, S. K. 2017. *Reactive distillation process for the esterification of furandicarboxylic acid*. World Intellectual Property Organization patent application WO 2017/017447 A1. 02.02.2017.

METZNER, M., GERMER, J. & HENGGE, R. 2004. Multiple stress signal integration in the regulation of the complex σ^S-dependent *csiD-ygaF-gabDTP* operon in *Escherichia coli*. *Molecular Microbiology,* 51**,** 799-811.

MEYER, D., WALTER, L., KOLTER, G., POHL, M., MÜLLER, M. & TITTMANN, K. 2011. Conversion of Pyruvate Decarboxylase into an Enantioselective Carboligase with Biosynthetic Potential. *Journal of the American Chemical Society,* 133**,** 3609-3616.

MILIC, M., DOMINGUEZ DE MARIA, P. & KARA, S. 2023. A patent survey on the biotechnological production of 2,5-furandicarboxylic acid (FDCA): Current trends and challenges. *EFB Bioeconomy Journal,* 3**,** 100050.

MINAMI, H., KIM, J. S., IKEZAWA, N., TAKEMURA, T., KATAYAMA, T., KUMAGAI, H. & SATO, F. 2008. Microbial production of plant benzylisoquinoline alkaloids. *Proceedings of the National Academy of Sciences of the United States of America,* 105**,** 7393-7398.

MIRANDA, A. S. D., MILAGRE, C. D. F. & HOLLMANN, F. 2022. Alcohol Dehydrogenases as Catalysts in Organic Synthesis. *Frontiers in Catalysis,* 2.

MOHEDANO, M. T., KONZOCK, O. & CHEN, Y. 2022. Strategies to increase tolerance and robustness of industrial microorganisms. *Synthetic and Systems Biotechnology,* 7**,** 533-540.

MUKHOPADHYAY, A. 2015. Tolerance engineering in bacteria for the production of advanced biofuels and chemicals. *Trends in Microbiology,* 23**,** 498-508.

MULLIGAN, C., FISCHER, M. & THOMAS, G. H. 2011. Tripartite ATP-independent periplasmic (TRAP) transporters in bacteria and archaea. *FEMS Microbiology Reviews,* 35**,** 68-86.

MUNEKATA, M. & TAMURA, G. 1981. Antitumor Activity of 5-Hydroxy-methyl-2-furoic Acid. *Agricultural and Biological Chemistry,* 45**,** 2149-2150.

MUÑOZ DE DIEGO, C., SCHAMMEL, W., DAM, M. A. & GRUTER, G. J. M. 2011a. *Method for the preparation of 2,5-furandicarboxylic acid and esters thereof*. World Intellectual Property Organization patent application WO 2011/043660 A2. 14.04.2011.

MUÑOZ DE DIEGO, C., SCHAMMEL, W., DAM, M. A. & GRUTER, G. J. M. 2011b. *Method for the preparation of 2,5-furandicarboxylic acid and for the preparation of the dialkyl ester of 2,5-furandicarboxylic acid*. World Intellectual Property Organization patent application WO 2011/043661 A1. 14.04.2011.

MURAKAMI, S., NAKASHIMA, R., YAMASHITA, E., MATSUMOTO, T. & YAMAGUCHI, A. 2006. Crystal structures of a multidrug transporter reveal a functionally rotating mechanism. *Nature,* 443**,** 173-179.

MUSCHIOL, J., PETERS, C., OBERLEITNER, N., MIHOVILOVIC, M. D., BORNSCHEUER, U. T. & RUDROFF, F. 2015. Cascade catalysis - strategies and challenges *en route* to preparative synthetic biology. *Chemical Communications,* 51**,** 5798-5811.

MUTALIK, V. K., GUIMARAES, J. C., CAMBRAY, G., LAM, C., CHRISTOFFERSEN, M. J., MAI, Q. A., TRAN, A. B., PAULL, M., KEASLING, J. D., ARKIN, A. P. & ENDY, D. 2013. Precise and reliable gene expression via standard transcription and translation initiation elements. *Nature Methods,* 10**,** 354-60.

NARANCIC, T., SALVADOR, M., HUGHES, G. M., BEAGAN, N., ABDULMUTALIB, U., KENNY, S. T., WU, H. H., SACCOMANNO, M., UM, J., O'CONNOR, K. E. & JIMÉNEZ, J. I. 2021. Genome analysis of the metabolically versatile *Pseudomonas umsongensis* GO16: the genetic basis for PET monomer upcycling into polyhydroxyalkanoates. *Microbial Biotechnology,* 14**,** 2463-2480.

NARCROSS, L., FOSSATI, E., BOURGEOIS, L., DUEBER, J. E. & MARTIN, V. J. J. 2016. Microbial Factories for the Production of Benzylisoquinoline Alkaloids. *Trends in Biotechnology,* 34**,** 228-241.

NELSON, K. E., WEINEL, C., PAULSEN, I. T., DODSON, R. J., HILBERT, H., DOS SANTOS, V. A. P. M., FOUTS, D. E., GILL, S. R., POP, M., HOLMES, M., BRINKAC, L., BEANAN, M., DEBOY, R. T., DAUGHERTY, S., KOLONAY, J., MADUPU, R., NELSON, W., WHITE, O., PETERSON, J., KHOURI, H., HANCE, I., LEE, P. C., HOLTZAPPLE, E., SCANLAN, D., TRAN, K., MOAZZEZ, A., UTTERBACK, T., RIZZO, M., LEE, K., KOSACK, D., MOESTL, D., WEDLER, H., LAUBER, J., STJEPANDIC, D., HOHEISEL, J., STRAETZ, M., HEIM, S., KIEWITZ, C., EISEN, J., TIMMIS, K. N., DÜSTERHÖFT, A., TÜMMLER, B. & FRASER, C. M. 2002. Complete genome sequence and comparative analysis of the metabolically versatile *Pseudomonas putida* KT2440. *Environmental Microbiology,* 4**,** 799-808.

NEUMANN, M., MITTELSTADT, G., IOBBI-NIVOL, C., SAGGU, M., LENDZIAN, F., HILDEBRANDT, P. & LEIMKUHLER, S. 2009. A periplasmic aldehyde oxidoreductase represents the first molybdopterin cytosine dinucleotide cofactor containing molybdo-flavoenzyme from *Escherichia coli*. *FEBS Journal,* 276**,** 2762-74.

NEUMANN, M., SEDUK, F., IOBBI-NIVOL, C. & LEIMKÜHLER, S. 2011. Molybdopterin Dinucleotide Biosynthesis in *Escherichia coli*. *Journal of Biological Chemistry,* 286**,** 1400-1408.

NGUYEN, T. D. & DANG, T. T. T. 2021. Cytochrome P450 Enzymes as Key Drivers of Alkaloid Chemical Diversification in Plants. *Frontiers in Plant Science,* 12.

NICOLAOU, S. A., GAIDA, S. M. & PAPOUTSAKIS, E. T. 2010. A comparative view of metabolite and substrate stress and tolerance in microbial bioprocessing: From biofuels and chemicals, to biocatalysis and bioremediation. *Metabolic Engineering,* 12**,** 307-331.

NIELSEN, J. & KEASLING, J. D. 2016. Engineering Cellular Metabolism. *Cell,* 164**,** 1185-1197.

NIELSEN, J. R., WEUSTHUIS, R. A. & HUANG, W. E. 2023. Growth-coupled enzyme engineering through manipulation of redox cofactor regeneration. *Biotechnology Advances,* 63.

NIKAIDO, H. & SAIER, M. H. 1992. Transport Proteins in Bacteria - Common Themes in Their Design. *Science,* 258**,** 936-942.

NIKEL, P. I., CHAVARRIA, M., DANCHIN, A. & DE LORENZO, V. 2016a. From dirt to industrial applications: *Pseudomonas putida* as a Synthetic Biology chassis for hosting harsh biochemical reactions. *Current Opinion in Chemical Biology,* 34**,** 20-29.

NIKEL, P. I., CHAVARRÍA, M., FUHRER, T., SAUER, U. & DE LORENZO, V. 2015. *Pseudomonas putida* KT2440 Strain Metabolizes Glucose through a Cycle Formed by Enzymes of the Entner-Doudoroff, Embden-Meyerhof-Parnas, and Pentose Phosphate Pathways. *Journal of Biological Chemistry,* 290**,** 25920-25932.

NIKEL, P. I. & DE LORENZO, V. 2018. *Pseudomonas putida* as a functional *chassis* for industrial biocatalysis: From native biochemistry to *trans*-metabolism. *Metabolic Engineering,* 50**,** 142-155.

NIKEL, P. I., FUHRER, T., CHAVARRÍA, M., SÁNCHEZ-PASCUALA, A., SAUER, U. & DE LORENZO, V. 2021. Reconfiguration of metabolic fluxes in as a response to sub-lethal oxidative stress. *ISME Journal,* 15**,** 1751-1766.

NIKEL, P. I., MARTÍNEZ-GARCÍA, E. & DE LORENZO, V. 2014. Biotechnological domestication of pseudomonads using synthetic biology. *Nature Reviews Microbiology,* 12**,** 368-379.

NIKEL, P. I., PÉREZ-PANTOJA, D. & DE LORENZO, V. 2016b. Pyridine nucleotide transhydrogenases enable redox balance of *Pseudomonas putida* during biodegradation of aromatic compounds. *Environmental Microbiology,* 18**,** 3565-3582.

NOGALES, J., GARCÍA, J. L. & DÍAZ, E. 2019. Degradation of Aromatic Compounds in *Pseudomonas*: A Systems Biology View. *In:* ROJO, F. (ed.) *Aerobic Utilization of Hydrocarbons, Oils, and Lipids. Handbook of Hydrocarbon and Lipid Microbiology.*

O'BRIEN, P. J., SIRAKI, A. G. & SHANGARI, N. 2005. Aldehyde sources, metabolism, molecular toxicity mechanisms, and possible effects on human health. *Critical Reviews in Toxicology,* 35**,** 609-662.

OLIVARES, J., ALVAREZ-ORTEGA, C. & MARTINEZ, J. L. 2014. Metabolic compensation of fitness costs associated with overexpression of the multidrug efflux pump MexEF-OprN in *Pseudomonas aeruginosa*. *Antimicrobial Agents and Chemotherapy,* 58**,** 3904-13.

OLIVEIRA, E. R., GOMEZ, J. G. C., TACIRO, M. K. & SILVA, L. F. 2021. *Burkholderia sacchari* (synonym *Paraburkholderia sacchari*): An industrial and versatile bacterial chassis for sustainable biosynthesis of polyhydroxyalkanoates and other bioproducts. *Bioresource Technology,* 337.

ORSI, E., CLAASSENS, N. J., NIKEL, P. I. & LINDNER, S. N. 2021. Growth-coupled selection of synthetic modules to accelerate cell factory development. *Nature Communications,* 12.

OSHRI, R. D., ZRIHEN, K. S., SHNER, I., BENDORI, S. O. & ELDAR, A. 2018. Selection for increased quorum-sensing cooperation in *Pseudomonas aeruginosa* through the shut-down of a drug resistance pump. *ISME Journal,* 12**,** 2458-2469.

OTTO, M., WYNANDS, B., LENZEN, C., FILBIG, M., BLANK, L. M. & WIERCKX, N. 2019. Rational Engineering of Phenylalanine Accumulation in *Pseudomonas taiwanensis* to Enable High-Yield Production of *Trans*-Cinnamate. *Frontiers in Bioengineering and Biotechnology,* 7**,** 312.

OTTO, M., WYNANDS, B., MARIENHAGEN, J., BLANK, L. M. & WIERCKX, N. 2020. Benzoate Synthesis from Glucose or Glycerol Using Engineered *Pseudomonas taiwanensis*. *Biotechnology Journal,* 15.

PAL, R. & CHATTARAJ, P. K. 2023. Electrophilicity index revisited. *Journal of Computational Chemistry,* 44**,** 278-297.

PANG, K., KOTEK, R. & TONELLI, A. 2006. Review of conventional and novel polymerization processes for polyesters. *Progress in Polymer Science,* 31**,** 1009-1037.

PANKE, S., WITHOLT, B., SCHMID, A. & WUBBOLTS, M. G. 1998. Towards a biocatalyst for (*S*)-Styrene oxide production: Characterization of the styrene degradation pathway of *Pseudomonas* sp. strain VLB120 *Applied and Environmental Microbiology,* 64**,** 3546-3546.

PAO, S. S., PAULSEN, I. T. & SAIER, M. H. 1998. Major facilitator superfamily. *Microbiology and Molecular Biology Reviews,* 62.

PARATE, R. D., DHARNE, M. S. & RODE, C. V. 2022. Integrated chemo and bio-catalyzed synthesis of 2,5-furandicarboxylic acid from fructose derived 5-hydroxymethylfurfural. *Biomass & Bioenergy,* 161.

PARTENHEIMER, W. & GRUSHIN, V. V. 2000. Synthesis of 2,5-Diformylfuran and Furan-2,5-Dicarboxylic Acid by Catalytic Air-Oxidation of 5-Hydroxymethylfurfural. Unexpectedly Selective Aerobic Oxidation of Benzyl Alcohol to Benzaldehyde with Metal=Bromide Catalysts. *Advanced Synthesis & Catalysis,* 343**,** 102-111.

PAYNE, K. A. P., MARSHALL, S. A., FISHER, K., CLIFF, M. J., CANNAS, D. M., YAN, C. Y., HEYES, D. J., PARKER, D. A., LARROSA, I. & LEYS, D. 2019. Enzymatic Carboxylation of 2-Furoic Acid Yields 2,5-Furandicarboxylic Acid (FDCA). *ACS Catalysis,* 9**,** 2854-2865.

PAYNE, K. A. P., WHITE, M. D., FISHER, K., KHARA, B., BAILEY, S. S., PARKER, D., RATTRAY, N. J. W., TRIVEDI, D. K., GOODACRE, R., BEVERIDGE, R., BARRAN, P., RIGBY, S. E. J., SCRUTTON, N. S., HAY, S. & LEYS, D. 2015. New cofactor supports α,β-unsaturated acid decarboxylation via 1,3-dipolar cycloaddition. *Nature,* 522**,** 497-501.

PEETERS, C., MEIER-KOLTHOFF, J. P., VERHEYDE, B., DE BRANDT, E., COOPER, V. S. & VANDAMME, P. 2016. Phylogenomic Study of *Burkholderia glathei*-like Organisms, Proposal of 13 Novel *Burkholderia* Species and Emended Descriptions of *Burkholderia sordidicola*, *Burkholderia zhejiangensis*, and *Burkholderia grimmiae Frontiers in Microbiology,* 7.

PEFERENCE. 2024. *The world's first commercial FDCA plant* [Online]. Available: https://peference.eu/fdca-flagship-plant/ [Accessed 23.02.2024].

PELLIS, A., HAERNVALL, K., PICHLER, C. M., GHAZARYAN, G., BREINBAUER, R. & GUEBITZ, G. M. 2016. Enzymatic hydrolysis of poly(ethylene furanoate). *Journal of Biotechnology,* 235**,** 47-53.

PETER, M. F., RULAND, J. A., DEPPING, P., SCHNEBERGER, N., SEVERI, E., MOECKING, J., GATTERDAM, K., TINDALL, S., DURAND, A., HEINZ, V., SIEBRASSE, J. P., KOENIG, P. A., GEYER, M., ZIEGLER, C., KUBITSCHECK, U., THOMAS, G. H. & HAGELUEKEN, G. 2022. Structural and mechanistic analysis of a tripartite ATP-independent periplasmic TRAP transporter. *Nature Communications,* 13.

PHAM, N. N., CHEN, C. Y., LI, H., NGUYEN, M. T. T., NGUYEN, P. K. P., TSAI, S. L., CHOU, J. Y., RAMLI, T. C. & HU, Y. C. 2020. Engineering Stable *Pseudomonas putida* S12 by CRISPR for 2,5-Furandicarboxylic Acid (FDCA) Production. *ACS Synthetic Biology,* 9**,** 1138-1149.

PHAN, H. B., LUONG, C. M., NGUYEN, L. P., BUI, B. T., NGUYEN, H. T., MAI, B. V., MAI, T. V. T., HUYNH, L. K. & TRAN, P. H. 2022. Eco-Friendly Synthesis of 5-Hydroxymethylfurfural and Its Applications as a Starting Material to Synthesize Valuable Heterocyclic Compounds. *ACS Sustainable Chemistry & Engineering*.

PIANCATELLI, G., SCETTRI, A. & DAURIA, M. 1982. Pyridinium Chlorochromate - a Versatile Oxidant in Organic-Synthesis. *Synthesis*, 245-258.

PLAGGENBORG, R., OVERHAGE, J., STEINBÜCHEL, A. & PRIEFERT, H. 2003. Functional analyses of genes involved in the metabolism of ferulic acid in *Pseudomonas putida* KT2440. *Applied Microbiology and Biotechnology,* 61, 528-535.

POBLETE-CASTRO, I., BECKER, J., DOHNT, K., DOS SANTOS, V. M. & WITTMANN, C. 2012. Industrial biotechnology of *Pseudomonas putida* and related species. *Applied Microbiology and Biotechnology,* 93, 2279-2290.

PRASAD, B. R., PADHI, R. K. & GHOSH, G. 2023. A review on key pretreatment approaches for lignocellulosic biomass to produce biofuel and value-added products. *International Journal of Environmental Science and Technology,* 20, 6929-6944.

PRIEFERT, H., RABENHORST, J. & STEINBÜCHEL, A. 2001. Biotechnological production of vanillin. *Applied Microbiology and Biotechnology,* 56, 296-314.

QUARTA, B. & ANESE, M. 2012. Furfurals removal from roasted coffee powder by vacuum treatment. *Food Chemistry,* 130, 610-614.

RAAIJMAKERS, J. M., DE BRUIJN, I., NYBROE, O. & ONGENA, M. 2010. Natural functions of lipopeptides from *Bacillus* and *Pseudomonas*: more than surfactants and antibiotics. *FEMS Microbiology Reviews,* 34, 1037-1062.

RABNAWAZ, M., WYMAN, I., AURAS, R. & CHENG, S. 2017. A roadmap towards green packaging: the current status and future outlook for polyesters in the packaging industry. *Green Chemistry,* 19, 4737-4753.

RABUS, R., JACK, D. L., KELLY, D. J. & SAIER, M. H. 1999. TRAP transporters: an ancient family of extracytoplasmic solute-receptor-dependent secondary active transporters. *Microbiology,* 145, 3431-3445.

RAGAUSKAS, A. J., WILLIAMS, C. K., DAVISON, B. H., BRITOVSEK, G., CAIRNEY, J., ECKERT, C. A., FREDERICK, W. J., HALLETT, J. P., LEAK, D. J., LIOTTA, C. L., MIELENZ, J. R., MURPHY, R., TEMPLER, R. & TSCHAPLINSKI, T. 2006. The path forward for biofuels and biomaterials. *Science,* 311, 484-489.

RAJESH, R. O., GODAN, T. K., RAI, A. K., SAHOO, D., PANDEY, A. & BINOD, P. 2019. Biosynthesis of 2,5-furan dicarboxylic acid by *Aspergillus flavus* APLS-1: Process optimization and intermediate product analysis. *Bioresource Technology,* 284, 155-160.

RAMOS, J. L., DUQUE, E., GALLEGOS, M. T., GODOY, P., RAMOS-GONZÁLEZ, M. I., ROJAS, A., TERÁN, W. & SEGURA, A. 2002. Mechanisms of solvent tolerance in gram-negative bacteria. *Annual Review of Microbiology,* 56, 743-768.

RAMOS, J. L., SOL CUENCA, M., MOLINA-SANTIAGO, C., SEGURA, A., DUQUE, E., GOMEZ-GARCIA, M. R., UDAONDO, Z. & ROCA, A. 2015. Mechanisms of solvent resistance mediated by interplay of cellular factors in *Pseudomonas putida*. *FEMS Microbiology Reviews,* 39, 555-66.

RAVI, K., GARCIA-HIDALGO, J., NOBEL, M., GORWA-GRAUSLUND, M. F. & LIDEN, G. 2018. Biological conversion of aromatic monolignol compounds by a *Pseudomonas* isolate from sediments of the Baltic Sea. *AMB Express,* 8, 32.

ROCA, A., RODRÍGUEZ-HERVA, J. J., DUQUE, E. & RAMOS, J. L. 2008. Physiological responses of *Pseudomonas putida* to formaldehyde during detoxification. *Microbial Biotechnology,* 1, 158-169.

ROMÁN-LESHKOV, Y., CHHEDA, J. N. & DUMESIC, J. A. 2006. Phase Modifiers Promote Efficient Production of Hydroxymethylfurfural from Fructose. *Science,* 312, 1933-1937.

RÖNITZ, J., HERRMANN, F., POLEN, T., WYNANDS, B. & WIERCKX, N. 2024. SIGHT-A system for solvent-tight incubation and growth monitoring in high throughput. *under review*.

ROSA, L. T., BIANCONI, M. E., THOMAS, G. H. & KELLY, D. J. 2018. Tripartite ATP-Independent Periplasmic (TRAP) Transporters and Tripartite Tricarboxylate Transporters (TTT): From Uptake to Pathogenicity. *Frontiers in Cellular and Infection Microbiology,* 8.

ROSATELLA, A. A., SIMEONOV, S. P., FRADE, R. F. M. & AFONSO, C. A. M. 2011. 5-Hydroxymethylfurfural (HMF) as a building block platform: Biological properties, synthesis and synthetic applications. *Green Chemistry,* 13, 754-793.

ROSENAU, T., POTTHAST, A., ZWIRCHMAYR, N. S., HETTEGGER, H., PLASSER, F., HOSOYA, T., BACHER, M., KRAINZ, K. & DIETZ, T. 2017. Chromophores from hexeneuronic acids: identification of HexA-derived chromophores. *Cellulose,* 24, 3671-3687.

ROSENBOOM, J. G., LANGER, R. & TRAVERSO, G. 2022. Bioplastics for a circular economy. *Nature Reviews Materials,* 7, 117-137.

ROSENFELD, C., KONNERTH, J., SAILER-KRONLACHNER, W., SOLT, P., ROSENAU, T. & VAN HERWIJNEN, H. W. G. 2020. Current Situation of the Challenging Scale-Up Development of Hydroxymethylfurfural Production. *ChemSusChem,* 13, 3544-3564.

ROZENBERG, A., INOUE, K., KANDORI, H. & BÉJÀ, O. 2021. Microbial Rhodopsins: The Last Two Decades. *Annual Review of Microbiology,* 75, 427-447.

RUDROFF, F. 2019. Whole-cell based synthetic enzyme cascades-light and shadow of a promising technology. *Current Opinion in Chemical Biology,* 49, 84-90.

RUIJSSENAARS, H. J. 2016. *Dehydrogenase-catalysed production of FDCA*. World Intellectual Property Organization patent application WO 2016/133384 A1. 25.08.2016.

RUIJSSENAARS, H. J., WIERCKX, N. J. P., KOOPMAN, F. W., STRAATHOF, A. J. J. & DE WINDE, J. H. 2011. *Polypeptides having oxidoreductase activity and their use*. World Intellectual Property Organization patent application WO 2011/026913 A1. 10.03.2011.

SAGRIPANTI, J. L., EKLUND, C. A., TROST, P. A., JINNEMAN, K. C., ABEYTA, C., KAYSNER, C. A. & HILL, W. E. 1997. Comparative sensitivity of 13 species of pathogenic bacteria to seven chemical germicides. *American Journal of Infection Control,* 25**,** 335-339.

SAIBIL, H. 2013. Chaperone machines for protein folding, unfolding and disaggregation. *Nature Reviews Molecular Cell Biology,* 14**,** 630-642.

SAILER-KRONLACHNER, W., ROSENFELD, C., BÖHMDORFER, S., BACHER, M., KONNERTH, J., ROSENAU, T., POTTHAST, A., GEYER, A. & VAN HERWIJNEN, H. W. G. 2022. Scale-Up of production of 5-hydroxymethylfurfural-rich adhesive precursors and structural features of humin side products. *Biomass Conversion and Biorefinery*.

SALIS, H. M., MIRSKY, E. A. & VOIGT, C. A. 2009. Automated design of synthetic ribosome binding sites to control protein expression. *Nature Biotechnology,* 27**,** 946-50.

SANDBERG, T. E., SALAZAR, M. J., WENG, L. L., PALSSON, B. O. & FEIST, A. M. 2019. The emergence of adaptive laboratory evolution as an efficient tool for biological discovery and industrial biotechnology. *Metabolic Engineering,* 56**,** 1-16.

SAYED, M., GABER, Y., JUNGHUS, F., MARTÍN, E. V., PYO, S. H. & HATTI-KAUL, R. 2022. Oxidation of 5-hydroxymethylfurfural with a novel aryl alcohol oxidase from *Mycobacterium* sp. MS1601. *Microbial Biotechnology,* 15**,** 2176-2190.

SCHMIDT, N. G., EGER, E. & KROUTIL, W. 2016. Building Bridges: Biocatalytic C-C-Bond Formation toward Multifunctional Products. *ACS Catalysis,* 6**,** 4286-4311.

SCHOBER, L., DOBIASOVÁ, H., JURKAS, V., PARMEGGIANI, F., RUDROFF, F. & WINKLER, M. 2023. Enzymatic reactions towards aldehydes: An overview. *Flavour and Fragrance Journal,* 38**,** 221-242.

SCHWANEMANN, T., OTTO, M., WIERCKX, N. & WYNANDS, B. 2020. *Pseudomonas* as Versatile Aromatics Cell Factory. *Biotechnology Journal,* 15.

SCHWANEMANN, T., URBAN, E. A., EBERLEIN, C., GÄTGENS, J., RAGO, D., KRINK, N., NIKEL, P. I., HEIPIEPER, H. J., WYNANDS, B. & WIERCKX, N. 2023. Production of (hydroxy)benzoate-derived polyketides by engineered Pseudomonas with *in situ* extraction. *Bioresource Technology,* 388.

SHELDON, R. A. 2014. Green and sustainable manufacture of chemicals from biomass: state of the art. *Green Chemistry,* 16**,** 950-963.

SHEN, H. Y., SHAN, H. Z. & LIU, L. 2020. Evolution Process and Controlled Synthesis of Humins with 5-Hydroxymethylfurfural (HMF) as Model Molecule. *ChemSusChem,* 13**,** 513-519.

SHENG, Y., TAN, X., ZHOU, X. & XU, Y. 2020. Bioconversion of 5-Hydroxymethylfurfural (HMF) to 2,5-Furandicarboxylic Acid (FDCA) by a Native Obligate Aerobic Bacterium, *Acinetobacter calcoaceticus* NL14. *Applied Biochemistry and Biotechnology* 192**,** 455-465.

SHI, N., LIU, Q. Y., ZHANG, Q., WANG, T. J. & MA, L. L. 2013. High yield production of 5-hydroxymethylfurfural from cellulose by high concentration of sulfates in biphasic system. *Green Chemistry,* 15**,** 1967-1974.

SHORTALL, K., DJEGHADER, A., MAGNER, E. & SOULIMANE, T. 2021. Insights into Aldehyde Dehydrogenase Enzymes: A Structural Perspective. *Frontiers in Molecular Biosciences,* 8.

SHREAZ, S., WANI, W. A., BEHBEHANI, J. M., RAJA, V., IRSHAD, M., KARCHED, M., ALI, I., SIDDIQI, W. A. & HUN, L. T. 2016. Cinnamaldehyde and its derivatives, a novel class of antifungal agents. *Fitoterapia,* 112**,** 116-131.

SIMON, O., KLAIBER, I., HUBER, A. & PFANNSTIEL, J. 2014. Comprehensive proteome analysis of the response of *Pseudomonas putida* KT2440 to the flavor compound vanillin. *Journal of Proteomics,* 109**,** 212-227.

SIMONS, C., WALSH, S. E., MAILLARD, J. Y. & RUSSELL, A. D. 2000. *Ortho*-Phthalaldehyde: proposed mechanism of action of a new antimicrobial agent. *Letters in Applied Microbiology,* 31**,** 299-302.

SINGHANIA, R. R., PATEL, A. K., SINGH, A., HALDAR, D., SOAM, S., CHEN, C. W., TSAI, M. L. & DONG, C. D. 2022. Consolidated bioprocessing of lignocellulosic biomass: Technological advances and challenges. *Bioresource Technology,* 354.

SINHA, A. K., VERMA, S. C. & SHARMA, U. K. 2007. Development and validation of an RP-HPLC method for quantitative determination of vanillin and related phenolic compounds in *Vanilla planifolia*. *Journal of Separation Science,* 30**,** 15-20.

SOKOLOVSKII, V., MURPHY, V. J., BOUSSIE, T. R., DIAMOND, G. M., DIAS, E. L., ZHU, G., LONGMIRE, J. M., HERRMANN, S., TORSSELL, S. & LAVRENKO, M. 2017. *Processes for the preparation of 2,5-furandicarboxylic acid and intermediates and derivatives thereof*. World Intellectual Property Organization patent application WO 2017/123763 A1. 20.07.2017.

SON, J., CHOI, I. H., LIM, C. G., JANG, J. H., BANG, H. B., CHA, J. W., JEON, E. J., SOHN, M. G., YUN, H. J., KIM, S. C. & JEONG, K. J. 2022. Production of Cinnamaldehyde through Whole-Cell Bioconversion from *trans*-Cinnamic Acid Using Engineered *Corynebacterium glutamicum*. *Journal of Agricultural and Food Chemistry,* 70**,** 2656-2663.

SONG, C. X., SUNDQVIST, G., MALM, E., DE BRUIJN, I., KUMAR, A., VAN DE MORTEL, J., BULONE, V. & RAAIJMAKERS, J. M. 2015. Lipopeptide biosynthesis in *Pseudomonas fluorescens* is regulated by the protease complex ClpAP. *BMC Microbiology,* 15.

STEGMANN, P., DAIOGLOU, V., LONDO, M., VAN VUUREN, D. P. & JUNGINGER, M. 2022. Plastic futures and their CO_2 emissions. *Nature,* 612**,** 272-276.

STORA ENSO. 2023. *Plastic as we know it is at the edge of a revolution, and this is how FuraCore® by Stora Enso can help* [Online]. Available: https://www.storaenso.com/en/newsroom/news/2023/7/furacore-by-stora-enso-here-to-revolutionise-plastic [Accessed 04.03.2024].

STORA ENSO. 2024. *FuraCore® — The innovative FDCA Process for bio-based plastics* [Online]. Available: https://www.storaenso.com/en/products/bio-based-materials/furacore-fdca [Accessed 04.03.2024].

STRLIC, M., THOMAS, J., TRAFELA, T., CSÉFALVAYOVÁ, L., CIGIC, I. K., KOLAR, J. & CASSAR, M. 2009. Material Degradomics: On the Smell of Old Books. *Analytical Chemistry,* 81**,** 8617-8622.

TAKAI, K., NAKAMURA, K., TOKI, T., TSUNOGAI, U., MIYAZAKI, M., MIYAZAKI, J., HIRAYAMA, H., NAKAGAWA, S., NUNOURA, T. & HORIKOSHI, K. 2008. Cell proliferation at 122°C and isotopically heavy CH_4 production by a hyperthermophilic methanogen under high-pressure cultivation. *Proceedings of the National Academy of Sciences of the United States of America,* 105**,** 10949-10954.

TAN, H. H., ZHOU, F., LIAO, D. M., OUYANG, J. & ZHENG, Z. J. 2020. Improved biosynthesis of 2,5-Furandicarboxylic acid through coupling of heterologous pathways in *Escherichia coli* and native pathways in *Pseudomonas putida* KT2440. *Biochemical Engineering Journal,* 161.

TAN, Y. S., ZHANG, R. K., LIU, Z. H., LI, B. Z. & YUAN, Y. J. 2022. Microbial Adaptation to Enhance Stress Tolerance. *Frontiers in Microbiology,* 13.

TENHAEF, N., STELLA, R., FRUNZKE, J. & NOACK, S. 2021. Automated Rational Strain Construction Based on High-Throughput Conjugation. *ACS Synthetic Biology,* 10**,** 589-599.

TEONG, S. P., YI, G. S. & ZHANG, Y. G. 2014. Hydroxymethylfurfural production from bioresources: past, present and future. *Green Chemistry,* 16**,** 2015-2026.

TEREOS. 2022. *How our fructose can be turned into "green" packaging* [Online]. Available: https://tereos.com/en/news/how-our-fructose-can-be-turned-into-green-packaging/ [Accessed 23.02.2024].

TETARD, A., FOLEY, S., MISLIN, G. L. A., BRUNEL, J. M., OLIVA, E., ANZOLA, F. T., ZEDET, A., CARDEY, B., PELLEQUER, Y., RAMSEYER, C., PLÉSIAT, P. & LLANES, C. 2021. Negative Impact of Citral on Susceptibility of *Pseudomonas aeruginosa* to Antibiotics. *Frontiers in Microbiology,* 12.

TETARD, A., ZEDET, A., GIRARD, C., PLÉSIAT, P. & LLANES, C. 2019. Cinnamaldehyde Induces Expression of Efflux Pumps and Multidrug Resistance in *Pseudomonas aeruginosa*. *Antimicrobial Agents and Chemotherapy,* 63.

THORWALL, S., SCHWARTZ, C., CHARTRON, J. W. & WHEELDON, I. 2020. Stress-tolerant non-conventional microbes enable next-generation chemical biosynthesis. *Nature Chemical Biology,* 16**,** 113-121.

TIAN, Z. X., FARGIER, E., MAC AOGÁIN, M., ADAMS, C., WANG, Y. P. & O'GARA, F. 2009. Transcriptome profiling defines a novel regulon modulated by the LysR-type transcriptional regulator MexT in *Pseudomonas aeruginosa*. *Nucleic Acids Research,* 37**,** 7546-7559.

TIDWELL, T. T. 2008. Hugo (Ugo) Schiff, Schiff bases, and a century of β-lactam synthesis. *Angewandte Chemie-International Edition,* 47**,** 1016-1020.

TISO, T., NARANCIC, T., WEI, R., POLLET, E., BEAGAN, N., SCHRÖDER, K., HONAK, A., JIANG, M. Y., KENNY, S. T., WIERCKX, N., PERRIN, R., AVÉROUS, L., ZIMMERMANN, W., O'CONNOR, K. & BLANK, L. M. 2021. Towards bio-upcycling of polyethylene terephthalate. *Metabolic Engineering,* 66**,** 167-178.

TISO, T., WINTER, B., WEI, R., HEE, J., DE WITT, J., WIERCKX, N., QUICKER, P., BORNSCHEUER, U. T., BARDOW, A., NOGALES, J. & BLANK, L. M. 2022. The metabolic potential of plastics as biotechnological carbon sources-Review and targets for the future. *Metabolic Engineering,* 71**,** 77-98.

TODEA, A., BÎTCAN, I., APARASCHIVEI, D., PAUSESCU, I., BADEA, V., PÉTER, F., GHERMAN, V. D., RUSU, G., NAGY, L. & KÉKI, S. 2019. Biodegradable Oligoesters of ε-Caprolactone and 5-Hydroxymethyl-2-Furancarboxylic Acid Synthesized by Immobilized Lipases. *Polymers,* 11.

TOMAS, R. A. F., BORDADO, J. C. M. & GOMES, J. F. P. 2013. *p*-Xylene Oxidation to Terephthalic Acid: A Literature Review Oriented toward Process Optimization and Development. *Chemical Reviews,* 113**,** 7421-7469.

TORRENS-SPENCE, M. P., GLINKERMAN, C. M., GÜNTHER, J. & WENG, J. K. 2021. Imine chemistry in plant metabolism. *Current Opinion in Plant Biology,* 60.

TROIANO, D., ORSAT, V. & DUMONT, M. J. 2020. Status of Biocatalysis in the Production of 2,5-Furandicarboxylic Acid. *ACS Catalysis,* 10**,** 9145-9169.

TRUDGILL, P. W. 1969. The metabolism of 2-furoic acid by *Pseudomanas* F2. *Biochemical Journal,* 113**,** 577-87.

TSILOMELEKIS, G., ORELLA, M. J., LIN, Z. X., CHENG, Z. W., ZHENG, W. Q., NIKOLAKIS, V. & VLACHOS, D. G. 2016. Molecular structure, morphology and growth mechanisms and rates of 5-hydroxymethyl furfural (HMF) derived humins. *Green Chemistry,* 18**,** 1983-1993.

UJOR, V. C. & OKONKWO, C. C. 2022. Microbial detoxification of lignocellulosic biomass hydrolysates: Biochemical and molecular aspects, challenges, exploits and future perspectives. *Frontiers in Bioengineering and Biotechnology,* 10.

VAN DER HOEK, S. A. & BORODINA, I. 2020. Transporter engineering in microbial cell factories: the ins, the outs, and the in-betweens. *Current Opinion in Biotechnology,* 66**,** 186-194.

VAN PUTTEN, R. J., SOETEDJO, J. N. M., PIDKO, E. A., VAN DER WAAL, J. C., HENSEN, E. J. M., DE JONG, E. & HEERES, H. J. 2013a. Dehydration of Different Ketoses and Aldoses to 5-Hydroxymethylfurfural. *ChemSusChem,* 6**,** 1681-1687.

VAN PUTTEN, R. J., VAN DER WAAL, J. C., DE JONG, E., RASRENDRA, C. B., HEERES, H. J. & DE VRIES, J. G. 2013b. Hydroxymethylfurfural, a versatile platform chemical made from renewable resources. *Chemical Reviews,* 113**,** 1499-597.

VERGALLI, J., BODRENKO, I. V., MASI, M., MOYNIE, L., ACOSTA-GUTIERREZ, S., NAISMITH, J. H., DAVIN-REGLI, A., CECCARELLI, M., VAN DEN BERG, B., WINTERHALTER, M. & PAGES, J. M. 2020. Porins and small-molecule translocation across the outer membrane of Gram-negative bacteria. *Nature Reviews Microbiology,* 18**,** 164-176.

VIDAL, L. S., ISALAN, M., HEAP, J. T. & LEDESMA-AMARO, R. 2023. A primer to directed evolution: current methodologies and future directions. *RSC Chemical Biology,* 4**,** 271-291.

VIGNOLI, J. A., VIEGAS, M. C., BASSOLI, D. G. & BENASSI, M. D. 2014. Roasting process affects differently the bioactive compounds and the antioxidant activity of arabica and robusta coffees. *Food Research International,* 61**,** 279-285.

VISVALINGAM, J., HERNANDEZ-DORIA, J. D. & HOLLEY, R. A. 2013. Examination of the genome-wide transcriptional response of *Escherichia coli* O157:H7 to cinnamaldehyde exposure. *Applied and Environmental Microbiology,* 79**,** 942-950.

VOLK, M. J., TRAN, V. G., TAN, S. I., MISHRA, S., FATMA, Z., BOOB, A., LI, H. X., XUE, P., MARTIN, T. A. & ZHAO, H. M. 2023. Metabolic Engineering: Methodologies and Applications. *Chemical Reviews,* 123**,** 5521-5570.

VOLKE, D. C., FRIIS, L., WIRTH, N. T., TURLIN, J. & NIKEL, P. I. 2020. Synthetic control of plasmid replication enables target- and self-curing of vectors and expedites genome engineering of *Pseudomonas putida*. *Metabolic Engineering Communications,* 10**,** e00126.

VOLKE, D. C., MARTINO, R. A., KOZAEVA, E., SMANIA, A. M. & NIKEL, P. I. 2022. Modular (de)construction of complex bacterial phenotypes by CRISPR/nCas9-assisted, multiplex cytidine base-editing. *Nature Communications,* 13.

VOLMER, J., NEUMANN, C., BUHLER, B. & SCHMID, A. 2014. Engineering of *Pseudomonas taiwanensis* VLB120 for Constitutive Solvent Tolerance and Increased Specific Styrene Epoxidation Activity. *Applied and Environmental Microbiology,* 80**,** 6539-6548.

VU, T. T. T., LIU, S. T., JONUSIS, M., JONUSIENE, S., CHOI, J., KAWANO, R., REHNBERG, N., HATTI-KAUL, R. & PYO, S. H. 2023. Sustainable One-Pot Synthesis of 5-(Hydroxymethyl)furfural from C6-Sugars by Enhanced H^+ Exchange Heterogeneous Catalysis. *ACS Sustainable Chemistry & Engineering,* 11**,** 17130-17141.

WACHTMEISTER, J. & ROTHER, D. 2016. Recent advances in whole cell biocatalysis techniques bridging from investigative to industrial scale. *Current Opinion in Biotechnology,* 42**,** 169-177.

WANG, G. H., QI, S., XIA, Y., PARVEZ, A. M., SI, C. L. & NI, Y. H. 2020a. Mild One-Pot Lignocellulose Fractionation Based on Acid-Catalyzed Biphasic Water/Phenol System to Enhance Components' Processability. *ACS Sustainable Chemistry & Engineering,* 8**,** 2772-2782.

WANG, G. L., LI, Q., ZHANG, Z., YIN, X. Z., WANG, B. Y. & YANG, X. P. 2023. Recent progress in adaptive laboratory evolution of industrial microorganisms. *Journal of Industrial Microbiology & Biotechnology,* 50.

WANG, H. Y., LI, Q., KUANG, X. L., XIAO, D. F., HAN, X. B., HU, X. D., LI, X. & MA, M. G. 2018. Functions of aldehyde reductases from *Saccharomyces cerevisiae* in detoxification of aldehyde inhibitors and their biotechnological applications. *Applied Microbiology and Biotechnology,* 102**,** 10439-10456.

WANG, T. F., NOLTE, M. W. & SHANKS, B. H. 2014. Catalytic dehydration of C_6 carbohydrates for the production of hydroxymethylfurfural (HMF) as a versatile platform chemical. *Green Chemistry,* 16**,** 548-572.

WANG, W. P. & SHAO, Z. Z. 2014. The long-chain alkane metabolism network of *Alcanivorax dieselolei*. *Nature Communications,* 5.

WANG, X., ZHANG, X. Y., ZONG, M. H. & LI, N. 2020b. Sacrificial Substrate-Free Whole-Cell Biocatalysis for the Synthesis of 2,5-Furandicarboxylic Acid by Engineered *Escherichia coli*. *ACS Sustainable Chemistry & Engineering,* 8**,** 4341-4345.

WASSENAAR, T. M. & ZIMMERMANN, K. 2020. How industrial bacterial cultures can be kept stable over time. *Letters in Applied Microbiology,* 71**,** 220-228.

WEBER, D., PATSCH, D., NEUMANN, A., WINKLER, M. & ROTHER, D. 2021. Production of the Carboxylate Reductase from *Nocardia otitidiscaviarum* in a Soluble, Active Form for *in vitro* Applications. *ChemBioChem,* 22**,** 1823-1832.

WEHRMANN, M., ELSAYED, E. M., KÖBBING, S., BENDZ, L., LEPAK, A., SCHWABE, J., WIERCKX, N., BANGE, G. & KLEBENSBERGER, J. 2020. Engineered PQQ-dependent alcohol dehydrogenase for the oxidation of 5-(hydroxymethyl)furoic acid. *ACS Catalysis,* 10**,** 7836-7842.

WEIMER, A., KOHLSTEDT, M., VOLKE, D. C., NIKEL, P. I. & WITTMANN, C. 2020. Industrial biotechnology of *Pseudomonas putida*: advances and prospects. *Applied Microbiology and Biotechnology,* 104**,** 7745-7766.

WEINBERGER, S., CANADELL, J., QUARTINELLO, F., YENIAD, B., ARIAS, A., PELLIS, A. & GUEBITZ, G. M. 2017. Enzymatic Degradation of Poly(ethylene 2,5-furanoate) Powders and Amorphous Films. *Catalysts,* 7.

WERPY, T. & PETERSEN, G. R. 2004. *Top Value Added Chemicals from Biomass: Volume I - Results of Screening for Potential Candidates from Sugars and Synthesis Gas* [Online]. Available: https://doi.org/10.2172/15008859 [Accessed 07.03.2024].

WIERCKX, N., ELINK SCHUURMAN, T. D., BLANK, L. M. & RUIJSSENAARS, H. J. 2015. Whole-Cell Biocatalytic Production of 2,5-Furandicarboxylic Acid. *In:* KAMM, B. (ed.) *Microorganisms in Biorefineries. Microbiology Monographs, vol 26.*

WIERCKX, N., KOOPMAN, F., BANDOUNAS, L., DE WINDE, J. H. & RUIJSSENAARS, H. J. 2010. Isolation and characterization of *Cupriavidus basilensis* HMF14 for biological removal of inhibitors from lignocellulosic hydrolysate. *Microbial Biotechnology,* 3**,** 336-43.

WIERCKX, N., KOOPMAN, F., RUIJSSENAARS, H. J. & DE WINDE, J. H. 2011. Microbial degradation of furanic compounds: biochemistry, genetics, and impact. *Applied Microbiology and Biotechnology,* 92**,** 1095-105.

WIERCKX, N. J., BALLERSTEDT, H., DE BONT, J. A. & WERY, J. 2005. Engineering of solvent-tolerant *Pseudomonas putida* S12 for bioproduction of phenol from glucose. *Applied and Environmental Microbiology,* 71**,** 8221-7.

WIERCKX, N. J. P., ELINK SCHUURMAN, T. D., KUIJPER, S. M. & RUIJSSENAARS, H. J. 2012. *Genetically modified cell and process for use of said cell*. World Intellectual Property Organization patent application WO 2012/064195 A2. 18.05.2012.

WINDLE, C. L., MÜLLER, M., NELSON, A. & BERRY, A. 2014. Engineering aldolases as biocatalysts. *Current Opinion in Chemical Biology,* 19**,** 25-33.

WINKLER, M. & LING, J. G. 2022. Biocatalytic Carboxylate Reduction - Recent Advances and New Enzymes. *ChemCatChem,* 14.

WINSOR, G. L., GRIFFITHS, E. J., LO, R., DHILLON, B. K., SHAY, J. A. & BRINKMAN, F. S. 2016. Enhanced annotations and features for comparing thousands of *Pseudomonas* genomes in the *Pseudomonas* genome database. *Nucleic Acids Research,* 44**,** D646-53.

WONG, M. K., LOCK, S. S. M., CHAN, Y. H., YEOH, S. J. & TAN, I. S. 2023. Towards sustainable production of bio-based ethylene glycol: Progress, perspective and challenges in catalytic conversion and purification. *Chemical Engineering Journal,* 468.

WOODLEY, J. M. 2022. Ensuring the Sustainability of Biocatalysis. *ChemSusChem,* 15.

WORDOFA, G. G. & KRISTENSEN, M. 2018. Tolerance and metabolic response of *Pseudomonas taiwanensis* VLB120 towards biomass hydrolysate-derived inhibitors. *Biotechnology for Biofuels,* 11.

WU, K., MINSHULL, T. C., RADFORD, S. E., CALABRESE, A. N. & BARDWELL, J. C. A. 2022. Trigger factor both holds and folds its client proteins. *Nature Communications,* 13**,** 4126.

WU, Q., ZONG, M. H. & LI, N. 2023. One-Pot Chemobiocatalytic Production of 2,5-Bis(hydroxymethyl)furan and Its Diester from Biomass in Aqueous Media. *ACS Catalysis,* 13**,** 9404-9414.

WYNANDS, B., KOFLER, F., SIEBERICHS, A., DA SILVA, N. & WIERCKX, N. 2023. Engineering a 4-coumarate platform for production of para-hydroxy aromatics with high yield and specificity. *Metabolic Engineering,* 78**,** 115-127.

WYNANDS, B., LENZEN, C., OTTO, M., KOCH, F., BLANK, L. M. & WIERCKX, N. 2018. Metabolic engineering of *Pseudomonas taiwanensis* VLB120 with minimal genomic modifications for high-yield phenol production. *Metabolic Engineering,* 47**,** 121-133.

WYNANDS, B., OTTO, M., RUNGE, N., PRECKEL, S., POLEN, T., BLANK, L. M. & WIERCKX, N. 2019. Streamlined *Pseudomonas taiwanensis* VLB120 Chassis Strains with Improved Bioprocess Features. *ACS Synthetic Biology,* 8**,** 2036-2050.

XU, C., PAONE, E., RODRIGUEZ-PADRON, D., LUQUE, R. & MAURIELLO, F. 2020a. Recent catalytic routes for the preparation and the upgrading of biomass derived furfural and 5-hydroxymethylfurfural. *Chemical Society Reviews,* 49**,** 4273-4306.

XU, Q., ZHENG, Z., ZOU, L., ZHANG, C., YANG, F., ZHOU, K. & OUYANG, J. 2020b. A versatile *Pseudomonas putida* KT2440 with new ability: selective oxidation of 5-hydroxymethylfurfural to 5-hydroxymethyl-2-furancarboxylic acid. *Bioprocess and Biosystems Engineering,* 43**,** 67-73.

XU, Z. W., YANG, Y. W., YAN, P. F., XIA, Z., LIU, X. B. & ZHANG, Z. C. 2020c. Mechanistic understanding of humin formation in the conversion of glucose and fructose to 5-hydroxymethylfurfural in [BMIM]Cl ionic liquid. *RSC Advances,* 10**,** 34732-34737.

YANG, C. F. & HUANG, C. R. 2016. Biotransformation of 5-hydroxy-methylfurfural into 2,5-furan-dicarboxylic acid by bacterial isolate using thermal acid algal hydrolysate. *Bioresource Technology,* 214**,** 311-318.

YILMAZ, S., NYERGES, A., VAN DER OOST, J., CHURCH, G. M. & CLAASSENS, N. J. 2022. Towards next-generation cell factories by rational genome-scale engineering. *Nature Catalysis,* 5**,** 751-765.

YOSHIMURA, A. & ZHDANKIN, V. V. 2016. Advances in Synthetic Applications of Hypervalent Iodine Compounds. *Chemical Reviews,* 116**,** 3328-3435.

YOU, L., LIU, T. X., LIU, D. H. & ZHAO, X. B. 2023. Efficient conversion of glucose to 5-hydroxymethylfurfural by synergetic catalysis of enzymes and chemical catalysts towards potential large-scale continuous operation. *Chemical Engineering Journal,* 459.

YUAN, H., LIU, H., DU, J., LIU, K., WANG, T. & LIU, L. 2020. Biocatalytic production of 2,5-furandicarboxylic acid: recent advances and future perspectives. *Applied Microbiology and Biotechnology* 104**,** 527-543.

YUAN, H. B., LI, J. H., SHIN, H. D., DU, G. C., CHEN, J., SHI, Z. P. & LIU, L. 2018a. Improved production of 2,5-furandicarboxylic acid by overexpression of 5-hydroxymethylfurfural oxidase and 5-hydroxymethylfurfural/furfural oxidoreductase in *Raoultella ornithinolytica* BF60. *Bioresource Technology,* 247**,** 1184-1188.

YUAN, H. B., LIU, Y. F., LI, J. H., SHIN, H. D., DU, G. C., SHI, Z. P., CHEN, J. & LIU, L. 2018b. Combinatorial synthetic pathway fine-tuning and comparative transcriptomics for metabolic engineering of *Raoultella*

ornithinolytica BF60 to efficiently synthesize 2,5-furandicarboxylic acid. *Biotechnology and Bioengineering,* 115**,** 2148-2155.

YUAN, H. B., LIU, Y. F., LV, X. Q., LI, J. H., DU, G. C., SHI, Z. P. & LIU, L. 2018c. Enhanced 2,5-furandicarboxylic acid (FDCA) production in *Raoultella ornithinolytica* BF60 by manipulation of the key genes in FDCA biosynthesis Pathway. *Journal of Microbiology and Biotechnology,* 28**,** 1999-2008.

YUE, H. R., ZHAO, Y. J., MA, X. B. & GONG, J. L. 2012. Ethylene glycol: properties, synthesis, and applications. *Chemical Society Reviews,* 41**,** 4218-4244.

YUN, H. & KIM, B. G. 2008. Enzymatic production of (*R*)-phenylacetylcarbinol by pyruvate decarboxylase from *Zymomonas mobilis*. *Biotechnology and Bioprocess Engineering,* 13**,** 372-376.

ZHENG, Z., XU, Q., TAN, H., ZHOU, F. & OUYANG, J. 2020. Selective Biosynthesis of Furoic Acid From Furfural by *Pseudomonas Putida* and Identification of Molybdate Transporter Involvement in Furfural Oxidation. *Frontiers in Chemistry,* 8**,** 587456.

ZHOU, F., HEARNE, Z. & LI, C. J. 2019a. Water-the greenest solvent overall. *Current Opinion in Green and Sustainable Chemistry,* 18**,** 118-123.

ZHOU, J., CHEN, Z. & WANG, Y. 2020a. Bioaldehydes and beyond: Expanding the realm of bioderived chemicals using biogenic aldehydes as platforms. *Current Opinion in Chemical Biology,* 59**,** 37-46.

ZHOU, Y. Y., LI, Z. H., WANG, X. N. & ZHANG, H. R. 2019b. Establishing microbial co-cultures for 3-hydroxybenzoic acid biosynthesis on glycerol. *Engineering in Life Sciences,* 19**,** 389-395.

ZHOU, Y. Y., LIN, L., WANG, H., ZHANG, Z. C., ZHOU, J. Z. & JIAO, N. Z. 2020b. Development of a CRISPR/Cas9n-based tool for metabolic engineering of *Pseudomonas putid*a for ferulic acid-to-polyhydroxyalkanoate bioconversion. *Communications Biology,* 3.

ZHU, Y., ZHOU, C., WANG, Y. & LI, C. 2020. Transporter Engineering for Microbial Manufacturing. *Biotechnology Journal,* 15.

ZOBEL, S., BENEDETTI, I., EISENBACH, L., DE LORENZO, V., WIERCKX, N. & BLANK, L. M. 2015. Tn7-Based Device for Calibrated Heterologous Gene Expression in *Pseudomonas putida*. *ACS Synthetic Biology,* 4**,** 1341-51.

ZOU, L., ZHENG, Z., TAN, H., XU, Q. & OUYANG, J. 2020. Synthesis of 2,5-furandicarboxylic acid by a TEMPO/laccase system coupled with *Pseudomonas putida* KT2440. *RSC Advances,* 10**,** 21781-21788.

ZOU, L. H., JIN, X. Z., TAO, Y. M., ZHENG, Z. J. & OUYANG, J. 2022. Unraveling the mechanism of furfural tolerance in *Pseudomonas putida* engineered by genomics. *Frontiers in Microbiology,* 13.

5. Appendix

5.1. Supplementary material to chapter 2.1

Engineering 5-hydroxymethylfurfural oxidation (HMF) in *Pseudomonas* boosts tolerance and accelerates 2,5-furandicarboxylic acid (FDCA) production

Thorsten Lechtenberg[a], Benedikt Wynands[a], and Nick Wierckx[a*]

[a]Institute of Bio- and Geosciences IBG-1: Biotechnology, Forschungszentrum Jülich, 52425 Jülich, Germany

*Corresponding author:

Nick Wierckx, Institute of Bio- and Geosciences, IBG-1: Biotechnology, Forschungszentrum Jülich GmbH, 52425 Jülich, Germany, phone: +49 2461 61-85247

E-mail: n.wierckx@fz-juelich.de

Table S5.1-1: Overview of the 32 ALDH-encoding genes of *P. putida* KT2440 according to Julián-Sánchez *et al.* (Julian-Sanchez et al., 2020) and their corresponding homologs in *P. taiwanensis* VLB120. Gene names were adopted from Pseudomonas Genome DB (Winsor et al., 2016). Protein sequence identities were determined using the Emboss Needle Pairwise Sequence Alignment tool (Madeira et al., 2022).

Gene name	Annotation	Locus Tag (*P. putida* KT2440)	Locus Tag (*P. taiwanensis* VLB120)	Identity [%]
gabD-I	glutarate-semialdehyde dehydrogenase	PP_0213	PVLB_01255	98.1
aldB-I	aldehyde dehydrogenase	PP_0545	PVLB_22390	96.4
mmsA-I	methylmalonate-semialdehyde dehydrogenase	PP_0597	PVLB_22030	98.8
-	putative glyceraldehyde-3-phosphate dehydrogenase	PP_0665	-	-
-	betaine-aldehyde dehydrogenase	PP_0708	PVLB_21510	91.6
-	putative alpha-ketoglutarate semialdehyde dehydrogenase	PP_1256	PVLB_18510	86.3
patD	medium chain aldehyde dehydrogenase	PP_1481	PVLB_19745	92.8
-	benzaldehyde dehydrogenase	PP_1948	-	-
aldA	putative aldehyde dehydrogenase	PP_2487	-	-
sad-I	NAD^+-dependent succinate semialdehyde dehydrogenase	PP_2488	-	-
-	alpha-ketoglutaric semialdehyde dehydrogenase	PP_2585	PVLB_18550	70.2
-	aldehyde dehydrogenase family protein	PP_2589	PVLB_25000	52.9
aldB-II (*pedI*)	aldehyde dehydrogenase	PP_2680	PVLB_22390	86.6
-	aldehyde dehydrogenase family protein	PP_2694	-	-
prr	gamma-aminobutyraldehyde dehydrogenase	PP_2801	PVLB_10550	79.7
sad-II	NAD^+-dependent succinate semialdehyde dehydrogenase	PP_3151	PVLB_12155	94.8
phaL	bifunctional aldehyde dehydrogenase/enoyl-CoA hydratase	PP_3270	PVLB_12525	95.3
vdh	vanillin dehydrogenase	PP_3357	-	-
-	glyceraldehyde-3-phosphate dehydrogenase	PP_3443	PVLB_12010	93.1
peaE	phenylacetaldehyde dehydrogenase	PP_3463	PVLB_12825	96.2
-	ketoglutarate semialdehyde dehydrogenase	PP_3602	PVLB_11380	92.2

-	aldehyde dehydrogenase	PP_3646	PVLB_11105	98.0
gabD-II	succinate-semialdehyde dehydrogenase	PP_4422	PVLB_22540	49.8
astD	succinylglutamic semialdehyde dehydrogenase	PP_4478	PVLB_17530	95.1
mmsA-II	methylmalonate-semialdehyde dehydrogenase	PP_4667	PVLB_03765	97.6
proA	gamma-glutamyl phosphate reductase	PP_4811	PVLB_22325	95.0
putA	trifunctional transcriptional regulator/proline dehydrogenase/pyrroline-5-carboxylate dehydrogenase	PP_4947	PVLB_02470	96.4
betB	betaine aldehyde dehydrogenase	PP_5063	PVLB_01845	97.8
calB	coniferyl aldehyde dehydrogenase	PP_5120	PVLB_01470	84.0
amaB	aldehyde dehydrogenase	PP_5258	PVLB_24885	98.8
kauB	aldehyde dehydrogenase	PP_5278	PVLB_25000	97.8
-	aldehyde dehydrogenase	PP_5372	-	-

Table S5.1-2: Aldehyde reducing enzymes deleted in the *E. coli* RARE strain and their homologs in *P. taiwanensis* VLB120. Protein sequence identities were determined using the Emboss Needle Pairwise Sequence Alignment tool (Madeira et al., 2022).

Gene name	Annotation	Type	Locus Tag (*P. taiwanensis* VLB120)	Identity [%]
dkgB (yafB)	2,5-diketo-D-gluconic acid reductase B	AKR	PVLB_14845	67.8
yeaE	aldo/keto reductase	AKR	PVLB_11635	56.7
dkgA (yqhE)	2,5-diketo-D-gluconic acid reductase A	AKR	PVLB_10970 PVLB_14845 PVLB_11635	36.4 34.4 29.4
yqhD	alcohol dehydrogenase	ADH	-	-
yahK	aldehyde reductase	ADH	PVLB_15055 PVLB_10545 PVLB_22260	54.8 27.5 23.6
yjgB (ahr)	aldehyde reductase	ADH	PVLB_15055 PVLB_10545 PVLB_22260	34.5 27.6 23.8

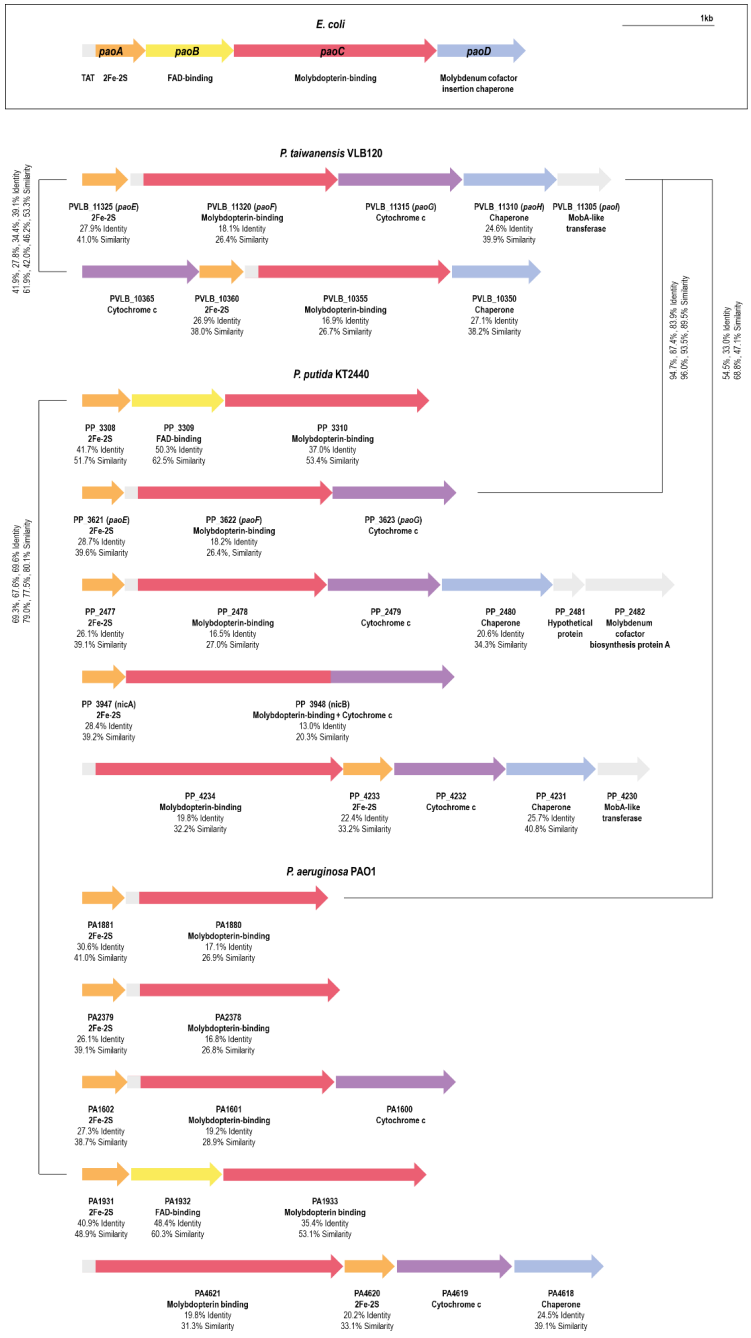

Figure S5.1-1: BLAST analysis screening for *paoABCD* homologs in *P. taiwanensis* VLB120, *P. putida* KT2440, and *P. aeruginosa* PAO1. In contrast to the last two both harboring *paoABC* but without a TAT-signal motif and the chaperone *paoD*, there is no homolog in *P. taiwanensis* VLB120. However, all strains possess related molybdenum-dependent enzymes. As *P. taiwanensis* VLB120 has only two operons encoding putative aldehyde oxidizing enzyme complexes, this bacterium was chosen for first experiments to reduce complexity. Sequence identities were determined using the Emboss Needle Pairwise Sequence Alignment tool (Madeira et al., 2022).

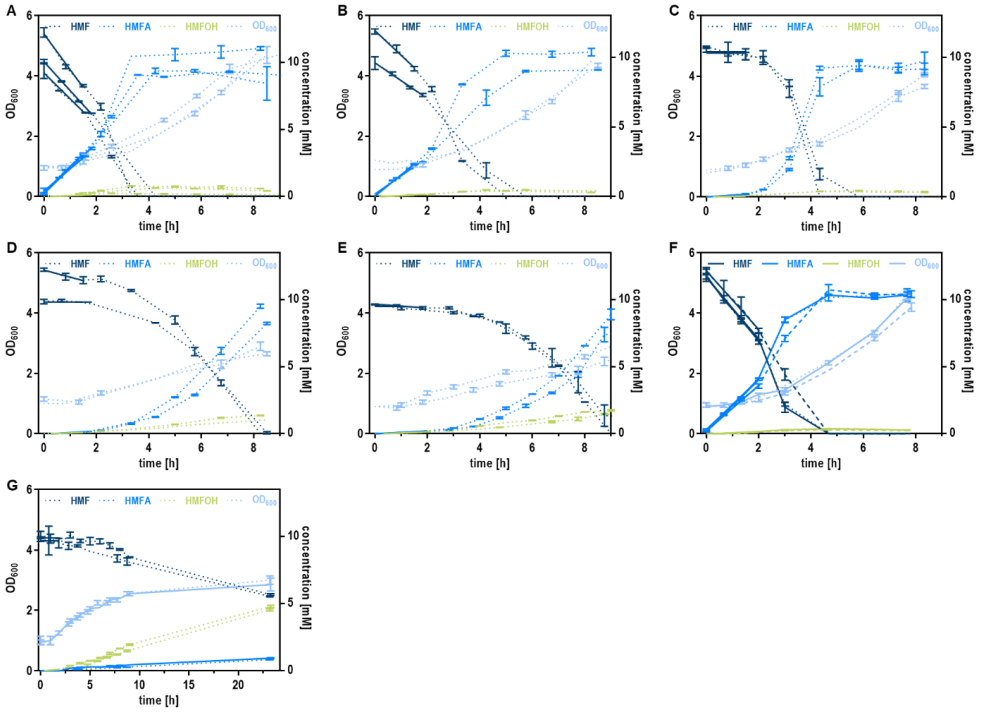

Figure S5.1-2: HMF conversion assays in shake flasks (four-fold buffered MSM with 40 mM glycerol, 2 mM glucose, and 10 mM HMF) using whole-cells of *P. taiwanensis* VLB120 GRC1 and selected mutant strains thereof. For the determination of initial HMF depletion and HMFA (and HMFOH) formation rates a linear fit covering the first 2 h of each experiment was performed (shown as solid line). The OD_{600} was considered constant within this period and equaled the starting conditions. The calculated rates are plotted in Fig. 2.1-1C. For each measurement, error bars represent the mean ± standard deviation of duplicates. Preferentially, at least two independent datasets were recorded. (**A**) GRC1 (three datasets). (**B**) GRC1 Δ*modABC* (two datasets). (**C**) GRC1 Δ*modABC* (-MoO_4^{2-}) (two datasets). (**D**) GRC1 Δ*paoEFG* (two datasets). (**E**) GRC1 Δ*paoEFG* ΔPVLB_10355-65 (two datasets). (**F**) GRC1 Δ*calB* (solid lines) (one dataset), GRC1 Δ*peaE* (dotted lines) (one dataset), and GRC1 Δ*aldB-I* (dashed lines) (one dataset). (**G**) GRC1 Δ*paoEFG* Δ*aldB-I* (GRC1 ROX) (two datasets).

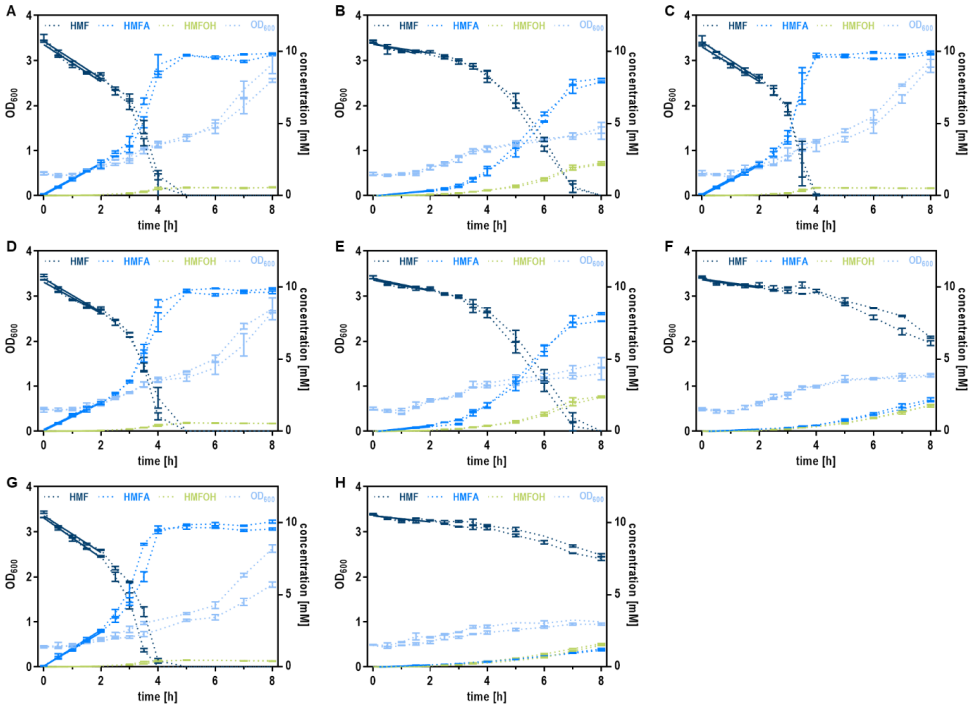

Figure S5.1-3: HMF conversion assays in 24-deepwell microplates (two-fold buffered MSM with 40 mM glycerol, 2 mM glucose, and 10 mM HMF) using whole-cells of *P. putida* KT2440 and deletion mutants thereof. For the determination of initial HMF depletion and HMFA (and HMFOH) formation rates a linear fit covering the first 2 h of each experiment was performed (shown as solid line). The OD_{600} was considered constant within this period and equaled the starting conditions. For each measurement, error bars represent the mean ± standard deviation of triplicates. (**A**) *P. putida* KT2440. (**B**) *P. putida* KT2440 Δ*paoEFG*. (**C**) *P. putida* KT2440 Δ*aldB-I*. (**D**) *P. putida* KT2440 Δ*aldB-II*. (**E**) *P. putida* KT2440 Δ*paoEFG*, Δ*aldB-I*. (**F**) *P. putida* KT2440 Δ*paoEFG*, Δ*aldB-II*. (**G**) *P. putida* KT2440 Δ*aldB-I*, Δ*aldB-II*. (**H**) *P. putida* KT2440 Δ*paoEFG*, Δ*aldB-I*, Δ*aldB-II*.

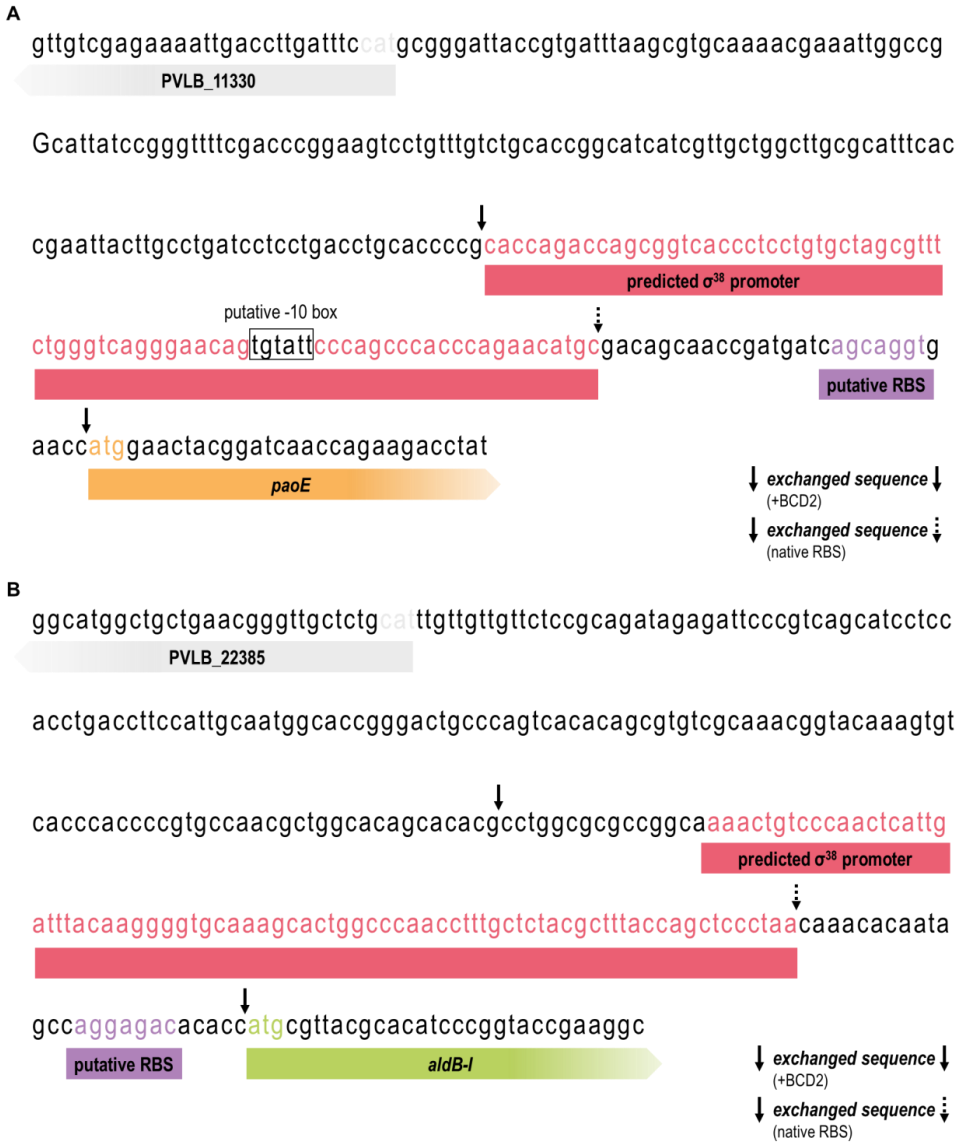

Figure S5.1-4: Bioinformatic prediction of promoter sequences upstream of *paoEFGHI* (A) and *aldB-I* (B). In each case a putative σ^{38} promoter was identified. Arrows indicate the sequence areas replaced by strong and constitutive promoters.

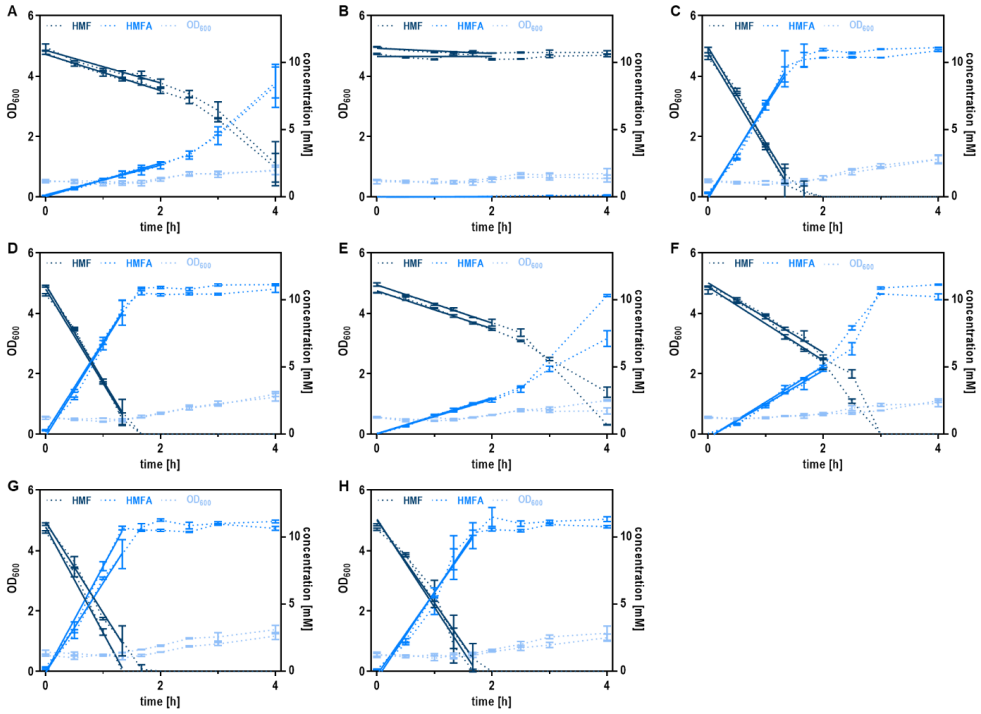

Figure S5.1-5: HMF conversion assays in 24-deepwell microplates (two-fold buffered MSM with 40 mM glycerol, 2 mM glucose, and 10 mM HMF) using whole-cells of GRC1 and promoter exchange mutants thereof with optimized expression of identified genes encoding HMF-oxidizing enzymes. For the determination of initial HMF depletion and HMFA formation rates a linear fit covering the first 2 h of each experiment was performed (shown as solid line). In cases HMF was fully converted faster this period was shortened accordingly. The OD_{600} was considered constant during that time and equaled the starting conditions. For each measurement, error bars represent the mean ± standard deviation of triplicates. Two independent experiments are shown for each strain. (**A**) GRC1. (**B**) GRC1 Δ*paoEFG* Δ*aldB-I* (GRC1 ROX). (**C**) BOX-P1 (P_{14c} promoter (+nRBS) upstream of *paoEFGHI* operon). (**D**) BOX-P2 (P_{14f} promoter (+nRBS) upstream of *paoEFGHI* operon). (**E**) BOX-C1 (P_{14f} promoter (+nRBS) upstream of *aldB-I*). (**F**) BOX-C2 (P_{14f} promoter (+BCD2) upstream of *aldB-I*). (**G**) BOX-C1P2 (P_{14f} promoter (+nRBS) upstream of *paoEFGHI* operon; P_{14f} promoter (+nRBS) upstream of *aldB-I*). (**H**) BOX-C2P2 (P_{14f} promoter (+nRBS) upstream of *paoEFGHI* operon; P_{14f} promoter (+BCD2) upstream of *aldB-I*).

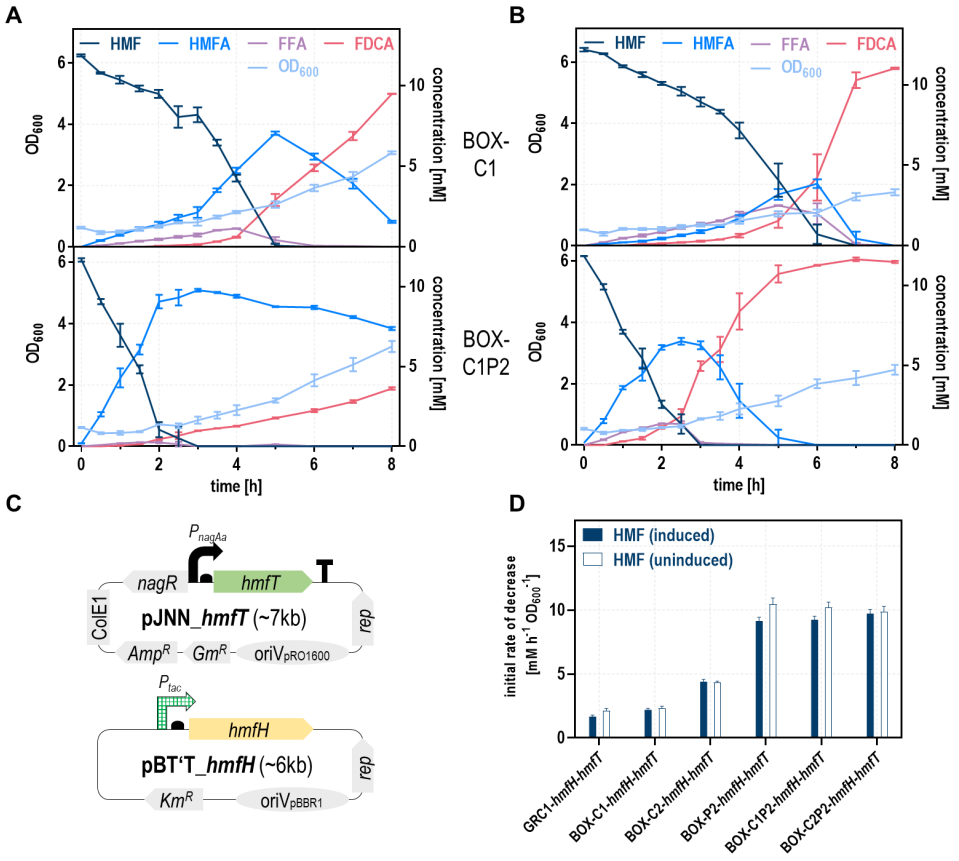

Figure S5.1-6: FDCA production experiments with oxidation-optimized BOX-C/P-*hmfH-hmfT* strains. Whole-cell HMF conversion assays in 24-deepwell microplates (two-fold buffered MSM with 40 mM glycerol, 2 mM glucose, and 10 mM HMF) using strains episomally expressing *hmfT* and *hmfH* from plasmids pBT'T_*hmfH* and pJNN_*hmfT*. For the transporter gene *hmfT* an inducible *nagR*/*PnagAa* promoter is used and expression of *hmfH* is controlled by a constitutive P_{tac} promoter. (**A**) Uninduced transporter expression. (**B**) Expression of the transporter induced by addition of 100 µM salicylate. The mean and standard deviation of three replicates is shown. (**C**) Schematic representation of the employed plasmids. (**D**) Initial rate of HMF decrease of all bioconversion experiments shown in Fig. 2.1-5 and Fig. S5.1-6. For the determination of initial HMF depletion rates a linear fit covering the first 2 h of each experiment was performed. The error bars correspond to the standard error of the slope of the linear regression.

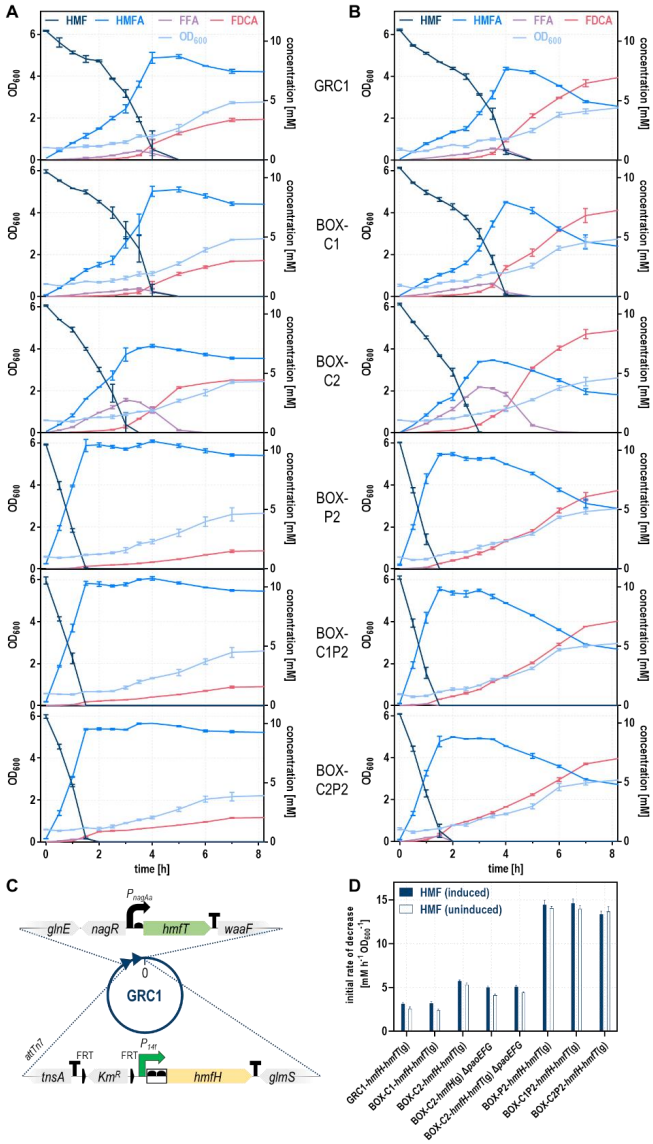

Figure S5.1-7: FDCA production experiments with oxidation-optimized BOX-C/P-*hmfH-hmfT*(g) strains. For large-scale bioprocesses, chromosomal integration of heterologous genes is advantageous enabling long-term expression of the targets without the need for continuous antibiotic selection. Consequently, the *hmfT* expression cassette from the pJNN_*hmfT* plasmid was integrated between *glnE* (PVLB_23545) and *waaF* (PVLB_23545) of each BOX-C/P strain and the GRC1 reference. This locus has recently been characterized as well suited for high level gene expression (Köbbing et al., 2024). In addition to the transporter gene, *hmfH* together with a P_{14f} promoter and a BCD2 element was integrated via Tn7 transposition eventually resulting in a set of BOX C/P-*hmfH-hmfT*(g) strains. Whole-cell HMF conversion assays in 24-deepwell microplates (two-fold buffered MSM with 40 mM glycerol, 2 mM glucose, and 10 mM HMF) using BOX-C/P-*hmfH-hmfT*(g) strains without (**A**) and with (**B**) induction of transporter expression by 100 µM salicylate. The mean and standard deviation of three replicates is shown. (**C**) Respective expression cassettes of the genomically modified strains. (**D**) Initial rate of HMF decrease of all bioconversion experiments shown in Fig. 2.1-5D and E, Fig. S5.1-7A and B. For the determination of initial HMF depletion rates a linear fit covering the first 2 h of each experiment was performed. In cases HMF was fully converted faster this period was shortened accordingly. The OD_{600} was assumed constant during this period and equaled the starting conditions. The error bars correspond to the standard error of the slope of the linear regression.

5.2. Supplementary material to chapter 2.2

Life with toxic substrates – PaoEFG forms the basis for growth of *Pseudomonas taiwanensis* VLB120 and *Pseudomonas putida* KT2440 on aromatic aldehydes

Thorsten Lechtenberg[a], Benedikt Wynands[a], Tino Polen[a], and Nick Wierckx[a*]

[a]Institute of Bio- and Geosciences IBG-1: Biotechnology, Forschungszentrum Jülich, 52425 Jülich, Germany

*Corresponding author:

Nick Wierckx, Institute of Bio- and Geosciences, IBG-1: Biotechnology, Forschungszentrum Jülich GmbH, 52425 Jülich, Germany, phone: +49 2461 61-85247

E-mail: n.wierckx@fz-juelich.de

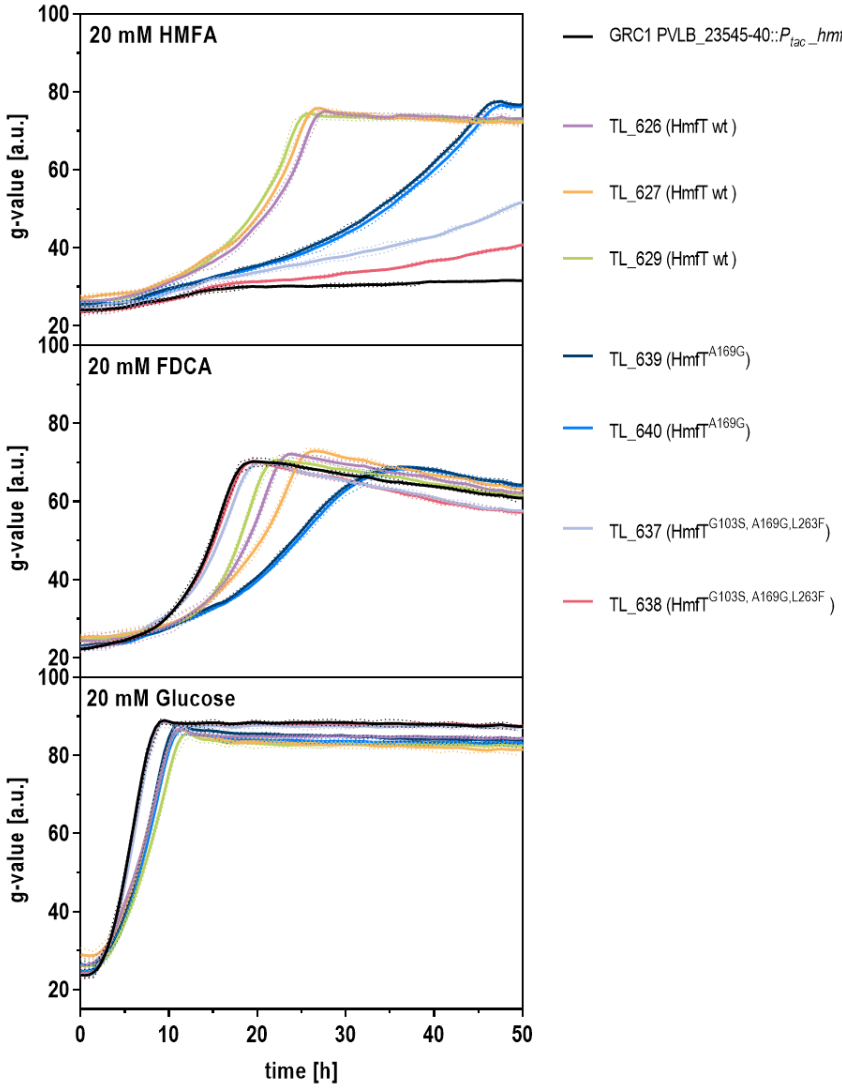

Figure S5.2-1: Analysis of selected strains resulting from the ALE of GRC1 PVLB_23545-40::*P*$_{tac}$*_hmfFGABCDEHT* on HMFA as sole carbon and energy source (first generation). Two-fold buffered MSM supplemented with 20 mM HMFA, FDCA, or glucose was inoculated with the evolved strains (refer to the legend for color-coding) and the parent strain GRC1 PVLB_23545-40::*P*$_{tac}$*_hmfFGABCDEHT* (black) to an OD_{600} of 0.1. Two precultures, one using LB and the second using MSM supplemented with 20 mM FA were conducted. Cells were cultivated in a Growth Profiler in 96-well microtiter plates. The growth curves result from a second-order smoothing to the mean values obtained from three replicates. The dots represent the standard deviation.

5.3. Supplementary material to chapter 2.3

Improving 5-(hydroxymethyl)furfural (HMF) tolerance of *Pseudomonas taiwanensis* VLB120 by automated adaptive laboratory evolution (ALE)

Thorsten Lechtenberg[a], Benedikt Wynands[a], Moritz-Fabian Müller[a], Tino Polen[a], Stephan Noack[a], and Nick Wierckx[a*]

[a]Institute of Bio- and Geosciences IBG-1: Biotechnology, Forschungszentrum Jülich, 52425 Jülich, Germany

*Corresponding author:

Nick Wierckx, Institute of Bio- and Geosciences, IBG-1: Biotechnology, Forschungszentrum Jülich GmbH, 52425 Jülich, Germany, phone: +49 2461 61-85247

E-mail: n.wierckx@fz-juelich.de

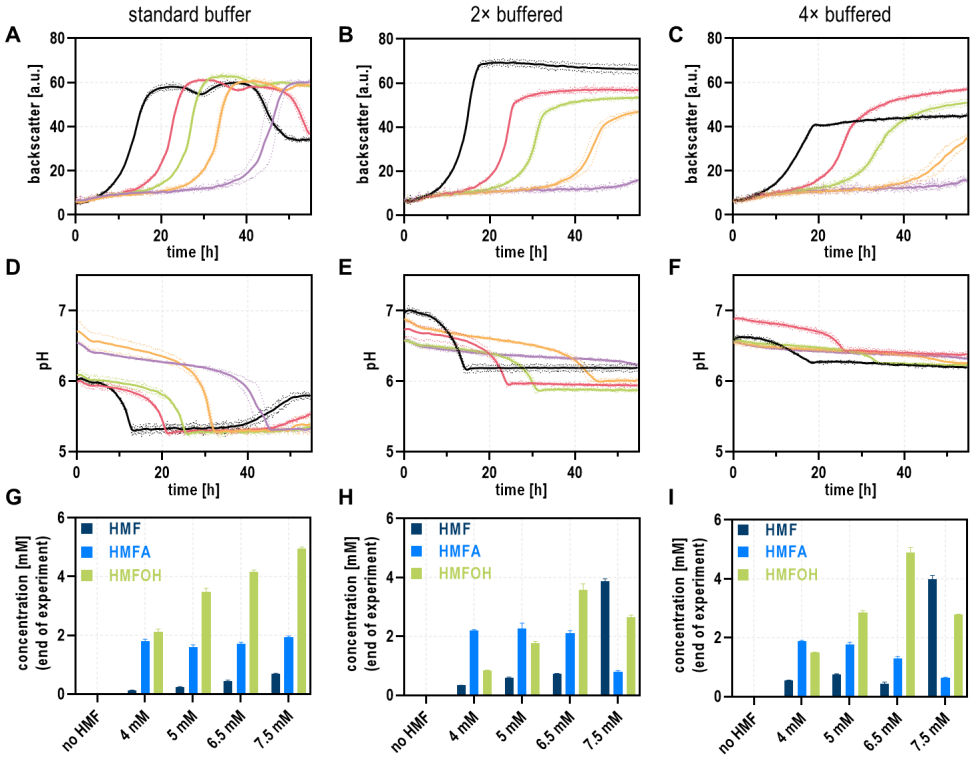

Figure S5.3-1: Evaluation of optimal culture conditions for an ALE with GRC1 ROX. All experiments were carried out in a 48-well FlowerPlate in a BioLector using MSM supplemented with 80 mM glycerol, 2 mM glucose, and varying concentrations of HMF (black: no HMF, red: 4 mM, green: 5 mM, orange: 6.5 mM, purple: 7.5 mM). Three buffer concentrations were tested: standard ((**A**), (**D**), (**G**)); two-fold ((**B**), (**E**), (**H**)); and four-fold ((**C**), (**F**), (**I**)). (**A**)-(**C**) Cell growth monitored by scattered light intensities. (**D**)-(**F**) pH values of the respective cultures. Graphs result from a second-order smoothing to the mean values obtained from three replicates. The dots represent the standard deviation. (**G**)-(**I**) HPLC analysis of final (55 h) HMF concentrations. The mean and standard deviation of three replicates is shown.

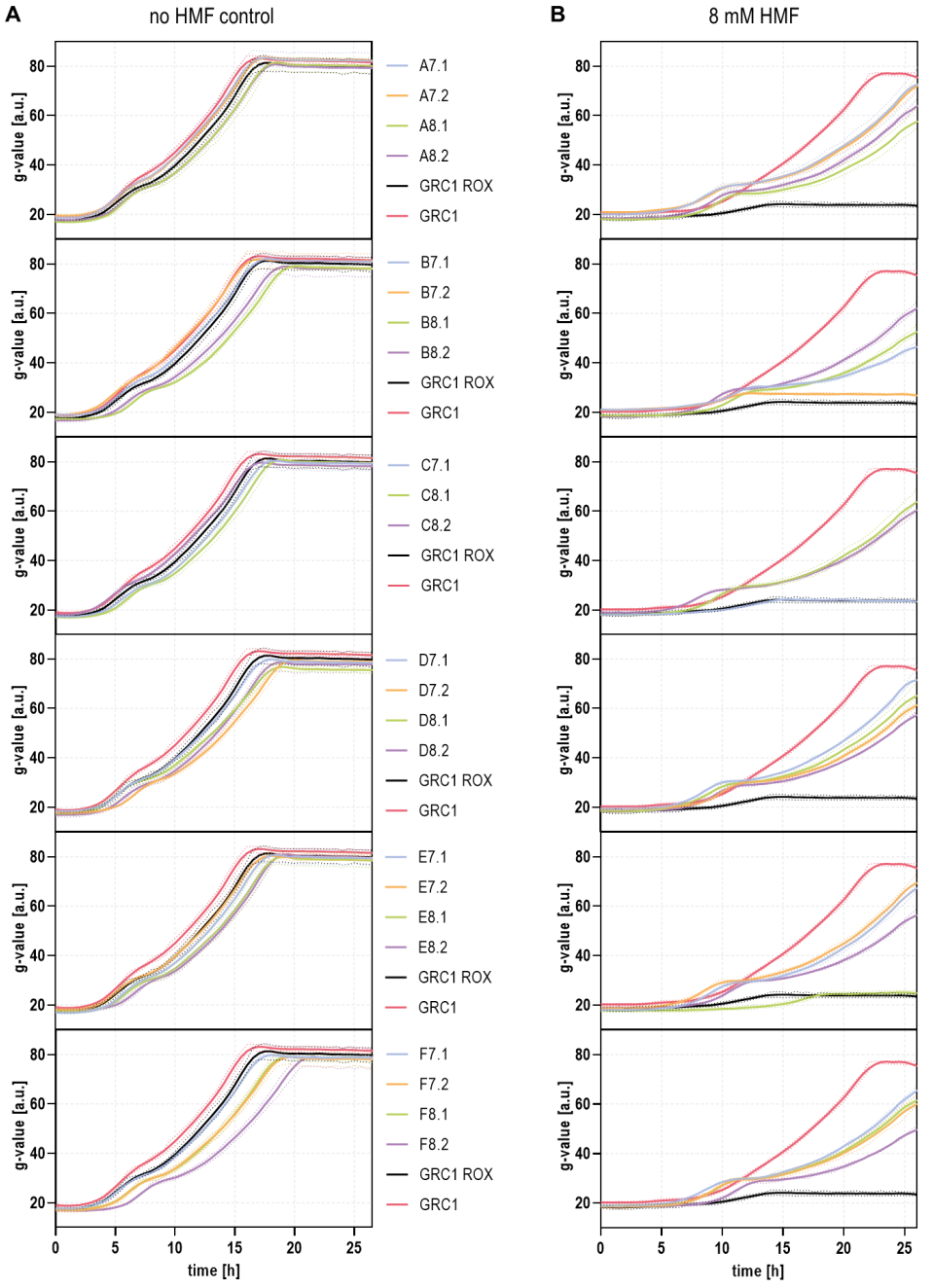

Figure S5.3-2: Analysis of all isolated clones from the ALE. Two-fold buffered MSM supplemented with 40 mM glycerol and 2 mM glucose as carbon sources was inoculated with the evolved strains (see legend for color coding), GRC1 ROX (black), and GRC1 (red) to an OD_{600} of 0.1. Cells were cultivated in a Growth Profiler in 96-well microtiter plates. The growth curves result from a second-order smoothing to the mean values obtained from three replicates. The dots represent the standard deviation. (**A**) No HMF added. (**B**) 8 mM HMF added. Because the preculture of clone C7.2 did not grow the respective isolate was not tested.

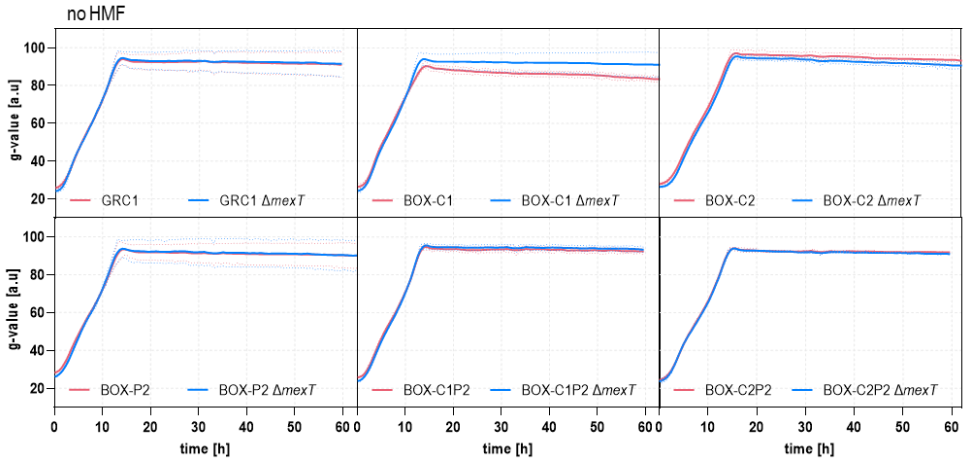

Figure S5.3-3: *MexT* deletion also confers a fitness advantage in strains with intact aldehyde oxidation machinery including the oxidation-optimized BOX strains (control experiments). Two-fold buffered MSM supplemented with 40 mM glycerol and 2 mM glucose as carbon sources in absence of HMF was inoculated with GRC1 or BOX derivatives (red) and the respective *mexT* deletion mutant (blue) to an OD_{600} of 0.1. Cells were cultivated in a Growth Profiler in 96-well microtiter plates. The growth curves result from a second-order smoothing to the mean values obtained from three replicates. The dots represent the standard deviation.

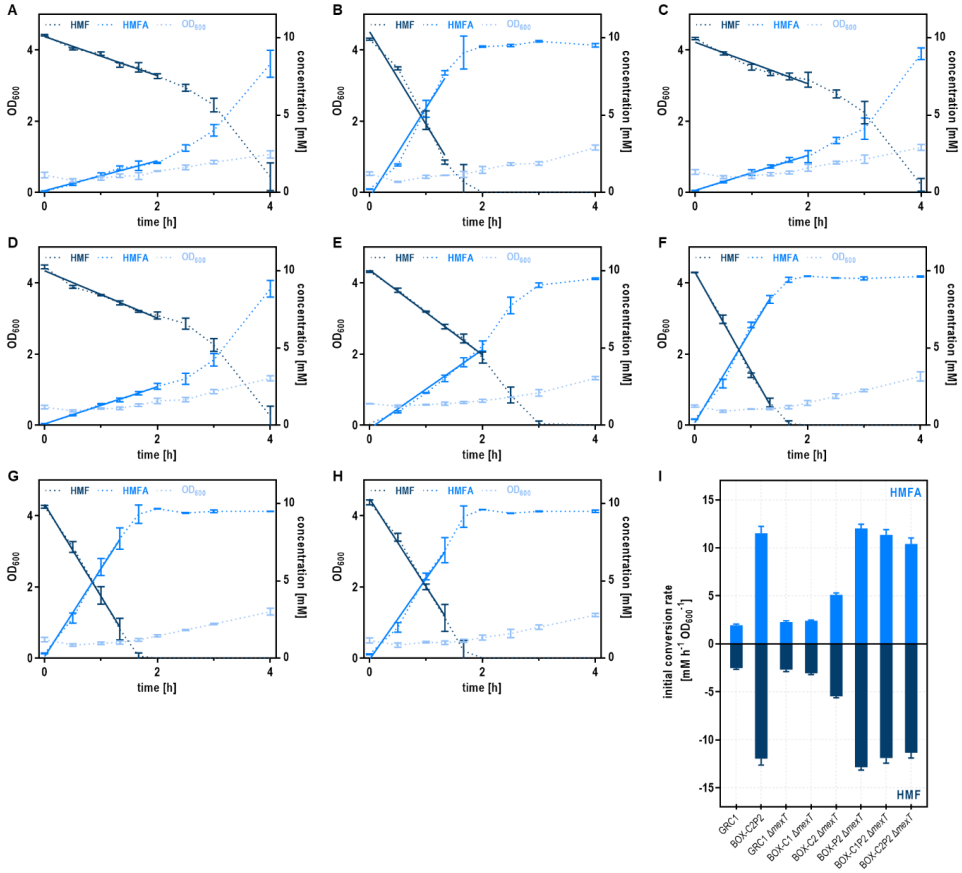

Figure S5.3-4: HMF conversion assays in 24-deepwell microplates (two-fold buffered MSM with 40 mM glycerol, 2 mM glucose, and 10 mM HMF) using whole-cells of GRC1 and derived BOX strains (increased expression of *paoEFG* and *aldB-I*) with deletion of *mexT*. For the determination of initial HMF depletion and HMFA formation rates a linear fit covering the first 2 h of each experiment was performed (shown as solid line). In cases HMF was fully converted faster this period was shortened accordingly. The OD_{600} was considered constant during that time and equaled the starting conditions. For each measurement, error bars represent the mean ± standard deviation of triplicates. (**A**) GRC1. (**B**) BOX-C2P2. (**C**) GRC1 Δ*mexT*. (**D**) BOX-C1 Δ*mexT*. (**E**) BOX-C2 Δ*mexT*. (**F**) BOX-P2 Δ*mexT*. (**G**) BOX-C1P2 Δ*mexT*. (**H**) BOX-C2P2 Δ*mexT*. (**I**) Initial HMF depletion and HMFA formation rates of all shown experiments. The error bars correspond to the standard error of the slope of the linear regression. *MexT* deletion does not alter HMF-oxidation properties of examined strains.

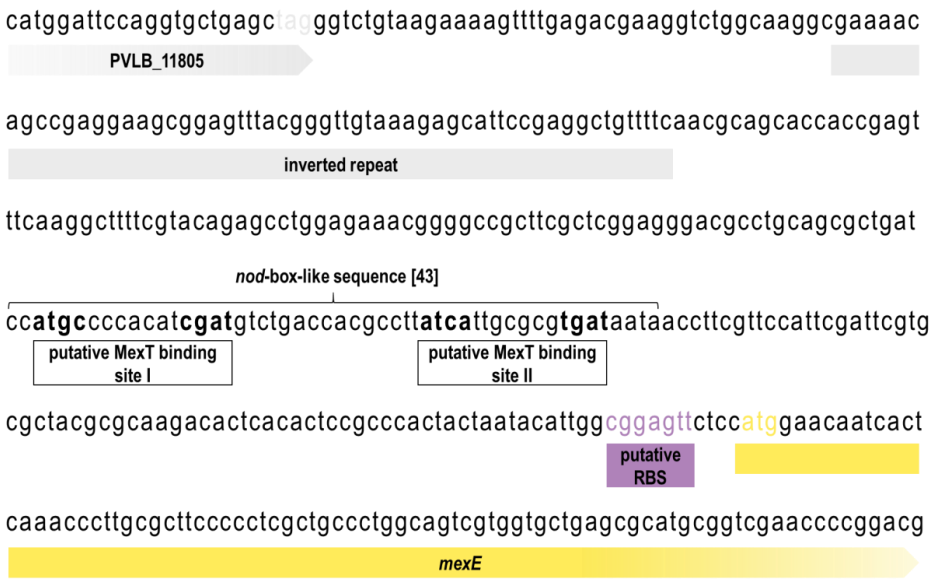

Figure S5.3-5: Genomic context of *mexEF-oprN* in *P. taiwanensis* VLB120 highlighting the *nod*-box-like sequence containing two putative MexT binding sites upstream of the operon. Annotations were made based on alignment with a previously determined consensus sequence ATCA(N)$_7$CGAT identified in *P. aeruginosa* (Kim et al., 2019).

5. Appendix

Table S5.3-1: Overview of the growth parameters of all strains under the tested conditions in chapter 2.3. The end of the lag phase was estimated based on the first increase in g-value by more than 5% between two measurements.

			no stressor						with HMF/furfural					
strain	figure	carbon source	maximum g-value [a.u.]				elapsed time to reach maximum g-value [h]	end of lag phase [h]	stressor concentration [mM]	maximum g-value [a.u.]				elapsed time to reach maximum g-value [h]	end of lag phase [h]
			replicates			***Avg.***				*replicates*			***Avg.***		
GRC1	2.3-2 and S5.3-2	40 mM glycerol 2 mM glucose	82.00	82.77	84.34	**83.03**	16.53	4	8	76.3	77	77.3	**76.88**	23.55	10.53
GRC1 ROX	2.3-2 and S5.3-2	40 mM glycerol 2 mM glucose	85.07	79.91	79.01	**81.33**	17.53	4	8	25.39	23.18	24.02	**24.20**	no growth	no growth
A7.1	2.3-2 and S5.3-2	40 mM glycerol 2 mM glucose	86.85	81.41	81.39	**83.22**	17.03	4	8	80.53	72.66	72.10	**75.10**	26.05	8
A7.2	2.3-2 and S5.3-2	40 mM glycerol 2 mM glucose	83.15	83.79	82.64	**83.20**	17.03	4	8	72.17	74.17	75.78	**74.04**	26.05	9.05
A8.1	2.3-2 and S5.3-2	40 mM glycerol 2 mM glucose	84.75	79.98	79.39	**81.37**	18.03	5	8	73.2	68.4	69.6	**70.38**	30.57	8.51
A8.2	2.3-2 and S5.3-2	40 mM glycerol 2 mM glucose	80.68	80.57	80.71	**80.65**	18.53	5	8	70.20	70.72	71.26	**70.73**	29.07	8
B7.1	2.3-2 and S5.3-2	40 mM glycerol 2 mM glucose	83.12	81.20	81.20	**81.84**	17.53	4	8	72.06	73.85	71.99	**72.63**	32.57	11.53
B7.2	2.3-2 and S5.3-2	40 mM glycerol 2 mM glucose	80.44	79.22	85.68	**81.78**	16.53	3	8	27.87	27.95	27.49	**27.77**	no growth	no growth
B8.1	2.3-2 and S5.3-2	40 mM glycerol 2 mM glucose	78.96	80.08	78.22	**79.08**	19.53	6	8	70.06	71.09	71.21	**70.79**	31.57	11.03
B8.2	2.3-2 and S5.3-2	40 mM glycerol 2 mM glucose	77.81	76.83	82.61	**79.08**	18.53	4.5	8	69.26	70.02	73.15	**70.81**	29.07	8
C7.1	2.3-2 and S5.3-2	40 mM glycerol 2 mM glucose	83.64	79.14	78.53	**80.44**	17.53	4.5	8	23.87	23.87	24.95	**24.23**	no growth	no growth
C7.2	2.3-2 and S5.3-2	40 mM glycerol 2 mM glucose	-	-	-	-	-	-	8	-	-	-	-	-	-
C8.1	2.3-2 and S5.3-2	40 mM glycerol 2 mM glucose	82.72	79.86	79.26	**80.61**	18.03	5	8	74.10	69.67	70.17	**71.31**	30.57	9.53
C8.2	2.3-2 and S5.3-2	40 mM glycerol 2 mM glucose	80.32	80.34	78.60	**79.75**	16.53	3.5	8	70.57	71.08	70.08	**70.58**	34.6	7

D7.1	2.3-2 and S5.3-2	40 mM glycerol 2 mM glucose	79.97	79.87	79.16	**79.67**	17.53	4.5	8	74.31	73.99	73.37	**73.89**	26.05	7.5
D7.2	2.3-2 and S5.3-2	40 mM glycerol 2 mM glucose	77.59	78.01	82.54	**79.38**	19.53	6	8	70.23	69.36	73.83	**71.14**	29.07	9.05
D8.1	2.3-2 and S5.3-2	40 mM glycerol 2 mM glucose	75.64	77.51	77.75	**76.96**	18.53	4	8	67.27	69.96	69.05	**68.76**	29.07	8
D8.2	2.3-2 and S5.3-2	40 mM glycerol 2 mM glucose	77.68	75.53	82.55	**78.58**	18.53	5	8	69.75	69.11	72.81	**70.55**	29.57	8
E7.1	2.3-2 and S5.3-2	40 mM glycerol 2 mM glucose	83.68	79.26	79.65	**80.86**	17.53	4.5	8	71.70	68.90	69.43	**70.01**	31.57	8.52
E7.2	2.3-2 and S5.3-2	40 mM glycerol 2 mM glucose	80.65	79.71	81.49	**80.62**	17.53	4.5	8	69.00	72.13	72.82	**71.31**	26.05	8
E8.1	2.3-2 and S5.3-2	40 mM glycerol 2 mM glucose	83.34	78.92	77.59	**79.95**	18.53	5	8	25.95	24.02	25.02	**25.00**	no growth	no growth
E8.2	2.3-2 and S5.3-2	40 mM glycerol 2 mM glucose	81.41	81.15	80.38	**80.98**	19.03	6	8	71.05	71.65	70.71	**71.14**	29.57	9.53
F7.1	2.3-2 and S5.3-2	40 mM glycerol 2 mM glucose	79.58	79.11	79.97	**79.55**	18.03	4.5	8	70.14	70.99	70.31	**70.48**	31.56	8
F7.2	2.3-2 and S5.3-2	40 mM glycerol 2 mM glucose	77.73	76.76	82.58	**79.02**	19.03	4.5	8	71.12	69.00	74.18	**71.43**	29.07	8.52
F8.1	2.3-2 and S5.3-2	40 mM glycerol 2 mM glucose	78.47	80.44	78.63	**79.18**	19.03	5.5	8	71.93	70.21	70.25	**70.80**	29.07	8.52
F8.2	2.3-2 and S5.3-2	40 mM glycerol 2 mM glucose	78.21	75.72	82.61	**78.85**	21.53	6.5	8	69.02	67.95	73.92	**70.30**	34.6	10.53
GRC1	2.3-2	20 mM glucose	99.7	100	103	**100.97**	9.58	2.48	10	94.2	96	98.4	**96.19**	13.08	7.58
GRC1 ROX	2.3-2	20 mM glucose	92.4	93.3	95.5	**93.72**	10.58	3.5	10	33.7	33.9	30.8	**32.79**	no growth	no growth
A7.1	2.3-2	20 mM glucose	91.7	92.6	92.9	**92.39**	9.58	1.5	10	83.9	85.1	84.3	**84.44**	19.08	12.08
E7.2	2.3-2	20 mM glucose	96.1	97.3	99.3	**97.59**	10.08	2.48	10	86.9	87.2	89.4	**87.85**	19.08	9.58
F8.1	2.3-2	20 mM glucose	99	97.5	96	**97.48**	13.08	6.05	10	88.3	88.1	86.8	**87.73**	22.62	13.08
GRC1	2.3-3	40 mM glycerol 2 mM glucose	100	101	99.7	**100.25**	15.03	3.53	8	96.8	96.4	88.3	**93.81**	20.07	9.03
GRC1 ROX	2.3-3	40 mM glycerol 2 mM glucose	93.5	93.7	100	**95.75**	15.03	3.03	8	30.2	30.9	29.3	**30.14**	no growth	no growth
F8.1	2.3-3	40 mM glycerol 2 mM glucose	95.1	101	97.7	**97.82**	16.53	4.03	8	92.1	92.6	-	**92.35**	24.57	7.53

5. Appendix

GRC1 ROX *mexT*^{G231E}	2.3-3	40 mM glycerol 2 mM glucose	100	97.1	101	**99.39**	16.03	3.53	8	92.5	91.5	91.1	**91.74**	24.57	6.53
GRC1 ROX Δ*mexT*	2.3-3	40 mM glycerol 2 mM glucose		101	98.8	**99.44**	16.03	4.03	8	87.2	94.6	94.6	**92.13**	23.07	6.53
GRC1	2.3-4A	40 mM glycerol 2 mM glucose	100	98.8	99.2	**99.38**	16.03	2.51	8	100	99.5	92.4	**97.45**	16.52	4.01
GRC1 Δ*mexT*	2.3-4A	40 mM glycerol 2 mM glucose	98.3	98	98.9	**98.42**	16.52	2.02	8	96.1	98.2	92.6	**95.63**	15.02	3.02
GRC1	2.3-4A	40 mM glycerol 2 mM glucose	100	98.8	99.2	**99.38**	16.03	2.51	20	28.2	26	25.8	**26.65**	no growth	no growth
GRC1 Δ*mexT*	2.3-4A	40 mM glycerol 2 mM glucose	98.3	98	98.9	**98.42**	16.52	2.02	20	88.1	95.5	88.7	**90.75**	40.07	27.57
GRC1	2.3-4A	40 mM glycerol 2 mM glucose	100	98.8	99.2	**99.38**	16.03	2.51	20 (furfural)	85.6	93.2	80.9	**86.57**	23.57	11.53
GRC1 Δ*mexT*	2.3-4A	40 mM glycerol 2 mM glucose	98.3	98	98.9	**98.42**	16.52	2.02	20 (furfural)	86.2	88.9	90.4	**88.52**	21.57	10.03
GRC1	2.3-4A	40 mM glycerol 2 mM glucose	90.2	95.4	96	**93.86**	13.58	1.05	40	35.5	35.7	36.3	**35.85**	no growth	no growth
GRC1 Δ*mexT*	2.3-4C	40 mM glycerol 2 mM glucose	90.6	95.6	97.3	**94.52**	13.58	2	40	78.8	77	81.1	**78.95**	47.13	33.1
BOX-C1	2.3-4C	40 mM glycerol 2 mM glucose	92	89.1	92.4	**91.18**	14.08	2	40	34.5	34.2	32.9	**33.85**	no growth	no growth
BOX-C1 Δ*mexT*	2.3-4C	40 mM glycerol 2 mM glucose	95.7	95.9	90.3	**93.96**	14.08	1.48	40	80.3	79.2	76.8	**78.79**	47.13	31.63
BOX-C2	2.3-4C	40 mM glycerol 2 mM glucose	94.9	97.4	98.9	**97.04**	15.08	2	40	79.1	79.5	75.5	**78.04**	65.63	45.13
BOX-C2 Δ*mexT*	2.3-4C	40 mM glycerol 2 mM glucose	94	96	96.9	**95.64**	15.08	3.02	40	79	78	78.8	**78.60**	55.13	37.63
BOX-P2	2.3-4C	40 mM glycerol 2 mM glucose	95.7	94.5	90	**93.40**	14.58	2	40	68.3	71.3	70.7	**70.08**	42.63	n. a.
BOX-P2 Δ*mexT*	2.3-4C	40 mM glycerol 2 mM glucose	96.3	95.8	88.4	**93.52**	14.08	2	40	77.1	70.1	73.1	**73.41**	32.62	17.08
BOX-C1P2	2.3-4C	40 mM glycerol 2 mM glucose	92.9	95.5	94.9	**94.39**	14.08	2	40	80.4	77.1	-	**78.73**	41.13	24.58
BOX-C1P2 Δ*mexT*	2.3-4C	40 mM glycerol 2 mM glucose	93.7	96.5	95.2	**95.12**	14.08	2	40	77.2	76.1	72	**75.12**	32.62	20.08
BOX-C2P2	2.3-4C	40 mM glycerol 2 mM glucose	94.2	94.4	93.4	**94.02**	14.58	1.48	40	76.9	80.1	74.4	**77.14**	57.13	20.58

BOX-C2P2 *ΔmexT*	2.3-4C	40 mM glycerol 2 mM glucose	93.4	94	93.7	**93.71**	15.08	2	40	75.6	76.9	79.3	**77.26**		15.83
GRC1 ROX	2.3-5	40 mM glycerol 2 mM glucose	95.9	94.4	95.3	**95.17**	14.02	1.5	8	35.9	36.7	35.7	**36.07**	no growth	no growth
GRC1 ROX *ΔmexT*	2.3-5	40 mM glycerol 2 mM glucose	95.8	95.5	92.2	**94.50**	15.52	2.5	8	89.7	89.2	88.9	**89.27**	21.52	3.52
GRC1 ROX *ΔmexEF-oprN*	2.3-5	40 mM glycerol 2 mM glucose	96.6	94.8	95.9	**95.78**	15.52	2	8	88.1	86.6	87.1	**87.26**	22.02	3.52
GRC1 ROX *ΔmexT ΔmexEF-oprN*	2.3-5	40 mM glycerol 2 mM glucose	95.2	95.8	93.9	**94.98**	14.52	2	8	89.7	90.7	89.3	**89.92**	21.02	3.52

5.4. Supplementary material to chapter 2.4

De novo production of *t*-cinnamaldehyde by engineered solvent-tolerant and oxidation-deficient *Pseudomonas taiwanensis* VLB120

Thorsten Lechtenberg[a], Benedikt Wynands[a], and Nick Wierckx[a*]

[a]Institute of Bio- and Geosciences IBG-1: Biotechnology, Forschungszentrum Jülich, 52425 Jülich, Germany

*Corresponding author:

Nick Wierckx, Institute of Bio- and Geosciences, IBG-1: Biotechnology, Forschungszentrum Jülich GmbH, 52425 Jülich, Germany, phone: +49 2461 61-85247

E-mail: n.wierckx@fz-juelich.de

Expanded information on plasmid cloning

DNA fragments were PCR amplified using Q5 High-Fidelity DNA polymerase (New England Biolabs, Ipswich, MA, USA). For subsequent NEBuilder HiFi DNA Assembly (New England Biolabs, Ipswich, MA, USA) primers were designed with adequate overhangs and acquired as unmodified DNA oligonucleotides from Eurofins Genomics. Plasmid correctness was verified by PCR using OneTaq 2X Master Mix with Standard Buffer (New England Biolabs, Ipswich, MA, USA) followed by Sanger sequencing. *At*PAL was previously codon-optimized for *P. taiwanensis* VLB120 and amplified from pBG14f-*phdBCDE-4cl-pal* (Otto et al., 2020). *No*CAR and *Ec*PPTase were multiplied from pETDuet_1_*Ec*PPTase_His-*No*CAR (Weber et al., 2021).

Table S1: Strains used in this thesis.

strain	relevant characteristics	reference	chapter
***Paraburkholderia caribensis* DSM 13236**	native HMF and furfural degrader	(Achouak et al., 1999)	2.1, 2.2
E. coli			
PIR2	F$^-$, Δ*lac169*, *rpoS(Am)*, *robA1*, *creC510*, *hsdR514*, *endA*, *recA1*, *uidA(ΔMluI)*::*pir*; host for *oriV*(R6K) vectors in low copy number	Thermo Fisher Scientific	2.1, 2.2, 2.3, 2.4
EC100D™ *pir*$^+$	F$^-$, *mcrA*, Δ(*mrr-hsdRMS-mcrBC*), *φ80dlacZΔM15*, Δ*lacX74*, *recA1*, *endA1*, *araD139*, Δ*(ara, leu)7697, galU*, *galK*, *λ–rpsL (Str^R)*, *nupG*, *pir$^+$(DHFR)*, host for *oriV*(R6K) vectors in low copy number	LGC, Biosearch Technologies	2.1, 2.2, 2.4
HB101 pRK2013	Sm^R, *hsdR-M$^+$*, *proA2*, *leuB6*, *thi-1*, *recA*; bears plasmid pRK2013	(Ditta et al., 1980)	2.1, 2.2, 2.3, 2.4
DH5α	F Φ80 *lac*ZΔM15 Δ(*lac*ZYA-*arg*F)U169 *recA1 endA1 hsdR17* (r_K^-, m_K^+) *pho*A *sup*E44 *thi*-1 *gyr*A96 *rel*A1 λ$^-$	Thermo Fisher Scientific	2.1
DH5α pSW-2	DH5α bearing pSW-2	(Martinez-Garcia and de Lorenzo, 2011)	2.1, 2.2, 2.3, 2.4
DH5αλpir pTNS1	DH5αλpir bearing plasmid pTNS1	de Lorenzo lab	2.1, 2.4
P. taiwanensis			
GRC1	genome reduced chassis of *P. taiwanensis* VLB120, ΔpSTY, Δprophage1/2, Δprophage3, Δprophage4, Δflag1, Δflag2, Δlap1, Δlap2, Δlap3	(Wynands et al., 2019)	2.1, 2.2, 2.3, 2.4
GRC1 Δ*modABC*	GRC1 with Δ*modA* (PVLB_15900), Δ*modB* (PVLB_15905), Δ*modC* (PVLB_15910)	this work MiKat #533	2.1
GRC1 Δ*paoEFG*	GRC1 with Δ*paoE* (PVLB_11325), Δ*paoF* (PVLB_11320), Δ*paoG* (PVLB_11315)	this work MiKat #530	2.1

GRC1 Δ*calB*	GRC1 with Δ*calB* (PVLB_01470)	this work MiKat #529	2.1
GRC1 Δ*peaE*	GRC1 with Δ*peaE* (PVLB_12825)	this work MiKat #531	2.1
GRC1 Δ*aldB-I*	GRC1 with Δ*aldB-I* (PVLB_22390)	this work MiKat #532	2.1
GRC1 Δ*paoEFG* ΔPVLB_10355-65	GRC1 with Δ*paoE*, Δ*paoF*, Δ*paoG* , ΔPVLB_10355, ΔPVLB_10360, ΔPVLB_10365	this work MiKat #657	2.1
GRC1 Δ*paoEFG* Δ*aldB-I* **(GRC1 ROX)**	GRC1 with Δ*paoE*, Δ*paoF*, Δ*paoG* , Δ*aldB-I*	this work MiKat #666	2.1, 2.3, 2.4
GRC1 Δ*paoEFG* Δ*aldB-I* ΔPVLB_10970	GRC1 with Δ*paoE*, Δ*paoF*, Δ*paoG* , Δ*aldB-I*, ΔPVLB_10970	this work MiKat #1202	2.1
GRC1 Δ*paoEFG* Δ*aldB-I* ΔPVLB_11635	GRC1 with Δ*paoE*, Δ*paoF*, Δ*paoG* , Δ*aldB-I*, ΔPVLB_11635	this work MiKat #1203	2.1
GRC1 Δ*paoEFG* Δ*aldB-I* ΔPVLB_14845	GRC1 with Δ*paoE*, Δ*paoF*, Δ*paoG* , Δ*aldB-I*, ΔPVLB_14845	this work MiKat #1204	2.1
GRC1 Δ*paoEFG* Δ*aldB-I* Δ*adhP*	GRC1 with Δ*paoE*, Δ*paoF*, Δ*paoG* , Δ*aldB-I*, Δ*adhP* (PVLB_10545)	this work MiKat #1205	2.1
GRC1 Δ*paoEFG* Δ*aldB-I* ΔPVLB_15055	GRC1 with Δ*paoE*, Δ*paoF*, Δ*paoG* , Δ*aldB-I*, ΔPVLB_15055	this work MiKat #675	2.1
GRC1 Δ*paoEFG* Δ*aldB-I* ΔPVLB_22260	GRC1 with Δ*paoE*, Δ*paoF*, Δ*paoG* , Δ*aldB-I*, ΔPVLB_22260	this work MiKat #1206	2.1
GRC1 Δ*paoEFG* Δ*aldB-I* Δ*adhP* ΔPVLB_10970	GRC1 with Δ*paoE*, Δ*paoF*, Δ*paoG* , Δ*aldB-I*, Δ*adhP*, ΔPVLB_10970	this work MiKat #1525	2.1
GRC1 Δ*paoEFG* Δ*aldB-I* Δ*adhP* ΔPVLB_11635	GRC1 with Δ*paoE*, Δ*paoF*, Δ*paoG* , Δ*aldB-I*, Δ*adhP*, ΔPVLB_11635	this work MiKat #1526	2.1
GRC1 Δ*paoEFG* Δ*aldB-I* Δ*adhP* ΔPVLB_14845	GRC1 with Δ*paoE*, Δ*paoF*, Δ*paoG* , Δ*aldB-I*, Δ*adhP*, ΔPVLB_14845	this work MiKat #1527	2.1

Table S1: Strains used in this thesis.

GRC1 Δ*paoEFG* Δ*aldB-I* Δ*adhP* ΔPVLB_15055 **(GRC1 ROAR)**	GRC1 with Δ*paoE*, Δ*paoF*, Δ*paoG* , Δ*aldB-I*, Δ*adhP*, ΔPVLB_15055	this work MiKat #1524	2.1
GRC1 Δ*paoEFG* Δ*aldB-I* Δ*adhP* ΔPVLB_22260	GRC1 with Δ*paoE*, Δ*paoF*, Δ*paoG* , Δ*aldB-I*, Δ*adhP* ΔPVLB_22260	this work MiKat #1528	2.1
BOX-P1	GRC1 with $P_{paoEFGHI}$::$P_{14c\_nRBS;}$ promoter of *paoEFGHI* exchanged to P_{14c}	this work MiKat #1028	2.1, 2.3
BOX-P2	GRC1 with $P_{paoEFGHI}$::$P_{14f\_nRBS;}$ promoter of *paoEFGHI* exchanged to P_{14f}	this work MiKat #987	2.1, 2.3
BOX-C1	GRC1 with P_{aldB-I}::$P_{14f\_nRBS;}$ promoter of *aldB-I* exchanged to P_{14f}	this work MiKat #988	2.1, 2.3
BOX-C2	GRC1 with P_{aldB-I}::$P_{14f\_BCD2;}$ promoter of *aldB-I* exchanged to P_{14f} + BCD2	this work MiKat #986	2.1, 2.3
BOX-C1P2	GRC1 with $P_{paoEFGHI}$::P_{14f_nRBS}, P_{aldB-I}::$P_{14f\_nRBS;}$ promoter of *paoEFGHI* exchanged to P_{14f}, promoter of *aldB-I* exchanged to P_{14f}	this work MiKat #1020	2.1, 2.3
BOX-C2P2	GRC1 with $P_{paoEFGHI}$::P_{14f_nRBS}, P_{aldB-I}::$P_{14f\_BCD2;}$ promoter of *paoEFGHI* exchanged to P_{14f}, promoter of *aldB-I* exchanged to P_{14f} + BCD2	this work MiKat #1019	2.1, 2.3
GRC1-*hmfH-hmfT*	GRC1 harboring pBT'T_*hmfH* and pJNN_*hmfT*	this work MiKat #428	2.1
BOX-P2-*hmfH-hmfT*	BOX-P2 harboring pBT'T_*hmfH* and pJNN_*hmfT*	this work MiKat #1751	2.1
BOX-C1-*hmfH-hmfT*	BOX-C1 harboring pBT'T_*hmfH* and pJNN_*hmfT*	this work MiKat #1752	2.1
BOX-C2-*hmfH-hmfT*	BOX-C2 harboring pBT'T_*hmfH* and pJNN_*hmfT*	this work MiKat #1750	2.1
BOX-C1P2-*hmfH-hmfT*	BOX-C1P2 harboring pBT'T_*hmfH* and pJNN_*hmfT*	this work MiKat #1754	2.1
BOX-C2P2-*hmfH-hmfT*	BOX-C2P2 harboring pBT'T_*hmfH* and pJNN_*hmfT*	this work MiKat #1753	2.1

5. Appendix

GRC1-*hmfH-hmfT*(g)	GRC1 with PVLB_23545-40::*nagR*/*PnagAa-hmfT* and *attTn7*::Kan_FRT_P_{14f_BCD2}_*hmfH*	this work MiKat #1162	2.1
BOX-P2-*hmfH-hmfT*(g)	BOX-P2 with PVLB_23545-40::*nagR*/*PnagAa-hmfT* and *attTn7*::Kan_FRT_P_{14f_BCD2}_*hmfH*	this work MiKat #1163	2.1
BOX-C1-*hmfH-hmfT*(g)	BOX-C1 with PVLB_23545-40::*nagR*/*PnagAa-hmfT* and *attTn7*::Kan_FRT_P_{14f_BCD2}_*hmfH*	this work MiKat #1165	2.1
BOX-C2-*hmfH-hmfT*(g)	BOX-C2 with PVLB_23545-40::*nagR*/*PnagAa-hmfT* and *attTn7*::Kan_FRT_P_{14f_BCD2}_*hmfH*	this work MiKat #1164	2.1
BOX-C1P2-*hmfH-hmfT*(g)	BOX-C1P2 with PVLB_23545-40::*nagR*/*PnagAa-hmfT* and *attTn7*::Kan_FRT_P_{14f_BCD2}_*hmfH*	this work MiKat #1167	2.1
BOX-C2P2-*hmfH-hmfT*(g)	BOX-C2P2 with PVLB_23545-40::*nagR*/*PnagAa-hmfT* and *attTn7*::Kan_FRT_P_{14f_BCD2}_*hmfH*	this work MiKat #1166	2.1
BOX-C2-*hmfH*(g) Δ*paoEFG*	BOX-C2 with Δ*paoE*, Δ*paoF*, Δ*paoG* and *attTn7*::Kan_FRT_P_{14f_BCD2}_*hmfH*	this work MiKat #1737	2.1
BOX-C2-*hmfH-hmfT*(g) Δ*paoEFG*	BOX-C2 with Δ*paoE*, Δ*paoF*, Δ*paoG* , PVLB_23545-40::*nagR*/*PnagAa-hmfT* and *attTn7*::Kan_FRT_P_{14f_BCD2}_*hmfH*	this work MiKat #1736	2.1
GRC3	inducibly solvent-tolerant genome reduced chassis of *P. taiwanensis* VLB120 , ΔpSTY, Δprophage1/2::*ttgVWGHI*, Δprophage3, Δprophage4, Δflag1, Δflag2, Δlap1, Δlap2, Δlap3	(Wynands et al., 2019)	2.2, 2.4
GRC3 Δ*paoEFG*	GRC3 with Δ*paoE*, Δ*paoF*, Δ*paoG*	this work MiCat #1140	2.2
GRC3 Δ*paoEFG* Δ*aldB-I* (**GRC3 ROX**)	GRC3 with Δ*paoE*, Δ*paoF*, Δ*paoG* , Δ*aldB-I*	this work MiCat #1157	2.2, 2.4
GRC1 PVLB_23545-40::P_{tac}_*hmfFGABCDEHT*	*hmf*-Cluster (*hmfFGABCDEHT*) integrated into landing pad PVLB_23545-40 (P_{tac}, RBS mutated to AGGGAC)	this work #TL_125	2.2
GRC1 PVLB_23545-40::*adh+hmfR1FGABCDEHT*	*adh+hmfR1* added to the previously integrated *hmf*-Cluster, native promoter sequences	this work MiCat #913	2.2
TL_626	GRC1 PVLB_23545-40::P_{tac}_*hmfFGABCDEHT* evolved on HMFA as sole carbon and energy source, HmfT wt (first generation ALE strain)	this work	2.2

Table S1: Strains used in this thesis.

TL_627	GRC1 PVLB_23545-40::P_{tac}_*hmfFGABCDEHT* evolved on HMFA as sole carbon and energy source, HmfT wt (first generation ALE strain)	this work	2.2
TL_629	GRC1 PVLB_23545-40::P_{tac}_*hmfFGABCDEHT* evolved on HMFA as sole carbon and energy source, HmfT wt (first generation ALE strain)	this work	2.2
TL_639	GRC1 PVLB_23545-40::P_{tac}_*hmfFGABCDEHT* evolved on HMFA as sole carbon and energy source, HmfT^{A169G} (first generation ALE strain)	this work	2.2
TL_640	GRC1 PVLB_23545-40::P_{tac}_*hmfFGABCDEHT* evolved on HMFA as sole carbon and energy source, HmfT^{A169G} (first generation ALE strain)	this work	2.2
TL_637	GRC1 PVLB_23545-40::P_{tac}_*hmfFGABCDEHT* evolved on HMFA as sole carbon and energy source, HmfT$^{G103S, A169G, L263F}$ (first generation ALE strain)	this work	2.2
TL_638	GRC1 PVLB_23545-40::P_{tac}_*hmfFGABCDEHT* evolved on HMFA as sole carbon and energy source, HmfT$^{G103S, A169G, L263F}$ (first generation ALE strain)	this work	2.2
TL_666	GRC1 PVLB_23545-40::P_{tac}_*hmfFGABCDEHT* evolved on HMFA as sole carbon and energy source, HmfT^{L40S} (second generation ALE strain)	this work	2.2
TL_671	GRC1 PVLB_23545-40::P_{tac}_*hmfFGABCDEHT* evolved on HMFA as sole carbon and energy source, HmfT^{G166A} (second generation ALE strain)	this work	2.2
TL_676	GRC1 PVLB_23545-40::P_{tac}_*hmfFGABCDEHT* evolved on HMFA as sole carbon and energy source, HmfT^{G166A} (second generation ALE strain)	this work	2.2
TL_666 BOX-C1	TL_666 with $P_{aldB\text{-}I}$::P_{14f_nRBS}; promoter of *aldB-I* exchanged to P_{14f}	this work MiCat #2214	2.2
TL_666 BOX-C2	TL_666 with $P_{aldB\text{-}I}$::P_{14f_BCD2}; promoter of *aldB-I* exchanged to P_{14f} + BCD2	this work MiCat #2213	2.2
TL_666 BOX-P2	TL_666 with $P_{paoEFGHI}$::P_{14f_nRBS}; promoter of *paoEFGHI* exchanged to P_{14f}	this work MiCat #2212	2.2
TL_666 BOX-C1P2	TL_666 with $P_{paoEFGHI}$::P_{14f_nRBS}, $P_{aldB\text{-}I}$::P_{14f_nRBS}; promoter of *paoEFGHI* exchanged to P_{14f}, promoter of *aldB-I* exchanged to P_{14f}	this work MiCat #2329	2.2
TL_666 BOX-C2P2	TL_666 with $P_{paoEFGHI}$::P_{14f_nRBS}, $P_{aldB\text{-}I}$::P_{14f_BCD2}; promoter of *paoEFGHI* exchanged to P_{14f}, promoter of *aldB-I* exchanged to P_{14f} + BCD2	this work MiCat #2328	2.2

ALE A7.1	GRC1 ROX after continuous exposure to 4 mM HMF, seven sequential cultures, evolution line A	this work	2.3
ALE E7.2	GRC1 ROX after exposure to increasing concentrations of HMF (4 – 6 mM), seven sequential cultures, evolution line E	this work	2.3
ALE F8.1	GRC1 ROX after exposure to increasing concentrations of HMF (4 – 6 mM), eight sequential cultures, evolution line F	this work	2.3
GRC1 ROX *mexT*^{G231E}	GRC1 ROX with *mexT*^{G231E} (reverse-engineered)	this work MiKat #1018	2.3
GRC1 ROX Δ*mexT*	GRC1 ROX with Δ*mexT* (PVLB_13900)	this work MiKat #974	2.3
GRC1 Δ*mexT*	GRC1 with Δ*mexT* (PVLB_13900)	this work MiKat #953	2.3
BOX-C1 Δ*mexT*	BOX-C1 with Δ*mexT* (PVLB_13900)	this work MiKat #2118	2.3
BOX-C2 Δ*mexT*	BOX-C2 with Δ*mexT* (PVLB_13900)	this work MiKat #2116	2.3
BOX-P2 Δ*mexT*	BOX-P2 with Δ*mexT* (PVLB_13900)	this work MiKat #2117	2.3
BOX-C1P2 Δ*mexT*	BOX-C1P2 with Δ*mexT* (PVLB_13900)	this work MiKat #2120	2.3
BOX-C2P2 Δ*mexT*	BOX-C2P2 with Δ*mexT* (PVLB_13900)	this work MiKat #2119	2.3
GRC1 ROX Δ*mexEF-oprN*	GRC1 ROX with Δ*mexEF-oprN* (PVLB_11790, PVLB_11795, PVLB_11800)	this work MiKat #1137	2.3
GRC1 ROX Δ*mexT* Δ*mexEF-oprN*	GRC1 ROX with Δ*mexT* (PVLB_13900) and Δ*mexEF-oprN* (PVLB_11790, PVLB_11795, PVLB_11800)	this work MiKat #1136	2.3
GRC3 PHE	phenylalanine platform strain, first published as GRC3 Δ8Δ*pykA-tap* GRC3 Δ*pobA*, Δ*hpd*, Δ*quiC*, Δ*quiC1*, Δ*quiC2*, Δ*phhAB*, Δ*katG*, ΔPVLB_10925, Δ*pykA*, *trpE*^{P290S}, *aroF-1*^{P148L}, *pheA*^{T310I}	(Otto et al., 2019)	2.4

Table S1: Strains used in this thesis.

GRC3 PHE ROX	oxidation-deficient GRC3 PHE GRC3 PHE with Δ*paoE*, Δ*paoF*, Δ*paoG* , Δ*aldB-I*	this work MiKat #1158	2.4
GRC3 PHE ROX *attTn7*::Kan_FRT_P_{14f}_*At*PAL	GRC3 PHE ROX with genomically integrated control operon for production of *t*-cinnamate	this work MiKat #1296	2.4
GRC3 *attTn7*::Kan_FRT_P_{14f}_*At*PAL_*No*CAR_*Ec*PPTase	GRC3 with genomically integrated operon for production of *t*-cinnamaldehyde	this work MiKat #1297	2.4
GRC3 PHE *attTn7*::Kan_FRT_P_{14f}_*At*PAL_*No*CAR_*Ec*PPTase	GRC3 PHE with genomically integrated operon for production of *t*-cinnamaldehyde	this work MiKat #1298	2.4
GRC3 ROX *attTn7*::Kan_FRT_P_{14f}_*At*PAL_*No*CAR_*Ec*PPTase	GRC3 ROX with genomically integrated operon for production of *t*-cinnamaldehyde	this work MiKat #1299	2.4
GRC3 PHE ROX *attTn7*::Kan_FRT_P_{14f}_*At*PAL_*No*CAR_*Ec*PPTase	GRC3 PHE ROX with genomically integrated operon for production of *t*-cinnamaldehyde	this work MiKat #1300	2.4
P. putida			
KT2440	mt-2 derivative, cured from the TOL plasmid pWW0	(Bagdasarian et al., 1981)	2.1, 2.2
KT2440 Δ*paoEFG*	KT2440 with Δ*paoE* (PP_3621), Δ*paoF* (PP_3622), Δ*paoG* (PP_3623)	this work MiKat #1536	2.1, 2.2
KT2440 Δ*aldB-I*	KT2440 with Δ*aldB-I* (PP_0545)	this work MiKat #1537	2.1, 2.2
KT2440 Δ *aldB-II*	KT2440 with Δ*aldB-II* (*pedI*, PP_2680)	this work MiKat #1538	2.1, 2.2
KT2440 Δ*paoEFG* Δ*aldB-I*	KT2440 with Δ*paoE*, Δ*paoF*, Δ*paoG*, Δ*aldB-I*	this work MiKat #1583	2.1, 2.2
KT2440 Δ*paoEFG* Δ*aldB-II*	KT2440 with Δ*paoE*, Δ*paoF*, Δ*paoG*, Δ*aldB-II*	this work MiKat #1584	2.1, 2.2
KT2440 Δ*aldB-I* Δ*aldB-II*	KT2440 with Δ*aldB-I*, Δ*aldB-II*	this work MiKat #1585	2.1, 2.2

KT2440 Δ*paoEFG* Δ*aldB-I* Δ*aldB-II*	KT2440 with Δ*paoE*, Δ*paoF*, Δ*paoG*, Δ*aldB-I*, Δ*aldB-II*	this work MiKat #1623	2.1, 2.2
KT2440 Δ*vdh*	KT2440 with Δ*vdh*	this work MiCat #1643	2.2
KT2440 Δ*paoEFG* Δ*vdh*	KT2440 with Δ*paoE*, Δ*paoF*, Δ*paoG*, Δ*vdh*	this work MiCat #1644	2.2
KT2440 Δ*aldB-I* Δ*vdh*	KT2440 with Δ*aldB-I*, Δ*vdh*	this work MiCat #1645	2.2
KT2440 Δ*aldB-II* Δ*vdh*	KT2440 with Δ*aldB-II*, Δ*vdh*	this work MiCat #1646	2.2
KT2440 Δ*paoEFG* Δ*aldB-I* Δ*vdh*	KT2440 with Δ*paoE*, Δ*paoF*, Δ*paoG*, Δ*aldB-I*, Δ*vdh*	this work MiCat #1727	2.2
KT2440 Δ*paoEFG* Δ*aldB-II* Δ*vdh*	KT2440 with Δ*paoE*, Δ*paoF*, Δ*paoG*, Δ*aldB-II*, Δ*vdh*	this work MiCat #1728	2.2
KT2440 Δ*aldB-I* Δ*aldB-II* Δ*vdh*	KT2440 with Δ*aldB-I*, Δ*aldB-II*, Δ*vdh*	this work MiCat #1729	2.2
KT2440 Δ*paoEFG* Δ*aldB-I* Δ*aldB-II* Δ*vdh*	KT2440 with Δ*paoE*, Δ*paoF*, Δ*paoG*, Δ*aldB-I*, Δ*aldB-II*, Δ*vdh*	this work MiCat #1730	2.2
KT2440 Δ*paoEFG* Δ*aldB-I* Δ*aldB-II* ΔPP_1948	KT2440 with Δ*paoE*, Δ*paoF*, Δ*paoG*, Δ*aldB-I*, Δ*aldB-II*, ΔPP_1948	this work MiCat #1731	2.2
KT2440 PP_0340-41::P_{tac}_*hmfFGABCDEHT*	*hmf*-Cluster (*hmfFGABCDEHT*) integrated into landing pad PP_0340-41 (P_{tac}, RBS mutated to AGGGAC)	this work MiCat #1026	2.2

Table S2: Plasmids used in this thesis.

plasmid	relevant characteristics	assembly description	reference	chapter
pRK2013	Km^R, *oriV*(RK2/ColE1), mob^+ tra^+		(Figurski and Helinski, 1979)	2.1, 2.2, 2.3, 2.4
pSW-2	Gm^R, *oriV*(RK2), mob^+, *xylS*, $P_m \rightarrow$ *I-sceI*		(Martinez-Garcia and de Lorenzo, 2011)	2.1, 2.2, 2.3, 2.4
pTNS1	Amp^R, *oriV*(R6K), mob^+, *tnsABC+D* operon for specific transposition		(Choi et al., 2005)	2.1, 2.4
pSNW2, pSNW4, pEMG, and derivatives				
pSNW2	Km^R, *oriV*(R6K), lacZα-MCS flanked by two I-SceI sites P_{14g} BCD2 → *msfgfp*		(Volke et al., 2020)	2.1, 2.2, 2.3
pSNW4	Str^R, *oriV*(R6K), lacZα-MCS flanked by two I-SceI sites P_{14g} BCD2 → *msfgfp*		(Volke et al., 2020)	2.1
pEMG	Km^R, *oriV*(R6K), lacZα-MCS flanked by two I-SceI sites		(Martinez-Garcia and de Lorenzo, 2011)	2.1, 2.2
pEMG-PVLB_23545-40	Km^R, *oriV*(R6K), pEMG equipped with homology arms for integration into genomic locus PVLB_23545-40 (coordinates: 5185817-5185816, genebank accession number CP003961.1) of *P. taiwanensis* VLB120 flanked by two I-SceI sites, P_{em7} BCD2 → *msfgfp* between the TS-sites		(Köbbing et al., 2024)	2.1, 2.2
pSNW2-*modABC* (pSNW2_PVLB_15900-10_KO)	pSNW2 bearing flanking sequences of *modABC*, *modABC* deletion delivery vector (VLB120)	HiFi DNA assembly; TS1-*modABC* and TS2-*modABC* were amplified from VLB120 gDNA and integrated into pSNW2 via EcoRI/SalI	this work #201	2.1

pSNW2-*paoEFG* (pSNW2_PVLB_11315-25_KO)	pSNW2 bearing flanking sequences of *paoEFG*, *paoEFG* deletion delivery vector (VLB120)	HiFi DNA assembly; TS1-*paoEFG* and TS2-*paoEFG* were amplified from VLB120 gDNA and integrated into pSNW2 via EcoRI/SalI	this work #198	2.1, 2.2, 2.4
pSNW2-*calB* (pSNW2_PVLB_01470_KO)	pSNW2 bearing flanking sequences of *calB*, *calB* deletion delivery vector (VLB120)	HiFi DNA assembly; TS1-*calB* and TS2-*calB* were amplified from VLB120 gDNA and integrated into pSNW2 via EcoRI/SalI	this work #197	2.1
pSNW2-*peaE* (pSNW2_PVLB_12825_KO)	pSNW2 bearing flanking sequences of *peaE*, *calB* deletion delivery vector (VLB120)	HiFi DNA assembly; TS1-*peaE* and TS2-*peaE* were amplified from VLB120 gDNA and integrated into pSNW2 via EcoRI/SalI	this work #199	2.1
pSNW2-*aldB-I* (pSNW2_PVLB_22390_KO)	pSNW2 bearing flanking sequences of *aldB-I*, *aldB-I* deletion delivery vector (VLB120)	HiFi DNA assembly; TS1-*aldB-I* and TS2-*aldB-I* were amplified from VLB120 gDNA and integrated into pSNW2 via EcoRI/SalI	this work #200	2.1, 2.2, 2.4
pSNW2_PVLB_10355-65_KO	pSNW2 bearing flanking sequences of PVLB_10355-65, PVLB_10355-65 deletion delivery vector (VLB120)	HiFi DNA assembly; TS1-PVLB_10355-65 and TS2-PVLB_10355-65 were amplified from VLB120 gDNA and integrated into pSNW2 via EcoRI/SalI	this work #219	2.1
pSNW2-*paoEFG*_PP (pSNW2_PP_3621-23_KO)	pSNW2 bearing flanking sequences of *paoEFG*, *paoEFG* deletion delivery vector (KT2440)	HiFi DNA assembly; TS1-*paoEFG* and TS2-*paoEFG* were amplified from KT2440 gDNA and integrated into pSNW2 via EcoRI/SalI	this work #492	2.1
pSNW2-*aldB-I*_PP (pSNW2_PP_0545_KO)	pSNW2 bearing flanking sequences of *aldB-I*, *aldB-I* deletion delivery vector (KT2440)	HiFi DNA assembly; TS1-*aldB-I* and TS2-*aldB-I* were amplified from KT2440 gDNA and integrated into pSNW2 via EcoRI/SalI	this work #493	2.1
pSNW4-*aldB-II*_PP (pSNW4_PP_2680_KO)	pSNW4 bearing flanking sequences of *aldB-II*, *aldB-II* deletion delivery vector (KT2440)	HiFi DNA assembly; TS1-*aldB-II* and TS2-*aldB-II* were amplified from KT2440 gDNA and integrated into pSNW4 via EcoRI/SalI	this work #494	2.1
pSNW2_PVLB_10970_KO	pSNW2 bearing flanking sequences of PVLB_10970, PVLB_10970 deletion delivery vector (VLB120)	HiFi DNA assembly; TS1-PVLB_10970 and TS2-PVLB_10970 were amplified from VLB120 gDNA and integrated into pSNW2 via EcoRI/SalI	this work #379	2.1

Table S2: Plasmids used in this thesis.

pSNW2_PVLB_11635_KO	pSNW2 bearing flanking sequences of PVLB_11635, PVLB_11635 deletion delivery vector (VLB120)	HiFi DNA assembly; TS1-PVLB_11635 and TS2-PVLB_11635 were amplified from VLB120 gDNA and integrated into pSNW2 via EcoRI/SalI	this work #380	2.1
pSNW2_PVLB_14845_KO	pSNW2 bearing flanking sequences of PVLB_14845, PVLB_14845 deletion delivery vector (VLB120)	HiFi DNA assembly; TS1-PVLB_14845 and TS2-PVLB_14845 were amplified from VLB120 gDNA and integrated into pSNW2 via EcoRI/SalI	this work #381	2.1
pSNW2-*adhP* (pSNW2_PVLB_10545_KO)	pSNW2 bearing flanking sequences of *adhP*, *adhP* deletion delivery vector (VLB120)	HiFi DNA assembly; TS1-*adhP* and TS2-*adhP* were amplified from VLB120 gDNA and integrated into pSNW2 via EcoRI/SalI	this work #382	2.1
pSNW2_PVLB_15055_KO	pSNW2 bearing flanking sequences of PVLB_15055, PVLB_15055 deletion delivery vector (VLB120)	HiFi DNA assembly; TS1-PVLB_15055 and TS2-PVLB_15055 were amplified from VLB120 gDNA and integrated into pSNW2 via EcoRI/SalI	this work #220	2.1
pSNW2_PVLB_22260_KO	pSNW2 bearing flanking sequences of PVLB_22260, PVLB_22260 deletion delivery vector (VLB120)	HiFi DNA assembly; TS1-PVLB_22260 and TS2-PVLB_22260 were amplified from VLB120 gDNA and integrated into pSNW2 via EcoRI/SalI	this work #383	2.1
pSNW2-P_ex-*paoEFGHI*-P_{14f_BCD2}	pSNW2 bearing flanking sequences of the promoter of the *paoEFGHI* operon and a synthetic P_{14f} promoter together with BCD2 translational coupler, *paoEFGHI* promoter exchange (P_{14f} + BCD2) delivery vector (VLB120)	HiFi DNA assembly; TS1-P_ex-*paoEFGHI* and TS2-P_ex-*paoEFGHI* were amplified from VLB120 gDNA, P_{14f} promoter and BCD2 were amplified from pBG14f (Zobel et al., 2015), fragments were integrated into pSNW2 via EcoRI/SalI	this work #280	2.1, 2.2
pSNW2-P_ex-*aldB-I*-P_{14f_BCD2}	pSNW2 bearing flanking sequences of the promoter of *aldB-I* and a synthetic P_{14f} promoter together with BCD2 translational coupler, *aldB-I* promoter exchange (P_{14f} + BCD2) delivery vector (VLB120)	HiFi DNA assembly; TS1-P_ex-*aldB-I* and TS2-P_ex-*aldB-I* were amplified from VLB120 gDNA, P_{14f} promoter and BCD2 were amplified from pBG14f (Zobel et al., 2015), fragments were integrated into pSNW2 via EcoRI/SalI	this work #281	2.1, 2.2

pSNW2-P_ex-*paoEFGHI-P*$_{14f\_nRBS}$	pSNW2 bearing flanking sequences of the promoter of the *paoEFGHI* operon, a synthetic P_{14f} promoter and the 29 bp sequence upstream of the first ORF including the native ribosome binding site (RBS) of the operon's first gene, *paoEFGHI* promoter exchange (P_{14f}) delivery vector (VLB120)	HiFi DNA assembly; P_ex-*paoEFGHI-P*$_{14f\_BCD2}$ was amplified in two parts and the resulting fragments reassembled. BCD2 translational coupler was replaced by the native 29 bp upstream sequence using adequate primer overhangs	this work #299	2.1, 2.2
pSNW2-P_ex-*aldB-I-P*$_{14f\_nRBS}$	pSNW2 bearing flanking sequences of the promoter of *aldB-I*, a synthetic P_{14f} promoter, and the 26 bp sequence upstream of the ORF including the native ribosome binding site (RBS), *aldB-I* promoter exchange (P_{14f}) delivery vector (VLB120)	HiFi DNA assembly; P_ex-*aldB-I-P*$_{14f\_BCD2}$ was amplified in two parts and the resulting fragments reassembled. BCD2 translational coupler was replaced by the native 26 bp upstream sequence using adequate primer overhangs	this work #300	2.1, 2.2
pSNW2-P_ex-*paoEFGHI-P*$_{14c\_nRBS}$	pSNW2 bearing flanking sequences of the promoter of the *paoEFGHI* operon, a synthetic P_{14c} promoter and the 29 bp sequence upstream of the first ORF including the native ribosome binding site (RBS) of the operon's first gene, *paoEFGHI* promoter exchange (P_{14c}) delivery vector (VLB120)	HiFi DNA assembly; P_ex-*paoEFGHI-P*$_{14f\_nRBS}$ was amplified in two parts and the resulting fragments reassembled. P_{14f} promoter was replaced by P_{14c} using adequate primer overhangs	this work #305	2.1, 2.2
pEMG-PVLB_23545-40-*nagR*/P$_{nagAa}$-*hmfT*	pEMG-PVLB_23545-40 harboring *nagR*/P_{nagAa}-*hmfT* instead of P_{em7} BCD2 → *msfgfp* between the TS-sites	HiFi DNA assembly, pEMG-PVLB_23545-40 was PCR amplified and merged with *nagR*/P_{nagAa}-*hmfT* amplified from pJNN_*hmfT*	this work #322	2.1
pEMG_PVLB_23545-40_P_{tac}	Km^R, *oriV*(R6K), pEMG equipped with homology arms for integration into genomic locus PVLB_23545-40 (coordinates: 5,185,817-5,185,816, genebank accession number NC_022738) of *P. taiwanensis* VLB120 flanked by two I-SceI sites, P_{tac} BCD2 → *msfgfp* (frameshifted) between the TS-sites	HiFi DNA assembly; vector backbone was amplified from pEMG_PVLB_23545-40 and merged with P_{tac} which was ordered as synthetic DNA fragment	this work (no fully correct version obtained)	2.2

Table S2: Plasmids used in this thesis.

pEMG_PVLB_23545_P_{tac}_*hmFGfABCDEHT*	Km^R, *oriV*(R6K), pEMG equipped with homology arms for integration into genomic locus PVLB_23545-40 of *P. taiwanensis* VLB120 flanked by two I-SceI sites, P_{tac} → *hmfFGABCDEHT* between the TS-sites (RBS mutated to AGGGAC)	HiFi DNA assembly; *hmfFGABCDEHT* was amplified from gDNA of *Paraburkholderia caribensis* and integrated into PCR-amplified pEMG_PVLB_23545_P_{tac}, the first 21 bp from *hmfF* were omitted (false priming problem with the respective primer) and instead integrated as spacer into the reverse primer for backbone amplification	this work #315	2.2
pEMG_PVLB_23545_*adh_hmfR1*_addition	pEMG bearing flanking sequences of the P_{tac} promoter of the *hmfFGABCDEHT* operon and *adh, hmfR1* and the native promoter sequence from *Paraburkholderia caribensis*. plasmid for modifying *hmf*-Cluster after integration into *P. taiwanensis* VLB120.	HiFi DNA assembly; *adh, hmfR1* and the native promoter sequence were amplified from gDNA of *Paraburkholderia caribensis* and integrated into PCR-amplified pEMG_PVLB_23545-40	this work #285	2.2
pEMG_PP_0340_P_{em7}	Km^R, *oriV*(R6K), pEMG equipped with homology arms for integration into genomic locus PP_0340-41 (coordinates: 414,043-414,044, genebank accession number NC_002947.3) of *P. putida* KT2440 flanked by two I-SceI sites, P_{em7} BCD2 → *msfgfp* between the TS-sites		(Köbbing et al., 2024)	2.2
pEMG_PP_0340_P_{tac}_*hmFGfABCDEHT*	Km^R, *oriV*(R6K), pEMG equipped with homology arms for integration into genomic locus PP_0340-41 of *P. putida* KT2440 flanked by two I-SceI sites, P_{tac} → *hmfFGABCDEHT* between the TS-sites (RBS mutated to AGGGAC)	restriction/ligation; promoter, RBS, and *hmfFGABCDEHT* were excised as one fragment from pEMG_PVLB_23545_P_{tac}_*hmFGfABCDEHT* (PacI/XbaI) and ligated into PacI/XbaI digested pEMG_PP_0340_P_{em7}	this work #316	2.2
pSNW2-*vdh* (pSNW2_PP_3357_KO)	pSNW2 bearing flanking sequences of *vdh*, *vdh* deletion delivery vector	HiFi DNA assembly; TS1-*vdh* and TS2-*vdh* were amplified from KT2440 gDNA and integrated into EcoRI/SalI digested pSNW2	this work #509	2.2

pSNW2-PP_1948 (pSNW2_PP_1948_KO)	pSNW2 bearing flanking sequences of PP_1948, PP_1948 deletion delivery vector	HiFi DNA assembly; TS1-PP_1948 and TS2-PP_1948 were amplified from KT2440 gDNA and integrated into EcoRI/SalI digested pSNW2	this work #541	2.2
pSNW2-*mexT*-G231E	pSNW2 bearing flanking sequences of *mexT* surrounding the full mutated version *mexT*^{G231E}, delivery vector to introduce *mexT* (PVLB_13900) point mutation c.692G>A (p.G231E)	HiFi DNA assembly; TS1-*mexT*, *mexT*^{G231E}, and TS2-*mexT* were amplified from ALE7.1 using colony PCR and integrated into pSNW2 via EcoRI/SalI	this work #307	2.3
pSNW2-*mexT* (pSNW2_PVLB_13900_KO)	pSNW2 bearing flanking sequences of *mexT*, *mexT* deletion delivery vector	HiFi DNA assembly; TS1-*mexT* and TS2-*mexT* were amplified from VLB120 gDNA and integrated into pSNW2 via EcoRI/SalI	this work #291	2.3
pSNW2-*mexEF-oprN* (pSNW2_PVLB_11790-11800_KO)	pSNW2 bearing flanking sequences of *mexEF-oprN*, *mexEF-oprN* deletion delivery vector	HiFi DNA assembly; TS1-*mexEF-oprN* and TS2-*mexEF-oprN* were amplified from VLB120 gDNA and integrated into pSNW2 via EcoRI/SalI	this work #360	2.3
Tn7-transposition				
pBG14f_FRT_Kan	Km^R flanked with FRT sites, *oriV*(R6K), pBG-derived, promoter *P*$_{14f}$, *msfGFP*		(Ackermann et al., 2021)	2.1, 2.4
pBG14f_FRT_Kan_*hmfH*	pBG14f_FRT_Kan derivative bearing *hmfH* from *P. caribensis* instead of *msfGFP*	HiFi DNA assembly; pBG14f_FRT_Kan backbone was PCR amplified and merged with *hmfH* amplified from *P. caribensis* gDNA,	this work #366	2.1
pBG14f-*phdBCDE-4cl-pal*	pBG14f with *phdBCDE* from *Corynebacterium glutamicum* ATCC 13032 (wildtype sequence), *4cl* from *Streptomyces coelicolor* (codon-optimized for *E. coli*), *pal* from *Arabidopsis thaliana* (codon-optimized for *P. taiwanensis* VLB120)		(Otto et al., 2020)	2.4

Table S2: Plasmids used in this thesis.

pBG14f_Kan_FRT_*At*PAL_*No*CAR_*Ec*PPTase	pBG14f_FRT_Kan with PAL from *A. thaliana* (codon-optimized for *P. taiwanensis* VLB120), CAR from *Nocardia otitidiscaviarum* (codon-optimized for *E. coli*), and PPTase from *E. coli* delivery vector for Tn7 transposition of expression cassette for *t*-cinnamaldehyde production	this work MiKat #367		2.4
pBG14f_Kan_FRT_*At*PAL	pBG14f_FRT_Kan with PAL from *A. thaliana* (codon-optimized for *P. taiwanensis* VLB120) delivery vector for Tn7 transposition of expression cassette for *t*-cinnamate production	this work MiKat #368		2.4
Expression plasmids				
pBT'Tmcs	pBT'mcs with RBS, Km^R, *oriV*(pBBR1), expression vector containing the constitutive P_{tac} promoter, no terminator		(Koopman et al., 2010b)	2.1
pJNNmcs(t)	also known as pTn-1, Amp^R, Gm^R, *oriV*(pRO1600), expression vector containing the salicylate-inducible *nagR*/P_{nagAa} promoter		(Wierckx et al., 2005)	2.1
pBT'T_*hmfH*	pBT'T harboring *hmfH* from *P. caribensis*, 5'UTR designed such as translation initiation rate was predicted to be 5000 (RBS calculator, Salis Lab) (Salis et al., 2009)	HiFi DNA assembly; pBT'Tmcs backbone was PCR amplified and merged with *hmfH* amplified from *P. caribensis* gDNA, desired spacer between RBS and start codon was introduced by adequate primer overhangs	this work #153	2.1
pJNN_*hmfT*	pJNN harboring *hmfT* from *P. caribensis*, native RBS	HiFi DNA assembly; pJNNmcs(t) backbone was PCR amplified and merged with *hmfT* amplified from *P. caribensis* gDNA	this work #155	2.1
pETDuet_1_*Ec*PPTase_His-*No*CAR	Amp^R, *oriV*(pMB1), *rop*, $P_{T7\text{-}lac} \rightarrow$ *Ec*PPTase, $P_{T7\text{-}lac} \rightarrow$ *No*CAR, *lacI*, CDS codon-optimized for *E. coli*		(Weber et al., 2021)	2.4

5. Appendix

Table S3: Oligonucleotides (name, sequence, and description) used in this thesis as PCR primers for cloning procedures. Lower case letters indicate overhangs, letters representing the binding sequence are capitalized, customly added spacers are italicized, and restriction sites are underlined. Oligonucleotides used for diagnostic PCRs and sequencing reactions are not included.

name	sequence (5' → 3')	description	chapter
TL_069	agggataacagggtaatctgAGGTACTGTCCAGCGCCAC	TS1-*modABC* forward primer (VLB120)	2.1
TL_070	cgacggatgcGAAGACGGCTCCAGAGGG	TS1-*modABC* reverse primer (VLB120)	2.1
TL_071	agccgtcttcGCATCCGTCGCACGCCTG	TS2-*modABC* forward primer (VLB120)	2.1
TL_072	gaagcttgcatgcctgcaggCATCCAGGTACTGGAACAGTGTCTG	TS2-*modABC* reverse primer (VLB120)	2.1
TL_045	agggataacagggtaatctgACACGTTGGGCACGATGTTG	TS1-*paoEFG* forward primer (VLB120)	2.1
TL_046	tcaatcctgtGGTTCACCTGCTGATCATCG	TS1-*paoEFG* reverse primer (VLB120)	2.1
TL_047	caggtgaaccACAGGATTGACCGATGGAAAG	TS2-*paoEFG* forward primer (VLB120)	2.1
TL_048	gaagcttgcatgcctgcaggGCGATCCGATAACGCCGATATAG	TS2-*paoEFG* reverse primer (VLB120)	2.1
TL_049	agggataacagggtaatctgATGGCTCCAGGGCCTGGTTGAACG	TS1-*calB* forward primer (VLB120)	2.1
TL_050	tgggcggcccTTCGGCTCCGGCGCGGCT	TS1-*calB* reverse primer (VLB120)	2.1
TL_051	cggagccgaaGGGCCGCCCATGCATCGC	TS2-*calB* forward primer (VLB120)	2.1
TL_052	gaagcttgcatgcctgcaggTGGCGCCATCCTTGCTCATTCG	TS2-*calB* reverse primer (VLB120)	2.1
TL_053	agggataacagggtaatctgCTGCTTGTCGGCCAGGTAC	TS1-*peaE* forward primer (VLB120)	2.1
TL_054	acaggaacggGGGGCTGAGCCTCTTGTC	TS1-*peaE* reverse primer (VLB120)	2.1
TL_055	ctcagccccCCGTTCCTGTGCCGGCCC	TS2-*peaE* forward primer (VLB120)	2.1

Table S3: Oligonucleotides (name, sequence, and description)

TL_056	gaagcttgcatgcctgcaggTCGCGTTTGTCAATCCTATGCGCAAC	TS2-*peaE* reverse primer (VLB120)	2.1
TL_041	agggataacagggtaatctgACACATCGAGCACCGCCA	TS1-*aldB-I* forward primer (VLB120)	2.1
TL_042	gcaacgcggtGGTGTGTCTCCTGGCTATTG	TS1-*aldB-I* reverse primer (VLB120)	2.1
TL_043	agacacaccACCGCGTTGCCTTCTTCG	TS2-*aldB-I* forward primer (VLB120)	2.1
TL_044	gaagcttgcatgcctgcaggGATGTCGAACAGGTTGGCTG	TS2-*aldB-I* reverse primer (VLB120)	2.1
TL_093	agggataacagggtaatctgATCATCAACGCCGCGATC	TS1-PVLB_10355-65 forward primer	2.1
TL_094	gtgccaccggCGAAGATCTCCTCATCTCC	TS1-PVLB_10355-65 reverse primer	2.1
TL_095	gagatcttcgCCGGTGGCACTCGCGCCA	TS2-PVLB_10355-65 forward primer	2.1
TL_096	gaagcttgcatgcctgcaggTCGAAGCCCAGTGCGCGG	TS2-PVLB_10355-65 reverse primer	2.1
TL_296	agggataacagggtaatctgACGATGTTGTTCTGCGACAG	TS1-*paoEFG* forward primer (KT2440)	2.1
TL_297	ccactccaatGGTTTCACCTGCCCGTCAC	TS1-*paoEFG* reverse primer (KT2440)	2.1
TL_298	aggtgaaaccATTGGAGTGGCACATGTACCG	TS2-*paoEFG* forward primer (KT2440)	2.1
TL_299	gaagcttgcatgcctgcaggTTTGCGCACACCCAGCGT	TS2-*paoEFG* reverse primer (KT2440)	2.1
TL_302	agggataacagggtaatctgCTGGTGCAGGCTGTTCATTTC	TS1-*aldB-I* forward primer (KT2440)	2.1

TL_303	gcgacgcggtGGTGTGTCTCCTTGGTATTG	TS1-*aldB-I* reverse primer (KT2440)	2.1
TL_304	gagacacaccACCGCGTCGCCTTCTTCG	TS2-*aldB-I* forward primer (KT2440)	2.1
TL_305	gaagcttgcatgcctgcaggTGCGGGCAAAGCCGTAGC	TS2-*aldB-I* reverse primer (KT2440)	2.1
TL_308	agggataacagggtaatctgGGCGCCACAAGAACTATGC	TS1-*aldB-II* forward primer (KT2440)	2.1
TL_309	gcgacgcggtGCTGAGCCTCTGCGGGTC	TS1-*aldB-II* reverse primer (KT2440)	2.1
TL_310	gaggctcagcACCGCGTCGCGGCCTTCG	TS2-*aldB-II* forward primer (KT2440)	2.1
TL_311	gaagcttgcatgcctgcaggCAGCAGCTCGAGGACCCAGC	TS2-*aldB-II* reverse primer (KT2440)	2.1
TL_276	agggataacagggtaatctgAATAACAGGCTGGTGCTC	TS1-PVLB_10970 forward primer (VLB120)	2.1
TL_277	atgggggcgcGAGAACTCCTTGTAGGGG	TS1-PVLB_10970 reverse primer (VLB120)	2.1
TL_278	aggagttctcGCGCCCCCATCGCCGCCA	TS2-PVLB_10970 forward primer (VLB120)	2.1
TL_279	gaagcttgcatgcctgcaggTGGCGCTGGCCGACTCGG	TS2-PVLB_10970 reverse primer (VLB120)	2.1
TL_270	agggataacagggtaatctgTGCGTCATCGTCGCGTAG	TS1-PVLB_11635 forward primer (VLB120)	2.1
TL_271	caacggccgtTCACGTAACGCATGTCACC	TS1-PVLB_11635 reverse primer (VLB120)	2.1
TL_272	cgttacgtgaACGGCCGTTGACAGCCCT	TS2-PVLB_11635 forward primer (VLB120)	2.1

Table S3: Oligonucleotides (name, sequence, and description)

TL_273	gaagcttgcatgcctgcaggGCTTGGGCACTACCCTCG	TS2-PVLB_11635 reverse primer (VLB120)	2.1
TL_264	agggataacagggtaatctgACTGACCTCTTCCACGCG	TS1-PVLB_14845 forward primer (VLB120)	2.1
TL_265	gctgctggttGTAGGCTCCTGATCAATGAAGTTC	TS1-PVLB_14845 reverse primer (VLB120)	2.1
TL_266	aggagcctacAACCAGCAGCGGGCTGGG	TS2-PVLB_14845 forward primer (VLB120)	2.1
TL_267	gaagcttgcatgcctgcaggCCGAAGAAGGCACCATGGTTGAG	TS2-PVLB_14845 reverse primer (VLB120)	2.1
TL_282	agggataacagggtaatctgTACTGCCCTGCTCAGCAC	TS1-*adhP* forward primer (VLB120)	2.1
TL_283	ttcgactgccACTCGCCTCCTTGTATTCC	TS1-*adhP* reverse primer (VLB120)	2.1
TL_284	ggaggcgagtGGCAGTCGAAGCAAGGCC	TS2-*adhP* forward primer (VLB120)	2.1
TL_285	gaagcttgcatgcctgcaggGTCGCCGGTTTCGTCGAG	TS2-*adhP* reverse primer (VLB120)	2.1
TL_099	agggataacagggtaatctgGAGTTTGCGCCTGCACTG	TS1-PVLB_15055 forward primer (VLB120)	2.1
TL_100	tggggttcgaACGGTACCTCATGGGAAG	TS1-PVLB_15055 reverse primer (VLB120)	2.1
TL_101	gaggtaccgtTCGAACCCCAGGTCGGCG	TS2-PVLB_15055 forward primer (VLB120)	2.1
TL_102	gaagcttgcatgcctgcaggGTAATGGCCCAGAACACGGC	TS2-PVLB_15055 reverse primer (VLB120)	2.1
TL_288	agggataacagggtaatctgTGAACGTGGCGCGCCTGG	TS1-PVLB_22260 forward primer (VLB120)	2.1
TL_289	cagacagaccGATGATTGTCTCCAGACTCACGCAACG	TS1-PVLB_22260 reverse primer (VLB120)	2.1

TL_290	gacaatcatcGGTCTGTCTGAAAAGTCTTG	TS2-PVLB_22260 forward primer (VLB120)	2.1
TL_291	gaagcttgcatgcctgcaggATCGTCTGCTGACCCAAC	TS2-PVLB_22260 reverse primer (VLB120)	2.1
TL_157	agtatagggataacagggtaatctgCTTCTTGACCGTGCAGCG	TS1-P_ex-*paoEFGHI* (P_{14f} + BCD2) forward primer (VLB120)	2.1
TL_158	cgggcttaattaaCGGGGTGCAGGTCAGGAG	TS1-P_ex-*paoEFGHI* (P_{14f} + BCD2) reverse primer (VLB120)	2.1
TL_159	acctgcaccccgTTAATTAAGCCCGTTGAC	P_{14f} + BCD2 (P_ex-*paoEFGHI*) forward primer	2.1
TL_160	ccgtagttccatTAGAAAACCTCCTTAGCATG	P_{14f} + BCD2 (P_ex-*paoEFGHI*) reverse primer	2.1
TL_161	aggaggttttctaATGGAACTACGGATCAAC	TS2-P_ex-*paoEFGHI* (P_{14f} + BCD2) forward primer (VLB120)	2.1
TL_162	ccctagaagcttgcatgcctgcaggCGTTAGCTTCAGCAGGTC	TS2-P_ex-*paoEFGHI* (P_{14f} + BCD2) reverse primer (VLB120)	2.1
TL_165	gtatagggataacagggtaatctgAGACACGTGCCGATGCCATTG	TS1-P_ex-*aldB-I* (P_{14f} + BCD2) forward primer (VLB120)	2.1
TL_166	cgggcttaattaaCGTGTGCTGTGCCAGCGT	TS1-P_ex-*aldB-I* (P_{14f} + BCD2) reverse primer (VLB120)	2.1
TL_167	gcacagcacacgTTAATTAAGCCCGTTGAC	P_{14f} + BCD2 (P_ex-*aldB-I*) forward primer	2.1
TL_168	tgcgtaacgcatTAGAAAACCTCCTTAGCATG	P_{14f} + BCD2 (P_ex-*aldB-I*) reverse primer	2.1
TL_169	aggaggttttctaATGCGTTACGCACATCCCG	TS2-P_ex-*aldB-I* (P_{14f} + BCD2) forward primer (VLB120)	2.1
TL_170	ccctagaagcttgcatgcctgcaggAGTTGCCAGCGGCCAAGG	TS2-P_ex-*aldB-I* (P_{14f} + BCD2) reverse primer (VLB120)	2.1

Table S3: Oligonucleotides (name, sequence, and description)

TL_205	*gacagcaaccgatgatcagcaggtgaacc*ATGGAACTACGGATCAACCAGAAG	pSNW2-P_ex-*paoEFGHI* (P_{14f}) first part forward primer	2.1
BW_712	ATGGGGCTCGATCCCCTC	pSNW2-P_ex-*paoEFGHI* (P_{14f}), pSNW2-P_ex-*aldB-I* (P_{14f}), and pSNW2-P_ex-*paoEFGHI* (P_{14c}) first part reverse primer	2.1
TL_206	gcgaggggatcgagccccatTCGCCATTCAGGCTGCGC	pSNW2-P_ex-*paoEFGHI* (P_{14f}) and pSNW2-P_ex-*aldB-I* (P_{14f}), and pSNW2-P_ex-*paoEFGHI* (P_{14c}) second part forward primer	2.1
TL_207	*ggttcacctgctgatcatcggttgctgtc*CCTAGGTCGCCACATTATACCCTC	pSNW2-P_ex-*paoEFGHI* (P_{14f}) second part reverse primer	2.1
TL_208	*caaacacaatagccaggagacacacc*ATGCGTTACGCACATCCC	pSNW2-P_ex-*aldB-I* (P_{14f}) first part forward primer	2.1
TL_209	*ggtgtgtctcctggctattgtgtttg*CCTAGGTCGCCACATTATACCCTC	pSNW2-P_ex-*aldB-I* (P_{14f}) second part reverse primer	2.1
TL_210	CCTAGGGACAGCAACCGATG	pSNW2-P_ex-*paoEFGHI* (P_{14c}) first part forward primer	2.1
TL_211	catcggttgctgtccctagg*tagttatattatacaacataaaaattgacatgtcaattcacttaattaa*CGGGGTGCAGGTCAGGAG	pSNW2-P_ex-*paoEFGHI* (P_{14c}) second part reverse primer	2.1
TL_105	GAATTCGAGCTCGGTACC	pEMG-PVLB_23545-40 forward primer and pBG14f_FRT_Kan forward primer	2.1, 2.2, 2.4
TL_229	TTAATTAAAGCGCTGATCGCAGC	pEMG-PVLB_23545-40 reverse primer	2.1
TL_230	gcgatcagcgctttaattaaTTATGCTTCAGAGAAAAGCTCGACG	*nagR*/P_{nagAa}-*hmfT* (pEMG-PVLB_23545-40-*nagR*/P_{nagAa}-*hmfT*) forward primer	2.1

TL_231	taccactcaggcccatccgtTCAGGAGGAACTGCGCGC	*nagR*/P_{nagAa}-*hmfT* (pEMG-PVLB_23545-40-*nagR*/P_{nagAa}-*hmfT*) reverse primer	2.1
TL_106	TAGAAAACCTCCTTAGCATG	pBG14f_FRT_Kan reverse primer	2.1, 2.4
TL_232	catgctaaggaggttttctaATGGATCGCTTCGACTACGTG	*hmfH* (pBG14f_FRT_Kan) forward primer	2.1
TL_233	cgggtaccgagctcgaattcTCAGTGCTCGGCGACGAAC	*hmfH* (pBG14f_FRT_Kan) reverse primer	2.1
TL_001	ACCGAATTCCTCGAGTCTAG	pBT'Tmcs forward primer	2.1
TL_002	ACCTCCTGTTTCCTGTGTG	pBT'Tmcs reverse primer	2.1
TL_003	tcacacaggaaacaggaggt*cgcgat*ATGGATCGCTTCGACTACGTG	*hmfH* (pBT'Tmcs) forward primer	2.1
TL_004	ctagactcgaggaattcggtTCAGTGCTCGGCGACGAAC	*hmfH* (pBT'Tmcs) reverse primer	2.1
TL_008	TCGAGTCTAGAGGAGCATG	pJNNmcs(t) forward primer	2.1
TL_009	GGAATTCGGTACCGCAAG	pJNNmcs(t) reverse primer	2.1
TL_010	agcttgcggtaccgaattccAGGAGATGCAAATGTCTGTAGCAG	*hmfT* (pJNNmcs(t)) forward primer	2.1
TL_011	gcatgctcctctagactcgaTCAGGAGGAACTGCGCGC	*hmfT* (pJNNmcs(t)) reverse primer	2.1
TL_149	catgctaaggaggttttctaATGATCATGGGAATTCATAAAGGTG	pEMG_PVLB_23545-40 forward primer (exchange to P_{tac})	2.2
TL_150	cccctgtggcagcggggcctTCAGCTCAAACCCAGCTC	pEMG_PVLB_23545-40 reverse primer (exchange to P_{tac})	2.2
P_{tac}	aggccccgctgccacaggggctgcgatcagcgctttaattaactgttgacaattaatcatcggctcgtataatgtgtggaattgtgagcggataacaatttcacacaggcctaggg cccaagttcacttaaaaaggagatcaacaatgaaagcaattttcgtactgaaacatcttaatcatgctaaggaggttttcta	P_{tac} promoter (synthetic DNA fragment)	2.2
TL_151	gtggaaagggtgccgtgcgt*cgcggcgtcgcgaatattcatctacgtct*CCTGTGTGAAATTGTTATCC	pEMG_PVLB_23545_P_{tac} reverse primer (*hmf*-Cluster integration)	2.2
TL_133	ACGCACGGCACCCTTTCC	*hmfFGABCDEHT* forward primer	2.2
TL_134	cgggtaccgagctcgaattcTCAGGAGGAACTGCGCGC	*hmfFGABCDEHT* reverse primer	2.2

Table S3: Oligonucleotides (name, sequence, and description)

TL_075	CAGGCATGCAAGCTTCTAG	pEMG_PVLB_23545-40 forward primer (*hmf*-cluster modification)	2.2
TL_171	CGCTGATCGCAGCCCCTG	pEMG_PVLB_23545-40 reverse primer (*hmf*-cluster modification)	2.2
TL_172	cacaggggctgcgatcagcgAACCCGGTTCACCAACGTC	adh/hmfR1 forward primer	2.2
TL_173	cctagaagcttgcatgcctgTGAATGCGGTTGATCGAGAC	adh/hmfR1 reverse primer	2.2
TL_332	agggataacagggtaatctgAAGCGACCTTCGGCCTGT	TS1-*vdh* forward primer	2.2
TL_333	cctgccgcggGCTCATTCCTCTTGTTGTCGTTATAG	TS1-*vdh* reverse primer	2.2
TL_334	aggaatgagcCCGCGGCAGGCCCAGACC	TS2-*vdh* forward primer	2.2
TL_335	gaagcttgcatgcctgcaggTTGCGACAACAGCGCGTAGGCC	TS2-*vdh* reverse primer	2.2
TL_346	agggataacagggtaatctgTGCCATCACTGGGCTACC	TS1-PP_1948 forward primer	2.2
TL_347	cgcacccgaaGCACTTTTGATTAATCGATTAAAATTTTTCCAC	TS1-PP_1948 reverse primer	2.2
TL_348	tcaaaagtgcTTCGGGTGCGAGCTGTTG	TS2-PP_1948 forward primer	2.2
TL_349	gaagcttgcatgcctgcaggTGAGAGGACGGATGTTTGAATAC	TS2-PP_1948 reverse primer	2.2
TL_191	agggataacagggtaatctgATACCGGATGCTCGTTGG	TS1-*mexT* forward primer	2.3
TL_192	ccccaaggctCGGTGCGCTTCACCTAAAG	TS1-*mexT* reverse primer	2.3
TL_193	aagcgcaccgAGCCTTGGGGCAGACGGG	TS2-*mexT* forward primer	2.3
TL_194	gaagcttgcatgcctgcaggATTCCACAGCCAGAGAGTGCG	TS2-*mexT* reverse primer	2.3
TL_241	agggataacagggtaatctgGAGAGCGGTGAGACCCATTTG	TS1-*mexEF-oprN* forward primer	2.3
TL_242	agtcgttgaaGGAGAACTCCGCCAATGTATTAG	TS1- *mexEF-oprN* reverse primer	2.3
TL_243	ggagttctccTTCAACGACTCCTTTGGTTG	TS2- *mexEF-oprN* forward primer	2.3
TL_244	gaagcttgcatgcctgcaggGTCATGCTCCAAATCTTG	TS2- *mexEF-oprN* reverse primer	2.3

TL_248	ttaatcatgctaaggaggttttctaATGGACCAGATCGAGGCC	*At*PAL forward primer	2.4
TL_249	gatgcatatgtatatctccttcttaTTAGCAGATAGGGATGGGG	*At*PAL reverse primer (production plasmid)	2.4
TL_257	atccccgggtaccgagctcgaattcTTAGCAGATAGGGATGGGG	*At*PAL reverse primer (control plasmid)	2.4
TL_250	TAAGAAGGAGATATACATATGC	*No*CAR forward primer	2.4
TL_251	TTAACCCTGAATCAGACC	*No*CAR reverse primer	2.4
TL_252	cctgttaggtctgattcagggttaaTAAGAAGGAGATATACCATGG	*Ec*PPTase forward primer	2.4
TL_253	atccccgggtaccgagctcgaattcTTAATCGTGTTGGCACAG	*Ec*PPTase reverse primer	2.4

Danksagung

Über ein Grundstudium mit dem Schwerpunkt organische Chemie und einem Master mit dem Titel „Biochemistry and Biophysics“ habe ich mich langsam aber stetig in Richtung Biochemie, Mikrobiologie und schließlich Biotechnologie gearbeitet. Ich möchte mich bei meinem Doktorvater Prof. Dr. Nick Wierckx bedanken, der mir spannende Forschung an der Schnittstelle zwischen mikrobieller Physiologie, nachhaltiger Chemie und Biotechnologie ermöglicht hat, wodurch ich diesen Weg erfolgreich fortsetzen konnte. Nick, vielen Dank, dass du mir dein Vertrauen geschenkt und ganz bewusst mich als Chemiker in dein zuletzt stark gewachsenes Team aufgenommen hast. Durch deine hervorragende Betreuung und uneingeschränkte Unterstützung konnten wir viele Hürden und Stolpersteine überwinden und der industriellen Anwendung von *Pseudomonas* Bakterien für die umweltverträgliche FDCA Produktion ein Stück näherkommen. Es war mir Freude und Ehre zugleich, das einst von dir selbst mit der Isolation und Charakterisierung eines HMF-abbauenden Bakteriums mitbegonnene Projekt weiterzuführen und zu vertiefen. Die äußerst lehrreiche Zeit in deiner Arbeitsgruppe am Forschungszentrum Jülich wird mir immer in guter Erinnerung bleiben.

Prof. Dr. Jörg Pietruszka danke ich für die Begleitung des Promotionsvorhabens als Mentor und die Übernahme des Zweitgutachtens.

Besonderer Dank gilt unserem Postdoc Benedikt Wynands dessen wertvolle Tipps und Tricks rund um unser Lieblingsbakterium maßgeblich zum Erfolg dieser Arbeit beigetragen haben. Es hat mich tief beeindruckt, dass dein wissenschaftliches Knowhow selbst in stressigen Situation immer von guter Laune und einem motivierenden Lächeln begleitet wird. Gemeinsam mit Tobias Schwanemann hast du mir den letzten molekularbiologischen Feinschliff gegeben, von dem ich noch lange profitieren werde.

Zusammen mit Jakob Rönitz sowie den Partnern vom UFZ Leipzig und der HHU Düsseldorf danke ich euch auch für die gute Zusammenarbeit und spannenden Meetings im Rahmen des NO-STRESS Projekts.

Ein großes Dankeschön geht an die gesamte Mannschaft der „Mikrobiellen Katalyse“, insbesondere Felix Herrmann, Thomas Konjetzko, Philipp Ernst, Jan de Witt und Yannic Ackermann. In Labor und Büro, sowie auf und neben dem Fußballplatz stimmte die Chemie und auf euch war und ist immer Verlass.

Abschließend danke ich meiner Familie, insbesondere meinen Eltern Katharina und Uwe, für ihre durchgehende Unterstützung während meiner gesamten bisherigen wissenschaftlichen

Laufbahn. Ihr habt mir viele Chancen im Leben eröffnet, mir jedoch gleichzeitig die Freiheit gelassen, meinen eigenen Weg zu wählen, auch wenn dieser weit weg von der Heimat und in einem unbekannten Berufsfeld verlief.

Im Laufe meines Studiums trat ein einzigartiger Mensch an meine Seite, der mich immer und überall bedingungslos und geduldig unterstützt, besonders in schwierigen Phasen. Ilka Hinxlage, jetzt Lechtenberg, du stehst hinter mir, wenn ich es brauche und gemeinsam meistern wir auch turbulente und fordernde Zeiten. Danke!

Eidesstattliche Erklärung

Ich versichere an Eides Statt, dass die Dissertation von mir selbständig und ohne unzulässige fremde Hilfe unter Beachtung der „Grundsätze zur Sicherung guter wissenschaftlicher Praxis an der Heinrich-Heine-Universität Düsseldorf“ erstellt worden ist. Die Dissertation wurde in der vorgelegten oder in ähnlicher Form noch bei keiner anderen Institution eingereicht. Ich habe bisher keine erfolglosen Promotionsversuche unternommen.

_____

Thorsten Lechtenberg

Band / Volume 279
Rare-earth atoms on two-dimensional materials: ab initio investigation of magnetic properties
J. P. Carbone (2024), 235 pp
ISBN: 978-3-95806-740-0

Band / Volume 280
Communities of Niche-optimized Strains (CoNoS) – a novel concept for improving biotechnological production
R. Zuchowski (2024), VIII, 168 pp
ISBN: 978-3-95806-743-1

Band / Volume 281
Enabling mixed microbial upcycling of plastic monomers
Y. S. Ackermann (2024), XVI, 203 pp
ISBN: 978-3-95806-749-3

Band / Volume 282
Folding and structural studies of *saccharomyces cerevisiae* Phosphoglycerate Kinase
N. Bustorff (2024), xxvi, 126 pp
ISBN: 978-3-95806-754-7

Band / Volume 283
The role of cellular development in multicellular antiphage defense of *Streptomyces*
T. Luthe (2024), vi, 173 pp
ISBN: 978-3-95806-768-4

Band / Volume 284
Probing the Transformation from Transition Metal Complexes to Extended Two-Dimensional Nanostructures
D. Baranowski (2024), XII, 103 pp
ISBN: 978-3-95806-772-1

Band / Volume 285
Neutron Scattering
Lectures of the JCNS Laboratory Course held at Forschungszentrum Jülich and at the Heinz-Maier-Leibnitz Zentrum Garching
edited by S. Förster, K. Friese, M. Kruteva, S. Nandi, M. Zobel, R. Zorn (2024), ca. 365 pp
ISBN: 978-3-95806-774-5

Band / Volume 286
***Ab initio* investigation of intrinsic antiferromagnetic solitons**
Amal Jawdat Nayef Aldarawsheh (2024), xv, 164 pp
ISBN: 978-3-95806-785-1

Schriften des Forschungszentrums Jülich
Reihe Schlüsseltechnologien / Key Technologies

Band / Volume 287
Understanding the dynamics of Plant- Bacteria-Bacteriophage interactions as a means to improve plant performance
S. H. Erdrich (2024), ix, 176 pp
ISBN: 978-3-95806-791-2

Band / Volume 288
Prediction of Magnetic Materials for Energy and Information Combining Data-Analytics and First-Principles Theory
R. Hilgers (2024), xv, 215 pp
ISBN: 978-3-95806-795-0

Band / Volume 289
Biodegradation and microbial upcycling of plastics
J. de Witt (2025), XVI, 259 pp
ISBN: 978-3-95806-804-9

Band / Volume 290
Practical Methods for Efficient Analytical Control in Superconducting Qubits
B. Li (2025), 202 pp
ISBN: 978-3-95806-807-0

Band / Volume 291
Ab initio investigation of topological magnetism in two-dimensional van der Waals heterostructures
N. Abuawwad (2025), xviii, 135 pp
ISBN: 978-3-95806-808-7

Band / Volume 292
Tolerance engineering of Pseudomonas for the efficient conversion and production of aldehydes
T. Lechtenberg (2025), XVI, 185 pp
ISBN: 978-3-95806-817-9

Weitere ***Schriften des Verlags im Forschungszentrum Jülich*** unter
http://wwwzb1.fz-juelich.de/verlagextern1/index.asp

Schlüsseltechnologien / Key Technologies
Band / Volume 292
ISBN 978-3-95806-817-9

Mitglied der Helmholtz-Gemeinschaft

JÜLICH
Forschungszentrum